



UNIVERSITAT_{DE}
BARCELONA

Inhibition of KRAS oncogenic activity by interfering with new KRAS interactors

Baraa Abuasaker



Aquesta tesi doctoral està subjecta a la llicència **Reconeixement- NoComercial – SenseObraDerivada 4.0. Espanya de Creative Commons.**

Esta tesis doctoral está sujeta a la licencia **Reconocimiento - NoComercial – SinObraDerivada 4.0. España de Creative Commons.**

This doctoral thesis is licensed under the **Creative Commons Attribution-NonCommercial-NoDerivs 4.0. Spain License.**

DOCTORAL PROGRAM IN BIOMEDICINE

UNIVERSITY OF BARCELONA



Inhibition of KRAS oncogenic activity by interfering with new KRAS interactors

Thesis presented by


Baraa Abuasaker

To qualify for the degree of Doctor by the University of Barcelona

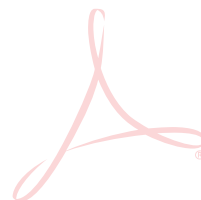
This thesis has been performed in the Department of Biomedicine
of the School of Medicine and Health Sciences of University of Barcelona,
under supervision of Prof. Neus Agell Jané and Dr. Montserrat Jaumot Pijoan

A blue ink signature of Baraa Abuasaker.

Baraa Abuasaker

A red ink signature of Prof. Neus Agell.

Prof. Neus Agell
(Supervisor and Tutor)

A red ink signature of Dr. Montserrat Jaumot.

Dr. Montserrat Jaumot
(Supervisor)

INDEX

INDEX

ABBREVIATIONS	7
INTRODUCTION	13
1. INTRODUCTION TO KRAS	15
1.1 KRAS structure and function	15
1.2 KRAS localisation in cell membranes	18
1.3 Regulators of KRAS	21
1.3.1 KRAS activity cycle: GAPs and GEFs	21
1.3.2 KRAS post-translational modifications (PTMs)	23
1.4 KRAS-mediated signalling pathways	26
1.4.1 The Mitogen-Activated Protein (MAP) kinase signalling pathway (RAF/MEK/ERK)	27
1.4.2 The PI3K/AKT pathway	30
1.4.3 The RAS/RASSF family pathway	31
1.5 KRAS mutations and cancer	34
1.5.1 Mutation characteristics of oncogenic KRAS	34
1.5.2 Mutations co-existing with oncogenic KRAS	36
1.5.3 KRAS mutations and inflammatory tumour microenvironment (TME)	38
1.6 KRAS inhibition	41
1.6.1 Indirect strategies of targeting KRAS	41
1.6.2 Direct strategies of targeting KRAS	46
1.7 Allosteric regulatory sites in KRAS potentially accelerate drug development	50
2. HYPOTHESIS AND OBJECTIVES	53
3. MATERIALS AND METHODS	57
3.1 Antibodies	59
3.2 Reagents and kits	60
3.3 Solutions and Buffers	63
3.4 Cell culture	65
3.4.1 Cell lines and maintenance	65
3.4.2 Cryopreservation	66
3.5 Organoids establishment	67
3.5.1 Human colorectal processing for organoids culture	67
3.5.2 Cryopreservation of organoids culture	67
3.5.3 Organoid thawing	68
3.5.4 Organoids passaging	69

3.6	3-Dimensional (3D) cell culture assay	69
3.6.1	Matrigel-based 3D cell culture <i>in vitro</i>	69
3.7	Bacterial selection and transformation	70
3.7.1	Transformation of BL21pLys cells. Protein expression and purification	71
3.7.2	Plasmid purification	75
3.8	Cell transfection	75
3.9	Electrophoresis and Western Blotting (WB)	76
3.9.1	Sample preparation	76
3.9.2	Protein quantification	76
3.9.3	SDS-Polyacrylamide Gel Electrophoresis (SDS-PAGE)	78
3.9.4	Protein transfer from gel to blotting membrane	79
3.9.5	Total protein detection: Ponceau S staining	80
3.9.6	Membrane blocking	81
3.9.7	Western blotting: Immunodetection	81
3.10	Treatment of cells with P14 and its derivatives, and EGF/FBS- dependent signalling activation	82
3.11	Co-immunoprecipitation	82
3.12	Ras Binding Domain-pull down assay (RBD-pull down)	84
3.13	Calmodulin-pull down (CaM-pull down)	84
3.14	Cell viability assays	85
3.14.1	MTS Tetrazolium assay:	85
3.14.2	Resazurin Reduction Assay:	87
3.15	Surface Plasmon Resonance (SPR)	88
3.16	UltraID proximity-dependent biotinylation method	91
3.16.1	Generation of the UltraID-KRAS-G12V vector	91
3.16.2	Streptavidin-pull down	94
3.16.3	Liquid chromatography-mass spectrometry analysis (LC-MS/MS)	96
3.16.4	Data analysis of the biotinylated proteins detected by LC-MS/MS	96
3.17	Immunofluorescence technique	97
3.18	Effect of P1.3 on orthotopic mice	98
3.18.1	Determination of the Maximum Tolerated Dose (MTD) of P1.3 in athymic mice	98
3.18.2	Repeated dose toxicity of P1.3 in athymic mice	99
4.	RESULTS	101
4.1	CHAPTER 1	103
4.1.1	BACKGROUND AND PREVIOUS DATA	105
I.	Generation of peptidomimetics designed to interfere with the interaction of Ras with its effectors	106
II.	Biological effect of peptidomimetics that bind to RAS effector domain.	109
4.1.2	RESULTS	111
4.1.2.1	Analysing the levels of RAS-GTP upon P1.3 treatment.	111
4.1.2.2	Studying the direct interaction of P1.3 with KRAS-GTP by surface plasmon resonance (SRP).	112
4.1.2.3	Toxicity profile assessment of P1.3 in athymic mice	112
I.	Determination of the Maximum Tolerated Dose (MTD) of P1.3 in athymic mice.	112

II.	Examination of the repeated dose toxicity of P1.3 in athymic mice-----	116
4.2	CHAPTER 2 -----	123
4.2.1	BACKGROUND AND PREVIOUS DATA -----	125
4.2.1.1	KRAS modelling, virtual screening and selection of the best compound as a KRAS interactor -----	126
4.2.2	RESULTS-----	127
4.2.2.1	Biological effects of the selected compound (P14) on colorectal cancer cells (CRC)-----	127
4.2.2.2	P14 derivatives formulation and biological effects on CRC cells-----	128
4.2.2.3	Studying the specificity of P14B on KRAS oncogenicity in CRC-----	131
4.2.2.4	P14B directly binds to oncogenic KRAS competing with CaM <i>in vitro</i> -----	133
4.2.2.5	P14B enhances oncogenic KRAS interaction with its effectors BRAF and P-CRAF, not affecting ARAF or CRAF-----	135
4.2.2.6	P14B decreases the viability of CRC cells expressing oncogenic KRAS in 2D and 3D culture conditions-----	136
4.2.2.7	P14B decreases the viability of Patient Derived Colorectal Cancer Organoids (PDCOs) -----	139
4.2.2.8	Biological effects of P14 and P14B on pancreatic ductal adenocarcinoma cell lines (PDAC) -----	140
4.2.2.9	Setting up the UltraID proximity-dependent biotinylation (PDB) technology in CRC cells-----	141
I.	Generation of the UltraID-KRAS-G12V vector. -----	142
II.	Functional validation of the UltraID-KRAS-G12V vector and setting up the PDB method. -----	144
III.	PDB technology reveals differential KRAS protein interactions upon P14B treatment in CRC. -----	146
5.	DISCUSSION-----	153
5.1.	The peptidomimetic P1.3 is designed to interact with RAS effector domain -----	155
5.2.	Small molecule binds directly to α 4- α 5 helices on surface of KRAS increases its signalling while inducing colorectal cancer (CRC) cell death -----	161
6.	CONCLUSIONS-----	175
7.	REFERENCES -----	178

ABBREVIATIONS

ABC: ammonium bicarbonate

AP-MS: affinity purification-mass spectrometry

APS: ammonium persulphate

ATCC: American type culture collection

BADs: Bcl-XL-2-associated death promoters

BSA: bovine serum albumin

CaM: calmodulin

Co-IP: co-immunoprecipitation

CR2: conserved region 2

CR3: conserved region 3

CRC: colorectal cancer

CXCL: Cys-X-Cys chemokines

DARPs: designed ankyrin repeat proteins

DBPs: differentially biotinylated proteins

DMEM: Dulbecco's modified Eagle's medium

DMSO: dimethyl sulfoxide

DNA: deoxyribonucleic acid

DPIs: dual prenyltransferase inhibitors

DTT: dithiothreitol

ECM: extracellular matrix

EGF: epidermal growth factor

EGFR: epidermal growth factor receptor

EM: electron microscopy

EMT: epithelial-mesenchymal transition

ER: endoplasmic reticulum

FBS: fetal bovine serum

FDR: false discovery rate

FTase: farnesyltransferase

FTIs: FTase inhibitors

GAP: GTPase activating protein

GDP: guanosine diphosphate

GEF: guanin exchange factors
GGTase: geranylgeranyltransferase
GGTI: GGTase inhibitor
GPCR: G protein-coupled receptor
GRB: growth-factor-receptor-bound protein
GST: glutathione-S-transferase
GTP: guanosine triphosphate
HDAC6: histone deacetylase 6
HRP: horseradish peroxidase
HVR: hypervariable region
IAA: iodoacetamide
ICAM-1: intracellular adhesion molecule 1
ICIs: immune checkpoints inhibitor
IL: interleukin
iNOS: inducible nitric oxide synthase
IP: intraperitoneal injection
KD: dissociation constant
KRAS: Kirsten rat sarcoma
LB: Luria-Bertani
LCMS: liquid chromatography-mass spectrometry
LUADs: lung adenocarcinoma
LZTR1: zipper-like transcription regulator 1
MAPK: mitogen-activated protein kinase
MCP-1: monocyte chemoattractant protein 1
MDSCs: myeloid-derived suppressor cells
MLB: Mg-containing lysis buffer
MTD: maximum tolerated dose
NETs: neuroendocrine tumours
NF1: neurofibromin
NSCLC: non-small cell lung cancer
NTA: N-terminal acidic motif

PALM: phosphatidylinositol-4,5-bisphosphate

PBD: proximal-dependent biotinylation

PBS: phosphate buffer saline

PCR: polymerase chain reaction

PD-L1: programmed death-ligand 1

PD: proteome discoverer

PDAC: pancreatic ductal adenocarcinoma

PDCOs: Patient-derived colorectal cancer organoids

PDEd: phosphodiesterase 6 delta subunit

PDK1: phosphoinositide-dependent kinase-1

PDOs: patient-derived organoids

PFA: paraformaldehyde

PH: pleckstrin homology

PI3K: phosphatidylinositol-3-kinase

PIP₂: phosphatidylinositol-4,5-bisphosphate

PIP₃: phosphatidylinositol-3,4,5-trisphosphate

PKC: protein kinase C

PKG2: cGMP-dependent protein kinase 2

PM: plasma membrane

PPIs: protein-protein interactions

pRb: retinoblastoma

PVDF: polyvinylidene fluoride

RASSF: RAS associated domain family

RBD: RAS binding domains

REB: RAS extraction buffer

RKIP: RAF kinase inhibitor protein

RT: room temperature

RTKs: receptor tyrosine kinases

RU: response unite

SAINT: significance analysis of INTeractome

SDS-PAGE: SDS-polyacrylamide gel electrophoresis

SDS: sodium dodecyl sulphate

SIRT2: sirtuin 2

SOS1: son of sevenless 1

SPR: surface plasmon resonance

TBS-T: TBS-tween 20

TBS: tris buffer saline

TCGA: cancer genome atlas

TEB: tissue extraction buffer

TME: tumour microenvironment

TNF-a: tumour activation factor-a

VEGF: vascular endothelial growth factor

WB: western blotting

WT: wild type

INTRODUCTION

1. Introduction to KRAS

1.1 KRAS structure and function

The Kirsten rat sarcoma oncogene (KRAS) homologue stands out as a prominent oncogene, distinguished by its notably elevated mutation rate compared to other oncogenes. This genetic anomaly is intricately linked to several highly lethal cancer types such as pancreatic ductal adenocarcinoma (PDAC), non-small cell lung cancer (NSCLC), and colorectal cancer (CRC) (L. Huang et al., 2021).

The KRAS gene is a member of the rat sarcoma viral oncogene family (RAS), alongside two other human isoforms: the Harvey and neuroblastoma rat sarcoma viral oncogenes (HRAS, NRAS). RAS proteins are small GTPases that transit between an active (GTP-bound) and an inactive (GDP-bound) state; and play a crucial role in regulating essential cellular processes by transducing signals originating from cell surface receptors.

In 1982, Weinberg and Barbacid isolated a gene from human bladder cancer cell lines, which was later identified as the human homologue of the RAS gene, known as HRAS, situated on the short arm of chromosome 11 (11p15.1–11p15.3) (Barbacid, 1987). Concurrently, another homologue, KRAS, was discovered in human lung cancer cells, positioned on the short arm of chromosome 12 (12p11.1–12p12.1) in the same year. The third member, NRAS, was detected in human neuroblastoma and resides on the short arm of chromosome 1 (1p22–1p32) (Chang et al., 1982; McBride et al., 1983).

The KRAS gene encodes two closely related protein isoforms, KRAS-4B and KRAS-4A, with 188 and 189 amino acids respectively, resulting from distinct cleavage patterns in the fourth exon (Karnoub & Weinberg, 2008), being KRAS-4B the predominant splice form of KRAS, henceforth referred to simply as KRAS. The crystallographic analysis of RAS elucidates two prominent domains: the catalytic G domain and the hypervariable region (HVR) (Vetter & Wittinghofer, 2001). The G domain of RAS, comprised of residues 1-166, forms the basis of biological functionality of the RAS GTPase proteins (Wittinghofer & Vetter, 2011). Furthermore, the G domain encompasses three pivotal regions, switch I, switch II, and the P loop (Figure 1A). Also, it contains the allosteric lobe for non-effector interactions (residues 87-166). The HVR, a flexible C-terminal structural element, is characterized by a membrane targeting domain housing the CAAX motif, where C denotes cysteine, A signifies any aliphatic amino acid, and X represents any amino acid (Figure 1B) (Bourne et al., 1991).

Based on homology with other RAS genes, KRAS can be delineated into three segments. The initial segment comprises the first 85 amino acid residues, constituting a highly conserved region. The subsequent 80 amino acid residues, referred to as the second segment, exhibit an 85% homology between any pair of human RAS genes. Finally, the last segment constitutes the HVR, a highly variable region, displaying a mere 8% homology (Figure 1B) (Huang et al., 2021).

As mentioned above, the switch regions I and II, within the G-domain, are essential for RAS function. These regions constitute the binding interface for effector proteins and serve as interaction sites for RAS regulators, including GTPase-activating proteins (GAPs) and guanine nucleotide exchange factors (GEFs) (detailed in 1.3.1). It is noteworthy that the characterization of switch regions in the literature involves several residue definitions, marked by a degree of arbitrariness stemming from the intrinsic flexibility of these regions. For instance, in the context of switch-II definitions, the initiation spans residues 58–60 and concludes within residues 67–76, encompassing or excluding the helix $\alpha 2$ either partially or in its entirety. For illustrative purposes in this context, the switch-I definition adopts residues 30–40, switch-II is defined by residues 58–72, and the P loop is outlined by residues 10–14. It is important to acknowledge that P-loop, also recognized as the Walker A motif, extends to the Ser17 and is an integral part of these intricate regulatory sequences (Walker et al., 1982). Emphasizing the significance, it is crucial to note that the hotspot mutations associated with cancer predominantly occur within the P-loop and switch II regions (Figure 1C).

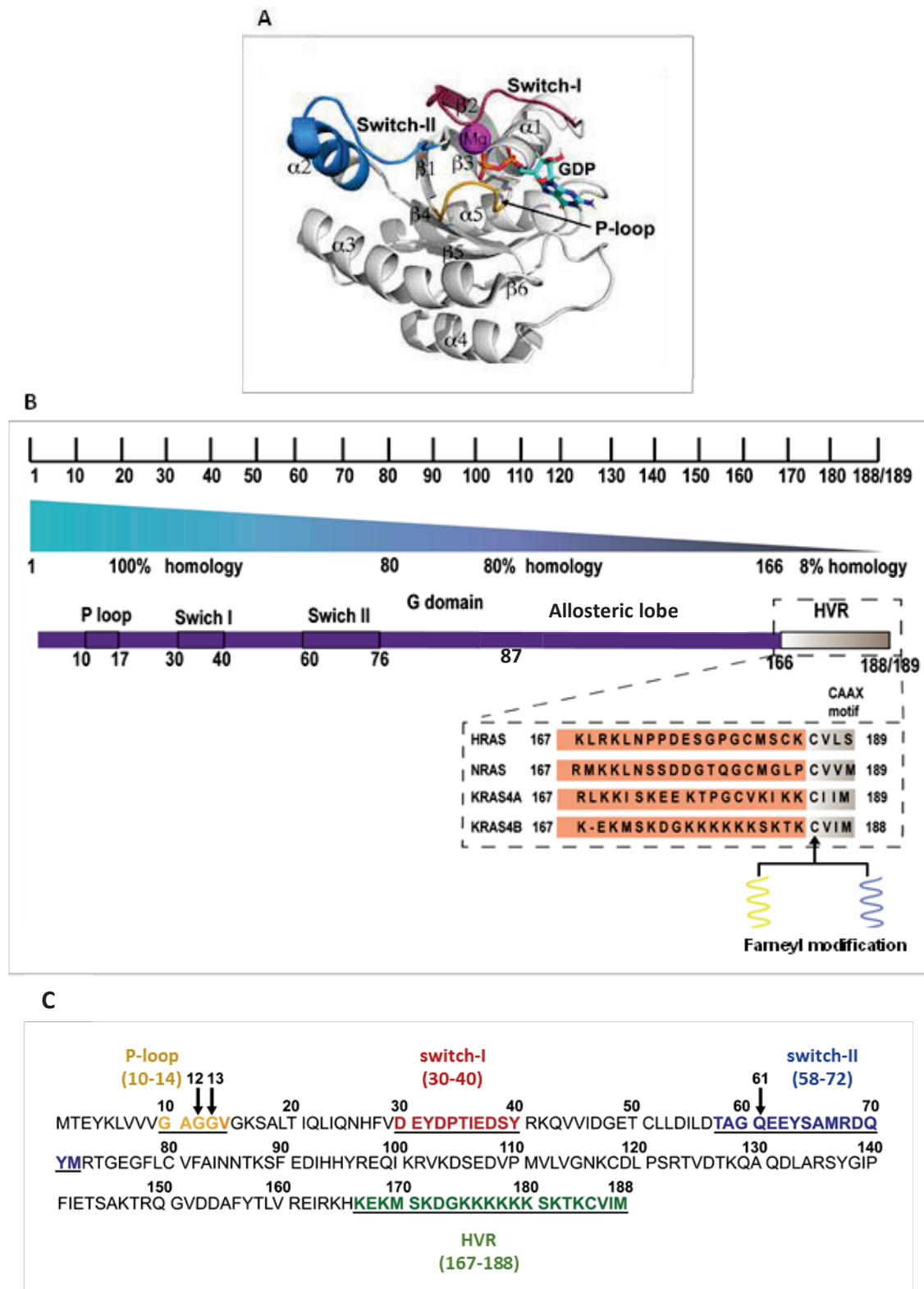


Figure 1: (A) Crystal structure of GDP-bound wild type KRAS. Adapted from (Pantsar., 2020). **(B) Comparative structure of RAS isoforms.** Adapted from (L. Huang et al., 2021). **(C) The sequence of KRAS4B.** Key structural regions in colours, and prominent mutations marked by arrows. Adapted from (Pantsar., 2020).

1.2 KRAS localisation in cell membranes

KRAS plasma membrane localization and recycling

The plasma membrane (PM) is an intricate and heterogeneous lipid bilayer, organised through a network of lipid-lipid, lipid-protein, and cytoskeleton interactions. This complexity is biologically significant, providing an appealing mechanism for regulating the lateral segregation and functional output of membrane-anchored signalling proteins (Simons & Toomre, 2000).

As previously mentioned, NRAS, HRAS, and KRAS are small GTPases that undergo cycling between inactive GDP-bound and active GTP-bound states to intricately regulate cell growth. In order to exhibit biological activity, RAS proteins do not only need to locate to the PM but also to organize precisely spatially within protein-lipid assemblies referred to as nanoclusters. This spatial arrangement is crucial for orchestrating and fine-tuning cellular processes associated with RAS-mediated signalling (Nan et al., 2015; Plowman et al., 2005; Tian et al., 2007; Zhou et al., 2018a; Zhou & Hancock, 2015). For biological activity, RAS proteins must localise to the PM using carboxy-terminal membrane anchor (Hancock et al., 1989). The RAS plasma membrane anchor comprises two essential components. The initial anchor component, shared across all RAS isoforms, is a carboxyl-terminal S-farnesyl cysteine carboxymethyl ester. This ester is formed through a series of sequential, irreversible posttranslational modifications of the conserved carboxy-terminal CAAX motif found in the nascent RAS proteins as it will be detailed in 1.3.2 (Zhou et al., 2018a). The second anchor component encompasses monopalmitoylation in NRAS, duopalmitoylation in HRAS, combination of cysteine palmitoylation across cysteine and lysine residues in KRAS4A (Laude & Prior, 2008; F. D. Tsai et al., 2015) and a polybasic domain (PBD) featuring six consecutive lysins in KRAS4B (KRAS) (Figure 2). (Silvius et al., 2005).

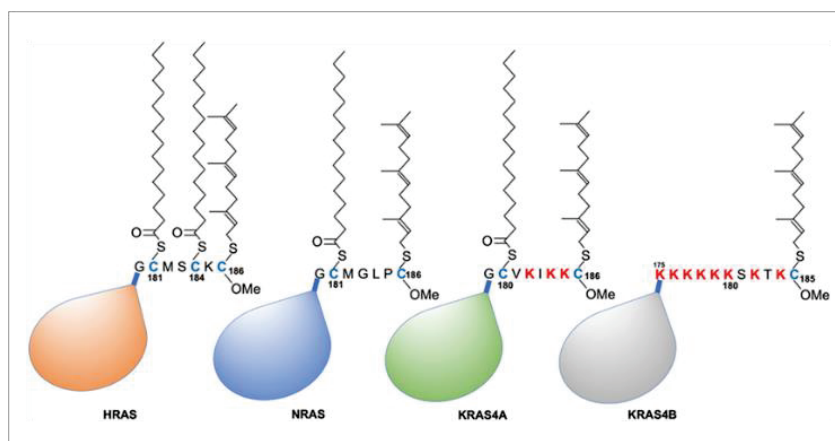


Figure 2: Carboxy-terminal PM anchor component in RAS isoforms. Adapted from (Zhou & Hancock., 2023).

Palmitoylation is facilitated by palmitoyltransferases localized in the endoplasmic reticulum (ER) and Golgi apparatus. It's worth noting that this bipartite membrane anchor structure is a common feature among various RAS superfamily proteins (Michaelson et al., 2001). Following the completion of anchor assembly on the cytosolic surface of the ER, HRAS and NRAS reach the PM via the exocytic pathway through the Golgi (Apolloni et al., 2000). In contrast, KRAS is transported to the PM bypassing the Golgi, utilizing the recycling endosome route (Figure 3, left) (Apolloni et al., 2000).

To maintain the spatial localisation of RAS proteins, the cell employs active transport and removal processes, ensuring RAS proteins reach their intended destinations and are removed before diffusion occurs (Schmick et al., 2015). HRAS and NRAS undergo cycles of depalmitoylation on the cytosolic surface of endosomes, facilitated by yet-to-be-fully-characterised thioesterases after internalisation. This is followed by repalmitoylation in the ER and Golgi, enabling vesicular transport back to the PM (Goodwin et al., 2005). Similarly, KRAS is released from endosomes immediately after internalisation due to the loss of anionic lipid asymmetry. It is then captured by the chaperone protein PDE δ . The KRAS-PDE δ complex is subsequently dissociated by binding the small GTPase Arl2 in the spatial vicinity of the ER. This allows KRAS to bind the cytosolic surface of ER vesicles for forward transport back to the PM (Figure 3, right) (Schmick et al., 2014). Inhibition of PDE δ hindered oncogenic signalling and tumorigenic growth (Dharmaiah et al., 2016).

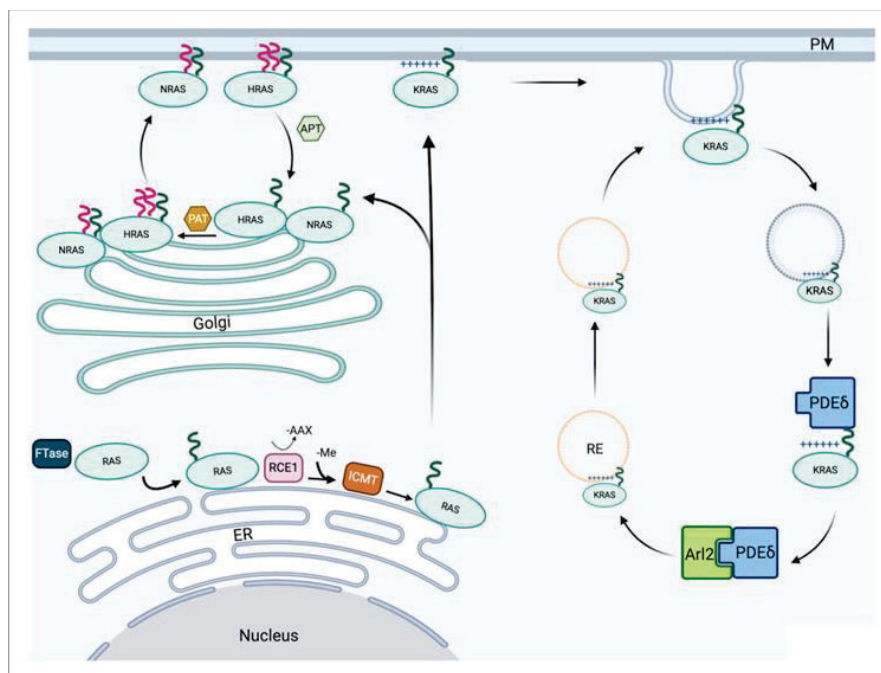


Figure 3: RAS post-translational modifications and transit to the PM (left). RAS recycling (right).
Adapted from (Kattan & Hancock, 2020)

Plasma membrane spatial organization of KRAS in nanoclusters

Advanced techniques have delved into the exploration of raft domains within intact cells. For instance, electron microscopy (EM) and fluorescence recovery after photobleaching analyses reveal that HRAS exhibits transient interactions with lipid rafts when bound to GDP, but clusters in cholesterol-insensitive, galectin-1-dependent, nonraft domains when bound to GTP. Similarly, KRAS forms clusters in cholesterol-insensitive nonrafts domains that are spatially distinct from the activated HRAS microdomains (Niv et al., 2002). These findings are further substantiated, in part, by FRET microscopy, illustrating the segregation of peptides to different domains on the inner surface of the PM based on distinct lipid anchors (Zacharias et al., 2002). Posterior studies, employing immune-electron microscopy (immune-EM), have revealed a previously unappreciated spatial mechanism governing the biological function of RAS. Specifically, RAS proteins were identified to assemble into 5-to-6-membered nanoclusters, serving as signalling scaffolds for recruiting and activating downstream effectors such as RAF and PI3K on the cell membrane (Figure 4) (Abankwa et al., 2007). This spatial mechanism presents a promising avenue for targeting mutant RAS in human cancers. Nevertheless, the immune-EM studies encountered limitations, such as the necessity to isolate membrane sheets from living cells to visualise RAS proteins on the inner leaflet of the membrane. Additionally, there was need to overexpress RAS to offset the low labelling efficiency associated with gold conjugated antibodies (Plowman et al., 2005).

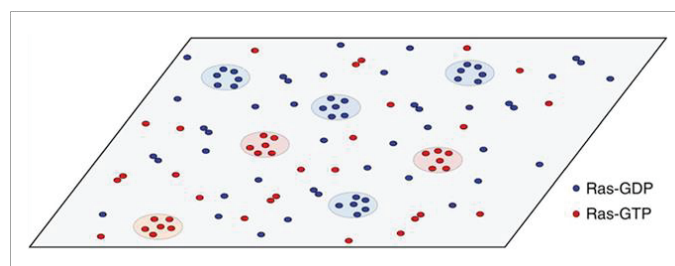


Figure 4: Spatial organization of RAS proteins in nanoclusters on the PM. RAS proteins are found in monomers, oligomers, and nanoclusters. *Adapted from (Zhou et al., 2018b).*

These constraints raise uncertainties regarding the nature, molecular organisation, and biological significance of the observed RAS nanoclusters. Advanced super-resolution light microscopy techniques, like photoactivated localisation microscopy (PALM), overcomes these constraints and empowers the imaging of intact biological samples with remarkable spatial resolution ranging from 10

to 20 nanometres and single-molecule sensitivity (Betzig et al., 2006), making it an ideal tool for investigating RAS nanoclusters (Durisic et al., 2014). In another study, PALM was combined with biochemical analysis, providing compelling evidence to indicate that, in addition to binding to GTP, RAS may also need to form dimers for the activation of the RAS-RAF-MEK-ERK effector pathway (MAPK kinase pathway) (Nan et al., 2015).

KRAS localization at cell endomembranes

Unsurprisingly, this compartmentalisation of RAS proteins is exploited for dynamically regulating RAS signalling. A critical observation is that RAS can signal from various domains, including the PM, Golgi apparatus (GA), and endoplasmic reticulum (ER), activating different signalling pathways from distinct subcellular locations (Bivona et al., 2003; Chiu et al., 2002; Santra et al., 2019). Coordinated waves of differential signalling can be envisioned emanating from distinct sites of RAS activation. For instance, PLC γ signalling induces fast and transient RAS activation at the PM and delayed but sustained RAS activation at the GA. This dynamic interplay is coordinated by PLC γ translocating the GEF RASGRP1 to the GA while activating GAP CAPRI at the PM (Bivona et al., 2003). The integration of signalling kinetics and differential pathway activation through subcellular compartmentalised and timed activation offers an attractive mechanism for controlling biological process with sequential activation events.

1.3 Regulators of KRAS

1.3.1 KRAS activity cycle: GAPs and GEFs

The functionality of RAS hinges on the switch I and switch II regions, serving as a guanosine diphosphate (GDP)/triphosphate (GTP) binary switch that orchestrates crucial signal transduction pathways from activated membrane receptors to intracellular molecules (Román et al., 2018). Two classes of regulatory proteins govern this binary switch: guanine nucleotide exchange factors (GEFs), exemplified by son of sevenless (SOS), and GTPase-activating proteins (GAPs), being neurofibromin 1 (NF1) the most studied (Drugan et al., 2000). Broadly speaking, GEFs activate signalling pathways by catalysing the exchange from GTPase-protein-bound GDP to GTP, while GAPs bring about the termination of signalling by promoting GTP hydrolysis (Figure 5). These multifaceted regulatory proteins, GEFs and GAPs, consist of multiple domains and are subject to intricate regulation by extracellular signals and localised cues (Bos et al., 2007). This dynamic regulation enables them to precisely control cellular events both temporally and spatially.

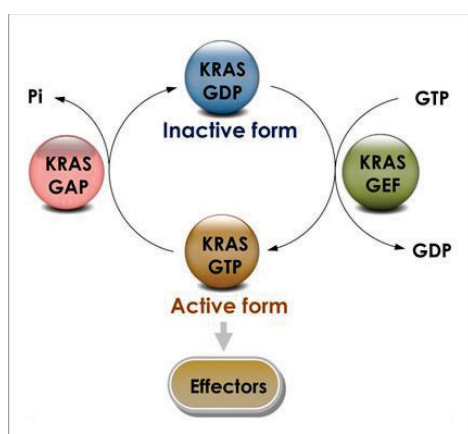


Figure 5: GTPase cycle of KRAS. *Extracted from (P. Liu et al., 2019).*

In its resting state, KRAS typically associates with GDP, maintaining an inactive state attributed to the intrinsic GTPase activity of KRAS, which facilitates the hydrolysis of GTP to GDP (Bos et al., 2007a). Upon exposure to relevant stimuli, such as the interaction between EGF (epidermal growth factor) and EGFR (EGF receptor), the KRAS-GDP complex exhibits reduced affinity for GDP in the presence of GEFs. GEFs association with KRAS cause a conformational change that results in an enhancement in the GDP ejection rate. Consequently, GDP is displaced by GTP, which boasts a higher affinity and a cellular concentration approximately tenfold greater than GDP (Iversen et al., 2014). GTP binding to KRAS induces a conformational change in switch I and II of the G-domain allowing binding to KRAS effectors. Subsequently, KRAS engages downstream molecules, initiating a series of signalling cascades. Conversely, GAPs binding to KRAS accelerates the slow intrinsic GTPase activity of KRAS, thereby leading to the inactive state of KRAS-GDP (Pamonsinlapatham et al., 2009). While both switch regions interact with GEFs, GAPs, and downstream effector proteins, switch I predominantly facilitate GTP hydrolysis by binding with GAP. On the other hand, switch II plays a substantial role in interacting with GEF, promoting nucleotide exchange (M. H. Yang et al., 2022).

Oncogenic RAS mutations commonly hinder GTP hydrolysis, affecting both intrinsic and GAP-mediated phosphate cleavage reactions. As will be further emphasized in section 1.5, the majority of oncogenic mutations (~97%) are concentrated at three major hot spots: G12 and G13 at P-loop and Q61 in switch II region, all in proximity to the reaction site (Papke et al., 2020). These oncogenic mutations can impair the GTPase activity of the RAS-GAP complex, though precise mechanisms that are yet to be fully established. Notably, different GAPs can exhibit varying hydrolysis rates on specific RAS mutants. For instant, NF1 shows higher activity on RAS G13D compared to p120GAP (Rabara et al., 2019), and RGS3, a non-canonical GAP, retains significant activity on RAS G12C (Li et al., 2021).

1.3.2 KRAS post-translational modifications (PTMs)

KRAS post-translational modifications (PTMs) (Figure 6) include phosphorylation, acetylation, ubiquitination, glycosylation, sumoylation, nitrosylation, and ADP-ribosylation; as well as farnesylation, proteolysis and carboxyl methylation.

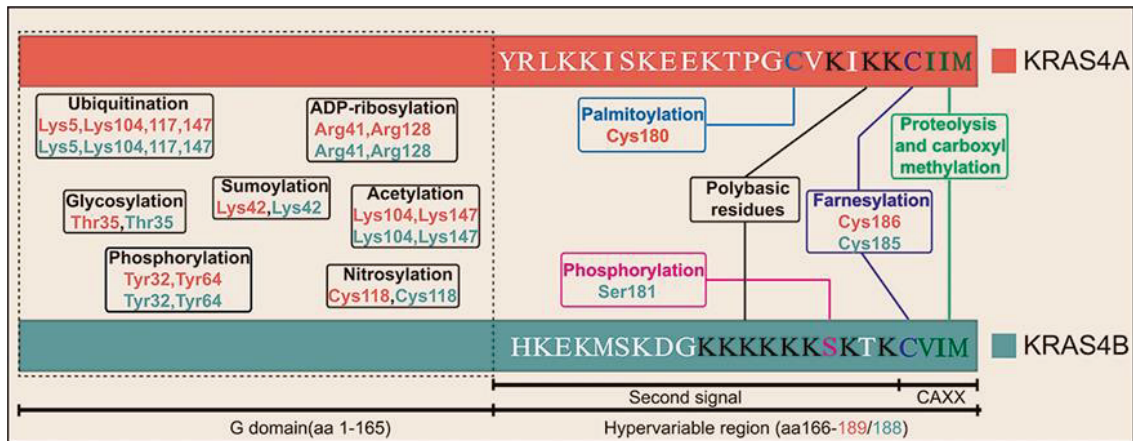


Figure 6: PTMs of KRAS (KRAS-4B) and KRAS-4A. The ones contained in the G-domain and in the HVR are shown separated. Adapted from (Wang et al., 2021).

Prenylation, proteolysis, and methylation

As mentioned in section 1.2, RAS proteins harbour a CAAX tetrapeptide in the C-terminus, undergoing a series of modifications collectively known as CAAX processing, which facilitate their attachment to specific proteins and membranes (Wright & Philips, 2006). The CAAX motif serves as the substrate for cytosolic prenyltransferases, namely farnesyltransferase (FTase) and geranylgeranyltransferase 1 (GGTase1), enabling weak affinity for plasma membranes (Seabra et al., 1991). While CAAX prenylation is generally considered immediate and unregulated, the guanine nucleotide exchange factor SmgGDS has been identified as a regulator of the farnesylation of multiple small GTPases (Berg et al., 2010). Additionally, interactions with noncoding, small nucleolar RNAs SNORD50A and SNORD50B have been reported to influence KRAS prenylation (Siprashvili et al., 2016). Notably, in the presence of an FTase inhibitor, KRAS can undergo modification by GGTase1, allowing for its full biological function (Whyte et al., 1997). Following prenylation, RAS relocates to the surface of the ER and interact with RAS-converting enzyme 1(RCE1). Prenylation appears to be a prerequisite for this step, as membrane transport mediates the colocalization of RAS with RCE1, ensuring substrate specificity (Otto et al., 1999). RCE1 then catalyses the removal of the last three amino acids (AAX) by proteolysis, converting

prenylcysteine into the new C-terminus (Manolaridis et al., 2013). Finally, the C-terminal prenylcysteine serves as a substrate for isoprenylcysteine carboxyl methylation catalysed by ICMT. The result of this processing is the remodelling of the globular hydrophilic region in the C-terminus of RAS proteins into the PM, fulfilling their biological activity.

KRAS phosphorylation

As shown in Figure 6, Tyr32 and Tyr 64 of KRAS are found to be phosphorylated (by SRC family kinases) in the G-domain. These modifications are involved in KRAS-effector interactions and in the KRAS GTP-cycle (Kano et al., 2019). These phosphorylations increase GAP binding and KRAS deactivation (Kano et al., 2019). This inhibitory phosphorylation is subsequently removed by the SHP2 phosphatase (Bunda et al., 2015). SHP2 also plays a pivotal role in developing resistance to KRAS G12C-specific inhibitors (G12C is a specific mutation deeply mentioned below) by facilitating receptor tyrosine kinase (RTK)-mediated feedback activation of wild-type KRAS. Combining KRAS G12C with SHP2 inhibitors disrupts this feedback loop, resulting in sustained KRAS inhibition (Ryan et al., 2019).

In the HVR of KRAS, the residue Ser181 is phosphorylated by protein kinase C (PKC) (Ballester et al., 1987). This PTM has been widely studied and some controversial models about its role in KRAS functionality and localization have been proposed. It has been showed that PKC phosphorylation at Ser181 interferes with the interaction of KRAS with calmodulin (CaM) favouring KRAS activity (Villalonga et al., 2002) (Alvarez-Moya et al., 2010). In Alvarez-Moya (2011) the authors present a model based on their experimental data demonstrating the role of Ser181 phosphorylation in the KRAS localization at the plasma membrane. Therefore, phosphorylated and non-phosphorylated KRAS would segregate in different PM signalling nanoclusters. Other investigation proposed that phosphorylation of Ser181 of KRAS would enable the translocation of KRAS from the PM to the ER, GA and mitochondria, where it would bind to Bcl-XL, promoting apoptosis (Bivona et al., 2006).

Thus, phosphorylation at Ser 181 has emerged as crucial regulatory mechanism influencing the normal and also the oncogenic properties of KRAS, although the exact role is not yet known. Relevant to this point, it has been shown that phosphorylation at Ser181 is required for KRAS to bind hnRNPA2/B1 protein favouring the activation of PI3K/AKT signalling in pancreatic cancer cells and for tumour growth in a xenograft mouse model (Barceló, et al., 2014). In CRC, KRAS phosphorylation at Ser 181 regulates gene expression (Cabot et al., 2021) and also the phosphorylation cycle of KRAS in this residue is shown

to be necessary to maintain the polarized phenotype of epithelial cells and as consequence is required for tumour growth in xenograft mouse models (Barceló et al., 2014a; Cabot et al., 2021).

Other studies indicate that KRAS phosphorylation at Ser181 inhibits tumour initiation by blocking the interaction with calmodulin, consequently abrogating the suppression of noncanonical Wnt signalling (M.-T. Wang et al., 2015).

It's also been shown that cGMP-dependent protein kinase 2 (PKG2) can phosphorylate KRAS at Ser181 triggering KRAS accumulation in the cytosol and on endomembranes thus impeding the proper KRAS recycling to the PM (Cho et al., 2016).

Acetylation- mediated regulation of KRAS

Recent findings have unveiled acetylation as a crucial posttranslational modification for KRAS, particularly at Lys104. Acetylation at this site was observed to result in a decrease nucleotide exchange facilitated by GEFs, leading to an elevated level of inactive GDP-bound state. This acetylation event effectively attenuated the transforming activity of KRAS (M. H. Yang et al., 2012a). Molecular dynamics modelling provided insights into the mechanism, revealing that acetylation at Lys104 perturbed the switch II region through electrostatic interactions, thereby disrupting the interaction between KRAS and GEFs (Baker et al., 2013). Histone deacetylase 6 (HDAC6) and sirtuin 2 (SIRT2) were identified as deacetylases responsible for regulating the acetylation status of KRAS. Interference with either enzyme significantly impaired the survival of cancer cells expressing mutant KRAS (M. H. Yang et al., 2013). Furthermore, a subsequent study identified Lys147 as a novel substrate for SIRT2-mediated deacetylation, highlighting the significant impact of its acetylation status on the oncogenic properties of KRAS (Song et al., 2016). Notably, Lys104 and Lys147, in addition to their roles in acetylation, also serve as a site for mono/diubiquitination, raising intriguing questions about potential competitive relationship between acetylation and ubiquitination that warrant further exploration. Beyond the C-terminus, recent mass spectrometric characterization and structural analysis revealed acetylation events in the N-terminus of KRAS. The acetylation of the N-terminus was found to contribute to the stability of the switch regions and the N-terminus, adding a layer of complexity to the regulatory landscape of KRAS (Dharmaiah et al., 2019).

Ubiquitination-mediated regulation of KRAS

PTM modification of proteins by ubiquitin, known as ubiquitination, is a tightly regulated process involving ubiquitin-activating enzyme (E1), ubiquitin-conjugating enzyme (E2), ubiquitin ligase (E3), and deubiquitylation enzymes. This process holds considerable significance for the stability, activity, and localization of proteins (Mansour, 2018). Recent studies have identified Lys104, Lys117, and Lys147 as critical sites for mono/diubiquitination, acting as reversible triggers for signal initiation in KRAS. Mono-ubiquitination at Lys147 of KRAS has been shown to impair GAP-mediated GTP hydrolysis, leading to increase GTP loaded and enhanced affinity to downstream effectors such as PI3K. Similarly, mono/diubiquitination at Lys117 accelerates nucleotide exchange, thereby enhancing KRAS activation (Sasaki et al., 2011). In contrast, mono-ubiquitination at Lys104 does not alter GAP-mediated GTP hydrolysis of nucleotide exchange (Baker et al., 2013). Considering the proximity of Lys104 to the GEF binding region and results from point mutation experiments, it is plausible that ubiquitination at Lys104 may influence GEF-mediated catalysis (Yin et al., 2017). The identification of the E3 ubiquitin ligases responsible for ubiquitination at Lys147, Lys117, and Lys104 in KRAS remains an ongoing area of investigation. Recently, the inactivation of leucine zipper-like transcription regulator 1 (LZTR1) was discovered to inhibit KRAS ubiquitination, introducing an unexpected layer of KRAS regulation (Bigenzahn et al., 2018a). This finding highlights the dynamic and intricate nature of ubiquitination-mediated regulation of KRAS, offering new avenues for exploration in understanding the underlying molecular mechanisms.

1.4 KRAS-mediated signalling pathways

Upon normal activation, Ras initiates a multitude of mitogenic signalling cascades that synergistically promote cell proliferation. The frequent aberrant activation of Ras in human tumours underscores its pivotal role in tumorigenesis (Prior et al., 2012). Intriguingly, alongside its potent pro-growth and transformation functions, Ras possesses the capability to induce apoptosis and senescence, suggesting a feedback mechanism to counteract prolonged survival with excessive RAS activity (Karnoub & Weinberg, 2008). The mitogenic pathways mediated by Ras involve multiple effectors, and similarly, the pathways leading to cell death are diverse.

1.4.1 The Mitogen-Activated Protein (MAP) kinase signalling pathway (RAF/MEK/ERK)

The RAF/MEK/ERK signalling pathway activated by RAS plays a pivotal role in regulating cellular proliferation, differentiation, and survival (Kolch et al., 1991). Originating from the identification of RAS small GTPases as the first oncogenes from viruses in the 1970s-1980s (Bonner et al., 1986; Rapp & Todaro, 1978), subsequent investigation on viral oncogenes revealed a N-terminal truncated version of the RAF Ser/Thr kinase (RAF1, CRAF) (Kozak et al., 1984; Rapp & Todaro, 1978). In the 1990s, the other two components of this pathway, MEK (or MAP kinase kinase (MAPKK)) and ERK (MAP kinase (MAPK)), were recognized as cytosolic protein kinases activated by mitogens (Kozak et al., 1984). Following these seminal discoveries, RAF (thus being the MAP Kinase Kinase Kinase (MAPKKK)) was identified as the upstream kinase of MEK in 1992 and the first direct effector of RAS in 1993 (Moelling et al., 1984), marking a milestone in understanding how cells sense external stimuli.

RAF kinase (MAPKKK)

Three RAF isoforms (CRAF, BRAF, and ARAF) and two closely related pseudokinases (KSR1 and KSR2) have been identified so far. The RAF isoforms share highly homologous sequences and similar structures, featuring three conserved regions (Figure 7): conserved region 1 (CR1) housing the RAS-binding domain (RBD) and a Cys-rich domain (Fischer et al., 2007), conserved region 2 (CR2) characterized by a Ser/Thr-rich sequence, conserved region 3 (CR3) comprising a putative kinase domain with a N-terminal acidic motif (NTA) (Köhler & Brummer, 2016); and a C-terminal regulatory tail (A. S. Dhillon et al., 2009; Kondo et al., 2019a). Despite these similarities, RAF isoforms exhibit variable kinase activities, with the order being BRAF > CRAF > ARAF. This variability is attributed to distinct NTA motifs and APE (Ala-Pro-Glu) motifs that contribute to dimerization-driven transactivation of RAFs (Beck et al., 1987; Hu et al., 2013; Huleihel et al., 1986; Yuan et al., 2018).

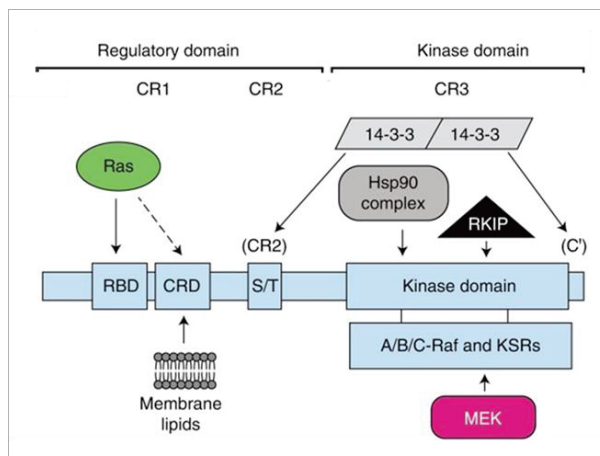


Figure 7: A/B/CRAF structure and some interacting proteins. RKIP (RAF kinase inhibitor protein). Adapted from (Terrell & Morrison, 2019).

In contrast to RAF, KSR proteins replacing the RBD at the N-terminus with a coiled-coil fused sterile α -motif and Pro-rich stretch, play a role in recruiting proteins to the PM upon stimulation. Importantly, they lack the catalytic Lys in the VAIK motif of the kinase domain, which impairs their catalytic activity (Rajakulendran et al., 2009). Historically, due to their associations with MEK and ERK, along with low kinase activity, KSR proteins have been considered scaffold proteins. However, recent studies challenge this perception, suggesting that KSR proteins can also function as allosteric activators, stimulating the catalytic activity of RAF proteins through dimerization (J. Hu et al., 2013; Rajakulendran et al., 2009; Yap et al., 2019). The side-to-side dimerization of RAF/KSR family kinases is crucial not only for their activation but also for their catalytic activity towards downstream kinases (Kondo et al., 2019; Park et al., 2019).

RAS-dependent CRAF activation is a very complex process that includes other RAF-protein interactions and chemical modifications such as phosphorylation and dephosphorylation of critical residues within the kinase (Riaud et al., 2024). Moreover, Nan et al. (2015) in conjunction with prior reports on RAF dimerization (Poulikakos et al., 2010) proposed a unified dimer model for RAS-RAF signalling (Figure 8). This model sheds new light on earlier observations of RAS-dependent formation of RAF dimers under both physiological and pharmacological conditions. Significantly, given the crucial role of the RAS-RAF-MEK-ERK signalling axis in human cancer, there is a potential avenue for targeting mutant RAS through the disruption of RAS dimers (Nan et al., 2015).

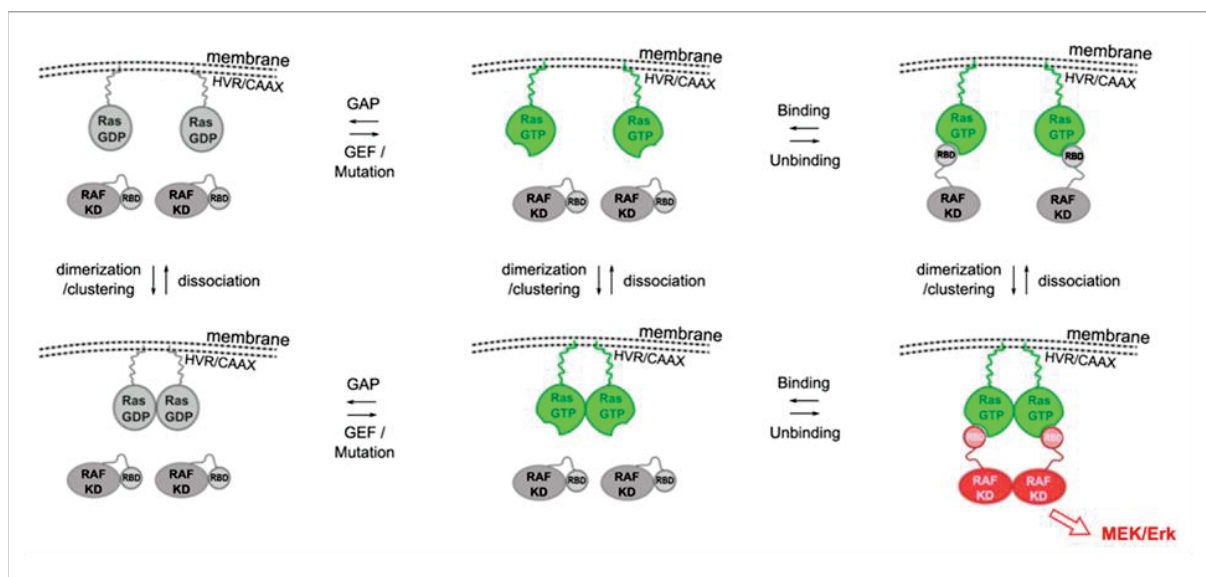


Figure 8: Dimer model for RAS-mediated activation of RAS/MAPK cascade. Adapted from (Nan et al., 2015).

MEK (MAPKK)

MEK1 and 2 are the MAPKK of ERK1 and 2, but the MAPKK serine/threonine kinase family is more extensive and includes other kinases activated in response to diverse signals. Its activation facilitates cell survival and apoptosis through various mediators besides ERK, such as JNK, SAPK, 14-3-3, and NF-KB (Figure 9) (Y. Guo et al., 2020; Schlesinger et al., 1998). Moreover, there are several cross talks between multiple signalling pathways and several negative feedback loops. Notably, MAPKKs are implicated in apoptosis induction by dysregulating pathways like ERK, JNK, and p38 (Karandikar et al., 2000).

ERK (MAPK)

The two ERK isoforms, ERK1 and 2, possess a central kinase domain flanked by short N- and C-terminal tails, exhibiting redundant functions with different expression patterns (Boulton et al., 1991). In contrast to RAFs and MEKs, which have limited substrates, ERKs recognize and phosphorylate numerous substrates, including transcription factors, protein kinases and phosphatases, as well as other functional proteins (Panka et al., 2006).

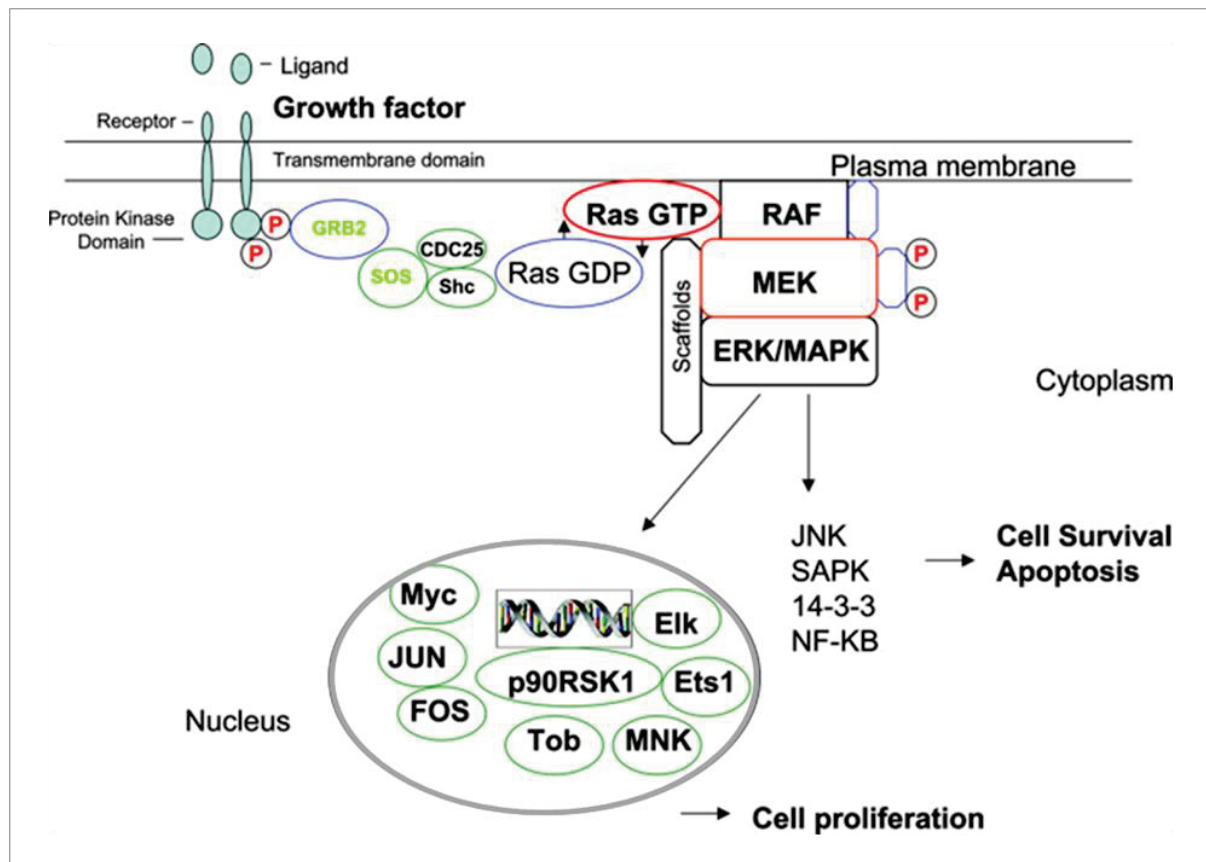


Figure 9: RAS/ MAPK pathway. Adapted from (Molina & Adjei, 2006).

1.4.2 The PI3K/AKT pathway

The phosphatidylinositol 3-kinase (PI3K)-AKT-mTOR signalling pathway, activated by various cellular stimuli or toxic insults, in which KRAS has been identified as a participant, plays a crucial role in regulating fundamental cellular functions, including transcription, translation, proliferation, growth, survival, apoptosis, glucose transport, and the development of tumour resistance (Fruman et al., 2017; Vivanco & Sawyers, 2002). In the depicted Figure 10, PI3Ks exist as heterodimers comprising a catalytic subunit (p110) and an adapter/regulatory subunit (p85). Activation of PI3K occurs by direct binding of the regulatory subunit to receptors with protein tyrosine kinase activity (Receptor Tyrosine Kinase, RTK) or to G protein-coupled receptors (GPCR). RTKs can also indirectly activate PI3K via RAS activation, which in turn activates PI3K by direct binding to p110 (Cuesta et al., 2021). Subsequently, the activated

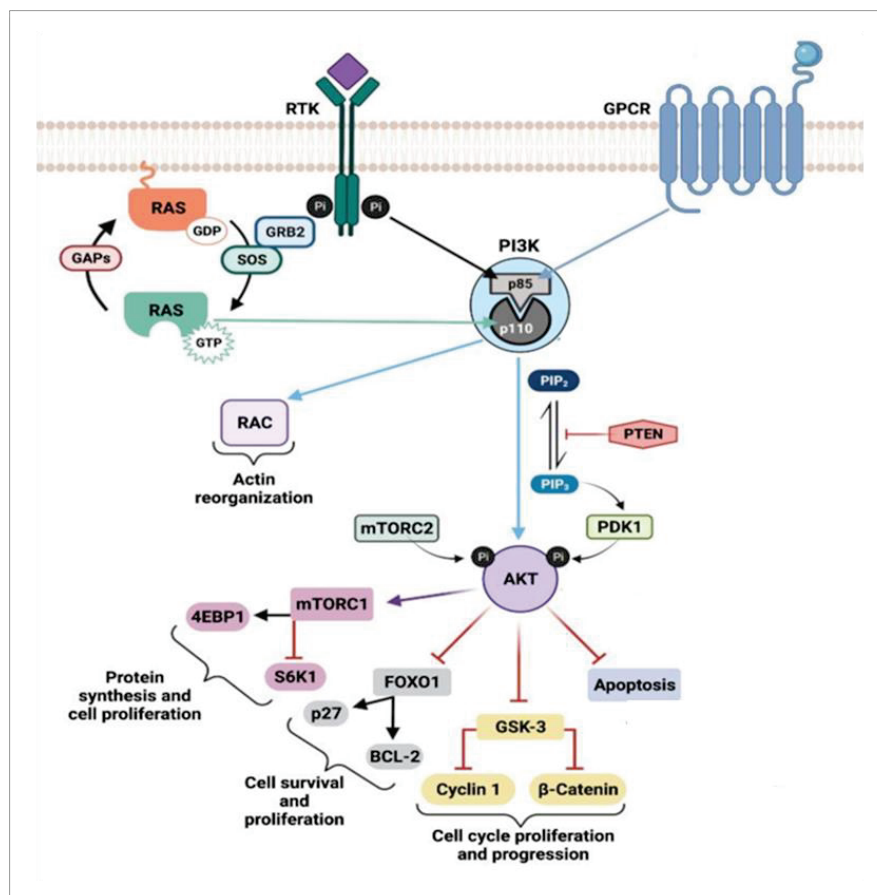


Figure 10: Model for the regulation of the RAS-PI3K-AKT signalling pathway. Adapted from (Cuesta et al., 2021)

PI3K converts the plasma membrane lipid PI (4,5) P2 to PI (3,4,5) P3, allowing the inactive cytosolic AKT to be recruited to the plasma membrane by direct binding to PIP3 through a PH binding domain. As a

consequence, AKT is phosphorylated at Thr308 by phosphoinositide-dependent kinase-1 (PDK1), and at Ser473 by mTORC2, leading to its complete activation (Kilic et al., 2017). Activated AKT modulates various downstream pathways, regulating cell proliferation, survival and metabolic processes (Hoxhaj & Manning, 2020). Moreover, AKT phosphorylates and activates Bcl-XL-2-associated death promoters (BADs), promoting the binding of BAD to the companion protein 14-3-3 rather than Bcl-XL, ultimately inhibiting apoptosis (She et al., 2005).

Other RAS effectors

Although RAF is the most extensively studied effector, several other RAS effector complexes have been resolved, including afadin, RALGDS, byr2, GRB14, PLC γ , PDE δ , shank3, and SIN1. Typically, only the RAS-binding domain (RBD) of effectors is resolved, with PI3K being a notable exception (Pacold et al., 2000). Transient binding interfaces with regulatory roles have been proposed for some effectors, such as the atypical SIN1-RBD in SIN1, and an additional interface suggested to modulate effector binding (Castel et al., 2021). Titration experiments indicate that oncogenic mutations can both enhance and diminish effector-RAS binding (Zheng et al., 2022). Recently, focus has shifted towards synthetic constructs (Guillard et al., 2017) and non-natural partners (Haza et al., 2021), some of which reveal binding interfaces beyond the biological switch I and II regions. However, a comprehensive and functionally competent structure of RAS remains elusive. This is primarily due to the lack of information on membrane-bound assemblies, the native cellular environment of RAS involving its dimerization and/or oligomerization.

1.4.3 The RAS/RASSF family pathway

A key group of Ras death effectors is the RASSF (Ras Association Domain Family) proteins. In 1998, Vavvas et al. identified a Novel Ras Effector (NORE1A) with a consensus Ras Association (RA) domain that binds to activated Ras (Karnoub & Weinberg, 2008). While initial controversy surrounded whether RASSF1 proteins formed complexes with Ras (Vos et al., 2000) or not (Ortiz-Vega et al., 2002), subsequent investigations supported RASSF1A as a physiological KRAS effector (Donninger et al., 2007a). In silico homology searches led to the discovery of four additional RASSF family members, all of which interact with activated KRAS in exogenous expression systems. Various isoforms of RASSF proteins, produced through splicing or differential promoter usage, exhibit down-regulation through epigenetic inactivation in human tumours (Donninger et al., 2007a). Lacking obvious enzymatic activity,

RASSF proteins function as scaffolding or sub-cellular targeting proteins. They are now recognized to link Ras to pathways regulating apoptosis, senescence, autophagy, inflammation, and DNA repair. These proteins interact with tumour suppressors, establishing connections between Ras and the precise control of two of them: p53 and retinoblastoma (pRb). RASSF1A and NORE1A (RASSF5) emerge as potential tumour suppressor hubs.

RASSF1A and RAS driven apoptosis

The MST kinases, identified as direct binding partners of RASSF proteins through two-hybrid studies (Khokhlatchev et al., 2002b), emerge as pro-apoptotic candidates for mediating RASSF-driven apoptosis. Particularly, RASSF1A plays a crucial role in the activation of MST kinases (Figure11), stabilizing their active, phosphorylated forms by inhibiting dephosphorylation through PP2A (C. Guo et al., 2011). MST kinases exhibit apoptotic effects through various substrates, including H2B and JNK (Cheung et al., 2003), but it is their involvement in the Hippo pathway that garners significant attention. In the Hippo pathway, MST kinases phosphorylate and activate LATs kinases, leading to the phosphorylation of the transcriptional regulators YAP and TAZ. This phosphorylation event regulates the localization of YAP/TAZ, restricting their oncogenic activity and influencing the stability of YAP (Pan, 2010; B. Zhao et al., 2007, 2010). RASSF1A further promotes the formation of a complex between YAP and p73 in the nucleus, enhancing the transcription of pro-apoptotic genes like PUMA (Yee et al., 2012). Seminal work from the Kolck group demonstrated that activated KRAS controls the Hippo pathway by binding to RASSF1A and promoting MTS activation (Matallanas et al., 2011). While subsequent studies supported this finding, siRNA studies revealed that the most critical target for RAS/RASSF1A/Hippo growth suppression might be the master tumour suppressor p53, rather than YAP (Matallanas et al., 2011). RASSF1A impacts p53 stability through its interaction with MDM2, forming a complex that promotes MDM2 auto-ubiquitination and subsequent proteasomal degradation. Additionally, MDM2, in association with LATS2, suppresses its ubiquitin ligase activity in a kinase-dependent manner, leading to enhanced p53 stability. The KRAS/RASSF1A interaction is implicated in inducing these regulatory actions (Matallanas et al., 2011).

NORE1A (RASSF5) induces apoptosis

Novel Ras effector 1 (NORE1), also known as RASSF5, was initially identified as the first member of the RASSF family through a yeast two-hybrid screen using activated RAS as bait (Vavvas et al., 1998). NORE1, closely homologous to RASSF1, exhibits multiple isoforms, with the primary ones being NORE1A and NORE1B, or RAPL (Hesson et al., 2003). While NORE1A demonstrates ubiquitous expression (Vos et al., 2003), NORE1B appears to have a more specific function in lymphocytic cells (Avruch et al., 2009). Compelling evidence supports NORE1A's role as a tumour suppressor. Exogenous expression of NORE1A robustly inhibits tumour cell growth (Vos et al., 2003), and its inhibition enhances cell proliferation (Calvisi et al., 2009). NORE1A^{-/-} MEFs are more susceptible to RAS-induced transformation than wild type MEFs, which necessitate p53 or pRb inactivation for RAS transformation (J. Park et al., 2010a). Despite not being as extensively epigenetically silenced as RASSF1A in primary tumours (Donninger et al., 2007b), NORE1A is frequently inactivated in many human cancers through promoter methylation. Loss of NORE1A is associated with a more malignant phenotype and heightened RAS activity in primary tumours (Calvisi et al., 2008). Furthermore, NORE1A inactivation through a translocation event is linked to the development of clear cell renal carcinomas, a rare form of familial cancer (Chen et al., 2003), confirming its role as a tumour suppressor *in vivo*. Crucially, NORE1A is a bona fide RAS effector, binding activated RAS directly both *in vitro* and *in vivo*, and executing its growth inhibitory function in RAS-dependent manner.

Similar to RASSF1A, NORE1A lacks enzymatic activity and executes its growth inhibitory functions by serving as a scaffold, regulating multiple pro-apoptotic pathways (Figure 11). NORE1A, akin to RASSF1A, forms complexes with the MTS kinases, thereby linking RAS to the Hippo pathway (Khokhlatchev et al., 2002a). However, in contrast to RASSF1A, NORE1A does not seem to activate the MTS kinases (Praskova et al., 2004), and the interaction between NORE1A and the MTS kinases is dispensable for NORE1A-mediated growth inhibition (Aoyama et al., 2004). This suggests that NORE1A exerts its growth suppressive effects independently of canonical Hippo signalling. NORE1A regulates various apoptotic pathways, including death receptor-mediated apoptosis (Elmetwali et al., 2016). It sensitises cells to TNF- α and TRAIL-mediated apoptosis, both *in vitro* and *in vivo*, with this effect being mediated by the stress-response MAP kinases (J. Park et al., 2010b). TNF- α treatment induces activation of p38 and JNK but not ERK. In NORE1A-depleted cells, TNF- α induced activation of p38 and JNK is significantly reduced (J. Park et al., 2010b). Similar findings were observed with another member of the TNF-receptor superfamily, CD40. In bladder cancer cells, NORE1A serves as a crucial mediator of

CD40/CD40- induced cell death, dependent on JNK signalling rather than ERK (Elmetwali et al., 2016). These results imply that NORE1A regulation of death receptor-mediated apoptosis may be RAS-independent.

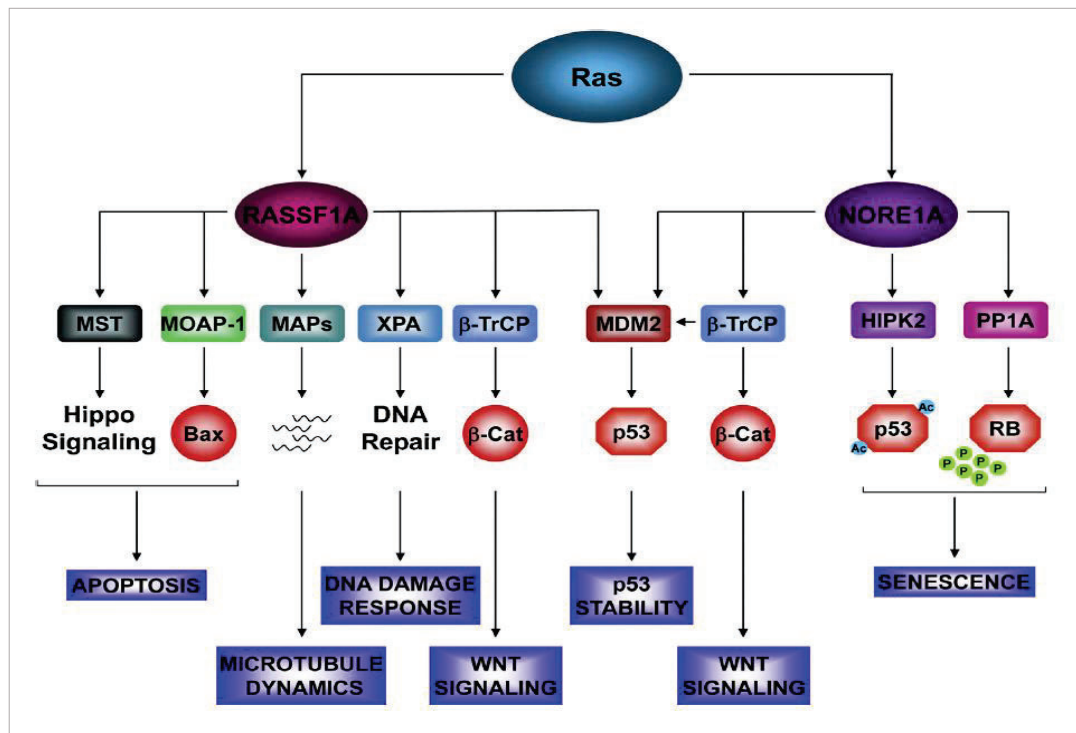


Figure 11: Summary of the major biological processes modulated by RASSF1A and NORE1A. Adapted from (Donninger et al., 2016).

1.5 KRAS mutations and cancer

1.5.1 Mutation characteristics of oncogenic KRAS

The KRAS gene is frequently mutated in various cancer types, including non-small cell lung cancer (NSCLC), colorectal cancer (CRC), and pancreatic ductal adenocarcinoma (PDAC) (Zhang et al., 2022). Predominantly, KRAS mutations manifest as single-base missense mutations, with approximately 98% occurring at codon 12 (G12), codon 13 (G13), or codon 61 (Q61) (Wood et al., 2016). Despite the prevalence of KRAS mutations across diverse cancers, there exists significant heterogeneity in mutation frequencies and subtypes. According to the Cancer Genome Atlas (TCGA) database, KRAS mutations are identified in about 11.6% of all carcinomas, with substantial variability in mutation rates and subtypes observed among different tumour types. PDAC exhibits the highest frequency of KRAS mutations, affecting 81.72% of patients, with G12D as the most frequent subtype.

In CRC, the mutation frequency of KRAS is 37.97%, while in NSCLC, it is approximately 21.20%. KRAS mutations are also found, albeit less frequently, in cholangiocarcinoma, uterine endometrial carcinoma, testicular germ cell cancer, and cervical squamous cell carcinoma, with mutation frequencies of about 12.7%, 14.1%, 11.7%, and 4.3%. The spectrum of KRAS mutations predominantly comprises 21 missense mutations, with G12D (29.19%), G12V (22.97%), and G12C (13.43%) being the most common. In CRC, the most common mutant subtypes are G12D and G12V. In NSCLC, G12C is the most prevalent subtype, constituting approximately 45% of all KRAS mutations, followed by G12V and G12D (Osta et al., 2019). In rare tumours, the overall mutations rate is 8.7%, with G12D, G12V, and G13D as the most common subtypes.

Understanding the landscape of KRAS mutations is crucial, as different mutant subtype and co-alterations may influence the clinicopathological features and prognoses of cancer patients. A summary of KRAS mutation frequency and subtype distributed in common cancers is provided in Table1.

Table 1. KRAS mutation rates and subtypes in most common cancers.

Cancer type	KRAS Mutation				
	N of Samples	Rate (%)	Top 3 subtypes (Proportion of all KRAS mutations, %)		
Pan-cancer	87.606	11.60	G12D (29.19)	G12V (22.97)	G12C (13.43)
Pancreatic adenocarcinoma	990	81.72	G12D (40.20)	G12V (31.96)	G12R (17.10)
Colorectal carcinoma	3853	37.97	G12D (28.04)	G12V (18.50)	G13D (18.10)
Non-small lung cancer	4584	21.20	G12D (45.42)	G12V (15.78)	G12D (13.03)

Data acquired from cBioPortal.org. G12: codon 12 encoding glycine; G13: codon 13 encoding glycine. *Adapted from* (Y. Yang et al., 2023a).

Association of KRAS mutations with clinicopathological characteristics

KRAS mutations exhibit distinct association with clinicopathological features across various tumour types. In CRC, a study focusing on left-sided, microsatellite-stable CRC revealed a higher proportion of KRAS-mutant patients in the lung-metastatic cohort, while the liver-metastatic cohort displayed a lower prevalence (Z. Wang et al., 2021). Another investigation in metastatic CRC indicated that regression of the KRAS mutation correlated with improved prognosis and oligo-metastatic status (Ottaiano et al., 2021). In NSCLC, KRAS mutations are observed in approximately 30% of lung adenocarcinomas and 5% of squamous lung cancers. These mutations are identified in 26% of Western and 11% of Asian populations, with a higher prevalence in smokers (30%) compared to non-smokers (10%) (Ceddia et al., 2022). Studies on lung adenocarcinoma patients revealed a significant association between KRAS mutations and older age (>45 years old) at diagnosis (Y. Yang et al., 2023a). Additionally, NSCLC patients with KRAS mutations exhibited a higher incidence of liver metastasis and brain metastasis compared to wild-type KRAS patients (Macerelli et al., 2014). KRAS mutation also serves as a biomarker for lower differentiation in neuroendocrine tumours (NETs).

A wealth of studies has investigated the influence of KRAS mutations on the prognoses of cancer patients. Yet findings across different studies often present contradictions in their specific impacts. The prevailing trend in current research suggests an association with a poor prognosis, acknowledging that specific subtypes and co-mutations may further contribute to varied outcomes.

1.5.2 Mutations co-existing with oncogenic KRAS

Diverse mutations patterns and co-mutations impacting KRAS function in cancer.

Beyond the varying levels and subtypes of mutations observed in different cancer tissues, KRAS mutations exhibit diverse co-mutation patterns that can influence KRAS function and contribution to the initiation and progression of tumours. The co-existence of genomic aberrations in oncogenic drivers and tumour suppressor genes has become a fundamental principle shaping molecular diversity in non-small lung cancer (NSCLC). This intricate co-mutation landscape is integral to understanding processes such as tumorigenesis, metastasis, immune microenvironment dynamics, and therapeutic vulnerabilities (Skoulidis & Heymach, 2019). Alterations in STK11 and KEAP1 exhibit a higher frequency in KRAS-altered tumours compared to wild-type (WT) tumours, while driver alterations in various disease types generally demonstrate mutual exclusivity with KRAS. Notably, an increased occurrence of co-alterations in MAPK/PI3K pathway genes is observed in KRAS G13D-mutated CRC and

endometrial cancers compared to G12D-mutated tumours (Lee et al., 2022). This finding further suggests that KRAS G13D-mutated tumours may manifest distinct biochemical and clinical mechanisms (Johnson et al., 2019). The variable responses to KRAS inhibitors in NSCLC, CRC and other solid tumours underscore the necessity for understanding the diverse genomic landscape of KRAS mutant cancers, both before treatment initiation and upon acquired resistance to therapies. As will be explained in the next section, ongoing combination trials involving KRAS, and other MAPK pathway (SHP2/MEK/ERK) inhibitors aim to enhance outcomes in patients with KRAS-mutated cancers, leveraging the presence of targetable co-alterations. Specifically, in NSCLC and other solid tumours, several KRAS G12C inhibitors are being evaluated in combination with immune checkpoint inhibitors (ICIs), SHP2 inhibitors, EGFR inhibitors and Bevacizumab (the vascular endothelial growth factors (VEGF) inhibitor (Leonard et al., 1997)) in clinical trials (Palma et al., 2021). Encouraging preliminary results have been reported in CRC trials exploring KRAS G12C inhibitors combined with anti-EGFR therapies, such as the combination of Adagrasib and Cetuximab, which demonstrated a 100% disease control rate (Weiss et al., 2021). The investigation of co-alterations in programmed death-ligand 1 (PD-L1) expression and mutational signatures, as prognostic and predictive markers for targeted therapies and immunotherapies in NSCLC and other KRAS-mutant tumour types, is a crucial area for future research. In the context of KRAS-driven lung adenocarcinoma (LUADs), intrinsic heterogeneity is evident, leading to classification into three predominant subgroups characterised by co-mutations in TP53, STK11 and CDKN2A/B (Skoulidis et al., 2015). Notably, KRAS/TP53 co-mutations correlate with an inflamed immune microenvironment and heightened tumoral PD-L1 expression (Jiao et al., 2020; Skoulidis et al., 2015). Conversely, LAUDs with KRAS/STK11 co-mutations exhibit an “immune-inert” profile, featuring fewer tumour-infiltrating T cells and lower PD-L1 expression (Jiao et al., 2020; Skoulidis et al., 2015, 2018). Furthermore, the characterisation of tumours with KRAS/STK11 co-mutation reveals a tumour microenvironment (TME) marked by a deficient immune response, notably deficient in CD8+ tumour-infiltrating lymphocytes while exhibiting an abundance of T regulatory cells. Conversely, in the TME associated with KRAS/TP53 co-mutation, there is a prevalence of CD8+ tumour-infiltrating lymphocytes and activated dendritic cells, with a notable scarcity of T regulatory cells (Bange et al., 2019). Clinical observations have also substantiated that patients harbouring ALK or EGFR/KRAS co-mutations exhibit poor responses to tyrosine kinase inhibitor therapy (Schmid et al., 2017). These intricate associations between co-mutation patterns and the immune landscape shed light on the potential challenges and opportunities in tailoring therapeutic strategies based on the specific genetic

context of NSCLC. The contrasting immune-related characteristics resulting from the different co-occurring mutations in KRAS-LAUDs underscore the significant impact of these interactions. This emphasizes the potential for enhancing prediction algorithms for cancer immunotherapy through a comprehensive understanding of co-mutation dynamics in NSCLC. The identification of these distinct immune profiles emphasizes the need for personalised approaches to treatment based on the intricate genomic makeup of individual tumours.

1.5.3 KRAS mutations and inflammatory tumour microenvironment (TME)

The tumour microenvironment (TME) is a dynamic network comprising not only tumour cells but also various non-tumour cell types, including stromal cells such as immune cells (macrophages, neutrophils, dendritic and natural killer cells, myeloid-derived suppressor cells (MDSCs), B and T cells), fibroblasts, adipocytes, endothelial cells, neurons, osteoblasts, osteoclasts, and the extracellular matrix (ECM). This non-cellular component, along with tumour and non-tumour cells forms a dynamic and challenging microenvironment that can be modulated and, in turn, modulates cancer cell activities, significantly influencing tumour progression (Figure 12) (Hamarsheh et al., 2020).

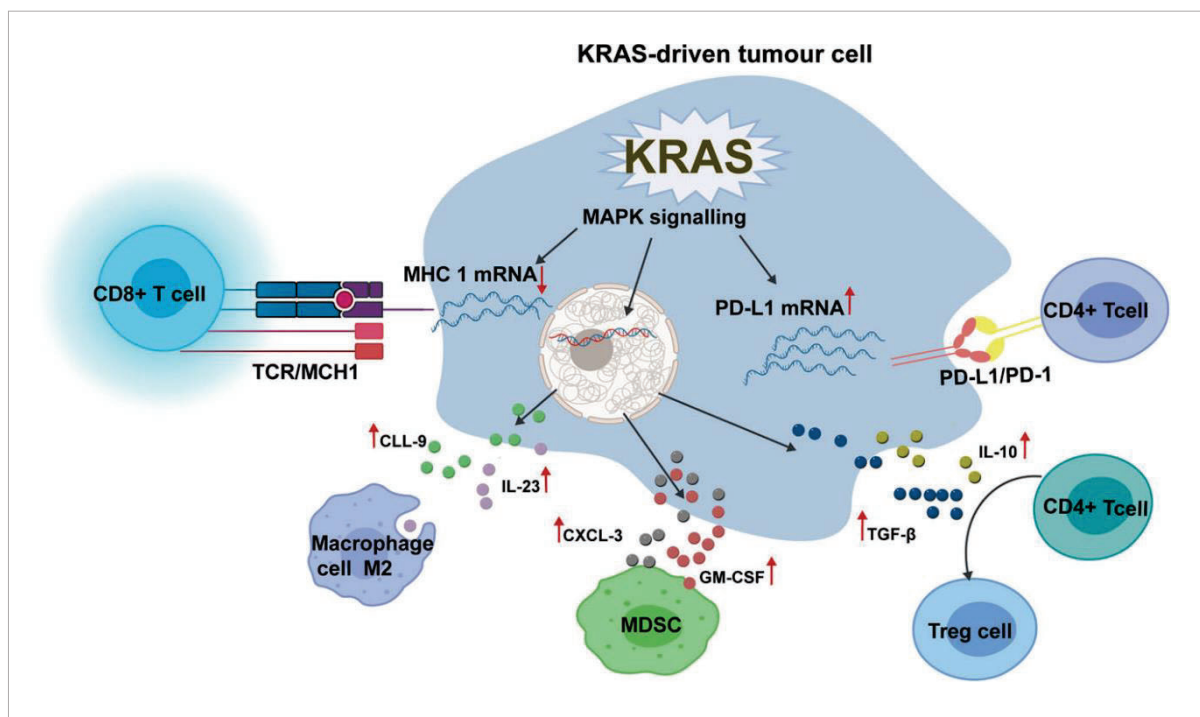


Figure 12: KRAS-driven immune evasion in the tumour microenvironment. *Extracted from (L. Huang et al., 2021)*

KRAS mutations have been closely linked to the modulation of tumour inflammation, increasingly recognised as a key contributor to tumorigenesis by impacting the immune response and treatment efficacy (M.-J. Tsai et al., 2014). Therefore, it is crucial to investigate how cancer cells harbouring oncogenic KRAS mutations may initiate the inflammatory TME, leading to chronic inflammation and stroma remodelling (H. Cheng et al., 2019).

Remarkably, the concept of tumour-promoting inflammation is closely linked to KRAS mutation (Hamarsheh et al., 2020). Notably, in CRC, instances with a high prevalence of KRAS mutations often coincide with chronic inflammatory conditions (Fu et al., 2020). KRAS, along with its downstream interactors, is recognised for its ability to shape the immune microenvironment by triggering NF- κ B signalling. This, in turn, leads to the transcriptional activation of various cytokines and chemokines, including interleukin (IL)-1b, IL-6, tumour activation factor- α (TNF- α), Cys-X-Cys chemokine (CXCL)-1,2,5, and 8, monocyte chemoattractant protein 1 (MCP-1 or CCL2), inducible nitric oxide synthase (iNOS), intracellular adhesion molecule 1 (ICAM-1), and endothelial leukocyte adhesion molecule 1 (ELAM1) (Cullis et al., 2018). In addition to NF- κ B, downstream partners like RAF/MAPK and PI3K may also independently induce the expression of IL-10, transforming growth factor- β (TGF- β), and granulocyte-macrophage colony-stimulating factor (GM-CSF) (Cullis et al., 2018).

Paradoxically, tumours with KRAS mutations are also linked to an immunosuppressive and anti-inflammatory microenvironment, as highlighted by numerous studies demonstrating that KRAS mutations are associated with the release of anti-inflammatory cytokines like IL-10 and TGF- β . This contributes the maintenance of an immunosuppressive TME. However, while ICAM-1 and IL-18 have commonly been associated with pro-inflammatory roles, IL-6 has been reported to exert an anti-inflammatory function in the context of KRAS mutations (Caetano et al., 2016). Studies using the CRC cell line C26 demonstrated that KRAS knockdown led to upregulation and secretion of IL-18 into the medium. The inhibition of C26 tumour growth in the liver was attributed to the production of IL-18 by hepatocytes, suggesting that KRAS-G12D mutation may suppress IL-18 chemokine production, potentially aiding evasion of the local immune system during tumour development (Smakman et al., 2005). While there are no reported findings regarding the pro-inflammatory functions mediated by KRAS in lung cancer, existing research underscores its versatile role in shaping the immune microenvironment across various cancer types. In colon cancer, KRAS- G12V mutants are reported to facilitate the differentiation of pro-inflammatory T cells into immunosuppressive T regulatory cells

(Tregs), promoting their infiltration in a KRAS-driven lung tumorigenesis mouse model (H. Cheng et al., 2019).

In pancreatic cells, oncogenic mutant KRAS-transfected normal acinar cells express elevated levels of ICAM-1, which is subsequently converted into a soluble form known as sICAM-1 (Storz, 2015). This sICAM-1 acts as a chemoattractant for pro-inflammatory M1-like macrophages, but not for anti-inflammatory M2-like macrophages. The attracted pro-inflammatory macrophages engage directly with acinar cells, providing enzymes for ECM degradation and releasing inflammatory cytokines and chemokines, such as TNF- α . This process is implicated in contributing to acinar cell metaplasia and initiating precancer lesions, ultimately progressing to pancreatic cancer (G. Liu et al., 2014; Storz, 2015). Moreover, in pancreatic cancer, it has also been reported that the effects of KRAS mutations could be mediated through exosomes. Exosomes containing KRAS-G12D, released by dead, dying, or stressed cells, such as cancer cells, are taken up by macrophages through an AGR (advanced glycosylation end product-specific receptor)-dependent mechanism. This process leads to the differentiation of macrophages into an M2-like pro-tumour/anti-inflammatory phenotype, facilitated by the signal transducer and activator of transcription 3 (STAT3)-dependent fatty acid oxidation mechanism (Jiang et al., 2015). KRAS mutations also influence the TME through IL-18, an inflammatory cytokine. Additionally, pancreatic cancer cells with KRAS-G12D mutations secrete high levels of anti-inflammatory mediators TGF- β and IL-10, crucial chemokines for maintaining an immunosuppressive environment and facilitating cancer cell immune escape (H. Cheng et al., 2019). IL-10 is well-known for inhibiting T cell activation, while TGF- β inhibits T cell activation and proliferation and promotes epithelial-to-mesenchymal transition, favouring cancer cell migration and invasion. Moreover, the released IL-10 and TGF- β by pancreatic cancer cells suppress the cytotoxic activity of CD8⁺ T cells (H. Cheng et al., 2019).

In lung cancer, KRAS mutations, particularly the KRAS-G12D mutation, are associated with elevated levels of Treg infiltration. This mutation induces apoptosis in CD3⁺ T cells and hinders the activation of cytotoxic CD8⁺ T cells (H. Cheng et al., 2019).

The influence of KRAS mutation on tumour immune evasion and progression is evident, yet their potential contribution to therapeutic efficacy remains ripe for further exploration in the near future. To this end, comprehensive investigations into the interplay between KRAS mutation and therapeutic response are essential for advancing and improving treatment outcomes.

1.6 KRAS inhibition

KRAS has been extensively validated as therapeutic target in CRC, in lung and pancreatic cancers. Targeting oncogenic KRAS has been always a central goal (as explained in Figure 13), but it is not until recently that all these efforts started to be fruitful.

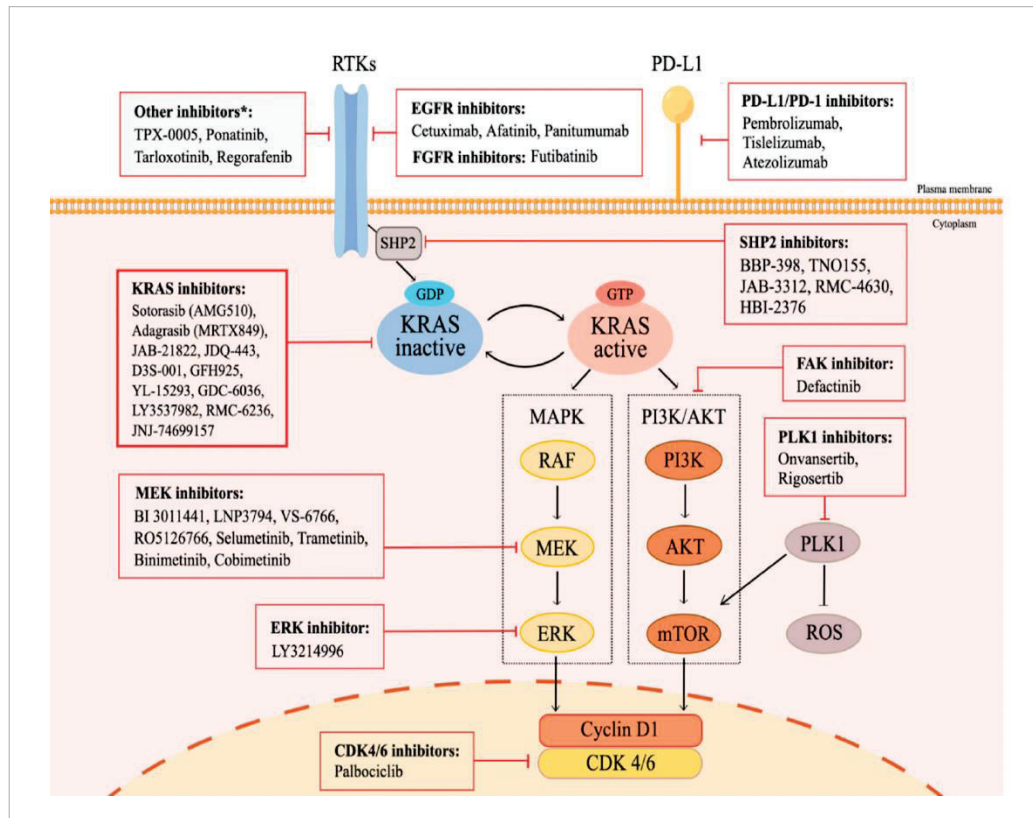


Figure 13: Potential targeting strategies developed against of oncogenic KRAS. Adapted from (Y. Yang et al., 2023b)

Oncogenic KRAS activates proliferative signalling pathways downstream and independently of EGFR stimulation (Bellio et al., 2021). For this reason, despite the specificity and the effectivity of therapies targeting EGFR (ex.: specific antibodies), it is not surprising that oncogenic KRAS mutations serve as a predictive factor for the inefficacy of therapies directed against the EGFR.

1.6.1 Indirect strategies of targeting KRAS

The main strategies to indirectly minimize oncogenic KRAS activity developed so far include: (i) addressing KRAS post-translational modifications; (ii) targeting synthetic lethal interactors of KRAS; (iii)

inhibiting KRAS plasma membrane association; (iv) blocking downstream signalling pathways; and (v) exploring immunotherapy (Dias Carvalho et al., 2019a; Zeitouni et al., 2016).

Targeting post-translational modifications of KRAS

RAS proteins undergo a continuous series of post-translational modifications, as previously discussed, some of them regulating their attachment to the plasma membrane and subcellular localisation. These processes in turn, modulate the activity and oncogenic capacity of KRAS and consequently, each step of the “maturation” of the KRAS protein represents a potential target for therapy.

Farnesylation, functioning as a prerequisite for subsequent modifications, has been a focus of intense research for anti-KRAS therapy (Kato et al., 1992). Inhibiting farnesylation can be achieved through two approaches: one involves using mimetic polypeptides of the CAAX motif to compete with KRAS for the enzyme farnesyl transferase (FTase), and the other utilises an analogy of farnesyl pyrophosphate (FPP) involved in the farnesylation reaction to compete for binding FTase (Basso et al., 2006). Peptides or small molecule inhibitors used to impair FTase’s catalytic activity during KRAS farnesylation are collectively termed farnesyltransferase inhibitors (FTIs). But, when FTIs were proved, cells reacted with the addition of a geranylgeranyl group by GGTase-I in KRAS (as a prenyl group) resulting in a failure of the clinical trials with FTIs. This finding supported the notion of combining FTIs with GGTIs to effectively inhibit KRAS prenylation.

Following prenylation, KRAS proteins undergo postprenylation processes involving RCE1 and ICMT, which mediate proteolysis and methylation. Since both farnesylated and geranylgeranylated KRAS undergo these postprenylation processes, concerns about selectivity may be less pronounced. Targeting prenylated KRAS can be achieved by inhibiting RCE1 and ICMT (Winter-Vann & Casey, 2005). Notably, deletion of RCE1 in a mouse model resulted in incorrect cellular localisation of the KRAS protein. However, the reduction of KRAS driven fibroblast transformation with conditional elimination of RCE1 was relatively small compared to FTIs treatment (Bergo et al., 2008).

Inhibition of other post-translational modifications of KRAS such as acetylation, ubiquitination, or phosphorylation, has not undergone extensive pre-clinical or clinical studies.

Targeting KRAS effector pathways

Given their pivotal role in mediating the proliferation, survival, and metabolic effects of the KRAS oncogene, considerable attention has been focused on the MAPK and PI3K pathways. Inhibitors targeting MEK and ERK kinases downstream in the MAPK pathway have demonstrated success in impeding MAPK pathway signalling. The efficacy of various targeted inhibitors in disrupting this pathway has been explored. Notably, the MEK1/2 inhibitors Trametinib (GSK1120212), Selumetinib (AZD6244) and RDEA119 have proven effective in preventing MEK activation (Gilmartin et al., 2011; Iverson et al., 2009; Yeh et al., 2007). While these targeted drugs effectively block the phosphorylation of MEK by RAF, MEK inhibition unexpectedly impacts the activation of other RAS signalling arms, particularly PI3K (Hoeflich et al., 2009; Mirzoeva et al., 2009; Sos et al., 2009). Interestingly, targeting ERK may present a viable therapeutic strategy, especially for malignancies resistant to MEK inhibition. Notably, SCH772985 and BVD-523 are effective ERK1/2 inhibitors. But responsive cells treated with SCH772985 exhibited elevated levels of P-MEK and P-AKT (Hatzivassiliou et al., 2012). Several inhibitors targeting PI3K, AKT, and mTOR have been developed to impede the PI3K pathway. Despite the promising anti-tumour effects observed in preclinical models of KRAS mutant cancers, MAPK and PI3K pathway inhibitors have not demonstrated significant therapeutic benefits in patients with KRAS mutant tumours, especially in pancreatic cancer (C.-S. Lee et al., 2019; T. L. Yuan et al., 2018). One explanation is that because KRAS interacts with numerous effector pathways, blocking only one or two of them is insufficient to halt its carcinogenic activity. Interestingly, SCH772985 (ERK1/2 inhibitor) in combination with the PI3K inhibitor AZD8186, synergistically enhanced the growth inhibitory effects and prevented AKT activation (Hatzivassiliou et al., 2012). Another argument is that effector pathway inhibitors possess a smaller therapeutic window, limiting the administration of higher doses due to on-target toxicity in normal tissue. Thirdly, KRAS mutant tumours even those originating from the same tissue, may vary in their sensitivity to the inhibition of specific RAS effector pathways. This variability is attributed to the heterogenous and context-dependent manner in which mutant KRAS utilizes effector pathways in cancer (C.-S. Lee et al., 2019; T. L. Yuan et al., 2018). Collectively, these studies emphasize that achieving a lasting impact on tumour growth involves targeting various RAS signalling pathways.

KRAS synthetic lethal inhibition and collateral dependence partners

Synthetic lethal partners of the KRAS oncogene exhibit highly effective interactions in RAS mutant cancer cells. The specific suppression of these synthetic lethal partners in KRAS mutant cells induces targeted toxicity. Many of the genes identified as synthetically lethal through RNAi and CRISPR-based genetic screens represent druggable targets (Aguirre & Hahn, 2018). Two noteworthy themes have surfaced from these investigations. Firstly, synthetically lethal interactions with KRAS frequently rely on the cellular environment and mirror the inherent genetic heterogeneity of cancer cell lines. Consequently, a particular synthetic lethality interaction is often observed only in a subset of KRAS mutant cancer cell lines. In general, blocking these pathways increases the susceptibility of KRAS mutant cells to oncogenic stress, reducing their viability (Luo et al., 2009). A study has identified the mitochondrial cation channel proteins VDAC2/3, which are not directly associated with RAS signalling but serve as targets for the compound Erastin, selectively inducing cell death in RAS mutant cells. Thus, inhibiting these proteins constitutes a form of synthetic lethality with the RAS oncogene (Yagoda et al., 2007).

These partners have a valuable roadmap for clinical studies exploring combinations of medications in KRAS mutant tumours.

Immunotherapy and combined therapeutic approaches in KRAS mutated cancers

Immunotherapy directed at immune checkpoint molecules, including PD-1, PD-L1 and CTLA-4, has emerged as a highly promising strategy in cancer treatment, exhibiting encouraging outcomes in KRAS mutated cancers (Dias Carvalho et al., 2019b; Uras et al., 2020). Particularly, for individuals with advanced-stage NSCLC, monoclonal antibodies targeting PD-1 and its primary ligand PD-L1 demonstrated notable survival benefits, highlighting the advantageous clinical prospects of anti-PD-1/PD-L1 immunotherapy (Figure 14) (C. Liu et al., 2020). In the context of CRC, anti-PD-1/PD-L1 therapy, exemplified by Pembrolizumab, has gained approval for a specific patient subset, notably those with mismatch repair deficient tumours characterised by heightened PD-L1 expression compared to mismatch repair proficient carcinoma (S. Liu et al., 2018; Uras et al., 2020). In pancreatic cancer, the clinical success of these immunotherapies has been constrained, resulting in their exclusion from the current clinical guidelines for this malignancy (Dias Carvalho et al., 2019a). Furthermore, it has been established that not all KRAS mutations confer benefits from immunotherapy, revealing divergences in immunotherapy efficacy among distinct KRAS mutant subtypes, particularly the KRAS

G12D mutation (Gao et al., 2020). While these findings may appear disheartening, the intricate impact of KRAS mutations on the TME could offer insights into the inefficacy of immunotherapy treatments. Therefore, delving into the influence of KRAS mutations on the TME could provide a fresh perspective on combined therapeutic strategies to surmount the therapeutic inefficiency and/or resistance associated with KRAS mutations.

Encouragingly, innovative strategies have been proposed to address acquired resistance and/or ineffectiveness, focusing on targeting both oncogenic signalling pathways and the microenvironment (Dias Carvalho et al., 2019a). Despite occasional limited clinical relevance, the exploration, in a murine KRAS-mutant CRC model, of combined therapies involving MEK inhibitors with antibodies targeting PD-1, PD-L1 or CTLA-4 has shown higher anti-tumour effects compared to monotherapy (Poon et al., 2017). The MEK inhibitor Selumetinib demonstrated the ability to attenuate anti-CTLA-4-mediated-T-cell activation and infiltration into tumours. Specifically, Selumetinib reduced CD11b⁺ Ly6G⁺ tumour-infiltrating neutrophils or Granulocytic-Myeloid-derived suppressor cells (gMDSC) and hindered monocyte differentiation into anti-inflammatory macrophages. MEK inhibitors were also observed to reverse the anti-CTLA-4-mediated induction of two key immunosuppressive factors, Arg1 and cyclooxygenase-2 (Cox-2) (Poon et al., 2017). Therefore, MEK inhibition, particularly with Selumetinib, confers beneficial effects to the TME in the context of CTLA-4 blockade (Poon et al., 2017). The combination of MEK inhibitors with CTLA-4 blocking antibodies effectively re-educates the TME, transforming it from an immunosuppressive to an immune-alert status and expanding the scope of therapeutic intervention (Figure 14) (Poon et al., 2017).

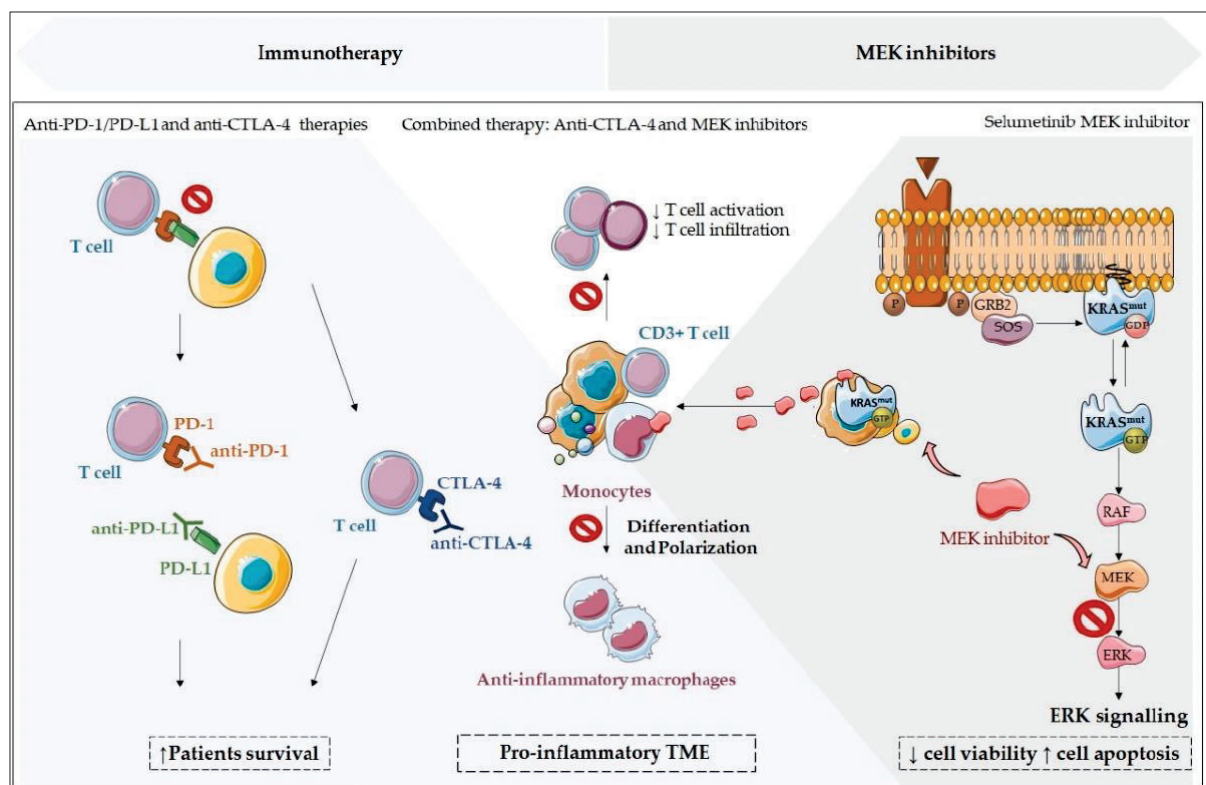


Figure 14: A comprehensive therapeutic strategy for cancers with KRAS mutations involves combining immunotherapy and MEK inhibitors. Adapted from (Pereira et al., 2022).

1.6.2 Direct strategies of targeting KRAS

Directly targeting KRAS has proven challenging due to the unique features of its molecular structure. Despite these challenges, the strategy to target KRAS directly remains an active area of investigation, with various approaches being explored.

Targeting the formation of the KRAS-GTP complex

In this strategy, competing GTP analogues were designed to compete for nucleotide binding to RAS. However, the effectiveness of these analogues in inhibiting KRAS activation was lower than anticipated, attributed to the high affinity of GTP to KRAS and elevated cellular GTP concentrations (Becher et al., 2013). An alternative strategy to impede KRAS-GTP complex formation is to inhibit the interaction of KRAS with GEFs. Among these, SOS1 is a well-known GEF, leading to the synthesis of SOS1 inhibitors to disrupt the KRAS-SOS1 interaction. Studies have demonstrated that these inhibitors suppress SOS1-mediated nucleotide exchange, thereby inhibiting RAS activation. This, in turn results

in the inhibition of cell proliferation and the downregulation of RAS signalling (Hillig et al., 2019). However, the binding activity of these inhibitors to KRAS is relatively weak, and it remains uncertain whether the inhibitors exert similar effects in the context of KRAS mutations (Maurer et al., 2012).

Disruptors of protein-protein interactions between KRAS and RAS effectors

Inhibiting KRAS's enzymatic function, specifically hydrolysing GTP to GDP, would counterproductively impede the transition from its on to off state, thus undermining the interruption of heightened signalling in the cancer setting. Instead, some KRAS inhibitors operate by disrupting the protein-protein Interaction (PPI) between KRAS and its downstream effectors, with RAF being extensively studied in this context. PPI inhibitors function by binding to the surface of one protein and competitively hindering the binding of the natural partner protein.

Specifically, the majority of KRAS-targeted inhibitors acting in the RAS/MAPK pathway bind to a cryptic pocket beneath the switch-II loop, rendering KRAS incapable of binding to RAF (J. M. Ostrem et al., 2013), and consequently disrupting downstream signalling. Notably, recent research by Hallin et al. emphasizes that this inhibitory effect is independent of the nucleotide state (Hallin et al., 2022). For example, the KRAS-G12D-targeted binder, MRTX1133, exhibits the ability to bind KRAS-G12D in both the GTP-bound and GDP-bound states, with X-ray crystal structures confirming the perturbation of the switch-II loop even in the GTP-bound state, rendering it incapable of binding RAF (Figure 15).

A distinct class of compounds operates differently by binding to the protein's exterior, akin to traditional PPI inhibitors. These compounds impede the binding of KRAS effector proteins. Specifically, they target a pocket situated between switch-I and switch-II loops on RAS. One of the earliest mentions of this class emerged from scientists at Genentech, who demonstrated the indole fragment's capability to bind KRAS, thereby obstructing SOS1 binding and concurrent nucleotide exchange (Maurer et al., 2012). In a SOS1 nucleotide exchange assay, the compound exhibited an IC₅₀ of 342 μM. Concurrently, the Fesik laboratory, during the same timeframe, identified several fragment-size compounds with binding affinity for multiple KRAS mutants, including G12D, G12V, and wild-type (Sun et al., 2012). A collaborative effort between the Fesik group and Boehringer Ingelheim subsequently resulted in the discovery of BI-2852. This compound demonstrated the disruption of KRAS binding to SOS1 nucleotide-exchange site, SOS1 allosteric activation site, C-RAF, and PI3K, with IC₅₀ ranging from 100 to 770 nM across KRAS-G12D and KRAS-G12C and KRAS WT. The authors observed that BI-2852 could inhibit P-ERK, P-AKT, and proliferation in cellular assays in a dose-dependent manner.

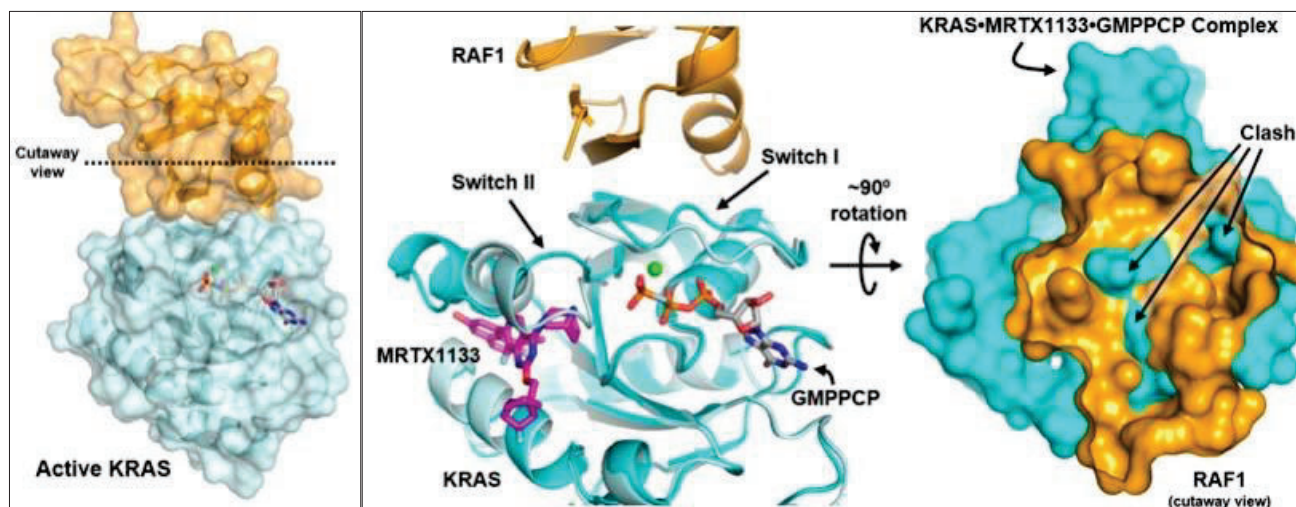


Figure 15: On the left, the X-ray crystal structure (PDB: 6VJJ) showcases the RAS binding domain of CRAF (depicted in orange) intricately bound with GMPPNP-KRAS (light blue), with GMPPNP serving as an analogue of GTP. In the middle, the structure of KRASG12D-MRTX1133-GMPPCP (PDB: 7T47, depicted in a cyan ribbon) is superimposed onto the KRAS-GMPPNP-RAF1 complex (depicted with light blue and orange ribbons). Here, GMPPCP also acts as an analogue of GTP. On the right, the KRAS-CRAF complex is rotated by 90 degrees, and a sectional view reveals clashes with the surface of KRAS-G12D-MRTX1133-GMPPCP depicted in cyan. *Adapted from* (Harwood et al., 2023).

Successfully targeting KRAS G12C

Small-molecule inhibitors were designed to directly target the G12C variant of KRAS in a conformation-specific manner (Xue et al., 2020). Distinct from other KRAS alleles like G12D and G12V, KRAS-G12C despite having an increased interaction with downstream effectors, maintains an active cycling between a GDP-bound and a GTP-bound state (Hunter et al., 2015). Targeting cysteine residues on KRAS-G12C can immobilize it in an inactive conformation, preventing reactivation by nucleotide exchange, interrupting the cycling phenomenon, and disrupting downstream signals (Xue et al., 2020). Following the successful proof-of-concept demonstration, ARS-853 emerged as a selective, covalent KRAS-G12C inhibitor and, at the time of its characterization, stood out as the first direct KRAS inhibitor with cellular potency in the range of a drug candidate (Patricelli et al., 2016). However, ARS-853 faced challenges related to poor bioavailability (Goebel et al., 2020). The inaugural direct KRAS-G12C inhibitor to progress into clinical trials was Amgen's Sotorasib, formerly known as AMG510. Later, Mirati Pharmaceuticals introduced Adagrasib, formerly known as MRTX849, as another covalent and

potent KRAS-G12C inhibitor. Additional promising KRAS-G12C allele-specific inhibitors, with potential therapeutic effects, include ARS-1620, SML-8–73–1, and ASP2453 (Goebel et al., 2020; Hallin et al., 2020; Nakayama et al., 2022; Patricelli et al., 2016).

Sotorasib (AMG510)

Sotorasib, a pioneering and selective KRAS inhibitor developed by Amgen, represents a first-in-class therapeutic agent (Blair, 2021). Specifically designed for the G12C mutant form of the protein, Sotorasib specifically and irreversibly binds to Cys12 in the inducible switch-II pocket and locks KRAS-G12C protein in an inactive status (Canon et al., 2019). Preclinical studies demonstrated its efficacy in inducing regression of KRAS- G12C tumours. Notably, it exhibited synergistic effects when combined with chemotherapy and other targeted agents, particularly the MEK inhibitor Trametinib (Canon et al., 2019). Sotorasib was found to induce a proinflammatory environment, either alone or in combination with immune checkpoint inhibitors targeting PD-1. This observation prompted further investigation through in-human studies, focusing on these combinations (Canon et al., 2019). In 2019, Fakih et al. reported outcomes of a phase I trial assessing the safety, tolerability, and efficacy of Sotorasib in adults with locally advanced or metastatic KRAS- G12C mutant solid tumour.

Adagrasib (MRTX849)

Adagrasib emerged as the second approved KRAS inhibitor following the path paved by Sotorasib (S. Dhillon, 2023). The continuous clinical investigation of MRTX849 presents a promising avenue for the effective targeting of KRAS-G12C proteins (Fell et al., 2020). On a conceptual level, MRTX849 boasts theoretical advantages, including a prolonged half-life (23h), dose-dependent pharmacokinetics, and penetration into the central nervous system (CNS) (Sabari et al., 2022). In December 2022, it received approval for adult patients with KRAS-G12C-mutated locally advanced or metastatic NSCLC based on encouraging results from the NSCLC cohort in the registrational study KRYSTAL-1 (S. Dhillon, 2023; Jänne et al., 2022). KRYSTAL-1, a multicohort phase I/II study, explored Adagrasib as monotherapy or in combination regimens for patients with advanced solid tumours harbouring a KRAS-G12C mutation. The ongoing phase III trial KRYSTAL-10 (NCT04793958) investigates Adagrasib with Cetuximab versus standard fluoropyrimidine-based chemotherapy in second-line metastatic KRAS-G12C-mutated colon cancer.

1.7 Allosteric regulatory sites in KRAS potentially accelerate drug development

As mentioned before, KRAS has been identified as an oncoprotein four decades ago (Tsuchida et al., 1982), with tens of thousands of scientific publications and over three hundred published structures of KRAS (Parker et al., 2022), the approval of clinical inhibitors for KRAS has only recently been achieved. The development of atlases highlighting allosteric sites holds the potential to significantly expedite drug discovery, particularly for proteins deemed “undruggable” due to the absence of an appropriate active site or their alliance on challenging to inhibit protein-protein interaction interfaces. Allosteric drugs, among their various advantages, often exhibit higher specificity compared to orthosteric drugs targeting conserved active sites (Changeux, 2013; J. Liu & Nussinov, 2016).

Focusing on residues where multiple mutations exert substantial allosteric effects, major allosteric sites were defined as those where the mean absolute change in binding free energy with the interaction partners upon mutation, equal or exceeds that in the binding interface (Weng et al., 2023). This approach identified a total of 18 major allosteric sites, with 10 located within the physiological allosteric site-the nucleotide binding pocket (Weng et al., 2023). The remaining 8 major allosteric sites encompass residues Val7, Gly10, Asp54, Thr58, Ala59, Pro110, Phe141, and Ile163. Additionally, KRAS exhibits four active surface pockets (including the effector binding domains) influenced by different mutations in its surface residues, as described below:

Pocket 1, also known as the switch I/II pocket, is situated behind switch II, positioned between the central β sheet and a helix 2. This pocket serves as the binding site for numerous inhibitors that have shown efficacy in pre-clinical models (Kessler et al., 2019; J. M. L. Ostrem & Shokat, 2016). The allosteric impact of mutations in pocket 1 is observed in 10 residues, aligning with the demonstrated ability of engaging pocket 1 to inhibit effector binding (Weng et al., 2023).

Pocket 2, also referred to as the switch II pocket, is positioned between switch II and a helix 3, serving as the binding site for Sotorasib (Canon et al., 2019). Allosteric inhibition of CRAF binding is observed in 9 residues affected by mutations that contact Sotorasib. Consequently, mutations and small molecules binding to pocket 1 and pocket 2 demonstrate the ability to allosterically inhibit KRAS activity (Weng et al., 2023).

Pocket 3 in KRAS is situated in the C-terminal lobe of the protein, representing the most distant pocket from the CRAF binding interface. While the effects of pocket 3 engagement have not been extensively documented (Grant et al., 2011), and this pocket has garnered limited attention for therapeutic

development (J. M. L. Ostrem & Shokat, 2016), recent insights revealed that pocket 3 is allosterically active, with 20 mutations identified in 6 residues within pocket 3 that inhibit KRAS binding to CRAF (Weng et al., 2023). Despite its spatial separation from the effector binding interface, a study underscores the importance of prioritising pocket 3 as a site for the development of KRAS inhibitors (Weng et al., 2023).

Lastly, pocket 4, situated immediately behind the flexible effector binding loop, encompasses 105 allosteric mutations distributed across 9 residues that do not directly contact CRAF.

All four surfaces' pockets of KRAS have been confirmed as allosterically active, with significant inhibitory effects on CRAF binding, observed following perturbations in all pockets (Weng et al., 2023). This compelling evidence supports the rationale for developing molecules that target all four pockets as potential KRAS inhibitors.

2. HYPOTHESIS AND OBJECTIVES

Our **hypothesis** inclusively posits that a promising avenue for combating oncogenic KRAS involves the targeted interaction with either the effector binding domain or the allosteric region of KRAS. By selectively binding to these regions, novel compounds, a peptidomimetic (P1.3) and a small molecule (P14B) have the potential to modulate the interaction between KRAS and effector or non-effector proteins, respectively, ultimately triggering apoptotic pathways leading to cell death. Through a comprehensive understanding of the mechanisms by which these compounds operate, we anticipate the refinement of therapeutic approaches and the development of enhanced treatment strategies. This deeper insight is crucial for optimizing clinical trial outcomes and ultimately improving patient prognosis.

Peptidomimetics binding to the effector domain of KRAS.

The **objectives** of this project are the following:

1. Building upon the experimental findings from P1.3 treatment of cells concerning KRAS downstream signalling and the binding dynamics between KRAS and its main effectors, CRAF and PI3K, our objective is to investigate the direct interaction between P1.3 and KRAS-GTP, and specifically, we aim to discern whether treatment with P1.3 influences the levels of KRAS-GTP.
2. To assess the toxicity profile of P1.3 through experimentation involving athymic mice. This investigation will provide valuable insights into the safety and tolerability of P1.3 in an *in vivo* model system.

Small compounds binding to the allosteric domain of KRAS.

The **objectives** of this project encompass a comprehensive investigation into the effects of P14 and its derivatives in both Colorectal Cancer (CRC) cells and Pancreatic Ductal Adenocarcinoma (PDAC) cells.

To achieve this, we delineate the following steps:

1. Exploration of P14 and P14B effects in cultured cell lines:
 - a. Assess the impact of P14 and P14B treatment on KRAS downstream signalling in CRC and PDAC cells.
 - b. Investigate the effects of various P14 derivatives (P14A, P14B, P14C, P14D, P14E, P14F, P14G, P14H, and P14I) in CRC cells.
 - c. Examine the differential influence of P14B on KRAS downstream signalling in cell lines with wild-type KRAS compared to those with oncogenic KRAS.

- d. Analyse the impact of P14B on the binding affinity between oncogenic KRAS and its main effectors: CRAF, BRAF, and ARAF.
 - e. Study the effect of P14B on the survival of CRC cells growing in 2D or 3D (Matrigel and CRC patients-derived organoids).
2. Characterization of P14B Interactions *in vitro*:
- a. Conduct surface plasmon resonance analysis to elucidate the potential direct interaction of P14B with oncogenic KRAS.
 - b. Employ *in vitro* calmodulin (CaM)-pulldown assay to investigate the effect of P14B on the CaM binding to KRAS.
3. Determine the protein interactions of KRAS affected by P14B treatment utilizing the proximity-dependent biotinylation technology (UltraID).

3. MATERIALS AND METHODS

3.1 Antibodies.

Primary Antibody	Reference	Source	Dilution/concentration
AKT	Cell signalling 9272	Rabbit	1:1000
C-RAF	BD Transduction 610151	Mouse	1:500
B-RAF	Cell signalling 14814	Rabbit	1:1000
A-RAF	Cell signalling 75804	Rabbit	1:1000
Cleaved Caspase-3 (Asp175)	Cell signalling 9661	Rabbit	1:1000
KRAS	AbCam 196630	Rabbit	1:500
Pan-RAS	CalbioChem OP40	Mouse	0.3 µg/ml
MEK	Cell signalling 9122	Rabbit	1:1000
Phospho-MEK1/2 Ser221	Cell signalling 2338	Rabbit	1:2000
p44/42 MAPK (ERK1,2)	Cell signalling 9102	Rabbit	1:2000
Phospho-AKT Ser473	Cell signalling 4060	Rabbit	1:1000
Phospho-C-RAF Ser338	Cell signalling 9427	Rabbit	1:500
Phospho-p44/42 MAPK Thr202/Tyr204	Cell signalling 9101	Rabbit	1:2000
Phospho-MEK Ser221	Cell signalling 9121	Rabbit	1:1000
α-Tubulin	Sigma-Aldrich T9026	Mouse	1:2000
RAS GAP120	Santa Cruz sc-63	Mouse	1:1000
PI3K-p110α	Cell signalling 4249	Rabbit	1:1000
Myc-tag	Cell signalling 2276	Mouse	1:8000

Table 2. Primary antibodies: commercial companies, reference number, and the dilution used.

Table 3. Secondary antibodies: commercial companies, reference number, and the dilution used.

Secondary antibodies	Reference	Dilution
Anti-mouse IgG (H+L) HRP Conjugate	BioRad 170-6516	1:3000
Anti-Rabbit IgG (H+L) HRP Conjugate	BioRad 170-6515	1:3000
Alexa 488 anti-mouse green	Invitrogen A21202	1:500

3.2 Reagents and kits

Table 4. Reagents: manufacturer and reference number.

Reagent	Reference
Acrylamide/Bis-Acrylamide (37:1) 30% (w/v)	Bio Basic A0011
Aprotinin	Sigma-Aldrich A1153
Bovine Serum Albumin (BSA)	Sigma-Aldrich A7906
DAPI	Sigma-Aldrich AD9564
DH5a cells	Life technology 18265-017
DMEM high glucose	Biological industry 01-055-1A
DMSO	Sigma-Aldrich D2650
Dithiothreitol (DTT)	Sigma-Aldrich D0632
Epidermal Growth Factor (EGF)	Sigma-Aldrich E4127
Foetal Bovine Serum (FBS)	Biological Industries 04-007-1A
Folin-Ciocalteu	Merck 109001
F12(HAM's) Nutrient mixture	Biological Industries 01-0951A
HA-tag antibody crosslinked to agarose beads clone HA-7	Sigma-Aldrich A20956
Igepal CA-630 (Nonidet-P40)	Sigma-Aldrich I3021

Immobilon®-P transfer membranes	Merck Millipore IPVH00010
Leupeptin	Sigma-Aldrich CL-2884
L-Glutamine	Sigma-Aldrich G8540
Lipofectamine[®]2000 reagent	Invitrogen 11668-019
Matrigel	Corning 356237
MEM Non-Essential Amino Acids Solution	Biological industries 01-340-1
Mowiol	Sigma-Aldrich 81381
Paraformaldehyde (PFA)	Electron Microscopy Science 15710
Penicillin-streptomycin	Biological Industries AAL-107
Phenylmethylsulphonyl Fluoride (PMSF)	Sigma-Aldrich S6508
Ponceau	Sigma-Aldrich P7170
Precision Plus protein[™] Unstained Standards	BioRad 161-0363
Pyruvic Acid	Sigma-Aldrich P5280
Sodium fluoride	Sigma-Aldrich S7920
Sodium Orthovanadate	Sigma-Aldrich S6508
TEMED	Sigma-Aldrich S6508
Trypsin	Gibco 15400-054
Guanine Triphosphate (GTP)	Roche 10106399001
Dynabeads My One Streptavidin C1 Beads	ThermoFisher #65001
Triton X-100	Sigma-Aldrich 102532625
pSF-UltraID bacteria	Addgene #172878
Myc-BioID vector system	Addgene #35700
Biotin	Sigma #B4501

Tween[®] 20	Sigma-Aldrich P1379
IPTG	Sigma-Aldrich 16758-1G
Coomassie stain	Sigma-Aldrich B0770-25G
Glutathione-Sepharose[™] 48	Cytiva 17075601
CaM-Sepharose beads	Merck GE17-0529-01
Raf-1 RBD, agarose	Sigma-Aldrich 14-278
EGTA	Sigma-Aldrich E4378-25G
EDTA	Sigma-Aldrich E5134-1KG
HEPES	Promega GX12485
2-Mercaptoethanol	Sigma-Aldrich M3148-250ML

Table 5: Kits: manufacturer and reference number.

Kits	Reference
CellTiter 96[®] Aqueous One Solution Cell Proliferation Assay	Promega G3580
EZ-ECL (Enhanced chemiluminescence Detection Kit for HRP)	Biological Industries 20-500-120
Nucleo Bond[®]Xtra Midi	Macherey-Nagel 740410
High Purity Plasmid Miniprep kit	Neo Biotech NB-03-0001
MyFi DNAPol kit	Bioline BIO-21117
NucleoSpin Gel and PCR Clean-up kit	Macherey-NAGEL 740609.50
CM5 Series S Chip	Cytiva 29104988
Slide-A-Lyzer[™] Mini Dialysis Device	ThermoFisher 69588

3.3 Solutions and Buffers

Table 6: Solutions and buffers composition

Solution	Composition
Electrolyte buffer	25mM Tris-HCl pH8.3, 192mM glycine and 0.2% SDS
Laemmli Sample buffer 4X	30mM phosphate buffer, 30% glycerol, 7% SDS, 0.15% DTT, and 0.05 % Bromophenol blue.
Phosphate-Buffered Saline (PBS) 10X	145mM NaCl, 6mM Na ₂ HPO ₄ , 2.5 mM NaH ₂ PO ₄
PBS-T	0.05% Tween in PBS 1X
PBS cell culture	131 mM NaCl, 1.54 mM KH ₂ PO ₄ and 5.06 mM Na ₂ HPO ₄
Ponceau Protein Stain Solution	0.1% Ponceau reagent and 5% Acetic acid.
Ras Extraction Buffer (REB)	20 mM Tris-HCl pH 7.5, 2 mM EDTA, 100 mM NaCl, 5 mM MgCl ₂ , 1%Triton X-100 and 10% Glycerol
Sodium dodecyl sulphate (SDS) lysis buffer	2% SDS and 67 mM Tris-HCl (pH 6.8)
Gel preparation solutions	Solution 1: 0.75 M Tris-HCl pH 8.8 and 0.2% SDS.
	Solution 2: 30% acrylamide and 0.8% bis-acrylamide
	Solution 3: 0.25% Tris-HCl pH 6.8 and 0.2% SDS
Lowry assay solutions	Solution 1: 2% Na ₂ CO ₃ and 0.1 N NaOH
	Solution 2: 0.5% CuSO ₄
	Solution 3: 1% Sodium potassium tartrate
Tris Buffer Saline (TBS) 10X	50 mM Tris-HCl pH 7.5 and 150 mM NaCl.
TBS-T	0.05% Tween in TBS 1X
Transfer buffer	25 mM Tris-HCl pH 8.8, 192 mM glycine, 0.2% SDS and 20% Ethanol or Methanol.

CaM-pull down buffer		50mM Tris-HCl pH 7.5, 150mM NaCl, and 0.1% Triton X-100
Tissue extraction buffer (TEB)		20mM Tris pH 7.5, 2mM EDTA, 25mM NaCl, 5mM MgCl ₂ , 1mM DTT, and 0.1%SDS
Magnesium-containing lysis buffer (MLB)		25mM HEPES pH 7.5, 150mM NaCl, 1% Igepal, 0.25% sodium deoxycholate, 10% glycerol, 10mM MgCl ₂ , and 1mM EDTA
Solutions for protein purification from bacteria	Bacterial lysis buffer	50mM Tris HCl pH 7.5, 100mM NaCl, 1mM EDTA, 5mM MgCl ₂ , 10% glycerol, 1% triton X-100, and 0.5% B-mercaptoethanol
	Exchange buffer	20mM Tris HCl pH 7.5, 50mM NaCl, 5% glycerol, and 0.1% Triton X-100
	Dialysis buffer	10mM Tris HCl pH7.5, 150mM NaCl, 2mM MgCl ₂ , 10% glycerol, and 0.1mM DTT
Running buffer for Surface Plasmon Resonance assay (SPR)		NaCl 150 mM, Tris-HCl 50 mM (pH 7.6), and MgCl ₂ 2mM
Solutions for streptavidin pull down assay	Cell lysis buffer	50 mM Tris pH7.5, 500 mM NaCl, 0.2% SDS, and 1mM EDTA
	Wash buffer 1	2% SDS
	Wash budder 2	0.5% Triton X-100, 1mM EDTA, 500mM NaCl, and 50mM Tris pH 7.5
	Wash buffer 3	0.5% IPEGAL, 1mM EDTA, 50mM Tris pH 7.5

3.4 Cell culture

3.4.1 Cell lines and maintenance

DLD-1^{KRASWT/KRASG13D} (DLD-1): The DLD-1 cell line, initially isolated by D.L.Dexter *et al.* in 1977, serves as a valuable model for human colorectal adenocarcinoma research. These cells carry a unique genetic profile, with one wild type (WT) allele of KRAS and another allele harbouring a G13D mutation in KRAS. Notably, the DLD-1 cell line's tumorigenic properties are reliant on the expression of this oncogenic KRAS allele, particularly under serum-limiting conditions. In addition to the KRAS-G13D mutation, DLD-1 cells exhibit mutations in crucial colorectal cancer (CRC) genes. TP53 contains an S241F mutation, and PIK3CA carries both E54K and D549K mutations. These genetic alterations contribute to the cell line's cancerous characteristics. DLD-1 cells are further characterised as CMS1, a specific subtype within the CRC classification, and they display microsatellite instability (MSI), among other distinctive features. Horizon Discovery Ltd. is the source from which the DLD-1 cell line was originally obtained, making it a valuable resource for research in the field of oncology and cancer biology.

DLD-1^{KRASWT/-} (DLD-1 KO): The DLD-1 cell line features a heterozygous knockout of the mutant KRAS allele and was sourced from Horizon Discovery Ltd., specifically clone D-WT7 (#HD105-002). The acquisition details can be found at <http://www.horizondiscovery.com>. These DLD-1 knockout (KO) cells were engineered through the utilization of Horizon Discovery's proprietary adeno-associated virus (AAV) gene targeting technology, known as GENESIS. This advanced technology enabled the precise genetic modification of the cells to achieve the desired KRAS allele knockout, making them an invaluable resource for studies related to KRAS and cancer research.

DLD-1 S2-6: DLD-1 KO cells stably expressing HA-KRAS-G12V were previously established in our laboratory (Cabot et al., 2021).

MPANC-96: Human pancreatic tumour cell line derived from metastatic site of pancreatic ductal adenocarcinoma (PDAC). This cell line features a notable heterozygous KRAS-G12D mutation and exhibits a dependency on KRAS, especially under serum-limiting conditions.

HPAF-II: Human pancreatic tumour cell line derived from a metastatic site of PDAC. This cell line is distinguished by its heterozygous KRAS-G12D mutation and a significant reliance on KRAS, particularly evident under serum-limiting conditions.

PA-TU 8902: Human pancreatic tumour cell line originating from PDAC. Notably, this cell line carries a heterozygous KRAS-G12V mutation and display a substantial dependency on KRAS, particularly evident under serum-limiting conditions.

SW1990: Human pancreatic tumour cell line that was established from a metastatic site in the spleen, specifically originating from PDAC. This cell line carries a notable heterozygous KRAS-G12V mutation. Interestingly, it exhibits independence from KRAS, evident under low serum conditions.

PA-TU 8988-T: Human pancreatic tumour cell line that was derived from a metastatic site in the liver, specifically originating from PDAC. Notably, this cell line carries a significant heterozygous KRAS-G12V mutation. What sets it apart is its remarkable independence from KRAS, evident under low serum conditions.

PANC-1: Human pancreatic tumour cell line established from PDAC. Distinguishing this line is its heterozygous KRAS-G12D mutation. Notably, it demonstrates a remarkable independence from KRAS, evident under low serum conditions.

hTERT-RPE: Human retinal pigmented epithelial normal cell line immortalised with hTERT. It was obtained from American Type Culture Collection (ATCC).

PDAC cell lines were kindly provided by Prof. Dr. Kimmelman (Harvard Medical School, Boston USA). DLD-1, DLD-1 KO, DLD-1 S2-6, and hTERT-RPE cell lines were cultured in DMEM-HAM'S F12 (1:1) medium, whereas PDAC cell lines were cultured in DMEM medium. All culture media were enriched with 10% foetal bovine serum (FBS), 2 mM L-glutamine, 50 µg/ml penicillin, 50µg/ml streptomycin, 1mM pyruvic acid, and 1% nonessential amino acids. To maintain sterility, supplements were meticulously filtered before incorporation into the medium.

3.4.2 Cryopreservation

To ensure long-term cell preservation, the cell lines were cryopreserved in liquid nitrogen with complete medium containing 10% dimethyl sulfoxide (DMSO), a cryoprotective agent that mitigates the formation of ice crystals.

The procedure involved the following steps: cells from 75cm² or 150cm² cell culture flasks (T75 and T150) were subjected to three washes with cell culture Phosphate-Buffered Saline (PBS). Subsequently, 2 ml or 4 ml of trypsin 1X was added, depending on the flask size. After trypsin inactivation with complete medium (containing 10% FBS), cells were detached from the flask, collected in sterile centrifuge tubes, and centrifuged at 650 g for 5 minutes at 4°C. Supernatants were then carefully removed, and the cell pellets were resuspended in 3 ml or 5 ml of complete medium. For T75 flasks, three cryotubes were labelled, while for T150 flasks, five were used. In each cryotube, 0.9 ml of the

cell suspension was transferred, and 100 µl of DMSO were added to achieve a final volume of 1 ml. The cryotubes were promptly agitated and transferred to dry ice, followed by storage in a liquid nitrogen container. When needed, frozen cells in cryotubes were gently thawed by adding small volumes of fresh complete medium. Subsequently, they were collected in a tube containing 10 ml of freshly supplemented medium to dilute DMSO. After centrifugation at 650 g for 5 minutes at 4°C, the supernatants were removed, and the cell pellets were resuspended in 5 ml or 10 ml of complete medium. Finally, these cell suspensions were transferred to 25cm² or 75cm² cell culture flasks, respectively.

3.5 Organoids establishment

3.5.1 Human colorectal processing for organoids culture

The tissue specimen was placed into a Petri dish designed for the tissue chopper. Any undesired fat or muscle tissue was removed, and depending on the size of specimen, small sections were precision-cut for histology blocks and fresh frozen samples. Employing the tissue chopper, the specimens were finely sliced into minuscule pieces, and subsequently, they were transferred and resuspended and reconstituted within a Falcon tube containing DMEM++ (composed of DMEM, 1/100 of penicillin-streptomycin (10,000 U/ml), and 1/500 of Primocin (50 mg/ml). Following this, a brief centrifugation at 1150 rpm for 3 minutes at 4°C allowed for the separation of the supernatant, which was then carefully discarded, while the pellet underwent a gentle wash with 10 ml of DMEM++. The centrifugation was repeated under the same conditions, and once again, the supernatant was removed without disturbing the pellet.

For specimens intended for tissue culture plates, the pellet was thoughtfully resuspended in Matrigel (at 40 µl per well) and subsequently plated into 24-well culture plates.

3.5.2 Cryopreservation of organoids culture

Cryopreservation of organoids culture: optimal timing, process, and essential steps

Note: Organoid cultures are best cryopreserved approximately seven days post-passage when they are in the early stages of re-establishment and still relatively small, without complex structures or budding.

Step 1: Prepare Cryopreservation Solution

- Prepare 1 ml of freeze mix for each vial to be stored. This freeze mix should consist of 50% FBS, 40% Advanced DMEM, and 10% DMSO. Place the solution in the freezer to cool.

Step 2: Organoid preparation

- Remove the culture medium from the organoids.
- Replace it with 500 μ L of Advanced DMEM.
- Mechanically dissociate the organoids and collect them into a 15 ml tube.
- Rinse the culture well with additional Advanced DMEM, collecting the rinsed solution in the same tube.

Step 3: Centrifugation

- Centrifuge the tubes at 1500 rpm for 5 minutes at 4°C.

Step 4: Vial labelling

- While the tubes are spinning, label cryovials with the organoid number, passage number, freeze date, and your initials. Write the organoid number on the vial lids. Place the labelled vials on ice.

Step 5: Resuspension

- Remove the supernatant from the centrifuged tubes and resuspend the pellet in an appropriate volume of the previously prepared freeze mix. Typically, the content from three wells of a 24-well culture should be cryopreserved into one vial.

Step 6: Vial preparation

- Aliquot 1 ml of the organoid suspension into each pre-labelled vial.
- Place the vials into a cool cell freezing container. Ensure that the cool cell is at room temperature before use.
- If there are any spare spaces, use dummy vials to fill them in.
- Promptly transfer the cool cell freezing container into a -80°C freezer. It's crucial to maintain the optimal temperature for successful organoid cryopreservation.

3.5.3 Organoid thawing

To initiate the organoid thawing process, retrieve the cryovial from liquid nitrogen storage and transport it back to the laboratory while keeping it on dry ice. Subsequently, gently agitate the vial in a 37°C water bath for a rapid thawing process, ensuring it is removed from the water bath as soon as the content have thawed, with some ice remaining. The entire vial content is then transferred into 10 ml of cold Advanced DMEM+RKi (at a 1/1000 dilution). Following this, centrifuge the tube for 5 minutes at 1500 rpm at 4°C. Remove the supernatant and resuspend the pellet in Matrigel. The resuspended

organoids in Matrigel are seeded into a 24-well plate and incubated in a CO₂ incubator for approximately 10 minutes until the Matrigel solidifies. Finally, overlay the organoids with media supplemented with RKi and return the plate to the incubator for further cultivation.

3.5.4 Organoids passaging

In the context of organoid passaging, the process unfolds as follows: firstly, remove the existing media from the well, and replace it with 500 µL of Advanced DMEM. Subsequently, employing a P1000 pipette, gently scrape the tip back and forth across the well to lift the gel, and then pipette the media up and down to further disintegrate the gel and facilitate the release of the organoids, ensuring no gel adheres to the well's bottom. Next, collect the dislodged organoids into a properly labelled 15 ml tube. Wash the wells again with fresh Advanced DMEM to retrieve any residual gel/organoids, adding them to the 15 ml tube.

Centrifuge the contents at 1500 rpm for 5 minutes at 4°C. Carefully aspirate the media and gel while keeping the cell pellet intact. Proceed to add 1 ml of Triple Express, pipetting up and down a few times to resuspend the pellet. Place the tube in a 37°C water bath for 5 minutes and ensure that all clumps are effectively broken down by additional pipetting. Top up the tube with Advanced DMEM media to halt the enzymatic reaction. Centrifuge the tube once again at 1500 rpm for 5 minutes at 4°C, aspirating the Advanced DMEM and preserving the cell pellet.

Subsequently, resuspend the pellet in Matrigel to achieve the desired cell density, and plate it into the appropriate tissue culture plate (typically 40 µL of Matrigel per well for a 24-well plate, equating to 960 µL for 24 wells, or 1440 µL for 36 wells). Allow the gel to set by incubating it for 10 minutes. Finally, overlay the gel with complete media and return the plate to the incubator, completing the passaging procedure.

3.6 3-Dimensional (3D) cell culture assay

3.6.1 Matrigel-based 3D cell culture *in vitro*

Matrigel, derived from the Engelbreth-Holm-Swarm (EHS) mouse carcinoma, is a sophisticated basement membrane mixture that embodies a rich blend of extracellular matrix (ECM) components such as laminin, collagen IV, heparan sulphate proteoglycans, entactin/nidogen, and various growth factors. This hydrogel serves as an invaluable tool in the realm of *in vitro* 3D cell culture, creating an environment that closely emulates the conditions of cell growth *in vivo*. In our study, we meticulously

conducted the 3D on-top Matrigel, adhering to the protocol outlined in Nat. Methods (G. Lee et al., 2007). Notably, it is imperative to maintain Matrigel and its associated materials at 4°C both before and during the experiment to prevent solidification. To initiate the assay, 24-well plates were uniformly coated with 120µl of Matrigel (8.1 mg/ml and < 1.5mg/ml endotoxin) and allowed to solidify at 37°C for 30 minutes. Subsequently, the plates were washed with 0.5 ml of non-supplemented medium to eliminate excess Matrigel. Following this preparatory phase, 2.5×10^4 cells suspended in 0.4 ml DMEM-HAM's F12, supplemented with 1% ITS (Insulin, Transferrin, and Sodium selenite), were meticulously seeded in triplicates onto the Matrigel-containing 24-well plates. The plates were then incubated at 37°C for 30 minutes with periodic gentle agitation every 5 minutes. Finally, a 10% Matrigel solution in DMEM-HAM's F12, supplemented with 1% ITS was overlaid onto the cells. In our experimental paradigm, we added P14B (10mM, 40mM, or 100mM) either at the time of seeding or 24 hours later, and three days post-seeding, the resulting colonies were subjected to analysis. Noteworthy, organoid-like structures, defined by their resemblance to the morphology of organoids, were captured using phase-contrast microscope. All scale bars in the images were standardised to 40mm providing a comprehensive view of the intricate cellular architecture developed within the 3D Matrigel environment.

3.7 Bacterial selection and transformation

Transformation is the genetic alteration of bacterial cells resulting from the direct uptake and incorporation of exogenous DNA through the cell membrane. In the context of bacterial culture for the purposes of this thesis, two distinct competent strains were employed: DH5α for the amplification and purification of plasmid DNA and BL21pLysS for the expression and purification of the proteins.

The selection of BL21pLysS bacteria was guided by specific characteristics that facilitate the expression and purification processes. Notably, these bacteria possess a non-resistant cell wall and express lysozyme, which is integrated into the pLys plasmid. These features greatly aid in the lysis and subsequent extraction of the protein intended for purification. Moreover, the expression of RNA polymerase T7, responsible for driving the expression of the GST-KRAS-G12V (1-166) gene, is regulated by the lacUV5 promoter present in the pLysS plasmid and can be induced by the addition of IPTG.

The culture medium used for the growth of these bacteria consisted of LB (Luria-Bertani) autoclaved culture medium, comprising 10 g/L of tryptone, 5 g/L of yeast extract, and 10g/L of NaCl in water with a pH of 7.5. Additionally, LB agar culture plates were prepared by incorporating 1.5% bacterial agar

into LB medium. For bacterial selection, DH5 α containing the pGEX-KG (GST-KRAS-1-166) plasmid were cultivated in the presence of 50 μ g/ml ampicillin. On the other hand, BL21pLys, due to its intrinsic resistance to chloramphenicol through the expression of the pLysS vector, required supplementation with ampicillin (used for resistance generated by the transformed plasmid pGEX-KG) and chloramphenicol at 20 μ g/ml to ensure proper selection and cultivation. These specific bacterial strains and culture conditions were essential components of the experimental setup for this study.

3.7.1 Transformation of BL21pLys cells. Protein expression and purification

Transformation of BL21pLys cells

The transformation process for BL21pLys cells underwent several key steps. Initially, competent BL21pLys cells (50 ml) were thawed on ice for 30 minutes. Then, 1 μ g of purified pGEX-KG (GST-KRAS-1-166) or pGEX-KG (GST) DNA plasmids were added, and the mixtures were incubated on ice for an additional 30 minutes. Heat-shocking was then performed by placing the tubes in a dry bath at 42°C for 45 seconds, quickly transferring them back to ice, and allowing a 2-minute incubation period.

Under sterile conditions, approximately 0.8 ml of sterile L-Broth without antibiotics was added, and after one hour at 37°C cells were harvested. Subsequently, 100 μ L of bacterial cells were plated on an L-Broth/agar plate containing the necessary antibiotics. The remaining cell suspension was centrifuged at 5000 rpm and most of the supernatant was removed, leaving only 100 μ L. The bacterial cells were then resuspended and plated on another plate. Plates were incubated upside down at 37°C overnight. To preserve the transformed colonies, three colonies were selected with an inoculation loop and placed in separate 15 mL tubes, each containing 5 ml L-Broth and the appropriate antibiotic. These tubes were incubated overnight at 37°C. Following incubation, 1.5 ml of bacteria were harvested and transferred to cryotubes, with the remaining volume available for plasmid purification. To ensure successful preservation, 500 μ L of a 60% glycerol solution was added and immediately shaken. The cryotube was then promptly stored at -80°C for future use in the research project. This process of BL21pLys transformation was vital for subsequent experimental phases.

Induction of BL21pLys cells for GST-KRAS and GST protein expression

To initiate the induction process, it was essential to obtain at least three glycerol stocks from distinct tubes. Subsequently, plasmid purification was performed on a small scale from all the glycerol stocks, followed by DNA sequencing to ensure their integrity.

BL21pLys cells transformed with pGEX-KG (GST-KRAS-1-166) or pGEX-KG (GST) DNA plasmids were inoculated from glycerol stocks into 10 ml of L-Broth supplemented with the appropriate antibiotics and incubated overnight with agitation at 37°C. Once the overnight culture was established, it was transferred to a larger Erlenmeyer flask containing 500 ml of L-Broth with antibiotics. Here, the bacterial cells were allowed to grow for four hours, and a 50 µL sample was collected and saved.

To induce protein expression, IPTG was added to the culture to achieve a final concentration of 0.5 mM. The incubation was continued for an additional 4 hours. Following induction, 50 µL of the culture was collected and saved for reference, and the remaining cells were subjected to centrifugation at 5000 rpm for 10 minutes at 4°C. The resulting cell pellet was then frozen at -80°C for further analysis. To verify the success of induction, a Coomassie staining method was employed. The collected bacterial samples, both induced and non-induced, were loaded onto the gel for SDS-PAGE. Subsequently, the gel was stained with Coomassie Brilliant Blue, a protein-binding dye. A successful induction was confirmed by the presence of two wide protein bands of 45kDa and 26kDa corresponding to GST-KRAS-G12V-1-166 and GST, respectively in the induced sample wells.

To perform Coomassie staining, the following steps were undertaken:

- Samples were prepared by adding 7 µL of Laemmli Sample Buffer 4X to 21 µL of bacterial cells.
- A 10% acrylamide gel was created and loaded with the prepared samples.
- The gel was run at 35 mA until proteins were resolved.
- Subsequently, the gel was immersed in a solution consisting of 0.25% Coomassie Brilliant Blue, 50% methanol, and 7.5% acetic acid.
- The gel was incubated for 10 minutes, and the staining solution was then removed.
- The gel was rinsed with water three times and incubated overnight in an unstaining solution composed of 20% methanol and 7.5% acetic acid.
- Presence of the protein bands was verified with a transilluminator, confirming the success of the induction processes.

Following a successful induction, the subsequent step involved cell lysis, and GST containing proteins purification by incubation with glutathione-sepharose beads. The purification process was carried out as follows:

1. The bacterial cell pellets induced in the previous step and kept at -80°C were thawed on ice, and meanwhile lysis buffer containing protease and phosphatase inhibitors, including aprotinin (150 nM), leupeptin (20 nM), PMSF (1 mM), sodium orthovanadate (0.2 mM), sodium fluoride (5 mM), and DTT (1 mM), was freshly prepared.
2. The two bacterial pellets were processed as follows: a) Incubated with lysis buffer for 20 minutes. b) Sonicated for three minutes in cycles of three seconds using a sonifier (Brandson SFX250). c) Centrifuged at 14,000 rpm for 10 minutes at 4°C. d) The supernatant was collected, and the pellet was stored at -80°C. e) 30 µL of the supernatant were reserved, and 800 µL of previously washed glutathione-sepharose beads (using 10-20 ml of lysis buffer) were added. f) Incubated for 1 hour at 4°C with rotation. g) After centrifugation at 3000 rpm for 3 minutes at 4°C, the supernatant was removed and stored at -80°C. h) The beads were washed with 20 ml of lysis buffer four times, centrifuged at 3000 rpm for 3 minutes at 4°C, retaining 20 µL of each wash for later analysis (to ensure that we did not lose the protein).
3. To ensure that all KRAS was loaded with GTP an incubation with GTP was performed, followed by a wash with exchange buffer as follows: a) The beads were incubated with 1600 µL of exchange buffer, complemented with 1 mM GTP, 10 mM EDTA, and 1 mM DTT. b) Incubated for 30 minutes at 30°C. c) MgCl₂ was added until a final concentration of 15 mM was reached, then cooled down to 4°C. e) The beads were washed with 15 ml of exchange buffer with 2 mM of magnesium ions and then with 15 ml of lysis buffer twice.
4. To elute GST-KRAS from the beads: a) 1 ml of lysis buffer supplemented with 20 mM of glutathione was added and mixed well by pipetting. b) Centrifuged at 3000 rpm for 3 minutes at 4°C, and the supernatant containing the eluted GST-KRAS was collected. c) 0.5 ml of lysis buffer, also supplemented with 20 mM of glutathione, was added to the pellet and mixed well by pipetting. d) Centrifuged at 3000 rpm for 3 minutes at 4°C, and the supernatant was collected, combining it with the first elution for further analysis and purification.

Typically, the purified proteins are not stored in the same buffer in which they were initially purified. To achieve a buffer exchange for KRAS, we employed the Slide-A-Lyzer™ Mini Dialysis Device. This device comprises a tube divided into two compartments, separated by a semi-permeable membrane with pores that permit the free movement of molecules with a molecular weight less than 3.5 KDa. Consequently, GST-KRAS is retained within the membrane, while the buffer components are either removed or exchanged through the dialysis process. By repeating this procedure several times, the protein ultimately becomes solubilized in the new dialysis buffer.

To perform the buffer exchange:

The solution containing KRAS, typically the supernatant from the final centrifugation step of the purification process, was collected and loaded into a Slide-A-Lyzer Device with a 2 ml capacity. Following this, 45 ml of the new dialysis buffer was added, and the system was gently agitated at 100 rpm for 2 hours at 4°C. Subsequently, the dialysis buffer was removed, and another 45 ml of fresh buffer was added, repeating the incubation step. The buffer exchange process was repeated overnight. Finally, the protein was collected from the Slide-A-Lyzer Device, now effectively solubilized in the new dialysis buffer, making it suitable for further experiments and analyses.

Protein verification

To ensure the purity and identity of the purified protein, a series of analyses were performed. The initial step involved a Lowry Protein assay to confirm the presence of protein within the final purified sample. Subsequently, to ascertain the specific identity of the purified protein as KRAS, two acrylamide gels were prepared, and electrophoresis was carried out. One of the gels was dedicated to Western blotting using an antibody capable of recognizing KRAS, such as Pan-Ras or a specific KRAS antibody, while the other gel was subjected to Coomassie staining. The following samples were loaded onto the gels for analysis:

- Purified protein (5 µl)
- Glutathione-sepharose beads (30 µl)
- Not-bound sample (30 µl)
- Bacterial lysate (30 µl)

The procedure encompassed the following steps:

- Preparation of two 10% acrylamide gels.
- Loading of the specified samples into the wells of each gel.
- Running the gels at 35 mA.
- Staining one of the gels with Coomassie Blue to visualize protein bands and transferring the proteins from the other gel to a PVDF membrane.
- Staining the PVDF membrane with Ponceau S, followed by blocking with bovine serum albumin (BSA).
- Incubating the membrane with the chosen antibody specific to KRAS.
- Washing the membrane and incubating it with the appropriate HRP-conjugated secondary antibody.
- Develop and capture an image of the membrane through chemiluminescence. These analyses collectively confirm the presence and identity of the purified KRAS protein.

3.7.2 Plasmid purification

The purification of amplified plasmids from transformed bacteria was accomplished utilizing either the PureYield™ Plasmid Miniprep System, yielding 15µg of DNA, or the NucleoBond®Xtra Midi system, capable of producing up to 750µg of DNA. In both instances, the purification protocols were meticulously executed in accordance with the manufacturer's instructions. Following plasmid purification, DNA concentration was quantified utilizing a nanodrop spectrophotometer provided by ThermoFisher Scientific. Additionally, to ensure the quality and integrity of the DNA, the crucial process of DNA sequencing was outsourced to the Sequencing Service of CSIC-IRTA, located at the UAB campus within the CRAIG building in Bellaterra. This comprehensive approach ensured the robustness and accuracy of DNA isolation and sequencing, crucial for the subsequent analyses and experiments detailed in this research.

3.8 Cell transfection

Cells were transiently transfected following the Lipofectamine™2000 commercial protocol, a technique that encapsulates vectors within liposomes for their introduction into the cells through the plasma membrane, enabling the expression of proteins of interest. To initiate the transfection process, cells were cultured in p100 plates until they reached approximately 70% confluence on the day of transfection. Subsequently, 24µg of DNA and 60µl of Lipofectamine were separately combined with

0.5 ml of non-supplemented DMEM in two different tubes. The two solutions were then thoroughly mixed and incubated for 20 minutes at room temperature (RT). During this incubation period, the cells were washed with cell culture PBS, and 9 ml of DMEM (supplemented, but devoid of antibiotics to prevent interference with Lipofectamine) was added to the plates. Following this, the DNA-Lipofectamine mixture was gently dispensed onto the cells and allowed to incubate for 6 hours. Ultimately, the medium was replaced with fresh complete medium, and cell collection was conducted 48 hours post-transfection.

3.9 Electrophoresis and Western Blotting (WB)

3.9.1 Sample preparation

Cell lysates

The cultured cells were carefully rinsed three times with cold PBS and subsequently lysed in a buffer composed of 67 mM, Tris-HCl at pH 6.8, and 2% sodium dodecyl sulphate (SDS). Cell lysates were collected by scraping, and following this, they were exposed to a temperature of 97°C in a dry bath for 15 minutes. After this heat treatment, the samples were subjected to centrifugation at 10,000g for 1 minute at RT. The resting supernatant was then preserved for subsequent protein quantification.

Tumour lysates

The tumour samples were initially placed in a tube and kept on ice. The amount of TEB (Tissue Extraction Buffer) used, ranging between 500 – 900 µl, depended on the size of the tumours. An effort was made to ensure that tissues from the pancreas and liver were cut into roughly equal-sized pieces. The next step involved disrupting and homogenizing the tumours while maintaining a cold environment. This was achieved using a Dissertator (Qiagen), which was operated through multiple cycles of 30 seconds at medium speed. Some cycles were performed at full speed when necessary to ensure complete homogenization of the samples. To enhance the efficiency of the process, the tip of the Dissertator was continuously stirred within the sample.

After the tumour samples were thoroughly homogenized, they were left to rest on ice for 10 minutes and subsequently subjected to centrifugation at 21,900 g for 10 minutes at 4°C. Finally, the resulting supernatant was preserved for further protein quantification.

3.9.2 Protein quantification

This thesis employed the Lowry assay to quantify protein concentration, which is based on the Biuret method and involves two essential reactions. In the initial step, peptides react with copper under alkaline conditions to form a cuprous complex. In the subsequent reaction, the Folin–Ciocalteu reagent (phosphomolybdic/phosphotungstic acid) is introduced, which interacts with the cuprous ions and oxidizes tyrosine, tryptophan, and cysteine, leading to the formation of a blue green colour heteropoly molybdenum complex that absorbs light at 750 nm. The Lowry assay was conducted in 96-well plates, and various concentrations of BSA, prepared from a 1 µg/µl stock solution, were used as calibration standards.

To perform the assay, both samples and standards were prepared twice, as outlined in Table 7. Subsequently, Lowry solution A was prepared by following the 48:1:1 ratio of three solutions: Solution 1 (2% Na₂CO₃ and 0.1 M NaOH), Solution 2 (0.5% CuSO₄), and Solution 3 (1% sodium potassium tartrate).

Table 7: Volumes required for standard curve and samples.

	BSA(µL)	Sample (µl)	Lysis buffer (µl)	H ₂ O (µl)
Standard Curve	0	-	2	43
	2	-	2	41
	4	-	2	39
	8	-	2	35
	16	-	2	27
	32	-	2	11
	40	-	2	3
Sample	-	2	-	43

Subsequently, 225µl of Lowry solution A was dispensed into each well, thoroughly mixed by pipetting, and incubated at RT for 10 minutes.

While this incubation took place, Lowry solution B was prepared by combining the Folin-Ciocalteu reagent and deionized water at a 1:1 ratio. Following this, 22.5µl of Lowry solution B was carefully added to each well and mixed by pipetting. After allowing the samples to incubate for 30 minutes at RT, their absorbance at 750 nm was measured using a multimode plate reader (Spark®, TECAN). A simple linear regression was performed using the absorbance values from the standards.

Finally, the average absorbance values of each sample were interpolated, and the protein concentration was determined. Once the protein concentrations were calculated, 15 or 20µg of protein per sample along with Laemmli sample buffer 4X, were prepared for SDS-PAGE in accordance with a 3:1 ratio.

3.9.3 SDS-Polyacrylamide Gel Electrophoresis (SDS-PAGE)

Electrophoresis is a technique employed for the separation and analysis of macromolecules and their fragments based on their size and charge. In this process, SDS-polyacrylamide gels are prepared at varying concentrations of acrylamide, which yield pores of different sizes, enabling the separation of proteins based on their molecular weight. Higher polymer concentrations are used for smaller molecules, and vice versa.

SDS is introduced into the samples, running buffer, and gels to impart a negative charge and denature the proteins. Consequently, when an electric field is applied, the proteins migrate towards the anode, with each protein moving at a distinct speed, depending on its size. This differential movement results in the physical separation of proteins from each other.

Table 8: Volumes of solutions required for resolving and stacking gel preparation.

Solutions	Resolving gel					Stacking gel
	6%	8%	10%	12%	15%	
Solution 1 (ml)	5	5	5	5	5	-
Solution 2 (ml)	2	2.8	3.4	4	5	0.36
Solution 3 (ml)	-	-	-	-	-	1.5
H₂O (ml)	3	2.2	1.6	1	-	1.2
Temed (µl)	14	14	14	14	14	7.5
Ammonium persulphate (APS) 13% (µl)	50	50	50	50	50	30

These gels consist of two key regions: the stacking section, characterized by larger pores that facilitate the alignment of proteins from the loaded samples, and the resolving section, which possesses appropriately sized pores for the separation of proteins based on their molecular weight. The specific

acrylamide concentrations used for gel preparation are determined based on the size of the proteins to be identified, as indicated in table 8.

Following the preparation of the resolving gel, the polymerizing agents (Temed and APS) were added last. The resulting mixture was then poured between the two glass plates of the gel assembly. To facilitate acrylamide polymerization, which necessitates oxygen-free conditions, 1 ml of deionized water was gently added on top. Once the water was removed, the freshly prepared stacking mixture was poured over the resolving gel, and a comb was swiftly inserted to create the loading wells.

Subsequently, the polymerized gel, along with the glass plates, was assembled onto the electrophoresis system (Mini-PROTEAN, BioRad) filled with running buffer, and the comb was removed. Samples and a molecular weight marker (such as Precision All Blue or Low or High Range Unstained Protein Standards from BioRad) were loaded into the wells using a Hamilton syringe. A constant current of 35 mA per gel was applied until the coloured front of the samples reached the end of the gel.

Following this separation step, the proteins were electro-transferred from the gel to a blotting membrane.

3.9.4 Protein transfer from gel to blotting membrane

After proteins had been separated according to their molecular weight in an SDS-gel, the next step involved transferring them onto a polyvinylidene fluoride (PVDF) Immobilon™-P membrane for WB. To prepare the PVDF membrane for this process, it was first hydrated to overcome its hydrophobic nature. This was achieved by briefly immersing it in a solution containing over 100% alcohol (in this case, methanol) for 30 seconds. Subsequently, the membrane was soaked in water and transfer buffer for 2 minutes each.

Once the PVDF membrane was appropriately prepared, it was assembled into a sandwich with the gel using a gel holder cassette. This assembly was then stacked and placed into a transfer tank. Within the transfer tank, a transfer buffer solution facilitated the process. To enhance contact and pressure, sponges and filter paper sheets (3mm CHR Blotting Paper, GE Healthcare) were pre-soaked in the transfer buffer and used inside the cassette. This method ensured efficient and consistent protein transfer to the PVDF membrane for subsequent WB analysis. The electro-transfer was carried out at a voltage of 70 V for 2 hours, or alternatively, it could be conducted at a lower voltage of 20 V overnight

in a refrigerated environment (4°C). Once the transfer process was completed, the membranes were then dried to prepare them for further analysis.

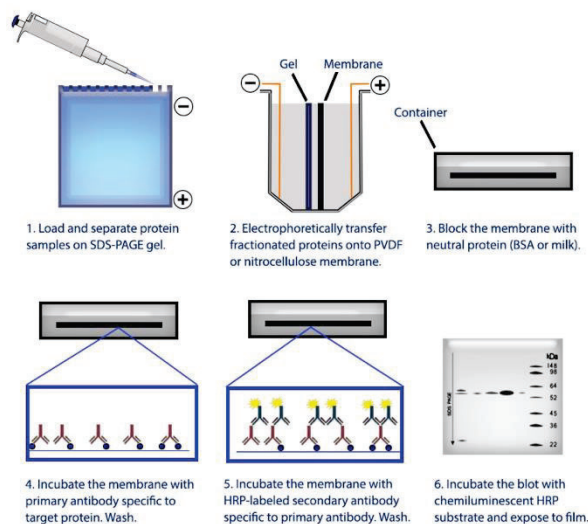


Figure 16: Overview of the WB procedure. Adapted from (<https://www.biolegend.com/de-at/western-blot>).

3.9.5 Total protein detection: Ponceau S staining

The Ponceau S staining method involves the use of a sodium salt of diazo dye to provide a quick and reversible stain, facilitating the visualization of protein bands on nitrocellulose or PVDF membranes. The dye can be easily removed when the membranes are washed with water. In the context of this thesis, Ponceau staining was employed to assess the effectiveness of both electrophoresis and protein transfer processes, as well as to verify the accurate loading of samples. Additionally, it served to visualize the protein standards.

As part of the procedure, once the membranes were thoroughly dried, they were subjected to a 1-minute incubation with Ponceau at RT. Subsequently, any excess staining was removed through several rinses with distilled water.

3.9.6 Membrane blocking

Given the PDVF membranes' propensity for high protein binding, it is imperative to prevent non-specific binding when incubating with antibodies. In this thesis, membranes were effectively precluded from such interactions by saturating them with a solution of BSA in Tris Buffer Saline (TBS).

Following the Ponceau staining procedure, the membranes were meticulously dried once more. Subsequently, they were rehydrated by immersing them in methanol for 30 seconds, followed by soaking them in water and TBS for 2 minutes each. To complete the blocking process, the membranes were incubated in a 5% BSA solution in TBS for 1 hour at RT, with periodic shaking. This blocking step ensured that specific antibody binding could be effectively achieved while minimizing non-specific interactions.

3.9.7 Western blotting: Immunodetection

Hybridisation with the antibodies

To pinpoint specific proteins among those transferred, the blotting membrane undergoes a two-step antibody incubation process. First, it is incubated with primary antibodies tailored to recognize the protein of interest. Subsequently, another round of incubation with secondary antibodies is conducted. These secondary antibodies are designed to target the constant domain of the primary antibodies and are typically linked to a reporter enzyme, facilitating visualisation. After blocking, the membranes were subjected to an overnight incubation with primary antibodies, diluted in TBS-Tween 20 (TBS-T) containing 5% BSA, at 4°C with gentle agitation. The following day, any excess primary antibodies were meticulously removed by washing the membrane three times for 10 minutes each with TBS-T at room temperature while shaking. Subsequently, the membranes were exposed to a solution of secondary antibodies, diluted in a 2.5% milk powder in TBS, for 1 hour at RT with periodic agitation. Finally, any residual secondary antibodies were removed by conducting a three-time, 10-minute wash with TBS-T at room temperature while shaking. The membranes were then maintained in TBS until protein visualisation.

Chemiluminescence detection and imaging

The final crucial step in WB is the identification of proteins of interest, which have been tagged with specific antibodies. In this thesis, a reporter enzyme, horseradish peroxidase, was employed, and it was linked to the secondary antibodies. This enzyme serves as a catalyst, initiating a chemical reaction

when hydrogen peroxide is introduced. This reaction results in the emission of light, a phenomenon known as chemiluminescence. The assessment of protein detection was accomplished using the Enhanced Chemiluminescence (ECL-EZ) system with the aid of a detection kit. The emitted light was captured and quantified using the ChemiDoc imaging system by BioRad. This process allowed for the precise identification and quantification of the targeted proteins.

3.10 Treatment of cells with P14 and its derivatives, and EGF/FBS- dependent signalling activation

The impact of P14 and its derivatives on KRAS downstream signalling pathways was assessed through various biological methods.

The cells were initially cultured in a medium supplemented with 10% FBS for 24 hours. Subsequently, they were subjected to serum starvation for the following 24 hours. After this, the cells were treated with various compounds for the durations specified in each respective figure (Results section). Additionally, in certain cases, to activate downstream KRAS cell signalling, a 10-minute treatment with epidermal growth factor (EGF) at 50 ng/ml or with 10% FBS for 30 minutes was administered as indicated.

3.11 Co-immunoprecipitation

Immunoprecipitation (IP) is a technique employed for the selective extraction of a protein of interest from a cell lysate. This is achieved through the use of an immune complex, consisting of an antibody that recognizes and binds specifically to the target protein. This antibody is coupled to agarose beads, which serve as the solid substrate enabling the isolation of the complex through centrifugation.

Co-immunoprecipitation (Co-IP) is a variant of IP specifically designed to capture intact protein complexes. It utilizes a particular antibody directed against a known protein within the complex to pull the entire complex. This approach facilitates the identification of the other components within the complex. In the context of this study, P14B ability to disrupt the interaction between oncogenic KRAS and its effectors was evaluated through co-IP.

For this analysis, DLD-1 S2-6 cells, which stably express HA-KRAS-G12V were subjected to a 24-hour starvation period. Following this, the cells were treated with P14B for 15 minutes, followed by treatment with EGF at 50 ng/ml for an additional 10 minutes. A co-IP procedure was then executed

using a monoclonal specific anti-HA antibody crosslinked to agarose beads. This allowed for the investigation of protein interactions within the complex.

To describe the process in a more precise and organized manner:

Cell collection and pellet preparation

- Cells were initially washed thrice with cold PBS.
- After washing, cells were collected by gentle scraping and suspended in 1 ml of cold PBS.
- The suspension was then centrifuged at 650 g for 5 minutes at 4°C.
- The resulting cell pellets were lysed with REB buffer, freshly supplemented with a cocktail of protease and phosphatase inhibitors (150nM aprotinin; 20μM leupeptin; 1 mM PMSF; 5 mM NaF; and 0.2 mM Na₃VO₄) as well as 1 mM DTT.
- The volume of REB buffer added varied depending on the pellet size, typically ranging between 500 – 800μl.
- These lysed samples were maintained on ice for 10 minutes and then centrifuged at 21,900 g for 10 minutes at 4°C.
- The supernatant, referred to as the soluble fraction, was retained for subsequent protein quantification (for more details, see section 3.9.2).
- After quantification, 40μg of protein per sample were separated as "input" and stored at -20°C.

Preparation of anti-HA antibody-agarose beads

Meanwhile, 50μl per sample of monoclonal anti-HA antibody-agarose beads were washed five times with PBS through centrifugation at 600 g for 30 seconds at RT. After washing, the beads were resuspended with a volume of REB buffer equivalent to the initial volume.

Immunoprecipitation

A total of 1,000 – 2,000μg of protein (soluble fraction) per sample were collected, and the volumes were adjusted by adding REB buffer. These samples were then incubated with the anti-HA antibody-agarose beads (50μl per sample) for 3 hours, allowing rotation at 4°C.

Subsequently, the samples were centrifuged at 21,900 g for 2 minutes at 4°C. The pellets containing the immunocomplexes were designated as the "bound fractions," while the supernatants were preserved as the "not bound" fractions.

Washing and Preparation

The bound fractions underwent five washes with 1 ml REB buffer through centrifugation at 600 g for 30 seconds at RT. Laemmli sample buffer 2X was added to the bound fraction in a 1:1 proportion. The "input" and "not bound" fractions were prepared as per standard procedure.

Western Blotting

All samples were then subjected to WB using the appropriate specific antibodies.

3.12 Ras Binding Domain-pull down assay (RBD-pull down)

The GST-fusion protein encompassing the human RAS-Binding Domain (RBD) of CRAF (residues 1-149), has been expressed in *Escherichia coli*. This fusion protein is conveniently provided pre-bound to glutathione agarose beads, ensuring ease of use. With a purity exceeding 80%, this high-quality construct exhibits a robust remarkable capability to specifically bind to and efficiently precipitate RAS-GTP, making it a reliable tool for elucidating the amount of active RAS in biological samples.

In detail: cells were grown until reaching approximately 75-80% confluence. Then, cells were starved overnight, followed by treatment with EGF for 10 minutes or P1.3 for 2 hours, and the last subsequently with EGF for additional 10 minutes. The cells were lysed using Mg-containing lysis buffer (MLB), with 0.4-0.8 ml of MLB utilised per 100 mm culture plate. Fresh cell lysate was diluted to approximately to 500µg-1mg of cell lysate per assay, allowing for one affinity reaction per lane for SDS-PAGE. The reaction mixture was gently rocked at 4°C for 30 minutes. Agarose beads were collected through pulsing (5 seconds in the microcentrifuge at 14,000 xg), and the supernatant was drained off. The beads were washed three times with MLB. The agarose beads were then resuspended in an appropriate amount of Laemmli Sample Buffer 2X and the samples were subjected to WB with anti-KRAS antibodies.

3.13 Calmodulin-pull down (CaM-pull down)

To investigate whether the interaction between KRAS and CaM is disrupted during incubation with P14B, an *in vitro* competence assay was conducted. This method involves the pull down of recombinant GTP-loaded GST-KRAS-G12V (1-166) using CaM-sepharose beads, followed by the introduction of varying concentrations of P14B. Analysis is performed using GTP-loaded KRAS in the presence of CaCl₂

since CaM binds only to the GTP form of KRAS. As negative control, incubation with EGTA as a calcium chelator is also assayed.

Initially, 5µg of recombinant GST-KRAS-G12V (1-166) (loaded with GTP, see Section 3.7.1) were mixed with 12.5µL of CaM-sepharose beads (Cytiva; Merck, Darmstadt, Germany). The beads had been previously washed with a pulldown buffer (PDB). This mixture was incubated in the presence of 1 mM CaCl₂ or 5 mM EGTA, in a total volume of 100µL in PDB, for 60 minutes at RT. The unbound fraction was collected through centrifugation, while the bound fraction underwent four washes with PDB containing either CaCl₂ or EGTA. The entire bound fraction was subsequently analysed by WB with anti-KRAS antibodies.

3.14 Cell viability assays

Assessing changes in cell viability constitutes a crucial technique for appraising cellular well-being, genotoxicity, and the efficacy of anti-cancer compounds. To gauge cell health, various pivotal indicators can be examined, including alterations in plasma membrane integrity, DNA synthesis, DNA content, enzyme activity, ATP presence, metabolic processes, and the cellular reducing environment. In this thesis, two different assays measuring certain aspects of cell metabolism or cellular reducing environment have been used. These tests consist of incubating viable cells with a reagent to transform a substrate to a coloured or fluorescent product that is proportional to the number of viable cells existing.

3.14.1 MTS Tetrazolium assay:

CellTiter 96® Aqueous One Solution Cell Proliferation Assay

The effect of the peptidomimetics and P14B in the viability of several CRC and PDAC lines harbouring different oncogenic KRAS mutations, and of one non-transformed cell line (hTERT-RPE cells) was evaluated using the CellTiter 96® Aqueous One Solution Cell Proliferation Assay (Promega G3580). It is a colorimetric method for determining the number of viable cells. The CellTiter 96® AQueous One Solution Reagent contains a novel tetrazolium compound [3-(4,5-dimethylthiazol-2-yl)-5-(3-carboxymethoxyphenyl)-2-(4-sulfophenyl)-2H-tetrazolium, inner salt; MTS] and an electron coupling reagent (phenazine ethosulphate; PES). PES has enhanced chemical stability, which allows it to be combined with MTS to form a stable solution. This advantageous “One Solution” format requires no volatile organic solvent to solubilize the formazan product.

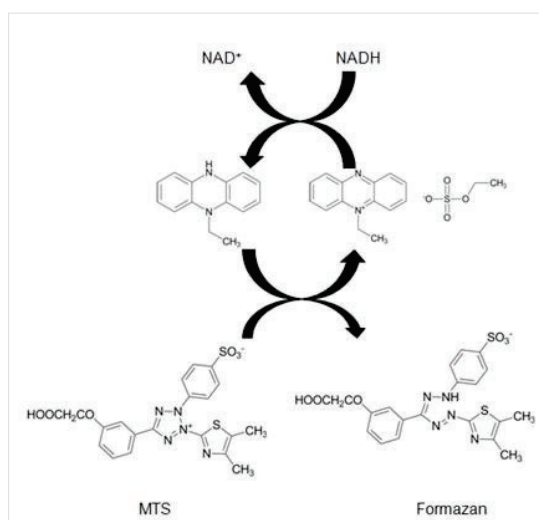


Figure 17: PES transfers electron from NADH to reduce MTS into formazan. *Extracted from* (Riss et al., 2013).

In this analysis, a total of 10,000 cells were suspended in 50µl of medium containing 10% FBS. These cells were then seeded in sextuplicate within a 96-well plate and allowed to incubate for 24 hours. Subsequently, different concentrations of peptidomimetics or P14B, diluted in 50µl of medium containing 10% FBS, were added and incubated for an additional 24 hours and for 48 hours following the pattern illustrated in Figure 18. Control groups received DMSO, which was diluted in the same 50µl volume. The total well volume remained constant at 100µl throughout the experiment.

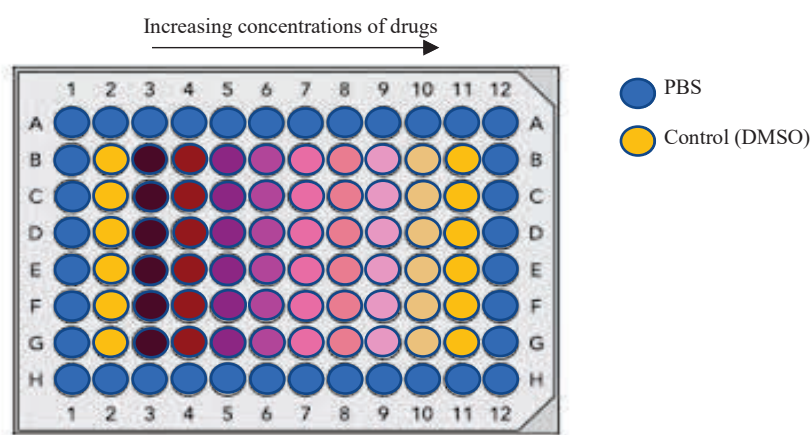


Figure 18: 96-well plate treatment pattern.

After the treatment, the MTS viability assay was conducted according to the manufacturer's instructions. Initially, 20µl of CellTiter 96® AQueous One Solution Reagent were introduced into each well, which already contained 100µl of cell culture medium, followed by thorough mixing using pipetting. Subsequently, the cells were incubated for 2 hours at 37°C, and the absorbance of each well was measured at 490 nm using a multimode plate reader (Spark, Tecan). To determine the percentage

of cell viability, the absorbance of each well was divided by the average absorbance of the control wells, which exhibited no significant deviation when analysed using a Student's t-test.

3.14.2 Resazurin Reduction Assay:

Presto-Blue® Cell Viability Reagent

The effect of P14B treatment in the viability of colorectal cancer or healthy patients-derived organoids (PDOs) was evaluated using the Presto-Blue® Cell Viability Reagent (Invitrogen, A13262). It is a fluorescent/colorimetric method for determining the number of viable cells. The Presto-Blue is a resazurin-based reagent, which infiltrating live cells, facilitates the reduction of resazurin to resorufin, a red and intensely fluorescent compound (see figure 19). Viable cells consistently transform resazurin into resorufin, causing a noticeable elevation in the overall fluorescence and colour of the surrounding cell culture medium. Furthermore, the conversion of resazurin into resorufin induces a striking shift in colour, making it feasible to detect cell viability through absorbance-based plate readers.

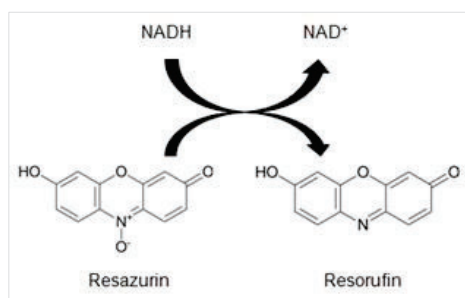


Figure 19: Resazurin substrate is reduced into the pink, fluorescent resorufin (Riss et al., 2013).

Steps followed to study the viability of PDOs upon P14B treatment:

Day -One:

- The culture medium was replaced with Advanced DMEM, and the organoids seeded in 24 well-plate were gently dislodged from the Matrigel matrix.
- The dislodged organoids were collected in a 15ml tube and centrifuged at 1500rpm for 5 minutes at 4°C.
- The resulting pellet was resuspended in 5ml of Advanced DMEM and passed through a 100µm cell strainer. Subsequently, another centrifugation was performed.
- The organoids were resuspended in Matrigel (21 wells were required, with 5 µl of Matrigel per well) and replanted into 96-well plates (triplicate per condition). The organoids were allowed

to set in the incubator for 10-15 minutes, after which they were overlaid with complete tumour media, and recovery was allowed overnight.

Day Zero of Five - Presto-Blue baseline measurement:

- The plates were labelled with the names of the drugs and their concentrations to be used.
- Presto-Blue was diluted at a 1:10 ratio with human tumour basal media.
- The media was removed from the organoids, and 100µl of the diluted Presto-Blue was added to each well, with an incubation period of 45 minutes.
- After 45 minutes, 90µl aliquots were transferred from each well to a black reader plate.
- Any remaining Presto-Blue in the wells was ensured to be removed before replacing it with 100µl of Advanced DMEM, and the plate was returned to the incubator.

Day Two of Five:

The steps from Day Zero were repeated, and in addition, 100µl of Advanced DMEM was removed from the wells. These were then replaced with different concentrations of P14B (as indicated in the results section), prepared in 100µl of complete media. The plate was subsequently returned to the incubator.

Day Five of Five - Presto-Blue final measurement:

The steps from Day Zero were repeated. To determine the percentage of cell viability, the absorbance of each well was divided by the absorbance obtained on Day Zero. This comparison revealed no significant variation upon analysis using a Student's t-test.

3.15 Surface Plasmon Resonance (SPR)

To investigate the presumed direct interaction between KRAS-G12V and P1.3 or P14B, we harnessed the power of SPR. Surface plasmons are coherent oscillations of electrons (electromagnetic waves) that occur at the interface between a metal and a dielectric material (or vacuum). These oscillations are excited when incident photons have a frequency matching the natural frequency of surface electrons. Since these waves occur at the metal-dielectric boundary (in our case, the water medium), they are exceptionally sensitive to any changes at the metal surface's edge. For instance, when molecules adsorb onto the conducting surface, they influence these electromagnetic waves, altering the range at which they are excited.

For this analysis, we employed the Biacore™ T-200 SPR Biosensor instrument equipped with chips featuring a gold layer within a matrix, capable of immobilizing one of the proteins of interest (the ligand). The other molecule under investigation (the analyte) was flowed over this layer. A light source directed light toward a prism, and the changes in the reflected angles were measured. These alterations correlate with variations at the surface layer, such as the interaction between the analyte and the ligand. By determining the dissociation constant (KD), we could quantify the strength of the interaction; smaller KD values indicate more prolonged interactions.

The raw data collected during the experiment was processed using Biacore T200 Evaluation Software 3.1, which transformed it into a sensogram. The sensogram reflects the changes in reflection angles while the sample is being injected.

To investigate the characteristics of the binding of P1.3 and P14B with KRAS-G12V, a CM5 Series S Chip (Cytiva 29104988) was employed. This chip features a dextran matrix to which the GST-tagged globular domain of KRAS-G12V (comprising residues 1-166) was covalently attached. Subsequently, P1.3 or P14 were introduced, and the change in resonance units (RUs) was measured to assess the interaction.

Chip preparation

Before introducing the analyte, it is essential to activate and prepare the chip matrix. This process involved several steps:

Step 1: Conditioning channels 1, 2, and 4

Channels 1, 2, and 4 were initially treated to ensure optimal chip performance.

This conditioning process involved sequential steps:

- 100 mM HCl
- 50 mM NaOH
- 0.1% SDS
- Rinse with water at a flow rate of 100µl/min.

Step 2: Activation of dextran

- The dextran matrix was activated to facilitate subsequent binding.
- This was achieved by injecting a mixture of N-hydroxy-succinimide and 1-Ethyl-3-[3-dimethylaminopropyl] carbodiimide (EDC) at a 1:1 ratio.
- The activation was performed at a flow rate of 10µl/min for 7 minutes.

Step 3: Immobilization of GST-KRAS-G12V (1-166)

- GST-KRAS-G12V, the target protein, was immobilized onto the dextran surface in channels 2 and 4.
- This step involved the injection of GST-KRAS-G12V at a concentration of 374nM in an acetate buffer with pH 4.5.
- The injection was carried out at a flow rate of 5µl/min, continuing until a response unit (RU) of 2000 was achieved in channel 2.
- To prevent non-specific binding, excess reactive sites on the dextran were blocked by injecting ethanolamine at a flow rate of 10 µl/min for 7 minutes.

Step 4: Immobilization of GST (Reference channel)

- As a reference control, GST was immobilized onto the dextran surface in channel 1.
- Similar to the previous step, GST was injected at a concentration of 1480nM, but this step was performed at a flow rate of 10µl/min for 3 minutes.
- A total of 1000 RUs were achieved.
- To minimize non-specific binding, excess reactive sites were also blocked with ethanolamine.

Step 5: Running Buffer Circulation

- Following the immobilization steps, the chip was prepared for the analysis, and the running buffer was continuously circulated within the chip.
- The composition of the running buffer was as follows:

NaCl 150 mM, Tris-HCl 50 mM (pH 7.6), and MgCl₂ 2mM

Injection of P14B and P1.3 after KRAS binding

Following the successful binding of KRAS to the dextran-coated surface, P14B and P1.3 were introduced in the system (refer to Figure 20, SPR steps) at various concentrations as specified in the results section. These injections were performed in a running buffer composed of 150 mM NaCl, 50 mM Tris-HCl (pH 7.5), 2mM MgCl₂, 0.1% Triton, and 5% DMSO. The flow rate during injection was set at 60µl/min, and the experiments were conducted at 25°C.

The dissociation phase was allowed to proceed for 10 minutes in the same buffer conditions. To ensure the reliability of the results, all runs were conducted in duplicate.

To eliminate nonspecific binding effects, we employed a subtraction method involving two linked channels (GST-KRAS-G12V minus GST). Furthermore, to assess the impact of different DMSO

concentrations (ranging from 3% to 8%) on the response units (RUs), a solvent correction was applied. This correction helped to reduce the errors associated with sample injection and provided more accurate data for the analysis.

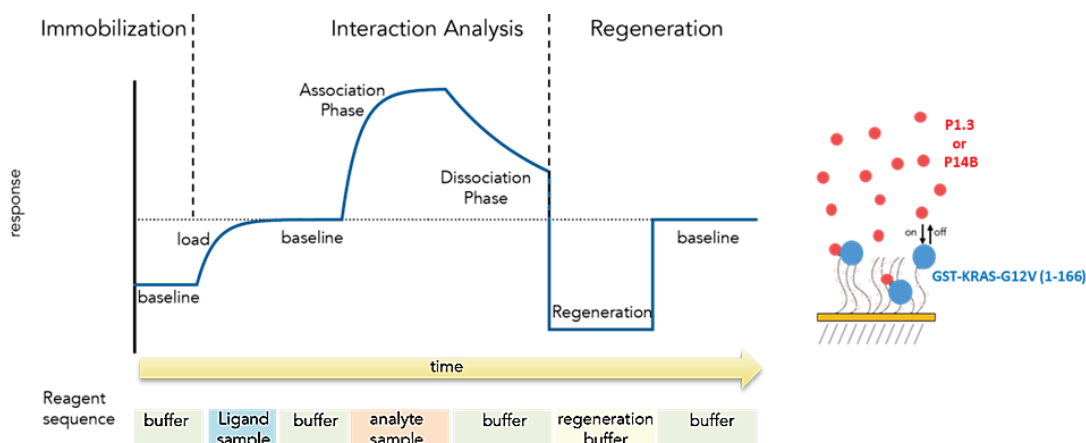


Figure 20: SPR protocol steps. Adapted from Centre for Macromolecular Interactions. (Harvard Medical School)

3.16 UltraID proximity-dependent biotinylation method

In brief, UltraID-KRAS-G12V vector was generated as detailed below and DLD-1 cells underwent transfection with this plasmid for a duration of 24 hours, following the protocol outlined in section 7.2. Subsequently, the cells were subjected to 24 hours of starvation and afterwards were treated with P14B for 1 hour, followed by exposure to biotin (Sigma # B4501) for 30 minutes as indicated in the Results section. Cells were then processed for streptavidin-pull down and LC-MC/MC or for immunofluorescence analysis as described hereunder.

Detailed description of the procedures:

3.16.1 Generation of the UltraID-KRAS-G12V vector

DH5 α *Escherichia coli* cells transformed with pCMV-C1-myc-UltraID or with mCherry KRAS-G12V were cultivated overnight in LB media, supplemented with 50 μ g/ml of ampicillin or 30 μ g/ml of kanamycin, respectively. Next, plasmids were isolated using the High Purity Miniprep Kit (Neo Biotech NB-03-0001) following manufacturer's instructions. DNA concentration was quantified using a nanodrop (ThermoFisher Scientific).

Polymerase chain reaction (PCR) amplification for the gene of interest, UltraID, was performed using a Fwd NheI AgeI myc-BioID C1 v2 primer initial forward oligonucleotide:

(5'-tccgctagcgctaccggtagccaccatggaacaaaaac-3') and

a Rev UltraID-C1 BsrGI primer terminal reverse oligonucleotide:

(5'-gagtcggaactgtacagcttctcctgaacttc-3').

PCR was conducted using the MyFi DNApol kit (Bioline-21117) with the following reaction and PCR program:

Table 9: PCR reaction.

	[Stock]	[Working]	Volume
MyFi PCR Buffer	5X	1X	5µl
pCMV-C1-myc--UltraID			0.1µl
Fwd BioID N1 AgeI*	10µM	0.4µM	1µl
Rev UltraID-C1 BsrGI	10µM	0.4µM	1µl
MyFi DNApol			1µl
H₂O DNase free	To 25µl		17µl

*Fwd BioID N1 AgeI: 100% compatible with UltraID sequence

Table 10: PCR program.

Initial denaturation	95°C	1 min	
Denaturation	95°C	15 min	
Annealing	49.3°C	15 min	30 cycles
Extension	72°C	45 sec	
Final extension	72°C	5 min	

Afterward, the PCR product underwent purification using the Macherey-Nagel NucleoSpin Gel and PCR Clean-Up Kit (Macherey-NAGEL 740609.50).

After the purification step, 2 µg each of the PCR product (UltraID) and the mCherry KRAS-G12V vector were subjected to digestion with AgeI and BsrGI for a duration of 2 hours at 37°C, employing the reaction specified in the table below. Vector was also single digested with restriction enzymes as control:

Table 11: Digestion reaction.

	[Stock]	[working]	PCR pCMV-C1-myc-UltraID	Vector (mCherry KRAS-G12V)	Vector (mCherry KRAS-G12V) CT* Agel	Vector (mCherry KRAS-G12V) CT* BsrGI
Backbone vector	-	2 µg	40 µl	3.68 µl	3.68 µl	3.68 µl
Buffer 2.1	10X	1X	5 µl	5 µl	5 µl	5 µl
Agel NEB	10U/µl	5U	0.5 µl	0.5 µl	0.5 µl	-
BsrGI	10U/µl	5U	0.5 µl	0.5 µl	-	0.5 µl
BSA	100X	1X	0.5 µl	0.5 µl	0.5 µl	0.5 µl
MilliQ H₂O	To 50 µl		3.5 µl	39.8 µl	40.3 µl	40.3 µl

*CT: Control.

Next, the resulting digested products underwent electrophoresis in a 1% agarose gel at 100V for 30 minutes (see Figure 46C in Results section). Subsequently, gel plugs containing the anticipated DNA bands were excised, and the DNA was extracted using the Macherey-Nagel NucleaSpin Gel and PCR Clean-Up Kit (Cat. No. 740609.50).

The purified DNA was then subjected to an overnight ligation at 4°C, employing the following reaction:

Table 12: DNA ligation reaction

	[Working]
mCherry KRAS-G12V Vector	20 fmol
pCMV-C1-myc-UltraID insert	120 fmol
Buffer ligase 10X	1X
ATP (10mM)	1mM
T4DNA ligase	1 µl
MilliQ H₂O	To 15 µl

Following this, 50 µl of DH5α competent bacteria (ThermoFisher Subcloning Efficiency DH5α Competent Cells, Cat. No. 18265-017) underwent transformation with 5 µl of the ligation product, adhering to the usual protocol. The transformed cells were then plated on kanamycin-resistant LB

plates overnight. Positive colonies were cultivated and cryopreserved for use in upcoming experiments.

Cloning procedure was verified in a 1% agarose gel at 100V for 30 minutes using the purified UltraID-KRAS-G12V vector (see Figure 46D in Results section) and plasmid was sequenced.

3.16.2 Streptavidin-pull down

Cell lysis

Cells (in p100 plate) expressing Myc-UltraID-KRAS-G12V and incubated or not with biotin as indicated in the Results section were washed three times with 10 ml 1X PBS to remove any excess biotin present in the culture medium. Next, 500 µl of Cell Lysis Buffer were added to each plate and lysates were transferred to pre-chilled 1.5 ml microfuge tubes. Then, 200 µl of 2% Triton-X100 were added, mixed well by pipetting and incubated for 30 minutes at 4°C by end-to-end rotation. After that time, 700 µl of chilled 50 mM Tris pH 7.5 were added and mixed by repeated pipetting. Subsequently, the lysates were subjected to centrifugation at 12,500g for 20 minutes at 4°C and the supernatants were transferred to new pre-chilled 2 ml microfuge tubes.

Lowry protein quantification was performed (see section 8.2) to ensure an equal amount of total protein between samples when incubated with streptavidin beads (Dynabeads My one streptavidin C1 Beads (Thermofisher #65001)). A minimum of 1 mg of total protein was required to be incubated with the beads.

Streptavidin beads preparation and incubation with the cell lysates

Streptavidin, a tetrameric protein with a molecular weight of 66 kDa, is purified from the bacterium *Streptomyces avidin* and demonstrates a notable binding affinity to biotin, with each unit capable of binding one biotin molecule. Streptavidin bound magnetic beads are commonly used to pull down biotinylated proteins from cell lysates.

Immediately following the aforementioned cell lysis step, the streptavidin magnetic beads were transferred to fresh 1.5 ml microfuge tubes at a volume of 50 µl per sample. The tubes were then subjected to a 3-minute incubation on a magnetic stand at RT, after which the clear solution was discarded. Subsequent to removal from the magnetic stand, the beads were equilibrated by adding 1 ml of Cell Lysis Buffer, and an end-to-end rotation was carried out for 5 minutes at RT. The tubes were then placed on the magnetic stand once more and incubated for an additional 3 minutes. Following

this step, the lysis buffer was discarded, and the sample lysates were transferred into new 1.5 ml microfuge tubes containing the previously equilibrated beads. The beads-lysate mixtures were incubated overnight at 4°C with end-to-end rotation.

Streptavidin-pull down of the biotinylated proteins

All steps were performed at RT unless indicated otherwise. The tubes containing the streptavidin beads-lysate mixtures were incubated on the magnetic stand for 5 minutes, and the lysates were carefully discarded without disturbing the beads. Next, the beads were washed by adding 1 ml of Wash Buffer 1 followed by end-to-end rotation for 5 minutes. The mixture was then incubated on the magnetic stand for 3 minutes, and the buffer 1 was carefully removed with a micropipette. Subsequently, the beads were washed by adding 1 ml of Wash Buffer 2, followed by end-to-end rotation for 5 minutes. The mixture was incubated on the magnetic stand for 3 minutes, and the buffer 2 was carefully removed with a micropipette. This washing process was repeated with 1 ml of Wash Buffer 3 with end-to-end rotation for 5 minutes, followed by incubation on the magnetic stand for 3 minutes. The buffer 3 was carefully removed with a micropipette. Finally, the beads were washed by adding 1 ml of 50 mM Tris pH 7.5, followed by end-to-end rotation for 5 minutes. The mixture was incubated on the magnetic stand for 3 minutes, and the Tris buffer was carefully removed with a micropipette.

Confirming the specific biotin-ligase activity of the Myc-UltraID-KRAS-G12V fusion protein expressed by the cells

Before conducting the LC-MS/MS analysis of the beads, a control test was performed in order to verify the presence of biotinylated proteins specifically pulled down by the beads, and thus to confirm that the Myc-UltraID-KRAS-G12V fusion protein expressed in the cells had biotin ligase activity. With this aim, the biotinylated proteins bound to the streptavidin beads were eluted and resolved by SDS-PAGE followed by streptavidin-HRP blotting analysis. The HRP-conjugated streptavidin is also particularly valuable for the precise detection and quantification of biotinylated proteins within a sample.

For this, 50 µl of Laemmli Sample Buffer 2X supplemented with 2 mM biotin were added to the beads obtained in the previous section and mixed by pipetting up and down five times using a cut 200 µl pipette tip. The beads were then heated at 90°C in a pre-heated heating block for 5 minutes to help to release the proteins bound to the beads. Following, the tubes were placed on the magnetic stand for

5 minutes. Subsequently, the eluate was transferred to a pre-chilled 1.5 ml microfuge tube and immediately frozen on dry ice for further analysis.

1. Approximately 5 to 10 μ l of each thawed eluate from each tube per condition were loaded onto a 10% SDS-polyacrylamide gel. Proteins were resolved by SDS-PAGE and electro-transferred to a blotting membrane.
2. The membrane was incubated in BSA Blocking Buffer for 1 hour at RT.
3. To detect biotin-labelled proteins, the membrane was incubated with streptavidin-HRP, which was diluted 1:30,000 in BSA Blocking Buffer, for 1 hour at RT.
4. The membrane was washed three times in 1X TBS-T, each time for 10 minutes at RT.
5. The membrane was processed for chemiluminescence detection through digital acquisition.

3.16.3 Liquid chromatography–mass spectrometry analysis (LC-MS/MS)

The streptavidin beads bound to the biotinylated proteins obtained in section 3.16.2 were washed twice with 100 mM ammonium bicarbonate at pH 8, undergoing end-to-end rotation for 5 minutes during each wash cycle. Subsequently, they were incubated on the magnetic stand for 3 minutes, and the supernatant was discarded. Following this, the beads were incubated with 5 mM DTT in 50 mM ammonium bicarbonate (ABC) at pH 8 for 30 minutes at 60°C and then cooled to room temperature. The magnetic stand was used for a 3-minute incubation, and the supernatant was discarded. The beads were then incubated with 3.75 mM IAA (iodoacetamide) in 50 mM ammonium bicarbonate at pH 8 and left in the dark for 20 minutes. Following this step, two washes with 50 mM ammonium bicarbonate (NH_4HCO_3) at pH 8 were conducted. The beads were manually digested. Briefly, proteins were reduced (DTT 200mM; 1h, 32°C) and alkylated (iodoacetamide 25mM; at RT for 30 min, in the dark). Afterwards, the samples were digested for 2 hours with trypsin (Sequence grade modified porcine trypsin, Promega; pH 8, 32°C) using 200ng of the enzyme and were then cleaned up with a C18 tip (ZipTip) as per manufacturer's protocol. Finally, the cleaned-up peptide solutions were deide-down and stored at -20°C until the LCMS analysis. These steps were performed in the Proteomics Unit, *Centres Científics i Tecnològics de la Universitat de Barcelona (CCiTUB)*.

3.16.4 Data analysis of the biotinylated proteins detected by LC-MS/MS

The samples underwent analysis by LCMS in the cutting-edge Orbitrap Fusion Lumos (CRG platform), employing a precisely calibrated 60-minute gradient. To ensure rigorous quality control, BSA controls

were concurrently digested and interleaved between sample runs to mitigate any potential carryover effects and meticulously evaluate instrument performance. Subsequently, the samples were interrogated against the SwissProt Human database (April 2023 edition) utilizing the Mascot v2.6 search algorithm (<http://www.matrixscience.com/>). Redundant protein identifications were automatically grouped using the built-in algorithm of Protein Discoverer. Peptides were filtered based on a stringent false discovery rate (FDR) criterion, with only those exhibiting an FDR below 1% being retained for further analysis.

For the subsequent data analysis, the SAINT software, and Proteome Discoverer 2.5 (PD) were employed to quantify, normalize the protein abundance, and compare their abundance between samples. PD is a commercial product of Thermo Fisher Scientific (Orsburn, 2021). Significance Analysis of INteractome (SAINT) is specifically designed for scoring protein-protein interactions in label-free quantitative proteomics data derived from affinity purification–mass spectrometry (AP-MS) experiments. Its robust functionality allows for the unbiased selection of authentic interactions while effectively eliminating nonspecific interactions (Teo et al., 2014).

The raw data files obtained in the mass spectrometry analyses were also visualized in PD (V2.5) and exported to Excel a list of identified proteins. The results have been filtered so only proteins identified with at least 2 peptides (and with $FDR \leq 5\%$) are included in the lists.

Cytoscape, a general-purpose modelling environment for integrating biomolecular interaction networks and states (Shannon et al., 2003) was used to analyse the physical and functional interaction of the differentially biotinylated proteins.

3.17 Immunofluorescence technique

After transfecting cells growing in glass coverslips, the following steps were performed: first, the cells were washed three times with PBS to eliminate any residual transfection reagents. Subsequently, the cells were fixed with 4% paraformaldehyde (PFA) in PBS for 10 minutes (for P60 plates, 3ml of fixative was added). Three more PBS washes were carried out to ensure complete PFA removal. Next, the cells were permeabilized with 0.2% Triton X-100 for 15 minutes. A blocking step was performed by incubating the cells in a solution of 1% BSA prepared in 0.1% Triton X-100 in PBS for 30 minutes. The cells were subsequently incubated with the primary antibody (anti-myc) for 1 hour, with the antibody prepared in a solution containing 1% BSA and 0.3% Triton X-100, at a 1:8000 dilution. Following another round of triple PBS wash, the cells were incubated with a fluorescent-labelled secondary antibody

(anti-mouse, Alexa Fluor 488) for 1 hour at 37°C, using a 1:500 dilution in PBS and 0.1% BSA. After the final round of PBS washes, the cell nuclei were stained with 1:5000 DAPI (1mg/ml) for 5 minutes, with 500µL added to each coverslip. The process was concluded with three PBS washes, followed by three washes with H₂O. Finally, the coverslip was affixed to slides using 6µL of Mowiol to complete the procedure. Confocal sections of the cells were obtained with the LSM880 confocal microscope (ZEISS).

3.18 Effect of P1.3 on orthotopic mice

3.18.1 Determination of the Maximum Tolerated Dose (MTD) of P1.3 in athymic mice

The aim of this study was to determine the MTD of P1.3 in healthy athymic mice.

A. Animals

- Species: *Mus musculus*
- Strain: Athymic Nude-Foxn1nu
- Age: 6-8 weeks
- Sex: Female
- Body weight: 22-24 g
- Animal supplier: Envigo

B. Housing conditions

Mice were housed in laminar flow rooms, maintaining a constant temperature (20-24°C) and humidity, with 5 animals per cage. The cages, made of polycarbonate, measured 300 mm x 180 mm x 150 mm; and the bedding material, corn cob, was changed weekly.

Throughout the entire study period, animals had free access to irradiation-sterilized dry food. They also had unrestricted access to sterile drinking water.

Cage identification involved labelling each cage with information such as the number of animals, sex, strain, arrival date, treatment, study number, group number, and the start date of the treatment.

Animal identification was achieved through ear coding.

C. Drug preparation

A 10% DMSO in serum solution was prepared for the vehicle, and once dissolved, it was stored at -20°C.

Intraperitoneal injections (IP) were administered.

For Dose A, a preparation of 0.750 mg of P1.3 was made with 0.750 ml of DMSO, resulting in a concentration of 1 mg/ml. The administered dose was 10 mg/kg, with a volume of 10 ml/kg.

For Dose B, a preparation of 1.5 mg of P1.3 was made with 0.750 ml of DMSO, resulting in a concentration of 2 mg/ml. The administered dose was 20 mg/kg, with a volume of 10 ml/kg.

For Dose C, a preparation of 3 mg of P1.3 was made with 0.750 ml of DMSO, resulting in a concentration of 4 mg/ml. The administered dose was 40 mg/kg, with a volume of 10 ml/kg.

D. Ethical observations

All procedures related to animal handling, care, and treatment in this study were conducted in accordance with the guidelines approved by the Ethical Committee of Animal Experimentation of the *Parc Científic de Barcelona* (PCB). The procedure applied was number 9928-P1 and received approval from the *Generalitat de Catalunya* (IP: Alberto Villanueva).

A. Experimental design

A set of 9 athymic mice was randomized into three homogeneous groups (n=3) to receive different treatments. At the specified time points, we collected blood samples from the mice's tail veins. The blood was utilized to separate plasma, and the plasma was maintained at 20°C.

Table 13: Treatment details for each group.

Group	N	Treatment	Dose	Duration	Blood sampling
A	3	P1.3	10 mg/Kg	Once	1h, 12h, 24h, 48h
B	3	P1.3	20 mg/Kg	Once	1h, 12h, 24h, 48h
C	3	P1.3	40 mg/Kg	Once	1h, 12h, 24h, 48h

3.18.2 Repeated dose toxicity of P1.3 in athymic mice

The aim of this study was to determine the repeated dose toxicity of intraperitoneal P1.3 (20 mg/kg, 5 days/week, 3 weeks) in healthy athymic mice.

A. Animals, house conditions and ethical observations were the same as described before.

B. *Drug preparation* P1.3 drug (30 mg) was dissolved in DMSO, achieving a stock concentration of 40 mg/ml. For the dosing solution, the stock was diluted 1:20 in saline, resulting in a concentration of 2 mg/ml (Dose: 20 mg/kg, volume: 10 ml/kg). The vehicle was prepared as 5% DMSO in saline.

C. *Experimental endpoints*

Mice underwent continuous monitoring of behaviour, body weight, and overall well-being throughout the treatment period. The relative body weight was determined using the formula:

$$\text{Relative body weight (\%)} = \left[\frac{\text{Body weight Day X}}{\text{Body weight Day 1}} \right] \times 100$$

The percentage of weight loss was then calculated as 100–Relative body weight. Ethical endpoint criteria for the experiment included weight loss exceeding 15% of the total body weight or any manifestation of distress. Notably, these criteria were not met in any instance during the course of the experiment.

4. RESULTS

4.1 CHAPTER 1

Characterisation of the peptidomimetic P1.3 as KRAS inhibitor

4.1.1 BACKGROUND AND PREVIOUS DATA

The elevated mutation frequency observed in KRAS, coupled with its pivotal involvement in human oncogenesis and in conferring resistance to cancer therapies, has instigated the pharmacologic interventions designed to impede mutant KRAS (Stalneck & Der, 2020).

Recently, methodological advances and new technologies developed with the aim of searching for KRAS direct inhibitors have had encouraging outcomes. One of the followed strategies has been to search for drugs able to disrupt the interaction of KRAS with its effectors (O'Bryan, 2019). In this sense, researchers have shed the light to the great potential of targeting protein-protein interactions (PPIs) as an intervention target for novel treatment of refractory disease such as cancer and it is widely regarded as a promising strategy in drug discovery (Hill et al., 2014; Nevola & Giralt, 2015).

However, because of the nature of the PPIs involved, regulation of these interactions is complicated, and some challenges in discovering PPIs modulators have arisen. The PPIs modulation through small molecules mainly focuses on protein-ligand interactions such as enzymes, ions, channels or receptors, because these proteins normally contain well-defined ligand-binding sites where small molecules generally fit with (Santos et al., 2016). Though, PPIs modulation through small molecules is generally considered difficult because of multiple reasons. First, the PPIs occur on the interface of a specific domain where two identical or different proteins are in contact (Gestwicki & Smith, 2012), and the complication is that this interface area of the interaction is larger than that of receptor-ligand contact area, and besides that the interface is highly hydrophobic (A. Cheng et al., 2007). Second, the flattened PPIs interface tends to have few pockets making it difficult for the designed small molecules to bind (Díaz-Eufracio et al., 2018). Third, the amino acid residues involved in PPIs are either continuous or discontinuous in their respective protein structures, thus results in high-affinity binding between the proteins, making it difficult for the small molecules to inhibit such high-affinity interaction (Ivanov et al., 2013). Accordingly, an alternative to small molecules should be considered, among them, peptides containing modified amino acids or chemical modifications named peptidomimetics, which show interesting advantages. Concretely, they have improved biological properties (Kuppusamy et al., 2019) and they are designed to be metabolically stable, bioavailable, and high selective. These qualities allow to overcome the challenge appeared with the synthesis and the purification of therapeutic peptides that are not straightforward because of low yields, chemical instability, hydrolysis, and short-half life.

Moreover, peptides are typically disordered and susceptible to proteolytic degradation, resulting in low binding affinities.

I. Generation of peptidomimetics designed to interfere with the interaction of Ras with its effectors

Virtual screening of RAS inhibitors: Virtual screening of chemical database through molecular docking protocols can help find novel potential leads suitable for further development (Cai et al., 2011; Liao et al., 2011). In our group, two molecular docking experiments were carried out using the SMINA docking program to identify and optimize novel inhibitors of RAS protein.

Based on the screening, a virtual library of 80,000 tri- and tetra-peptidomimetics containing at least one positively charged and both natural and non-natural amino acids in their structure was generated *in silico*. The peptidomimetics dataset was docked into RAS effector binding region around the substrate binding site previously identified; these were subsequently ranked according to the corresponding docking energy and finally filtered on the basis of their geometric and energetic properties. After filtering, a total of nine compounds were selected based on their favourable binding stability to RAS protein and cell membrane permeability, as well as their optimal overall binding mode (Table 14). As shown in Figure 21, the nine hit compounds share similar binding modes.

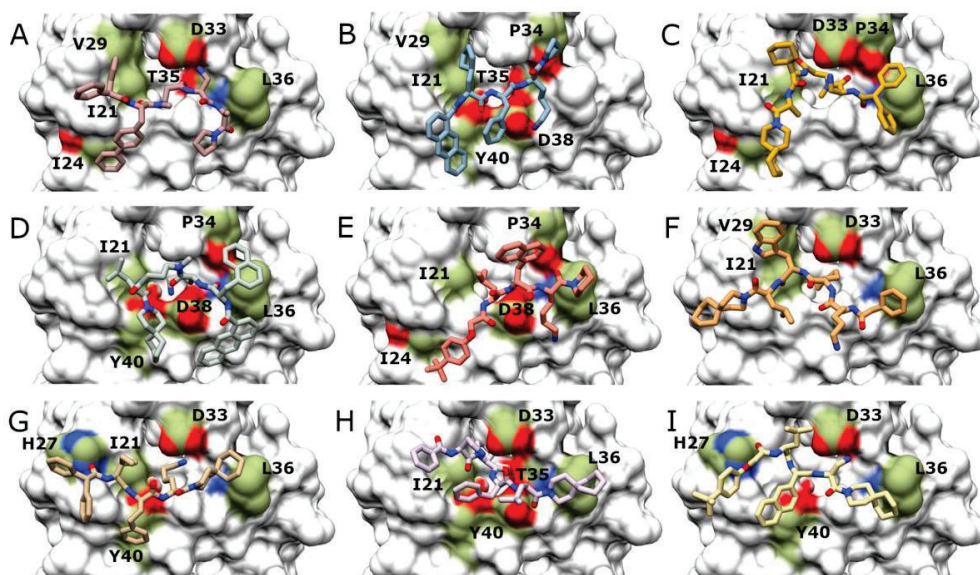
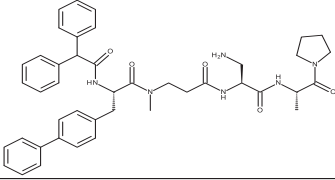
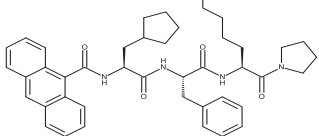
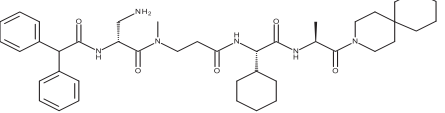
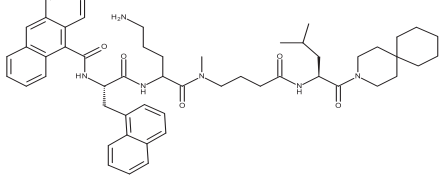
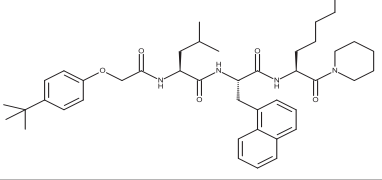
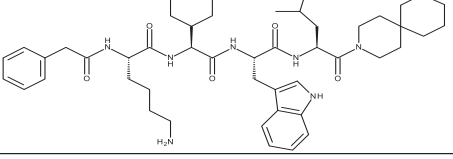
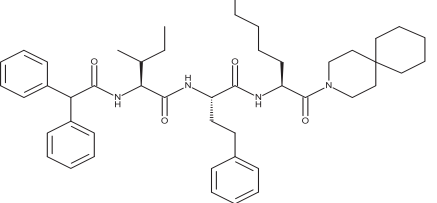
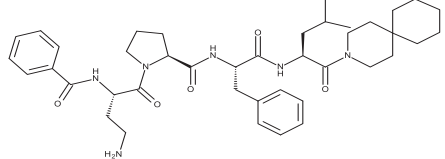
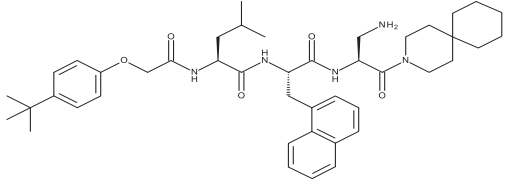


Figure 21: Peptidomimetic characteristics. *In silico* predicted binding modes of (A) P1, (B) P2, (C) P3, (D) P4, (E) P5, (F) P6, (G) P7, (H) P8 and (I) P9. Contact point residues on the RAS surface (PDB code 5P21) are shown in colour on the RAS protein surface: aliphatic areas are shown in green, areas with amino groups in blue and areas

containing carboxylic moieties in red. RAS residues involved in contact with the compounds are named using the one letter amino acid code; the residue number is shown next to the letter. *Extracted from* (Pallara et al., 2022).

Table 14: First set of inhibitors, docking scores and PASA. Modified from (Pallara et al., 2022).

Compound	Formula	Structure	Docking Score (Kcal/mol)	PASA (Å ²)
P1	C ₄₃ H ₅₁ N ₆ O ₅		-10,2	128
P2	C ₄₂ H ₅₂ N ₅ O ₄		-9,7	93
P3	C ₄₂ H ₆₁ N ₆ O ₅		-9,6	105
P4	C ₅₄ H ₆₉ N ₆ O ₅		-9,1	123
P5	C ₄₂ H ₆₀ N ₅ O ₅		-8,9	111
P6	C ₄₉ H ₇₂ N ₇ O ₅		-8,4	116
P7	C ₄₆ H ₆₄ N ₅ O ₄		-8,4	86
P8	C ₄₁ H ₅₉ N ₆ O ₅		-8,3	133
P9	C ₄₄ H ₆₂ N ₅ O ₅		-8,0	104

II. Biological effect of peptidomimetics that bind to RAS effector domain.

The detailed findings presented in Debora Cabot's Doctoral Thesis (2020) delineate the primary aim of investigating the effect of peptidomimetics targeting the RAS effector domain on RAS signalling following EGF activation. Initial experimentation involved treating hTERT-RPE serum-starved cells with selected peptidomimetics (50 μ M) for 2 hours, followed by EGF stimulation for 10 minutes. Notably, Figure 22A revealed that P1 and P8 efficiently inhibited RAF and ERK activation, while P1 and P3 induced significant reduction in the PI3K signalling pathway by inhibiting AKT activation. Subsequent investigations focused on identifying the most effective peptidomimetics for further study at lower concentrations. Figure 22B illustrated that P1 emerged as the most efficient in diminishing RAS signalling through multiple pathways in non-transformed cells. Mechanistic insights revealed that these inhibitory effects were attributed to blocking KRAS-effector binding, validated through co-immunoprecipitation (co-IP) assays (Figure 22C). Further exploration involved docking and selection of four P1 derivatives based on *in silico* binding stability and cell membrane permeability, with Figure 22D showing that P1.3 was the most effective in reducing P-RAF, P-ERK, and P-AKT levels. Notably, P1.3 disrupted the interaction between KRAS-G12V and its effectors CRAF and PI3K, as demonstrated in Figure 22E. Viability assays conducted on six PDAC cell lines with various oncogenic KRAS mutations, as illustrated in Figure 22F, revealed that P1.3 exhibited a remarkable ability to reduce cell viability, with an IC₅₀ of approximately 20 μ M, while showing minimal impact on normal cells. Although the specific mechanism of P1.3-induced cell death in PDAC cells requires further elucidation, these findings suggest its potential as a targeted therapeutic agent against pancreatic tumours with oncogenic KRAS mutations, sparing normal cells from adverse effects.

Based on the antecedent experimental outcomes, P1.3 emerges as a prospective candidate for direct therapeutic intervention targeting KRAS, recognising the significance of deepening the knowledge of the binding interaction between P1.3 and KRAS, along with assessing its impact in murine model. The results presented in this thesis, as outlined below, provide valuable insights into the ongoing investigation of this topic.

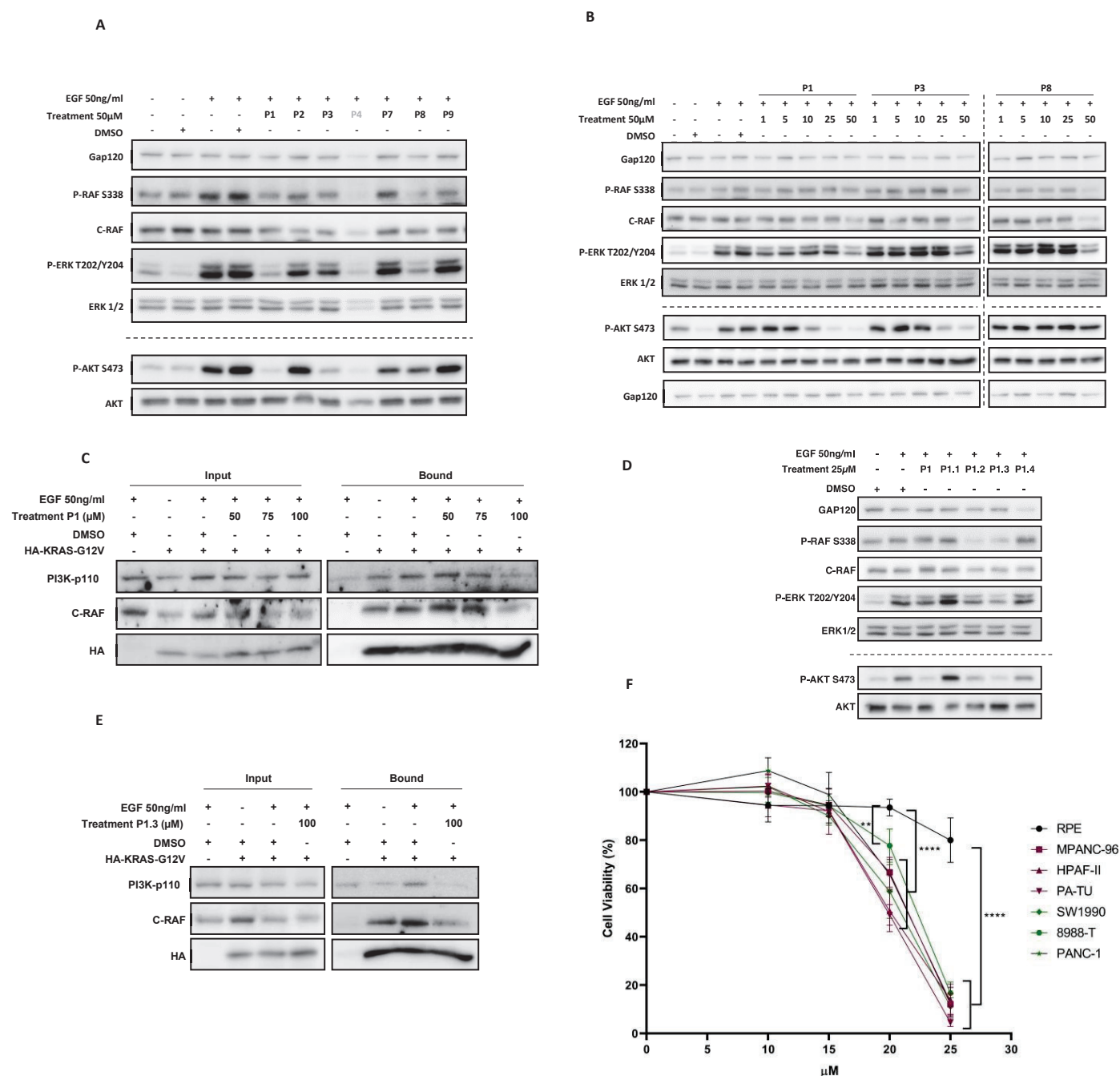


Figure 22: Biological effect of peptidomimetics that bind to RAS effector domain. (A) Effect of the indicated peptidomimetics on RAS signalling pathways. (B) The same analyses were performed as in (A) but incubating the cells with the indicated peptidomimetics in a range from 1, 5, 10, 25 and 50μM. (C) Co-IP of HA-KRAS-G12V with CRAF or with PI3K was analysed in starved Hela cells expressing HA-KRAS-G12V after being incubated with P1 (in a range from 50, 75 and 100μM) for 2 h, and EGF-stimulation for 10 min. (D) hTERT-RPE starved cells were incubated with 25μM of the indicated peptidomimetics for 2h and the activation of RAF/MEK/ERK and PI3K/AKT pathways after EGF stimulation for 10 min was studied by WB. (E) The same analyses as in (C) were done but

incubating the cells with 100 μ M of P1.3. (F) Effect of P1.3 on the cell viability of six PDAC cell lines (all harbouring oncogenic KRAS mutations) and on a non-transformed cell line (hTERT-RPE).

4.1.2 RESULTS

4.1.2.1 Analysing the levels of RAS-GTP upon P1.3 treatment.

As P1.3 showed high ability to inhibit RAS signalling, compatible with its effect on disrupting the binding capacity of KRAS with its main effectors CRAF and PI3K, in order to reinforce these results, an active RAS detection assay (RBD pull-down) was performed to check the cellular levels of RAS-GTP. Serum starved hTERT-RPE cells were treated for 2h with P1.3 followed by EGF activation for 10 min. RBD pull-down assay showed that the levels of RAS- GTP were not modified by P1.3 treatment of the cells (Figure 23) in agreement with the fact that the action of the peptidomimetic was to inhibit the interaction of RAS with its effectors.

Therefore, the observed decrease in P-CRAF, P-ERK and P-AKT levels were accounted by inhibition of KRAS-CRAF and KRAS-p110 α PI3K interactions.

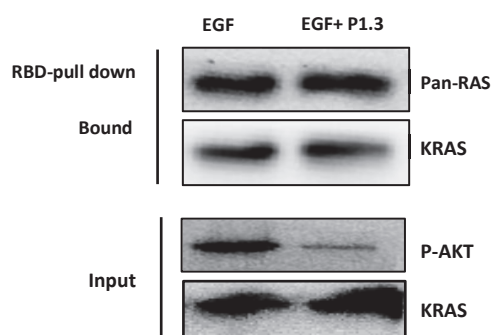


Figure 23: P1.3 treatment does not affect KRAS-GTP levels. Serum starved hTERT-RPE cells were preincubated or not with 25 μ M of P1.3 for 2h and then treated for 10 min with EGF. Cells were lysed and the RAS-GTP levels were determined by RBD-pull down as indicated in the methods section. P-AKT was also analysed in the input to confirm the inhibitory effect of P1.3 in this specific experiment.

4.1.2.2 Studying the direct interaction of P1.3 with KRAS-GTP by surface plasmon resonance (SRP).

To confirm the direct interaction between KRAS and P1.3, SRP analysis was performed. Purified GST-KRAS-G12V (amino acids 1 to 166) was immobilized and then GTP-loaded. After using different concentrations of P1.3 as the analyte, an affinity constant (KD) of 15.7 μ M of P1.3 for GTP-loaded KRAS was determined (Figure 24), while no stable sensorgrams could be obtained when analysing the interaction between KRAS-GDP and P1.3. These data further confirmed that, according to the initial design, P1.3 was directly interacting with RAS in its GTP loaded conformation.

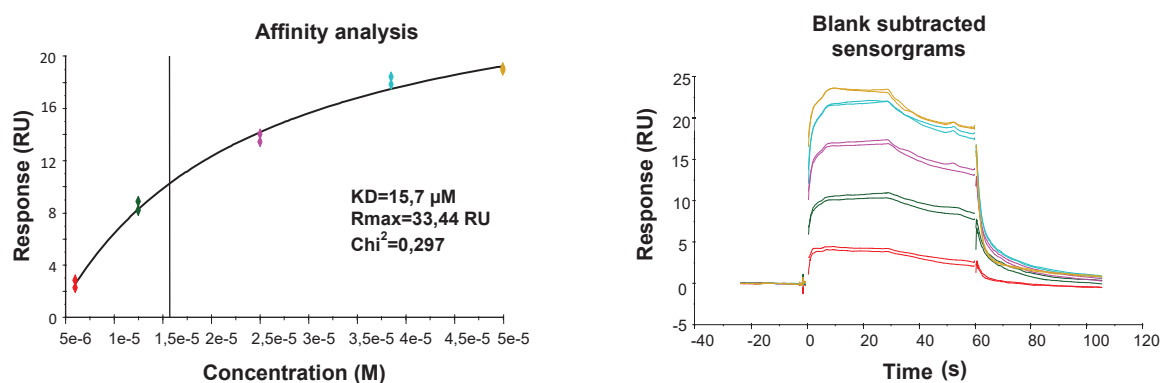


Figure 24: Direct interaction between KRAS-GST and P1.3 determined by SPR. Affinity analysis (left) and sensorgrams (right) were determined as indicated in the Methods section. (KD: dissociation constant). Colours in both graphs correspond to the same concentrations of P1.3.

4.1.2.3 Toxicity profile assessment of P1.3 in athymic mice

I. Determination of the Maximum Tolerated Dose (MTD) of P1.3 in athymic mice.

In order to study the antitumour efficacy of P1.3 in orthotopic xenograft model of pancreatic cancer, first we aimed to determine the maximum tolerated dose (MTD) of P1.3 in a healthy athymic mice (partially executed in Xenopat Company). A set of 12 athymic mice were distributed in four homogenous groups (n=3) to receive different concentrations of P1.3 as indicated in Table 15.

Table 15. Treatment detail for each group

Group	N	Treatment	Dose	Schedule	Route	Blood sampling*
A	3	Vehicle	-	Once	IP	1h, 12h, 24h, 48h
B	3	P1.3	10 mg/Kg	Once	IP	1h, 12h, 24h, 48h
C	3	P1.3	20 mg/Kg	Once	IP	1h, 12h, 24h, 48h
D	3	P1.3	40 mg/Kg	Once	IP	1h, 12h, 24h, 48h

*Mice from group A were injected 5 days later than all other mice. In all cases, the day of injection was considered day 0. N: number of mice; IP: intraperitoneal.

After injection, mice body weight was monitored during at least 10 days (Figure 25, Table 16).

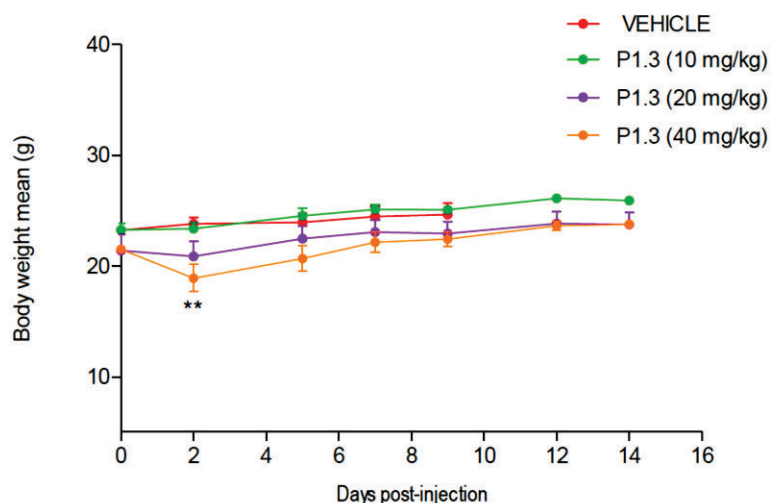


Figure 25: Mice body weight mean after P1.3 treatment. Statistically significant differences in body weight were found between groups (two-way RMANOVA test, * $p=0.031$). Bonferroni post-hoc test detected statistically significant differences between vehicle and P1.3 (40mg/kg) (** $p<0.01$) on day 2 after treatment.

In terms of local toxicity, no evidence of pain/distress was observed after intraperitoneal injection of vehicle, P1.3 at 10mg/kg or P1.3 at 20 mg/kg, however, injection of P1.3 at 40mg/kg induced some distress in mice that suggested pain/irradiation into the injection site.

In terms of systemic toxicity, P1.3 at 40mg/kg induced a significant reduction of mice body weight (>10%) after 48h of injection, that was recovered during the following few days as indicated in Figure 26 and Table 17.

Table 16: Body weight (g)

	Days post-injection							ID
	0	2	5	7	9	12	14	
P1.3 (10 mg/kg)	22,1	22,5	23,6	24,9	25,0	26,4	26,1	A1
	23,9	23,3	25,8	25,9	24,9	25,8	25,8	A2
	23,8	24,3	24,2	24,5	25,3	26,1	25,8	A3
Mean	23,3	23,4	24,5	25,1	25,1	26,1	25,9	
SD	1,0	0,9	1,1	0,7	0,2	0,3	0,2	
P1.3 (20 mg/kg)	23,1	22,4	24,0	24,6	24,6	25,7	25,6	A4
	18,6	18,2	20,2	21,0	21,0	22,1	21,7	A5
	22,5	22,0	23,2	23,6	23,2	23,7	23,9	B1
Mean	21,4	20,9	22,5	23,1	22,9	23,8	23,7	
SD	2,4	2,3	2,0	1,9	1,8	1,8	2,0	
P1.3 (40 mg/kg)	22,1	21,3	22,9	23,8	23,6	24,1	24,2	B2
	21,2	17,4	19,1	20,7	21,3	22,8	23,1	B3
	21,2	18,0	20,0	21,9	22,4	24,0	24,0	B4
Mean	21,5	18,9	20,7	22,1	22,4	23,6	23,8	
SD	0,5	2,1	2,0	1,6	1,2	0,7	0,6	
VEHICLE*	23,3	24,6	25,4	26,3	26,7			B5
	22,6	22,7	22,6	23,6	23,8			C1
	23,8	24,1	23,8	23,5	23,4			C2
Mean	23,2	23,8	23,9	24,5	24,6			
SD	0,6	1,0	1,4	1,6	1,8			

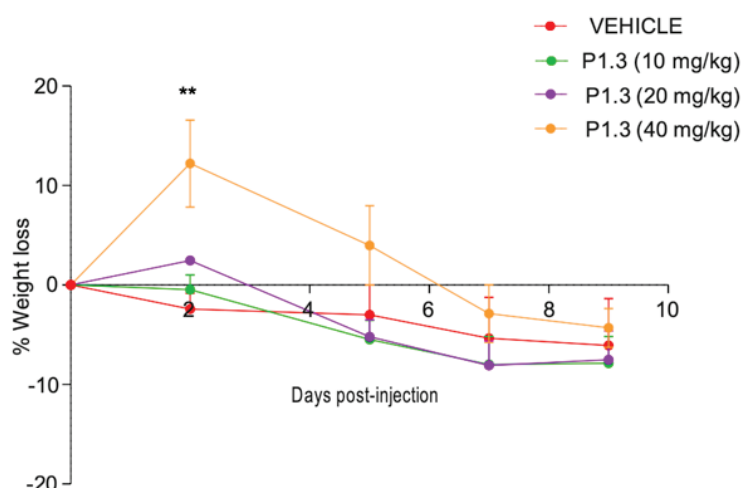


Figure 26: Percentage of mice body weight loss after treatment. Statistically significant differences in body weight were found between groups (two-way RMANOVA test, $*p=0.025$). Bonferroni post-hoc test detected statistically significant differences between vehicle and P1.3 (40mg/kg) ($**p<0.01$) on day 2 after treatment.

Table 17. Percentage of body weight loss (%)

	Days post-injection					ID
	0	2	5	7	9	
P1.3 (10 mg/kg)	0,0	-1,8	-6,8	-12,7	-13,1	A1
	0,0	2,5	-7,9	-8,4	-4,2	A2
	0,0	-2,1	-1,7	-2,9	-6,3	A3
Mean	0,0	-0,5	-5,5	-8,0	-7,9	
SD	0,0	2,6	3,3	4,9	4,7	
P1.3 (20 mg/kg)	0,0	3,0	-3,9	-6,5	-6,5	A4
	0,0	2,2	-8,6	-12,9	-12,9	A5
	0,0	2,2	-3,1	-4,9	-3,1	B1
Mean	0,0	2,5	-5,2	-8,1	-7,5	
SD	0,0	0,5	3,0	4,2	5,0	
P1.3 (40 mg/kg)	0,0	3,6	-3,6	-7,7	-6,8	B2
	0,0	17,9	9,9	2,4	-0,5	B3
	0,0	15,1	5,7	-3,3	-5,7	B4
Mean	0,0	12,2	4,0	-2,9	-4,3	
SD	0,0	7,6	6,9	5,0	3,4	
VEHICLE*	0,0	-5,6	-9,0	-12,9	-14,6	B5
	0,0	-0,4	0,0	-4,4	-5,3	C1
	0,0	-1,3	0,0	1,3	1,7	C2
Mean	0,0	-2,4	-3,0	-5,3	-6,1	
SD	0,0	2,8	5,2	7,1	8,2	

Additionally, within the scope of the study described in the Materials and Methods section, diverse concentrations of P1.3 were monitored in mice plasma over time via mass spectrometry. The findings illustrated that P1.3 exhibited a brief retention time in the plasma, regardless of the specific concentrations used, as depicted in Figure 27.

P1.3 in blood Maldi787.44 150 ppm ug/ml (standard curve with mice serum)

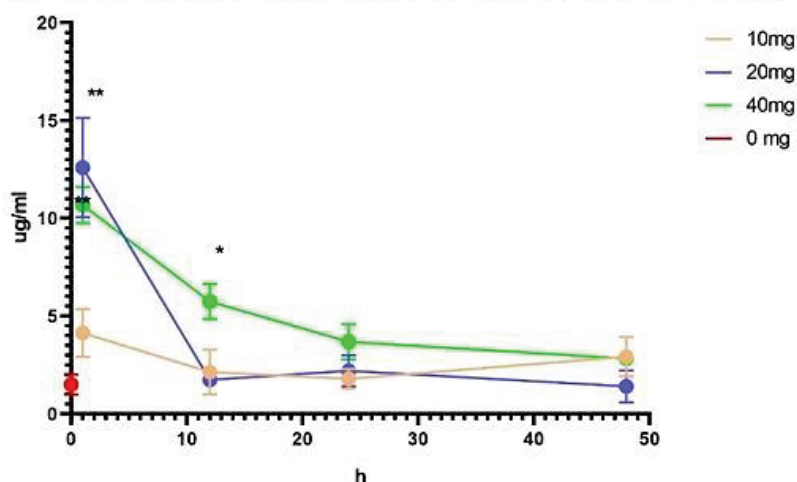


Figure 27: Mean values of the different concentrations of P1.3 in plasma plotted as time courses. Each error bar represents the standard error of the mean (SEM)

II. Examination of the repeated dose toxicity of P1.3 in athymic mice

After studying the toxicity of P1.3 in athymic mice subjected to high P1.3 doses, we opted against utilizing the 40mg/kg dosage for the repeated injection and instead focused on assessing the repeated dose toxicity of intraperitoneal P1.3 at a reduced 20mg/kg. This dosage was chosen based on prior findings that demonstrated its safety at a single dose in healthy athymic mice.

A set of 4 athymic mice were divided as follow: 1 mouse was used as a control, and 3 mice were subjected to P1.3 treatment. Treatment was done 5 times per week and the complete treatment duration was 3 weeks (Table 18).

Table 18: Treatment details for each group.

Group	N	Treatment	Dose	Schedule	Route	Duration
A	1	Vehicle	-	5 times/week	IP	3 weeks
B	3	P1.3	20 mg/kg	5 times/week	IP	3 weeks

N: number of mice; IP: intraperitoneal.

Mice body weight was monitored 3 times/week during the first 2 weeks of treatment, and daily during the third week. No statistical differences between mice treated with P1.3 and the control were observed (Figure 28, Table 19).

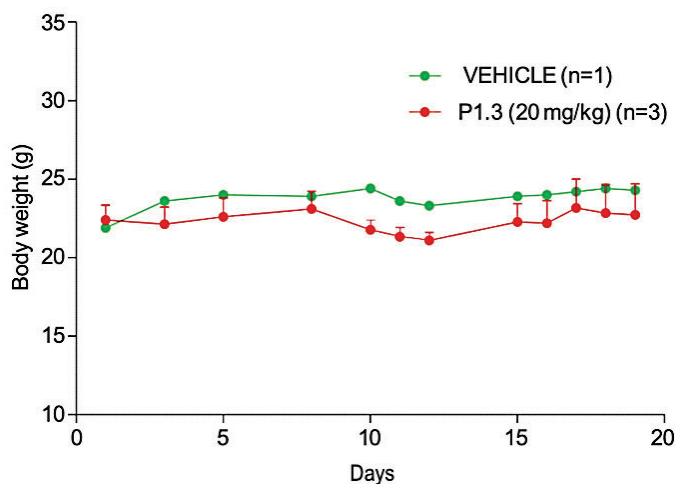


Figure 28: Mice body weight after P1.3 treatment. No statistically significant differences in the mice body weight were observed between groups (two-way RMANOVA test, $p=0.586$).

Table 19: Body weight (g)*

	Days of treatment												ID
	1	3	5	8	10	11	12	15	16	17	18	19	
VEHICLE	21,9	23,6	24,0	23,9	24,4	23,6	23,3	23,9	24,0	24,2	24,4	24,3	A1
P1.3 (20 mg/kg)	21,0	21,1	21,4	22,4	21,2	20,9	20,7	20,9	20,2	20,2	20,1	19,5	A2
	24,2	24,3	25,0	25,3	23,0	22,4	22,1	24,6	25,0	26,5	26,3	26,3	A3
	22,0	21,0	21,4	21,6	21,1	20,7	20,5	21,2	21,4	22,8	22,1	22,4	A4

* Relative body weight (%) = (Body weight Day X/ Body weight Day 1) x 100

However, at the end of the second week, P1.3-treated mice showed a gradual weight loss which was recovered during the weekend break, and during the third week a slight weight drop was observed again (Figure 29, Table 20). In conclusion, in terms of systemic toxicity, P1.3 at 20mg/kg was well tolerated, showing a slight body weight loss around 5% by the end of the second week. Moreover, local toxicity showed peritoneal organs adherence in addition to liver damage.

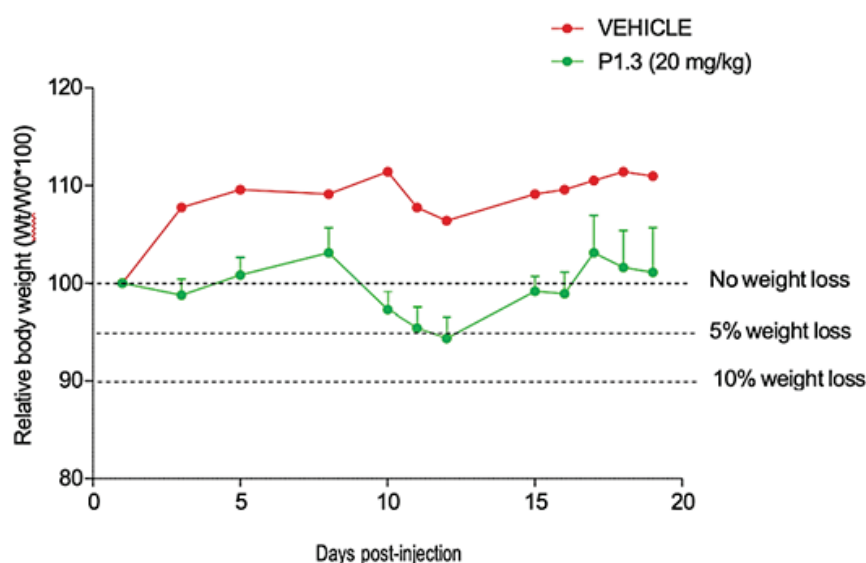


Figure 29: Relative body weight percentage during P1.3 treatment.

No statistically significant differences in relative to body weight were observed between vehicle and treatment (two-way RMANOVA, $p=0.058$). Relative body weight (%) = (body weight day X/ body weight day 1) x 100.

Table 20: Relative body weight (%) *

	Days of treatment												ID
	1	3	5	8	10	11	12	15	16	17	18	19	
VEHICLE	100,0	107,8	109,6	109,1	111,4	107,8	106,4	109,1	109,6	110,5	111,4	111,0	A1
P1.3 (20 mg/kg)	100,0	100,5	101,9	106,7	101,0	99,5	98,6	99,5	96,2	96,2	95,7	92,9	A2
	100,0	100,4	103,3	104,5	95,0	92,6	91,3	101,7	103,3	109,5	108,7	108,7	A3
	100,0	95,5	97,3	98,2	95,9	94,1	93,2	96,4	97,3	103,6	100,5	101,8	A4

* Relative body weight (%) = (Body weight Day X/ Body weight Day 1) x 100

Furthermore, we evaluated the organ toxicity at histological level after repeated P1.3 intraperitoneal injection (20mg/kg, 5 days/week, 3weeks) in healthy athymic mice. Liver, spleen, and pancreas hematoxylin-eosin (H&E) histologic sections from the 3 animals treated with P1.3 and one animal treated with the vehicle were analysed.

As shown in Figure 30 no signs of toxicity were observed in spleen. Pancreatic parenchyma did not show histologic alterations in their exocrine and endocrine components in any of the three mice that received P1.3 treatment (Figure 31). However, some histological alterations were found in liver. In two out of the three livers that received P1.3 treatment, geographical outlined areas of subcapsular pancreatic coagulative necrosis were observed (Figure 32). In view of these results, this coagulative necrosis was limited to subcapsular areas, and the remaining liver parenchyma had no histological alterations. These changes could probably be related to direct contact to the intraperitoneal administrated drug. In completable with the analyses of the origin of this coagulative necrosis as no signs of thrombosis or

vascular damage were objectivated after seriation of the paraffin blocs, ruling out the possibility of systemic thrombosis/embolism induced by P1.3. Furthermore, in these cases the remaining liver parenchyma that was away from the peritoneal surface, showed normal architecture without inflammatory activity, signs of cholestasis, steatosis, or abnormal deposit (Figure 33).

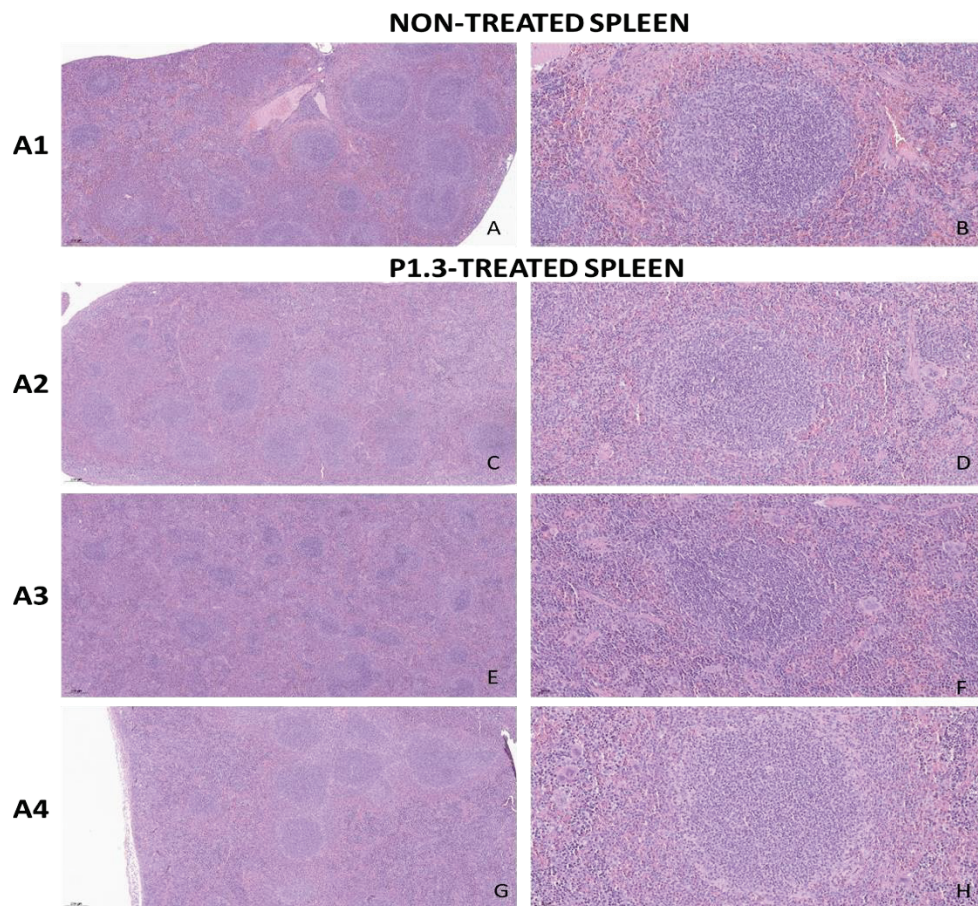


Figure 30: Histological appearance of the spleen in a non-treated mouse and three P1.3 treated mice. Representative H&E staining of spleen. A2, A3 and A4 mice were treated with P1.3. Original magnification 50x, scale bar 200 μ m (A, C, E, and G); or 200x, scale bar 50 μ m (B, D, F, and H).

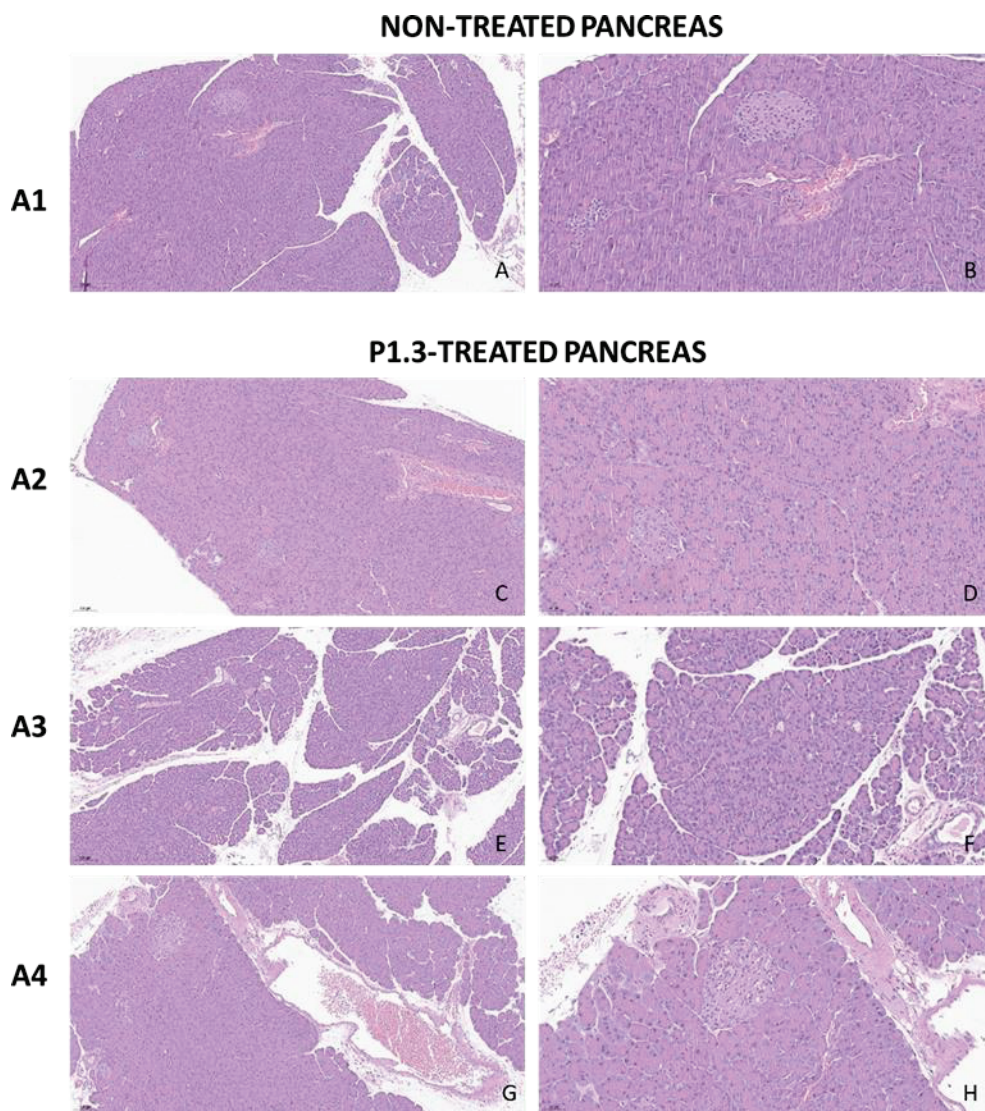


Figure 31: Histological appearance of the pancreas in a non-treated mouse and three P1.3 treated mice.

Representative H&E staining of the pancreas. A2, A3 and A4 mice were treated with P1.3. Original magnification 100x, scale bar 100µm (A, C, E and G); or 200x, scale bar 50µm (B, D, F and H).

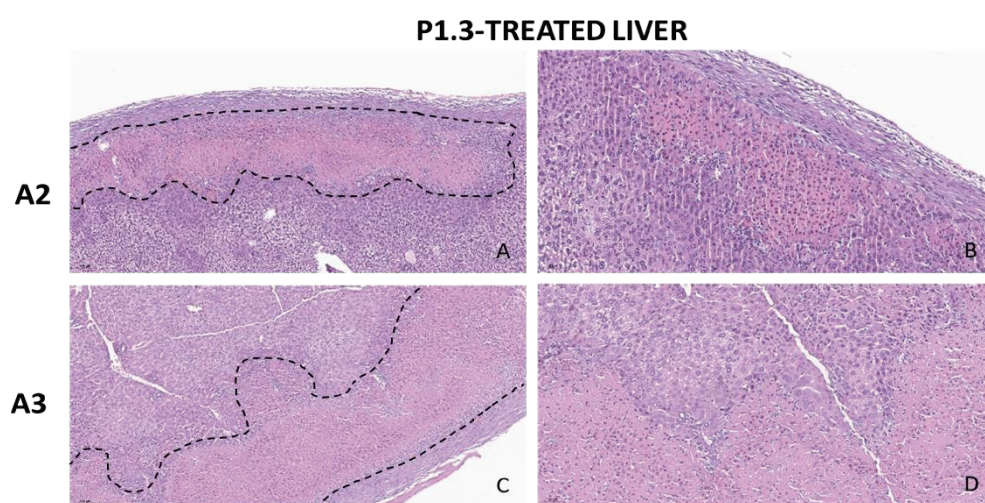


Figure 32: Histological appearance of the liver in P1.3- treated mice.

Representative H&E staining of the liver. Subcapsular pan-acinar coagulative necrosis highlighted by dashed

lines: A and B (mouse A2), C and D (mouse A3). Original magnification 100x, scale bar 100µm (A and C); or 200x, scale bar 50µm (B and D).

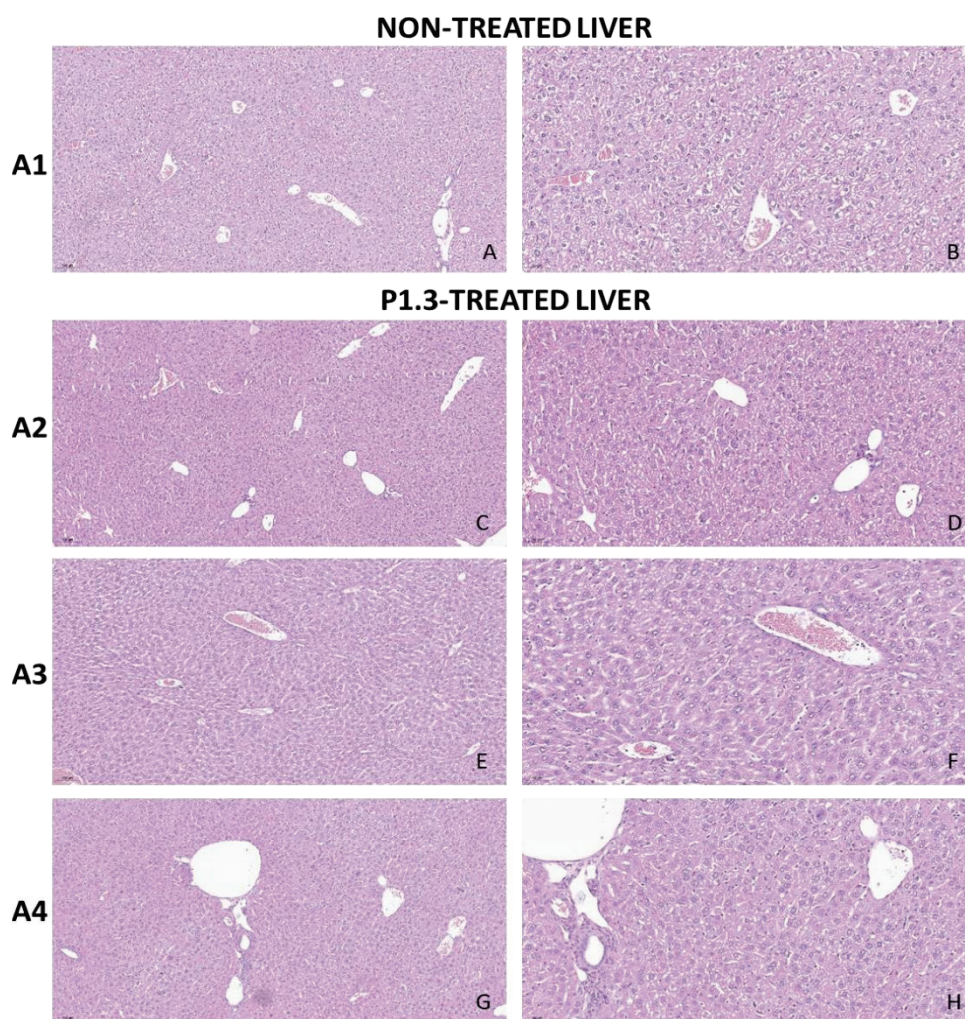


Figure 33: Histological appearance of the liver in P1.3-treated mice and control. Representative H&E staining of the liver. Normal liver parenchyma is shown in all images. A and B (mouse A1), C and D (mouse A2), E and F (mouse A3) and G and H (mouse A4). The images corresponding to mice A2 and A3 correspond to parenchyma away from the hepatic surface. Original magnification 100x, scale bar 100 μ m (A, C, E, G, I and K); or 200x, scale bar 50 μ m (B, D, F, H and J).

In conclusion, P1.3 does not induce any organ toxicity at the evaluated doses (20mg/kg) in spleen, pancreas, or liver but intraperitoneal injection can induce coagulative necrosis in liver.

4.2 CHAPTER 2

Searching for small molecules that bind directly to oncogenic KRAS interfering with its activity.

4.2.1 BACKGROUND AND PREVIOUS DATA

As deeply mentioned in the introduction, KRAS plays a central role in signal transduction, and KRAS mutations are closely related to tumour initiation and development. Successful targeting mutant KRAS will lead to a new platform for targeted oncology therapy. However, after 40 years of efforts, targeting KRAS has been challenging due to the difficulty to design a drug to recover the GTPase activity and the lack of druggable pockets. Researchers switched to other important molecules in the KRAS signalling pathway, such as RAF, MEK, and ERK. However, there has been no significant success in KRAS-driven tumours as they have obvious heterogeneity, which partly explains the poor efficacy of non-specifically targeting KRAS. Due to the lack of clear results and to the development of new *in silico* technologies, scientists concentrated again on directly targeting KRAS. Two different new strategies focused on regions other than the effector binding site opened the possibility of inhibiting oncogenic KRAS activity.

The first one is based on the identification of several post-translational modifications of KRAS such as phosphorylation, acetylation, ubiquitination, and others (Barceló, Paco, et al., 2014b; M. H. Yang et al., 2012b) that are able to modulate KRAS activity. Therefore, pharmacologically targeting these modifications could be a promising therapeutic strategy against oncogenic KRAS.

The second approach is supported by the fact that oncogenic KRAS activity can be modulated through interaction with non-effector proteins that bind to the HVR/and the allosteric lobe. PDE6- δ (Chandra et al., 2011), galectin 3 (Shalom-Feuerstein et al., 2008), calmodulin (CaM) (Garrido et al., 2018; Lopez-Alcalá et al., 2008; Villalonga et al., 2002), hnRNPA2 (Barceló et al., 2014b), nucleophosmin (Inder et al., 2010) and β catenin (Lee et al., 2018) are some examples. These interactions regulate either KRAS recycling, degradation, lipid binding, clustering at the plasma membrane, phosphorylation or other unknown features that are important for KRAS signalling (Seguin et al., 2017; Shalom-Feuerstein et al., 2008; Zimmermann et al., 2013). Thus, drugs that interfere with these binding sites might be useful to inhibit KRAS activity.

With the aim of searching new compounds that might be interfering with the interaction of KRAS and the non-effector proteins in the allosteric lobe, our group established a collaboration with Dr. J. Rubio (*Facultat de Química, Universitat de Barcelona*). Details of this in silico investigation are described in Dr. E. Garrido's Doctoral Thesis and published in Abuasaker et al. (2023) (Abuasaker et al., 2023). These results are the starting point of this chapter of the thesis.

4.2.1.1 KRAS modelling, virtual screening and selection of the best compound as a KRAS interactor

A sophisticated computational dynamic model of KRAS, specifically tailored to explore the diverse allosteric binding sites accessible within its structure had been previously developed by the group. Among these sites, pocket III stands out, positioned between the $\alpha 4$ and $\alpha 5$ helices (Figure 34A). This region gained significance due to its identification as the binding site for CaM, a finding supported both experimentally (Lopez-Alcalá et al., 2008a) and theoretically (Garrido et al., 2018a). The confirmation of pocket III's existence was further solidified through advanced computational tools, including LIGSTECSC and Pocket-Depth analyses (B. Huang & Schroeder, 2006; Kalidas & Chandra, 2008). Notably, this pocket remains conserved across all examined KRAS structures, including those in an inactive state, underscoring its potential significance. As such, the current investigation is centred on structure 4DSN from the Protein Data Bank, representing KRAS with the oncogenic mutation G12D and loaded with the GTP cofactor, a configuration ideal for targeting (further details provided in (Abuasaker et al., 2023)).

Utilizing state-of-the-art in silico docking techniques, as detailed in (Abuasaker et al., 2023), a meticulously screening of a library of compounds was performed, ultimately identifying nineteen candidates demonstrating the most favourable binding energies as potential KRAS interactors. Subsequently, the top-performing compounds underwent rigorous selection criteria, considering factors such as availability, solubility, and preliminary assessment of their negative impact on cancer cell viability (E. Garrido's Doctoral Thesis). Among these, P14 (depicted in Figure 34B) emerged as the optimal candidate for further biochemical examination of its interaction with KRAS, as well as exploration of its potential effects on signalling pathways and viability of treated cancer cells.

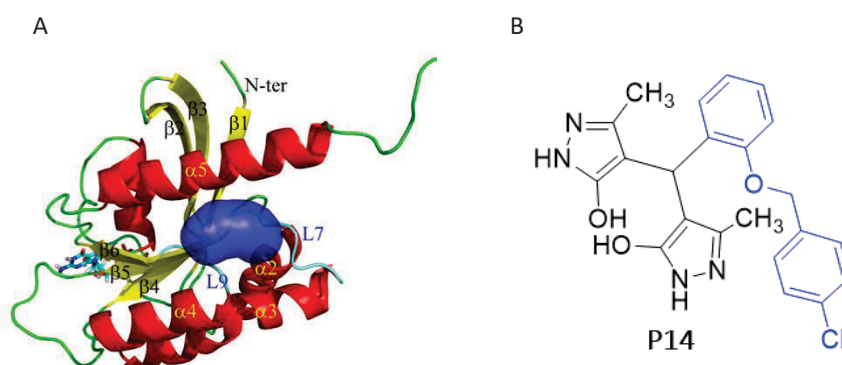


Figure 34: (A) Surface of the KRAS binding-site suggested to bind CaM in blue. (B) Formula of the selected compound P14. *Extracted from (Abuasaker et al., 2023).*

4.2.2 RESULTS

4.2.2.1 Biological effects of the selected compound (P14) on colorectal cancer cells (CRC)

As the data obtained from the docking analysis had demonstrated that the selected compound P14 was binding to a pocket near $\alpha5$ helix of KRAS (Figure 1A), and consequently this binding might prevent the interaction of KRAS with CaM, and since we had previously shown that CaM inhibited KRAS signalling (Alvarez-Moya et al., 2011), we aimed to analyse the effect of P14 on the activation of downstream KRAS signalling pathways (RAF/MEK/ERK and PI3K/AKT) in DLD-1 cells (CRC cell line harbouring one oncogenic KRAS-G13D allele).

In order to examine an expected impact on the activity of AKT and ERK upon P14 treatment, serum-starved DLD-1 cells (0.1% FBS) were subjected to 100 μ M of P14 at different times. As positive control of downstream KRAS signalling activation, cells incubated with 10% FBS containing medium for 30 minutes were also analysed. Western-blot (WB) against the phosphorylated active forms of AKT and ERK showed that the level of P-AKT increased after subjecting the cells to 100 μ M of P14 for 3 hours and remained elevated up to 6 hours, while activation of ERK started to appear after 45min of treatment and significantly increased after 3 and 6 hours (Figure 35). Based on this observation, for the subsequent experiments we

chose 3h-treatment as it was turned out to have the most significant effect on RAS downstream signalling.

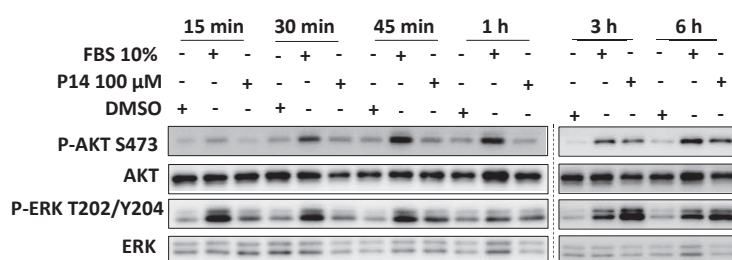


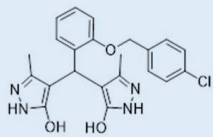
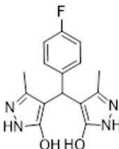
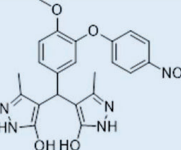
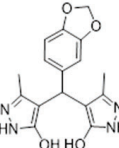
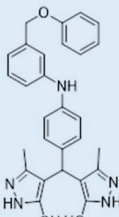
Figure 35: P14 treatment of DLD-1 cells increased endogenous downstream RAS signalling. DLD-1-starved cells were incubated for different times with 100 μ M P14, or for 30 min with 10%FBS. The levels of activation and the total levels of ERK and AKT were analysed by WB with specific antibodies against the active phosphorylated forms of the kinases or against the total forms of these proteins, respectively.

4.2.2.2 P14 derivatives formulation and biological effects on CRC cells

Following the observation of a remarkable biological impact upon treating CRC cells with P14, and concurrently with ongoing confirmation experiments, our research team initiated a collaborative effort with Dr. Maria Dolors Pujol (*Facultat de Farmàcia, Universitat de Barcelona*). The objective was to explore novel formulations of P14 that could further enhance its efficacy against cancer cells. Detailed descriptions of the chemical methodology employed to synthesize the P14 derivatives are explained in Abuasaker et al. (2023).

For inclusion in our investigation, four initial derivatives of P14 were formulated, designated from P14A to P14D (Table 21 left). Subsequently, six additional derivatives were synthesized, identified as P14E through P14J (Table 21 right).

Table 21: Chemical structure of the small molecule P14 and its derivatives.

Name	Formula	MW	Name	Formula	MW
P14		424,89	P14E		
P14A		302,31	P14F		
P14B		451,44	P14G		
P14C		328,33	P14H		
P14D		481,56	P14I		
			P14J		

Next, P14 derivatives potential effects on KRAS signalling were studied. Serum-starved DLD-1 cells (0.1% FBS) were treated with 100µM of P14A to P14J for 3 hours, and the activation of AKT and ERK was assessed by WB. As shown in Figure 36, P14, P14B, and P14C were able to activate AKT and ERK kinases, with P14 and P14B being the most efficient, whereas P14D, and from P14E to P14J had no impact on cell signalling.

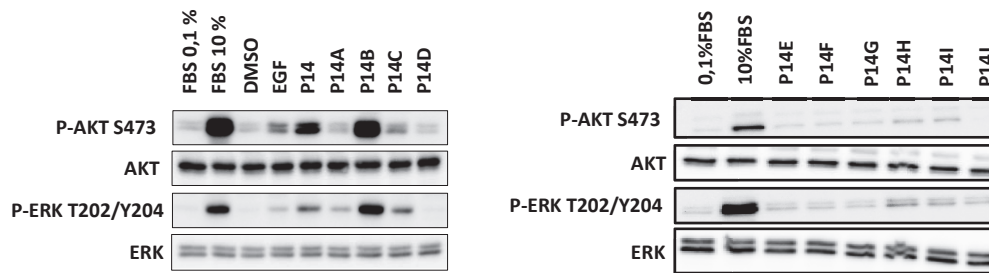


Figure 36: P14B derivative increased endogenous downstream RAS signalling the most. DLD-1-starved cells were incubated for 3 hours with 100 μ M P14 and derivatives, or for 30 min with 10%FBS. The levels of activation and the total levels of ERK and AKT were analysed by WB with specific antibodies against the active phosphorylated forms of the kinases or against the total forms of these proteins, respectively.

Since P14B exhibited the highest capacity to activate KRAS signalling, even at levels comparable to those achieved with 10% FBS (at 30 minutes), we selected it for further study. Figure 37 shows the spatial representation of the KRAS-P14 and KRAS-P14B complexes after been analysed by molecular dynamics (collaboration with Dr. Jaime Rubio).

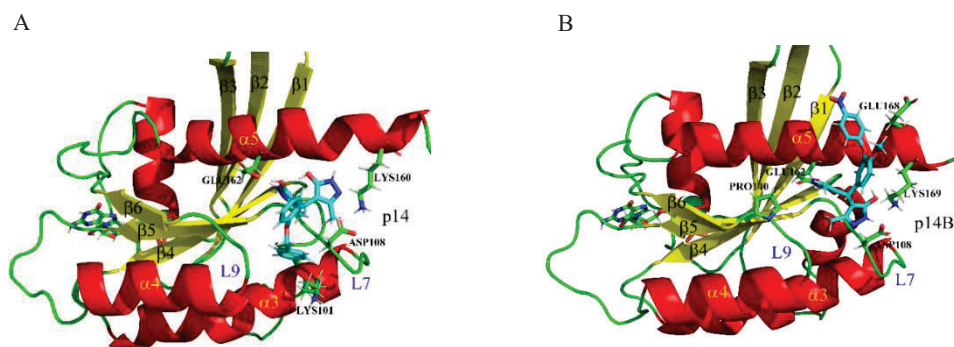


Figure 37: Spatial representations at the end of 100ns of conventional molecular dynamics of the complexes: (A) **KRAS-P14** (A) and **KRAS-P14B** (B). *Extracted from* (Abuasaker et al., 2023).

Following, the ability of P14B to affect the kinetics of RAS downstream signalling was analysed in DLD-1 cells treated with P14B at different times compared to 10% FBS. As shown in Figure 38, the kinetics of AKT, MEK, and ERK phosphorylation differed. The highest activation of ERK and MEK was clearly delayed in P14B-treated cells compared to 10% FBS. MEK and ERK activation began to appear after 15 minutes of P14B treatment, reaching their maximum levels after 3 hours. Additionally, MEK activation was no longer sustained after 3 hours, in contrast to ERK, which maintained a sustained level of P-ERK after 3 hours of treatment, extending up to 6 hours.

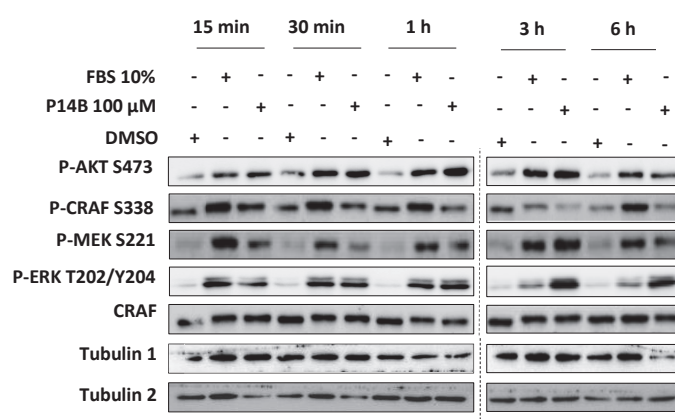


Figure 38: P14B treatment of DLD-1 cells induced a sustained increase in RAS signalling. DLD-1-starved cells were incubated for different times with 100 μ M P14B, or for 30 min with 10%FBS. The levels of activation and the total levels of CRAF, MEK, ERK and AKT were analysed by WB with specific antibodies against the active phosphorylated forms of the kinases or against the total forms of these proteins, respectively. WB anti-tubulin was used as a loading control.

Concluding, P14B, a small compound shown to interact with α 4- α 5 surface of KRAS in silico, induces a sustained increase in KRAS signalling in CRC cells.

4.2.2.3 Studying the specificity of P14B on KRAS oncogenicity in CRC

Since our experiments clearly showed that P14B treatment of CRC cells harbouring an oncogenic KRAS mutation (DLD-1) increased downstream RAS signalling, to study the effect of P14B in other cell lines, lacking oncogenic KRAS, was needed to confirm P14B specificity on oncogenic KRAS.

With this objective, we compared the effects of treating cell lines with different KRAS genetic background with P14B. For that, we took advantage of the existence of the isogenic CRC cell lines DLD-1 (expressing one oncogenic KRAS allele) and DLD-1-KO (DLD-1 from which oncogenic KRAS allele has been deleted). Additionally, the normal immortalized retinal pigment epithelium hTERT-RPE cells were included as a representative of non-transformed cell line.

Serum-starved cells (0.1% FBS) were treated for 3 hours with P14B (100 μ M), and the activation of AKT and ERK was evaluated by WB. As shown in Figure 39A, while AKT and ERK phosphorylation dramatically increased after P14B treatment in DLD-1 cells to almost the same levels as reached with 10%FBS, no significant variation was observed in hTERT-RPE treated cells. Concerning DLD-1-KO cells, P-AKT and P-ERK was observed in P14B-treated cells, but the activation of these kinases was very much lower than that achieved in DLD-1 treated cells. The quantification data from four independent experiments are presented in Figure 39B.

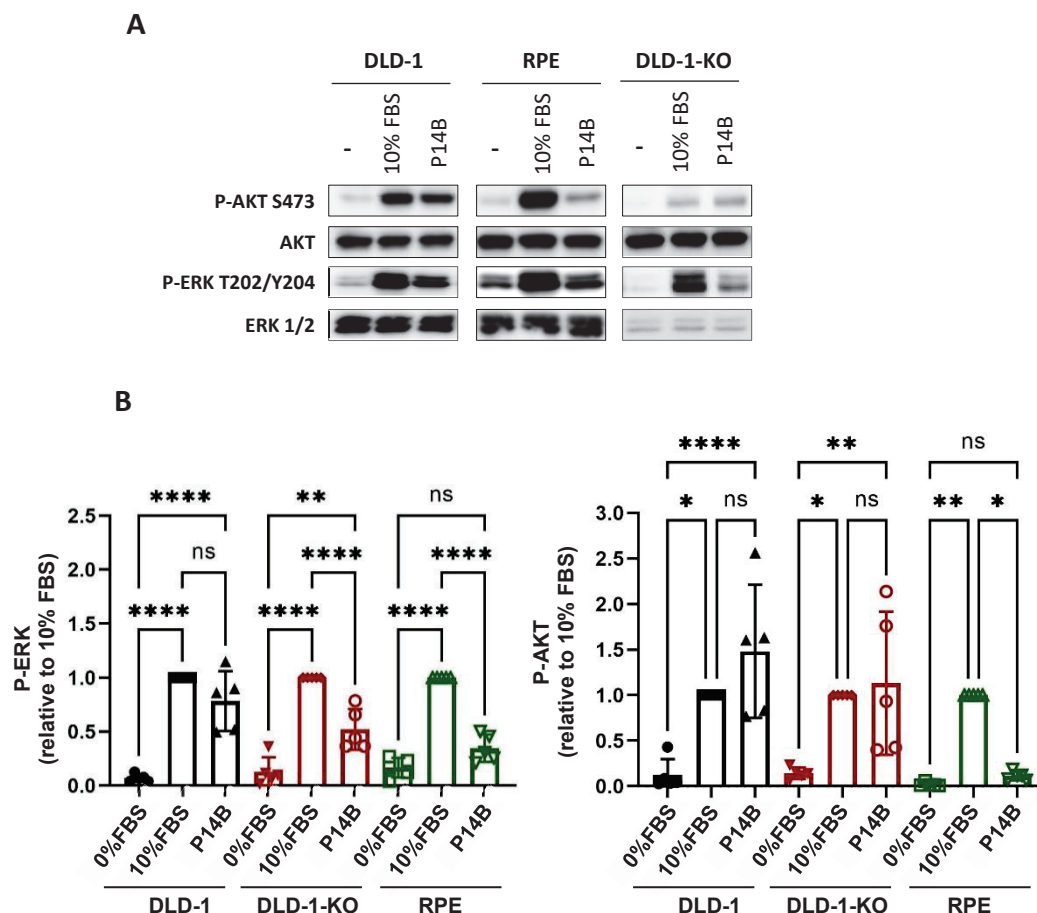


Figure 39: P14B treatment of CRC cells increased endogenous KRAS signalling depending on oncogenic KRAS expression. (A) DLD-1, DLD-1-KO, and hTERT-RPE starved cells were incubated with 100 μ M of P14B for 3 hours, and the levels of activation of ERK and AKT were analysed by WB. Specific antibodies against the active phosphorylated and total proteins were used. (B) The graphs display the quantification results from four independent experiments. Differences were assessed using one-way ANOVA and Multiple Comparisons Test and were considered significant when $p < 0.05$. *: p-value < 0.05 ; **: $p < 0.01$; ***: p-value < 0.0001 ; and ns: non-significant.

4.2.2.4 P14B directly binds to oncogenic KRAS competing with CaM *in vitro*

In summary, P14B demonstrates distinct ability to induce KRAS signalling in cells with oncogenic KRAS compared to those without. To investigate the potential direct interaction between oncogenic KRAS and P14B, we conducted surface plasmon resonance (SPR) analyses. In this experiment, the globular domain of KRAS (residues 1-166) tagged with GST was expressed, purified (as shown in Figure 40A), and immobilized on the CM5 sensor chip for SPR, following the procedure detailed in the Materials and Methods section. The sensor chip was loaded with GTP to ensure that KRAS was in the GTP-bound state. Various concentrations of P14B, ranging from 0 to 200 μ M, were then injected as the analyte to assess the interaction's affinity. As depicted in Figure 40B, we determined an affinity constant (KD) of 32.8 μ M for the binding of P14B to GTP-loaded KRAS.

Having P14B binding affinity to oncogenic KRAS, we wondered if this interaction occurred through the same surface region that KRAS uses to interact with CaM. To confirm this hypothesis, an *in vitro* competitive assay was conducted. This assay involved pulling down recombinant GTP-loaded GST-KRAS-G12V (1-166) using CaM-sepharose beads and subsequently incubating it with increasing concentrations of P14B. As depicted in Figure 40C, the calcium-dependent binding of GST-KRAS-G12V to CaM was attenuated in the presence of P14B.

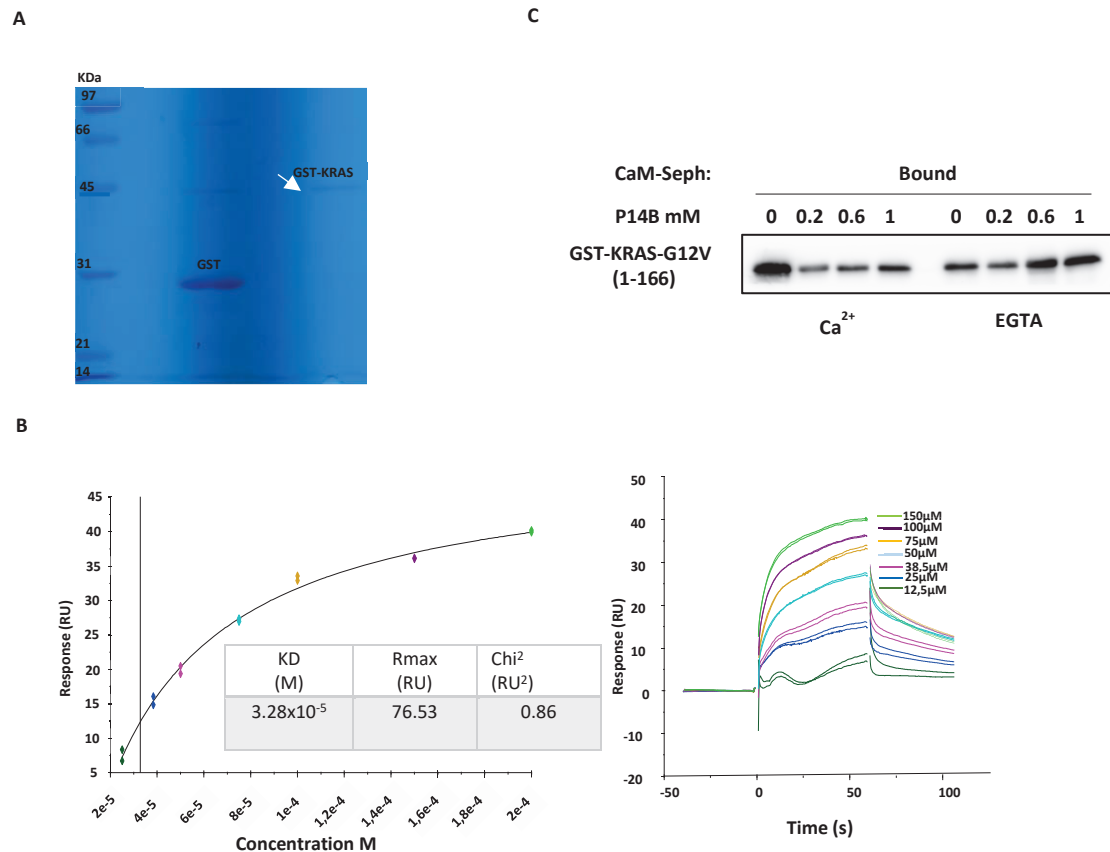


Figure 40: SPR analysis of P14B binding to oncogenic KRAS and competition with CaM: (A) GST-KRAS-G12V (1-166) and GST alone were purified from bacteria as described in Materials and Methods. The row collected bacterial samples were electrophoresed on a 10% acrylamide gel and subsequently stained with Coomassie brilliant blue, revealing the presence of both GST and GST-KRAS proteins. (B) Kinetic analysis (left) and sensograms (right) depicting the interaction between P14B and GST-KRAS-G12V (amino acids 1-166) as assessed through SPR. Resonance units (RU) are indicated on the vertical axis. The colour-coding utilised in the kinetic analysis is consistently applied in the sensogram to present each concentration of P14B. (C): CaM-sepharose pulldown assay conducted with GST-KRAS-G12V in the presence of P14B. Ca^{+2} or EGTA containing buffers indicate specific or non-specific KRAS-G12V binding to CaM, respectively. Bound fractions were analysed by WB with anti-KRAS specific antibodies.

4.2.2.5 P14B enhances oncogenic KRAS interaction with its effectors BRAF and P-CRAF, not affecting ARAF or CRAF.

After confirming the direct interaction between KRAS-G12V and P14B, we proceeded with a co-immunoprecipitation (co-IP) assay to investigate whether this interaction had any influence on the ability of oncogenic KRAS to bind to its effector proteins thereby favouring it and consequently leading to increase in downstream signalling.

We conducted a co-IP experiment to analyse the interaction of KRAS with various RAF family members following treatment with P14B at different times. This interaction was assessed after 10 min of P14B treatment, as P-CRAF and P-MEK were already observed after 15 min (see figure 38).

First of all, as a control over of the use of this cell line for the co-IP, serum-starved DLD-1 cells stably expressing HA-KRAS-G12V were treated for 30 min with 10%FBS or with P14B for 3 hours, and AKT and ERK activation analysis was performed by WB. We chose these cells to take advantage of that they express HA epitope tagged KRAS, which facilitates the co-IP. The results indicated that P14B induced the phosphorylation of AKT and ERK in these cells (Figure 41A), confirming that P14B effect was not influenced by the expression of the HA epitope in KRAS nor the type of KRAS oncogenic mutation. The co-IP confirmed the interaction between CRAF and oncogenic KRAS under serum- starvation conditions. However, we observed that only in response to EGF treatment, the immunoprecipitated CRAF was phosphorylated as illustrated in Figure 41B. Intriguingly, treatment with P14B significantly elevated the levels of phosphorylated CRAF (P-CRAF) that co-immunoprecipitated with KRAS, reaching levels similar to those achieved by EGF treatment. In contrast, BRAF did not form a complex with oncogenic KRAS under serum-starved conditions. Yet, upon EGF stimulation, we detected the interaction between these two proteins, as depicted in Figure 41B. Remarkably, P14B treatment induced a similar effect to the one caused by EGF, resulting in an increased interaction between KRAS and BRAF compared to non-treated cells. As CRAF, the interaction between ARAF and

oncogenic KRAS was already present under serum- starvation and no changes were detected due to the treatment with EGF nor P14B.

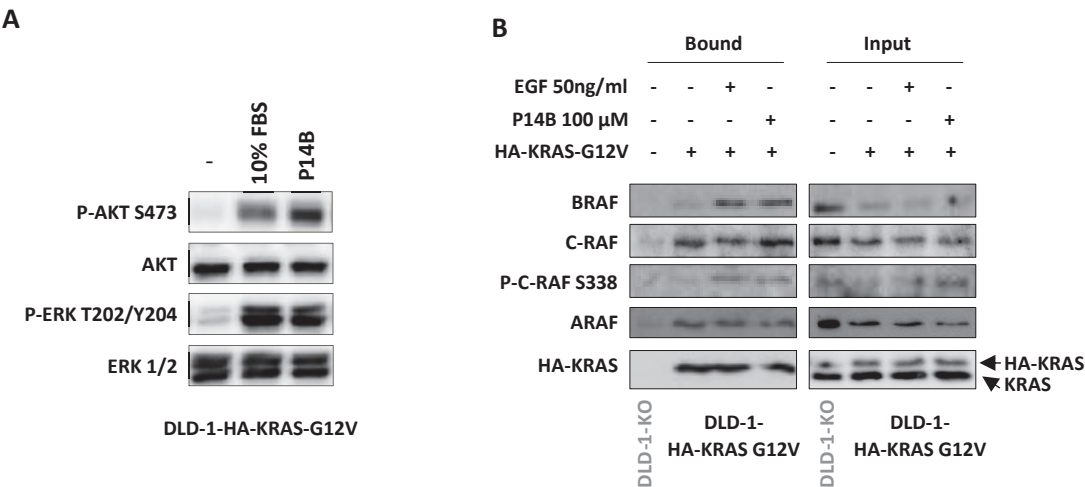


Figure 41: Treatment with P14B enhances the interaction of oncogenic KRAS with its effectors BRAF and CRAF/P-CRAF. (A) Serum-starved DLD-1 cells, which stably express HA-KRAS-G12V (DLD-1-HA-KRAS-G12V), were incubated with 100 μ M P14B for 3 hours of 10%FBS for 30 minutes. WB was performed using the specified antibodies against the phosphorylated and the total proteins indicated. (B) Co-IP of HA-KRAS-G12V with BRAF, CRAF/P-CRAF, or ARAF was examined in starved DLD-1- HA-KRAS-G12V cells after treatment with 100 μ M P14B or EGF for 10 minutes. Co-IP was carried out using anti-HA antibodies, and WB was performed on the bound and input fractions using antibodies specific for BRAF, CRAF, P-CRAF (S338), and ARAF. (-) represents the non-treated control.

4.2.2.6 P14B decreases the viability of CRC cells expressing oncogenic KRAS in 2D and 3D culture conditions

To elucidate the impact on cell viability of alterations in oncogenic KRAS signalling pathways and of the ability of oncogenic KRAS to interact with its effector proteins following P14B treatment, we conducted comprehensive analyses. Our assessments focused on the cell lines studied in Figure 39: DLD-1 (expressing oncogenic KRAS), DLD-1-KO (with the oncogenic KRAS allele deleted), and the non-transformed cell line hTERT-RPE. We performed dose-response experiments ranging from 0 to 100 μ M, with a 48-hour incubation period under 10% FBS conditions. As depicted in Figure 42A, P14B exhibited a significant reduction in the viability of DLD-1 cells, particularly at concentrations of 75 μ M and 100 μ M. The calculated IC₅₀ for DLD-

1 cells was approximately 80 μ M, where viability remained unaffected in both DLD-1-KO and non-transformed hTERT-RPE cells. Notably, no significant reduction in viability was observed between DLD-1-KO and hTERT-RPE cells, underscoring the specific impact of P14B on the viability of DLD-1 cells with oncogenic KRAS.

In this phase of our investigation, we aimed to ascertain whether cell death occurred through apoptosis. To achieve this, all three cell lines were exposed to P14B for 34h or 48h, after which we analysed the expression of cleaved caspase-3 by WB. As illustrated in Figure 42B, the presence of cleaved caspase-3 was solely discerned in the treated DLD-1 cells, while it remained undetectable in the samples from both DLD-1-KO and hTERT-RPE cells. These findings strongly suggest that the induction of apoptosis, as indicated by cleaved caspase-3 expression, was specific to P14B treatment in DLD-1 cells, reinforcing the selective impact of P14B on this cell line.

We also investigated the impact of P14B on DLD-1 cells implanted in 3D environment. When P14B was added during the initial cell seeding process, a marked reduction in the colony-forming capacity within Matrigel matrices was evident, even at a concentration as low as 10 μ M. Furthermore, when P14B was administered 24h after the cells had been seeded (at a point when colonies were already established), a discernible reduction in the size of the colonies became evident, particularly at a concentration of 40 μ M (Figure 42C). This observation underscores the potent effect of P14B in modulating the behaviour of DLD-1 cells within a 3D culture context.

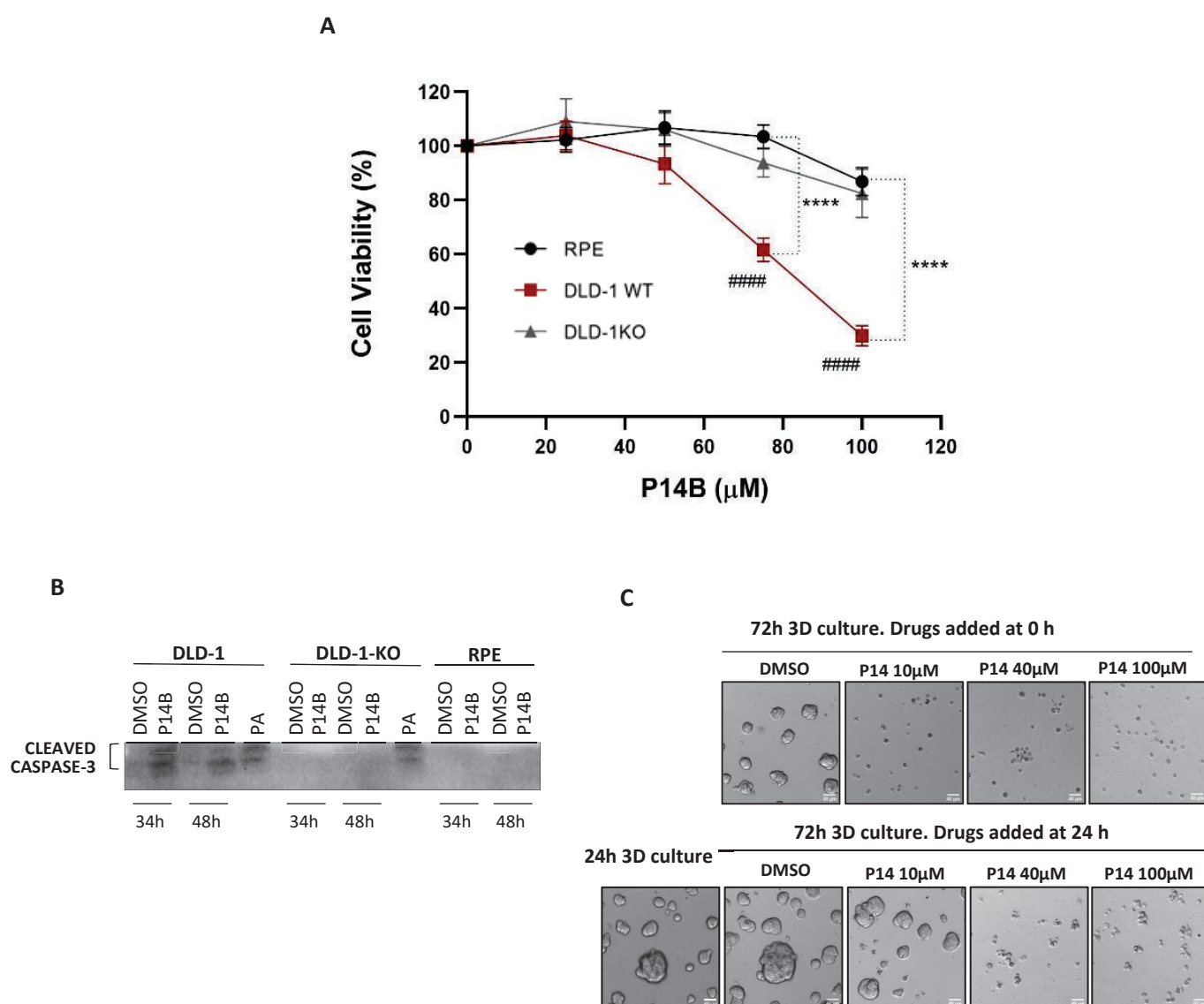


Figure 42: P14B treatment induces apoptotic cell death in DLD-1 cells. (A) DLD-1, DLD-1-KO, and RPE cells were subjected to P14B treatment across a range of doses from 0 to 100 μM and incubated for 48h. Cell viability assay (MTT) was conducted on a minimum of three separate occasions. Statistical differences were evaluated utilizing one-way ANOVA coupled with a Multiple Comparisons Test. Significance was established with a p-value of less than 0.0001 (****) indicating significance between DLD-1 and RPE or DLD-1-KO cells, and a p-value of less than 0.0001 (####) denoting significance between various concentrations of P14B treatment and non-treated DLD-1 cells. All results were considered significant at $p \leq 0.05$. (B) Cells were exposed to P14B (100 μM) for 34h and 48h, followed by cell lysis. WB was performed by using antibodies against the apoptosis marker, cleaved caspase-3. As a positive control, cells treated with the apoptosis inducer palmitic acid (PA) were included for the reference. (C) A total of 2.5×10^4 DLD-1 cells were cultivated on a thin basement membrane matrix

(Matrigel), which was overlaid with a diluted matrix solution, thereby establishing 3D on-top Matrigel assay. At the point of initial cell seeding or 24 hours thereafter, the cells received treatment with varying concentrations of P14B (10 μ M, 40 μ M, or 100 μ M). Subsequently, three days post-seeding, the formed colonies were subjected to analysis. Representative phase-contrast images are presented, with all scale bars set at 40 μ m.

4.2.2.7 P14B decreases the viability of Patient Derived Colorectal Cancer Organoids (PDCOs)

In pursuit of a more consistent and clinically relevant perspective, we sought to investigate the potential implications for cancer therapy. To achieve this, we established a collaboration with Abud's laboratory, at Monash Biomedicine Discovery institute, Department of Anatomy and Developmental Biology, Monash University, Australia. Our primary focus was to establish Patient Derived Colorectal Cancer Organoids (PDCOs) with the primary objective of faithfully recapitulating the architectural, physiological, and genetic characteristics of the original tissue. We conducted Presto-Blue assay (Figure 43B) over a span of five days, employing three technical triplicates. Our study focused on PDCOs (ORG148T) (Figure 43A left) harbouring oncogenic KRAS mutations and compared them to Patient Derived Normal Organoids derived from colorectal cancer patient (ORG141N) (Figure 43A right). The initial results yielded compelling insights. As indicated in Figure 43B, in a dose-response experiment spanning from 0 μ M to 100 μ M, ORG148T displayed a discernible response to P14B treatment over the course of five days. This response was characterised by a statistically significant difference across various doses, in contrast to the DMSO-treated control. Notably, at doses of 50 μ M, 75 μ M and 100 μ M, all responses exhibited remarkable distinctions from the control, with p-value equal or less than 0.0001. Conversely, P14B demonstrated no discernible effect on ORG141N even after five days of treatment. This observation reveals the specificity of P14B towards organoids bearing oncogenic KRAS mutations. These findings hold significant promise for the targeted therapeutic potential of P14B in colorectal cancer, as indicated by its selective impact on oncogenic KRAS-harboring organoids.

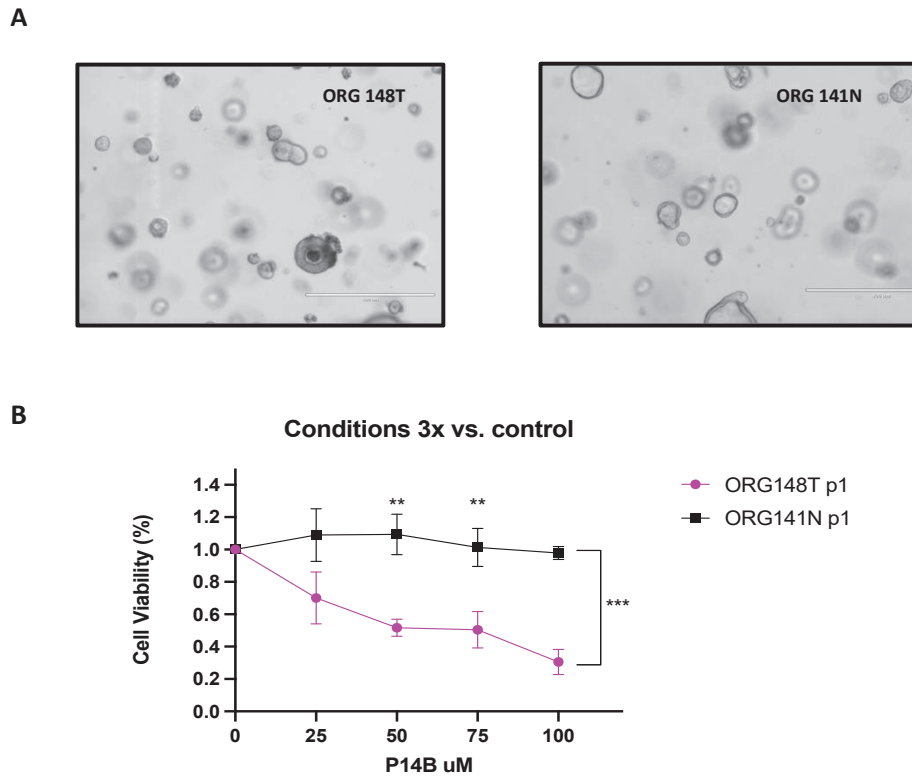


Figure 43: PDCOs viability is impaired by P14B treatment: A) Representative images of ORG 148T (left) and ORG 141N (right). Images were captured at 10x magnification on EVOS M7000. Scale bar= 400µm. (B) Graphical representation of the cell viability of ORG148T and ORG141N treated with P14B. Cell viability is displayed as a fold-change from the DMSO-treated control under each concentration, as measured with the PHERAstar FS plate reader following 45 minutes incubation with Presto-Blue reagent.

4.2.2.8 Biological effects of P14 and P14B on pancreatic ductal adenocarcinoma cell lines (PDAC)

Furthermore, we sought to broaden our investigation by examining the impact of P14 and P14B on pancreatic cancer. For this, we subjected six distinct PDAC cell lines, each bearing different KRAS mutations, to serum starvation and treated them with 100 µM of P14 for 3 hours. This allowed us to explore potential alterations in KRAS signalling under the same conditions as for CRC cells. As seen in Figure 44A, a slight elevation in the levels of P-AKT and P-ERK were observed after treating the PDAC cells with P14, with some variability of activation among them. Next, to gain initial insights into the impact of the chosen derivative, P14B, on PDAC cells, we selected PA-TU 8902 cell line to assess its potential in activating KRAS signalling. Serum-starved cells were treated for 3 hours with 100 µM of P14B, mirroring our

approach with the CRC lines DLD-1 and DLD-1 stably expressing oncogenic KRAS (HA-KRAS DLD-1), and with the hTERT-RPE cells. However, in PA-TU8902 cells as depicted in Figure 44B, we did not detect any significant further activation of AKT, CRAF or ERK levels following P14B treatment compared to the baseline levels of activation of these kinases. Further experiments should be conducted validate these findings across various PDAC cell lines.

In conclusion, while P14 amplifies KRAS downstream signalling in PDAC cells, P14B fails to exhibit similar effects. As a result, we opted to further pursue our investigation with a focus on CRC.

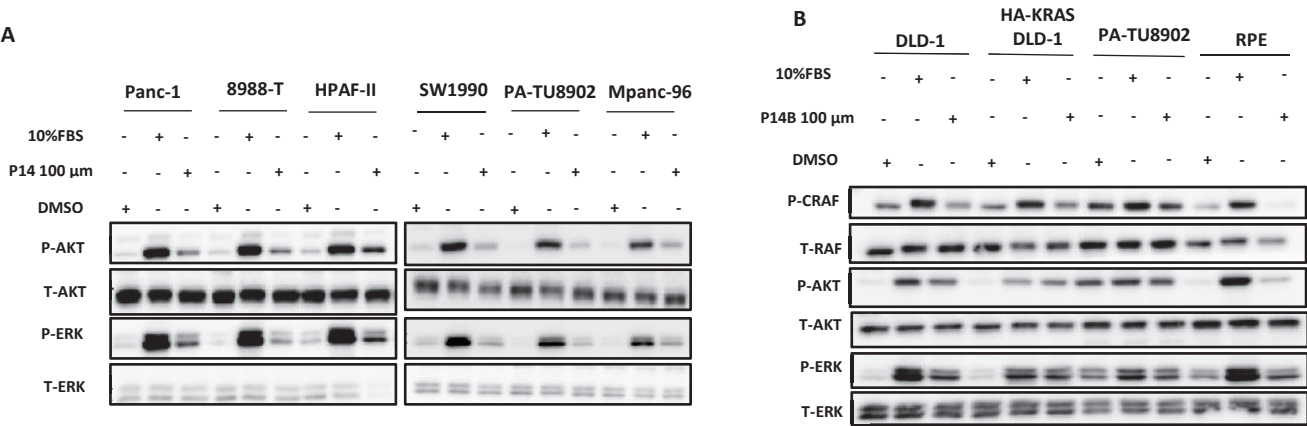


Figure 44: P14 but not P14B treatment of PDAC cell lines increased endogenous downstream RAS signalling. The indicated serum starved cell lines were incubated for 3 hours with 100μM P14 (A) or P14B (B), or for 30 min with 10%FBS. The levels of activation and the total levels of CRAF, ERK and AKT were analysed by WB with specific antibodies against the active phosphorylated forms of the kinases or against the total forms of these proteins.

4.2.2.9 Setting up the UltraID proximity-dependent biotinylation (PDB) technology in CRC cells

To elucidate potential interactors of oncogenic mutant KRAS in colorectal cancer (CRC) and gain insights into alterations induced by P14B treatment that might explain the results obtained up to the moment, the interactome of oncogenic KRAS-G12V was assessed using the proximal-dependent biotinylation technique (PDB). This method offers a distinct advantage over affinity purification, capturing weak or transient interactions within living cells

(Roux et al., 2012). In the original procedure (see Figure 45), an abortive variant of the protein biotin ligase (PBL) BirA, from *Escherichia coli*, fused to the protein studied was used. This PBL was called BioID. From BioID, other enzymes were developed over time (BioID2, BASU, TurboID, miniTurbo, and AirID) (Kubitz et al., 2022) in order to eliminate some obstacles detected when assessing the experiments with BioID. In this thesis, a deduced variant of microID (a truncation derived form of BioID2) named UltraID, being the smallest (below 20 kDa) and most efficient PBL available for PDB at the moment, has been used.

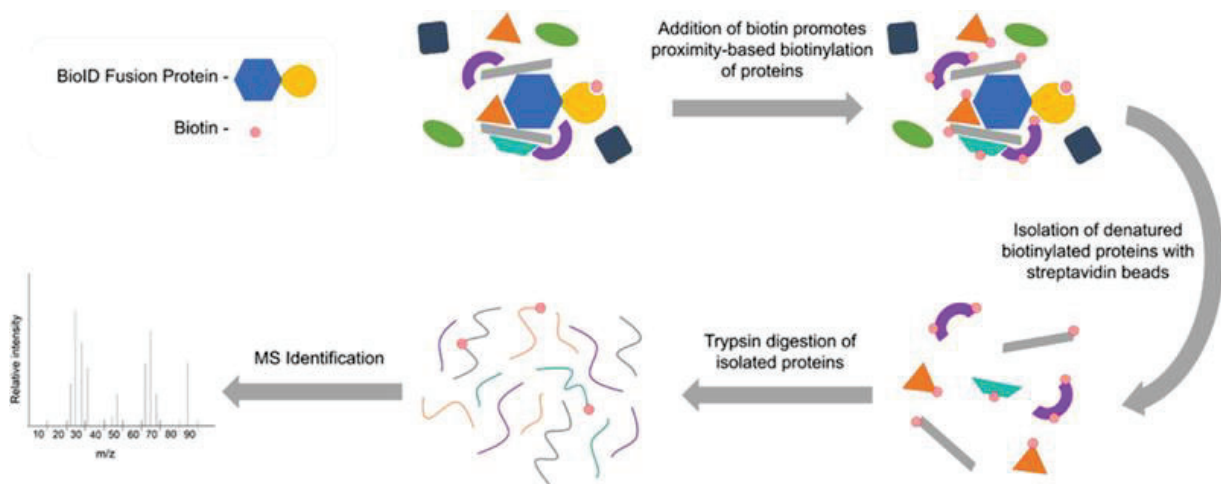


Figure 45: Schematic representation of the UltraID method (modification of the original BioID).

Adapted from Riannon M Sears et al. Methods in Molecular Biology 2019.

I. Generation of the UltraID-KRAS-G12V vector.

To ensure the generation of the KRAS-G12V-UltraID-C1 plasmid with unwavering precision, initially, the UltraID sequence from the pCMV-C1-myc-UltraID plasmid was amplified via PCR (depicted in Figure 46A) and, employing a meticulous approach to guarantee accuracy as detailed in Materials and Methods section. Subsequently, both the UltraID PCR product and the mCherry KRAS-G12V plasmid (Figure 46B) underwent digestion using AgeI and BsrGI enzymes. The resulting digestion products were analysed using 1% agarose gel electrophoresis, revealing distinct bands corresponding to UltraID (570 bp), KRAS-G12V (4500 bp), and Cherry (700 bp) confirming the successful amplification of the UltraID sequence and the precise digestion of the mCherry KRAS-G12V plasmid, as illustrated in Figure 46C. Following this, a precise fusion was achieved by linking the C-terminus of the myc-tagged UltraID to the N-terminus of KRAS-G12V, yielding the desired plasmid construct. Thorough

verification of this construct was conducted, as depicted in Figure 46D and E, ensuring its suitability for subsequent PDB assays in CRC cells.

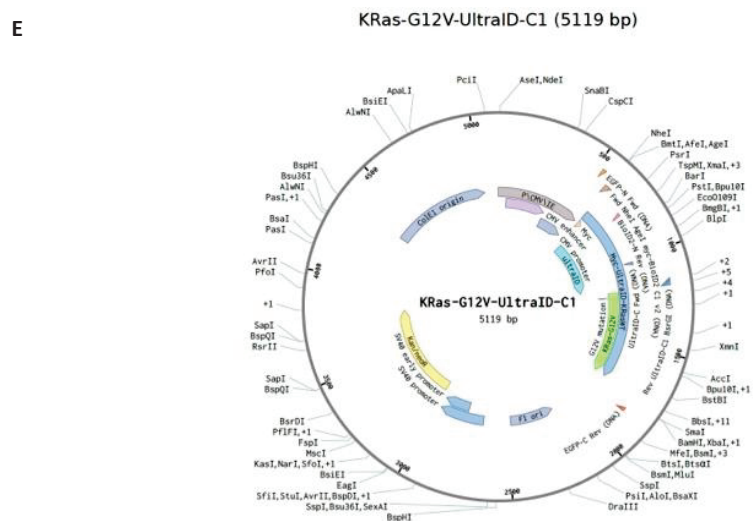
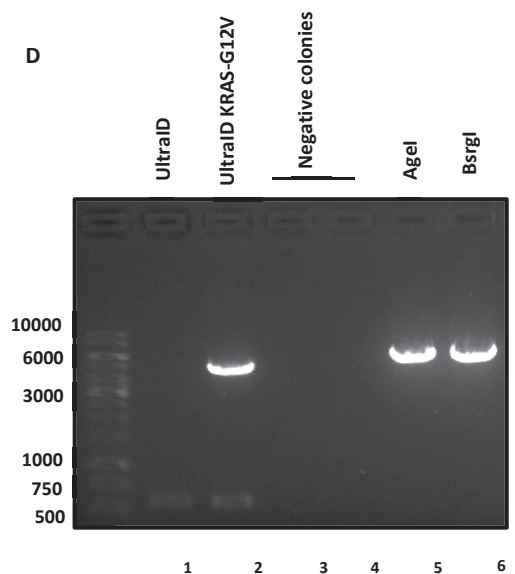
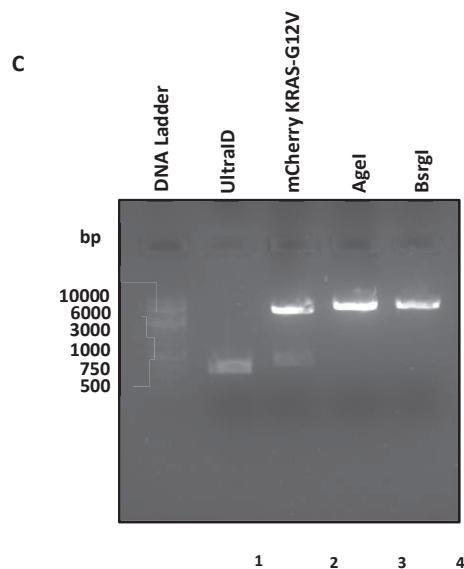
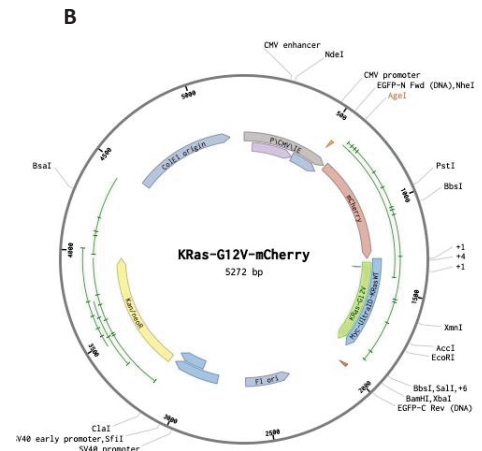
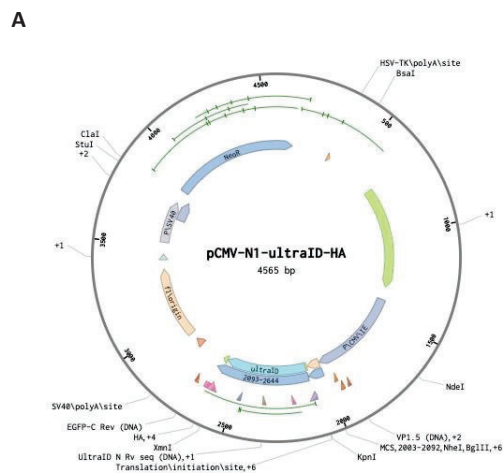


Figure 46: UltraID KRAS-G12V cloning. (A) pCMV-C1-myc-UltraID vector map. (B) mCherry KRAS-G12V vector map. (C) Agarose 1% gel electrophoresis showing the double digestion of the UltraID PCR product and 2 mg of mCherry KRAS-G12V with AgeI and BsrGI (lanes 1 and 2, respectively). As positive control: single digestions of the mCherry KRAS-G12V (lanes 3 and 4, respectively). (D) After ligation and plasmid purification, agarose 1% gel electrophoresis showing the double and single digestions of 2 mg of KRAS-G12V-UltraID-C1 with AgeI and BsrGI (lanes 2, 5 and 6). UltraID PCR product was resolved as a positive control (lane 1). (E) KRAS-G12V-UltraID-C1 vector map.

II. Functional validation of the UltraID-KRAS-G12V vector and setting up the PDB method.

To validate the functionality of UltraID-KRAS-G12V expression vector, a comprehensive series of experiments was conducted using DLD-1 cells. These cells were transiently transfected and incubated with or without biotin for a defined duration of 30 minutes. As positive control to verify biotinylation activity, DLD-1 cells were transiently transfected with the previously validated BioID-KRAS-G12V plasmid. Notably, these transfected cells underwent incubation with or without biotin for an extended period of 16 hours. To ascertain the specificity of biotinylation, DLD1 cells transiently expressing the fluorescent fusion protein Cherry-KRAS-G12V were employed as a negative control.

Moreover, to explore the potential influence of the growth factors on biotinylation, UltraID-KRAS-G12V expressing cells were subjected to either serum starvation or cultured in the presence of 10% FBS. Subsequently, protein cell lysates were obtained, subjected to SDS-PAGE and transferred onto a blotting membrane. Following, biotinylated proteins were detected by incubating the blotting membrane with streptavidin-conjugated horseradish peroxidase (HRP) as illustrated in Figure 47A. The following conclusions were drawn from this experiment: (a) biotinylated proteins exclusively manifest within cells transfected with BioID-KRAS-G12V or UltraID-KRAS-G12V and subsequently incubated with biotin; (b) BioID is more effective as PBL than UltraID, but it requires longer duration of biotin incubation; (c) the presence of FBS does not affect UltraID functioning.

Upon demonstrating this enzymatic activity, given that KRAS-G12V predominantly localizes in the plasma membrane, the next investigation aimed to validate the positioning of the UltraID-KRAS-G12V fusion protein within this cellular structure. To achieve this, DLD-1 cells

transiently transfected with the construct underwent immunofluorescence microscopy, leveraging an anti-myc antibody to exploit the myc-tag integrated into the expressed molecule. As illustrated in Figure 47B, the image clearly shows the localization of UltraID-KRAS-G12V at the plasma membrane.

Prior performing the definitive large-scale experiment, a crucial precursor in our investigation was to refine the purification process for the biotinylated proteins found within the cell lysate. DLD-1 cells transiently transfected with UltraID-KRAS-G12V were incubated with or without biotin. Post cell lysis, the biotinylated proteins were affinity-captured with streptavidin-conjugated beads. Following the protocol described in Materials and Methods section, the purified biotinylated proteins were resolved by SDS-PAGE, transferred to a blotting membrane, and incubated with streptavidin-HRP. This analysis demonstrated the successful purification of the ultraID-KRAS-G12V labelled proteins solely from the samples originating from cells incubated with biotin (Figure 47C).

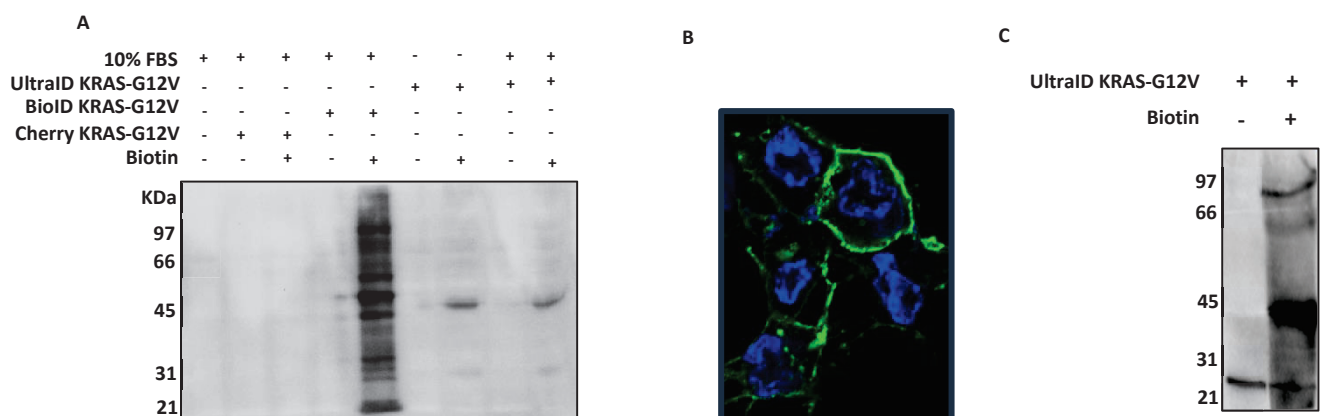


Figure 47: UltraID setup method. (A) DLD-1 cells transiently transfected with the indicated plasmids were incubated with or without 50 μ M biotin for 16 hours (for BioID-KRAS-G12V transfected cells) or for 30 minutes (for UltraID-KRAS-G12V transfected cells). Blotting analysis with streptavidin-HRP. (B) Representative image of DLD-1 cells transiently transfected with UltraID-KRAS-G12V subjected to immunofluorescence technique with anti-myc antibodies. Nuclei were evidenced with DAPI (blue). (C) DLD-1 cells transiently transfected with UltraID KRAS-G12V were incubated with 50 μ M biotin for 30 minutes. After cell lysis, biotinylated proteins were affinity captured with streptavidin-conjugated beads. Image shows the blotting analysis with streptavidin-HRP of the beads.

III. PDB technology reveals differential KRAS protein interactions upon P14B treatment in CRC.

In the pursuit of identifying proximal interacting proteins associated with KRAS and putative alterations induced by P14B treatment in CRC cells, a comprehensive experimental approach was undertaken. DLD-1 cells transiently transfected with UltraID-KRAS-G12V were cultured in triplicate, serum starved (24 hours) and then treated or untreated with P14B (1 hour). Biotin was added in the last 30 minutes of the treatment. Subsequently, a streptavidin pull-down was executed, followed by a thorough analysis using mass spectrometry (MS). After identification of the proteins, a compelling landscape, unveiling a total of 117 high-confidence KRAS-proximal interactors was obtained (refer to Figure 48A). Among these, 16 proteins were previously identified and strongly validated (score 0,4) as physically interacting with KRAS from the BioGrid database, featuring noteworthy candidates such as MAPK1, EGFR, BRAF, and ARAF (depicted in Figure 48B).

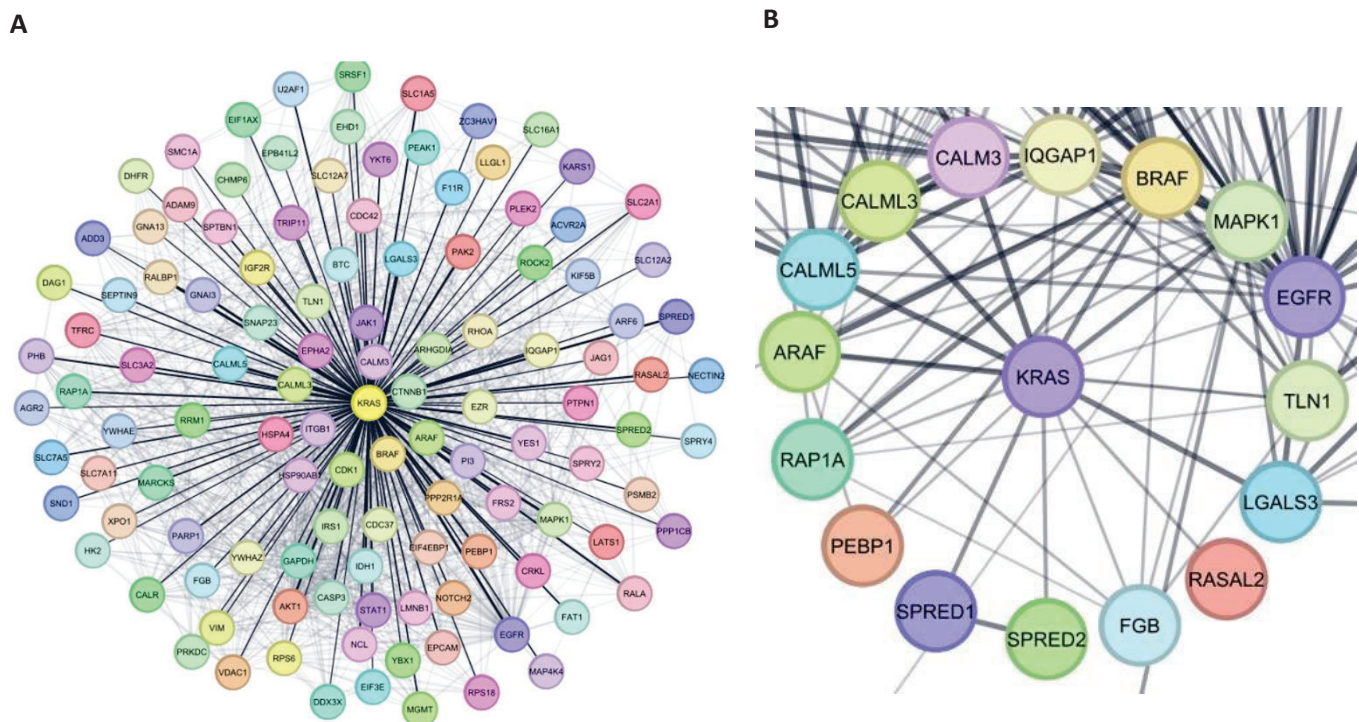


Figure 48: Identification of proteins interacting with KRAS-G12V through LC-MS/MS analysis using Cytoscape software. (A) A total of 117 KRAS proteins were detected to interact with KRAS-G12V, revealing a comprehensive view of the KRAS interactome. (B) Exploration of physically interacting partners with KRAS-G12V focuses on potential interactors.

Proteome Discoverer analysis and SAINT analysis allowed us to determine Differentially Biotinylated Proteins (DBPs) of KRAS interactors in cells treated or untreated with P14B (Table22).

Table 22. Table showing the previously described KRAS interactors detected as Differentially Biotinylated Protein (DBP). Cytoscape analysis with a cut score of 0,1 was used to determine the interactors.

ID	NAME	Log2 Fold Change	FDR	Known KRAS interactors (Physical & Functional)	Direct physical interactors	Indirect physical interactors
P29144	Tripeptidyl-peptidase 2	6,64	1,28E-16	✓		
Q9HDC5	Junctophilin-1	6,64	1,28E-16	✓	✓	
Q9NR45	Sialic acid synthase	6,64	1,28E-16	✓		
P09972	Fructose-bisphosphate aldolase C	6,64	1,28E-16	✓		
P30876	DNA-directed RNA polymerase II subunit RPB2	6,64	1,28E-16	✓		
P31939	Bifunctional purine biosynthesis protein purH	6,64	1,28E-16	✓		
Q13347	Eukaryotic translation initiation factor 3 subunit I	6,64	1,28E-16	✓		
Q15785	Mitochondrial import receptor subunit TOM34 (hTom34)	6,06	<1,3E-16	✓		
Q15003	Condensin complex subunit 2 (Barren homolog protein 1)	5,64	<1,3E-16	✓		✓
P54886	Delta-1-pyrroline-5-carboxylate synthase (P5CS)	5,32	<1,3E-16	✓		
P17812	CTP synthase 1 (CTP synthetase 1)	5,32	0,02	✓		
P00390	Glutathione reductase, mitochondrial (GR) (GRase)	4,74	0,01	✓		
Q7Z6Z7	E3 ubiquitin-protein ligase HUWE1 (ARF-binding protein 1)	4,74	0,01	✓		✓
Q9HAV7	GrpE protein homolog 1, mitochondrial (HMGE) (Mt-GrpE#1)	4,74	0,01	✓		
P12004	Proliferating cell nuclear antigen (PCNA) (Cyclin)	4,54	0,02	✓		
Q9Y3B7	Large ribosomal subunit protein uL11m	4,54	0,02	✓		
Q9HD45	Transmembrane 9 superfamily member 3 (EP70-P-iso)	4,32	0,03	✓		
P33991	DNA replication licensing factor MCM4	4,09	<1,3E-16	✓		
P33992	DNA replication licensing factor MCM5 (CDC46 homolog) (P1-CDC46)	3,91	<1,3E-16	✓		
Q06210	Glutamine--fructose-6-phosphate aminotransferase [isomerizing] 1	3,46	<1,3E-16	✓		✓
P52292	Importin subunit alpha-1 (Karyopherin subunit alpha-2) (KPNA2)	3,46	0,03	✓	✓	
Q7Z4W1	L-xylulose reductase (XR)	3,32	0,02			
P02452	Collagen alpha-1(I) chain (Alpha-1 type I collagen)	3,32	0,04	✓		
Q5SSJ5	Heterochromatin protein 1-binding protein 3 (Protein HP1-BP74)	3,32	0,04			

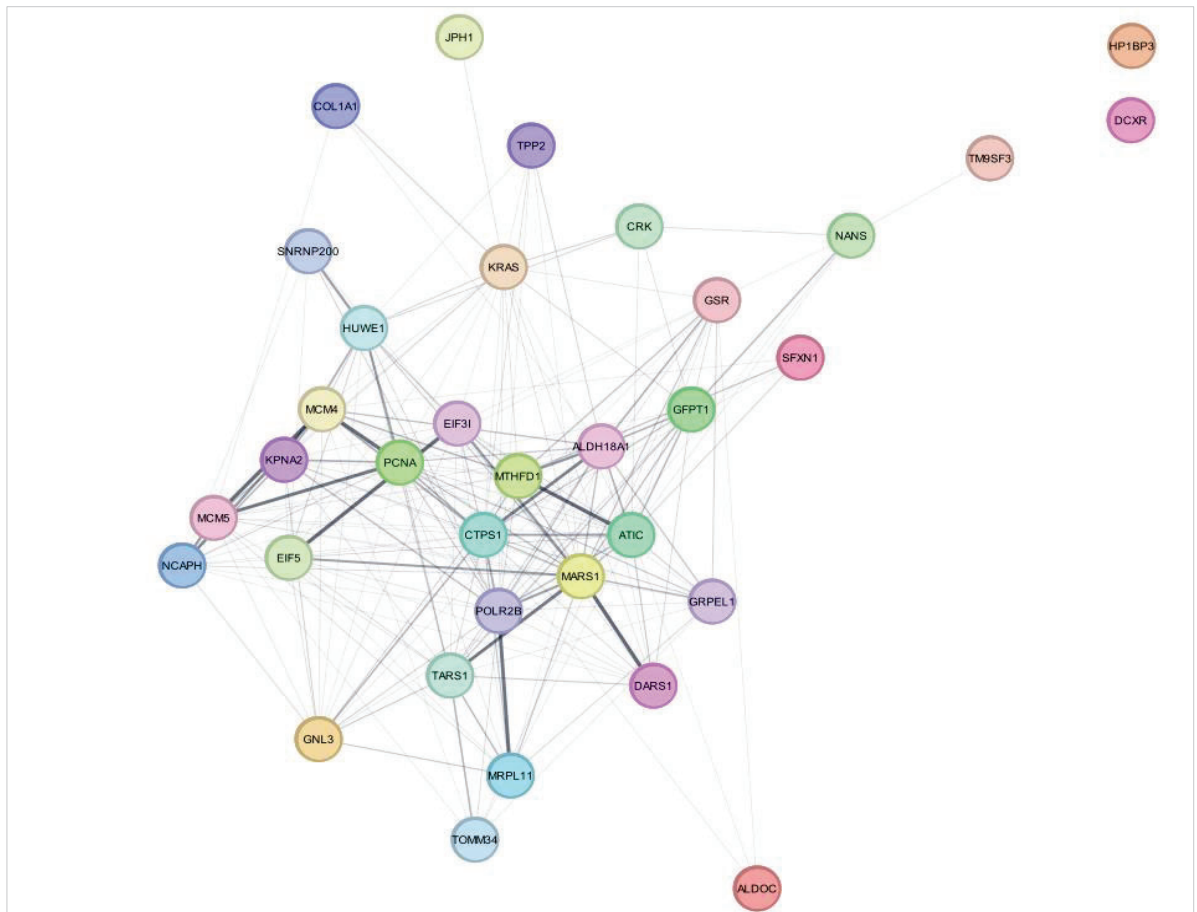
P14868	Aspartate--tRNA ligase, cytoplasmic (Aspartyl-tRNA synthetase) (DARS1)	3,25	<1,3E-16	✓	✓	
Q9BVP2	Guanine nucleotide-binding protein-like 3	3,25	0,01	✓		
P26639	Threonine--tRNA ligase 1, cytoplasmic	3,09	0,02	✓		
P55010	Eukaryotic translation initiation factor 5 (eIF-5)	3	0,05	✓		
P56192	Methionine--tRNA ligase, cytoplasmic	3	0,05	✓		✓
Q9H9B4	Sideroflexin-1	3	0,05	✓		
O75643	U5 small nuclear ribonucleoprotein 200 kDa	2,81	0,03	✓		
P11586	C-1-tetrahydrofolate synthase, cytoplasmic (C1-THF synthase)	2,25	<1,3E-16	✓		
P46108	Isoform Crk-I of Adapter molecule crk	-6,64	1,28E-16	✓		✓

As indicated in Table 22, 32 proteins displayed an increased interaction with KRAS upon P14B, while only one showed a decreased interaction. An exhaustive examination employing Cytoscape software, with confidence score 0.1, was performed revealing that almost all of these proteins had been previously described as interactors of KRAS, including functional interactions. However, only 3 of them were previously described as having a direct physical interaction with KRAS: **junctophilin-1** (Adhikari & Counter, 2018; Go et al., 2021a; Kovalski et al., 2019); **importin subunit alpha-1** (Go et al., 2021b) and **aspartate-tRNA ligase** (Rosenbluh et al., 2016). Interestingly, previously described interactors of these proteins were also found in the list of DBPs: **condensin complex subunit 2**, **E3 ubiquitin-protein ligase HUWE1**, **glutamine--fructose-6-phosphate aminotransferase**, **methionine--tRNA ligase** and **Crk-I** (labelled in the table as indirect interactors).

The network interaction between KRAS and the DBPs found in response to P14B treatment is shown in Figure 49. Figure 49A includes the physical and functional interactions, while Figure 49B exclusively presents the physical interactions. Additionally, a biological processes enrichment analysis of the proteins was performed in Figure 17B. It is evident that KRAS and junctophilin-1 appear to form an isolated complex independent of the other DBPs, whereas the remaining proteins form a highly interconnected network. Interestingly, a significant overrepresentation of proteins involved in metabolic and biosynthetic pathways was observed (Figure 49B)

This insightful analysis strongly suggests a discernible impact of P14B treatment on KRAS interactions, thereby influencing diverse biological functions.

A



B

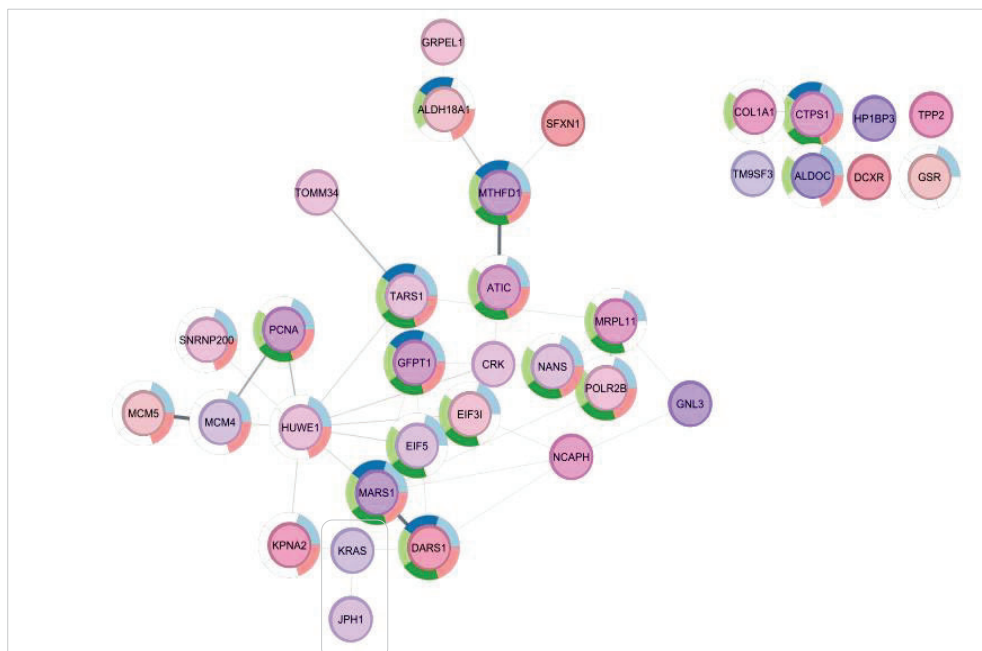


chart color	term name	description	FDR value
blue	GO:0034641	Cellular nitrogen compound metabolic process	0.0014
green	GO:0006520	Cellular amino acid metabolic process	0.0045
yellow	GO:0009058	Biosynthetic process	0.0045
red	GO:0044271	Cellular nitrogen compound biosynthetic process	0.0045
orange	GO:0046483	Heterocycle metabolic process	0.0045

Figure 49: Network analysis conducted using Cytoscape reveals the differential interactors detected by LC-MS/MS in P14B-treated DLD1 cells with a 0.1 cut score. (A) Network analysis of DBPs, encompassing both physical and functional previously described interactions. (B) Network of DBPs interactors encompassing the previously described physical interactions and the biological processes associated.

5. DISCUSSION

5.1. The peptidomimetic P1.3 is designed to interact with RAS effector domain

The KRAS protein stands out as one of the most frequently mutated proteins, wielding a pivotal role in propelling human oncogenesis. This profound significance has catalysed an intense quest for pharmacologic agents aimed at impeding mutant KRAS aberrant signalling. Given the adverse effects often associated with conventional cancer treatments like chemotherapy, the exploration of alternative therapies has become imperative (Mahmoudi Gomari et al., 2020; Quintal & Campos, 2020).

Bioactive peptides have emerged as a promising avenue due to their potential in combating chronic diseases such as cancer. However, realising the therapeutic potential of peptides poses formidable challenges. Issues such as low yields, chemical instability, hydrolysis, short half-life, and susceptibility to proteolytic degradation complicate their synthesis and purification processes.

To overcome these limitations, researchers have turned to the concept of peptidomimetics, which involves designing peptides containing modified amino acids or chemical alterations (Evans et al., 2020). Leveraging this strategy, our group has assessed the efficacy of various peptidomimetics, meticulously designed in silico against the RAS effector domain using the Iproteos technology.

Initial findings revealed a notable downregulation of RAS signalling in non-transformed cells (hTERT-RPE) grown under growth factor-limiting conditions, treated with the peptidomimetics, and subsequently stimulated with EGF. These cells showed **reduced levels of activation of the two main signal transduction pathways controlled by RAS** (RAS-MAPK and RAS-PI3K-AKT). An RBD-pull down assay discarded the possibility that the peptidomimetics might be interfering with the cellular levels of GTP-bound form of RAS wild-type, by means affecting on the guanine nucleotide exchange (GEFs) or the GTPase (GAPs) activities. RPE cells treated with EGF **plus P1.3 had the same levels of RAS-GTP** as the ones treated with only EGF. Furthermore, these peptidomimetics have demonstrated the ability to **disrupt the interaction between oncogenic KRAS and its principal effectors CRAF and PI3K-p110 in HeLa cells expressing HA-KRAS-G12V**, thereby becoming good aspirants to attenuate

the activity of the principal downstream signalling pathways associated with KRAS in cancer. Among the tested peptidomimetics, P1.3 has emerged as a particularly promising candidate. Building upon these observations, we proceeded to evaluate the impact of P1.3 on the viability of six pancreatic ductal adenocarcinoma (PDAC) cell lines harbouring diverse KRAS mutations under serum-saturating conditions, alongside non-transformed hTERT-RPE cells. Encouragingly, our data indicated that **P1.3 efficiently suppresses the proliferation of pancreatic cancer cells while exerting minimal effects on normal cells**. Specifically, P1.3 has demonstrated the capability to induce cell death in all tested tumour cells at concentrations ranging between 20-25 μ M. Thus, the heightened efficacy of P1.3 in reducing cell viability in PDAC cells compared to non-transformed epithelial cells bears significant implications for cancer therapy.

Notably, previous studies have suggested that mutations in KRAS alleviate a membrane-associated orientation that normally sequesters effector binding, potentially enhancing the binding affinity of possible drugs to the effector domain of oncogenic KRAS (Mazhab-Jafari et al., 2015). This may explain the inhibitory effect of P1.3 in the proliferation rate of PDAC cells harbouring oncogenic KRAS, compared with normal cells expressing wild type KRAS. Interestingly, Fang et al (2018) describe a new compound with a novel mechanism of action: it binds to a pocket in KRAS and simultaneously interacts with the plasma membrane. Consequently, the effector-binding site of the oncogenic KRAS becomes occluded, impeding RAF binding (Figure 50) (Fang et al., 2018). These findings underscore the significance of KRAS association with the plasma membrane and its profound influence on KRAS signalling.

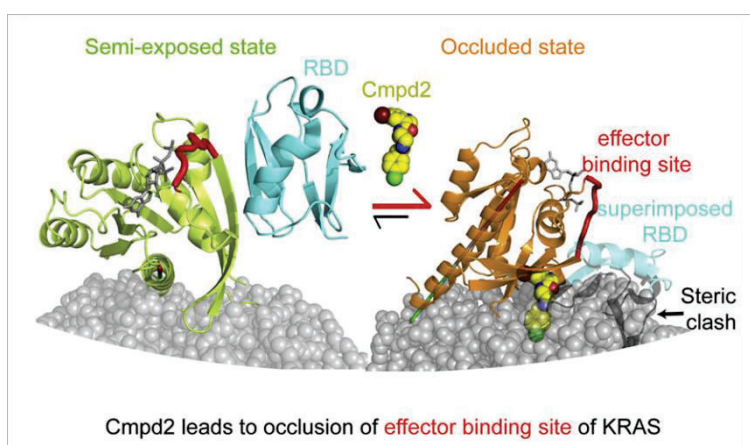


Figure 50: Novel mechanism of action of a drug that impedes the RBD of RAF binding to KRAS. *Extracted from (Fang et al., 2018).*

Hence, the ability of P1.3 to inhibit KRAS signalling in normal cells, its capacity to interfere with oncogenic KRAS binding with effectors, and its capability to reduce cell viability in treated PDAC cells, might be predominantly attributable to its tight binding to the active RAS-GTP form. Surface plasmon resonance technology allowed us to confirm this hypothesis by examining the kinetics of the binding between the purified G-domain (residues 1-166) of oncogenic KRAS-G12V (GTP-loaded) and P1.3. The analysis demonstrated the **direct interaction between the peptidomimetic and the conserved region of the GTP-loaded KRAS**, containing the effector domain, with a dissociation constant (K_D) of 15.7 μ M.

Supporting to this notion, recent discoveries have unveiled cyclic peptide inhibitors against KRAS with $K_D = 0.83 \mu$ M, effectively blocking the interaction between KRAS and its effector proteins (Upadhyaya et al., 2014). Other findings (Wu et al., 2013) highlight the potential for developing peptidomimetics as direct RAS inhibitors, suggesting they may offer greater utility than macrocyclic compounds. This presents promising avenues for advancing cancer therapeutics.

Once this point has been reached, the next step to advance the project is moving the research to an *in vivo* model. In this way, in order to test the putative beneficial therapeutic effects of P1.3 in tumours, the orthotopic xenograft model of pancreatic cancer in mice was chosen.

The first step of the formal protocol, prior treating xenograft mice, is to determine the maximum tolerated dose (MTD) of the compound in healthy athymic mice. For the length of time of a study that involves treatment of mice with a compound, the MTD is the maximum dose that can be dispensed to the animal that will not affect the survival, only generates an acceptable low reduction in body weight and very few over signs of toxicity. Local toxicity assessments after intraperitoneal injection of P1.3 revealed no evidence of pain or distress at doses of 10 or 20 mg/kg, but distress was observed at 40 mg/kg, suggesting potential irritation. Although these effects appeared temporary, caution is warranted, particularly with repeated injections. Subsequent histological evaluations of **organ toxicity** following five days per week injections at 20 mg/kg for three weeks, showed **no adverse effects on the spleen, pancreas, or liver**.

Additionally, samples of mice plasma were analysed by mass spectrometry to identify the presence of the peptidomimetic. **P1.3 exhibited a brief retention time in the mice plasma** with the diverse concentrations used.

Accordingly, arise the possibility that P1.3 prepared and administrated in the current form in mice, has low availability. Two different factors were taken into account for the next experiments with the peptidomimetic: method of administration and solubility.

At what concerns to the way of administration of P1.3, intravenous injection will be further assayed.

In regard to P1.3 solubility, preparation as injected in mice (2mg/ml) was used to analyse the solubility of P1.3 by electron microscopy. As shown in Figure 51 (left), some small precipitates invisible to naked eye or under phase contrast microscopy (40x), are visible under 120,000x magnification.

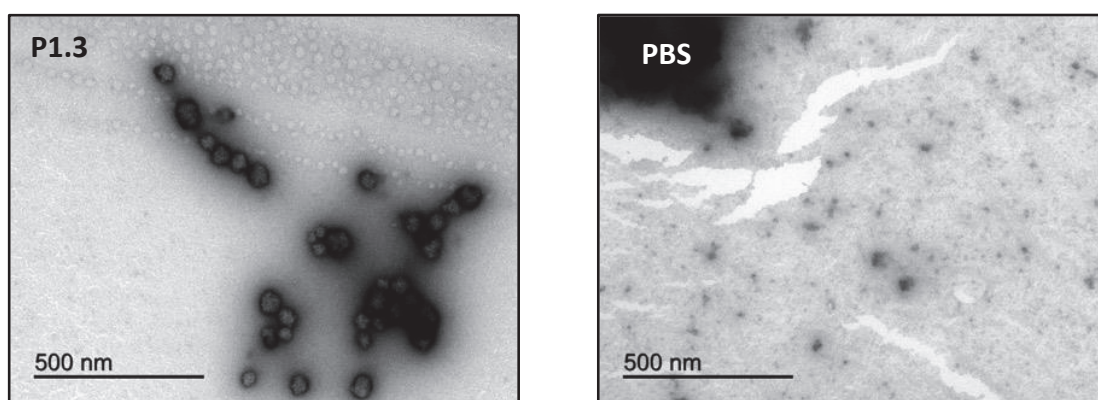


Figure 51: Figures illustrate the solubility of compound P1.3 at a concentration of 2mg/ml (left) compared to PBS (right) using electron microscopy (EM). P1.3 was prepared in PBS at 2mg/ml, centrifuged, and analysed by EM. Images were captured at 120,000x magnification with a scale bar of 500nm.

Although there is a possibility that the precipitates could be captured by the cells without problem due to their small size, a possible decrease in the final concentration of the peptidomimetic administered must also be considered.

As a result, through a collaborative effort with Dr. Francesc Rabanal (*Dpt. Química Inorgànica i Orgànica*, UB), novel derivatives of P1.3 have been designed and synthesized with the aim of assessing their bioavailability, expected to surpass that of P1.3. Currently, our laboratory is diligently evaluating the efficacy of these compounds in selectively killing PDAC cells. Interestingly, one such compound named P1.70, exhibits heightened cytotoxicity against PDAC cells compared to P1.3.

Concurrently, in partnership with Dr. Francesc Rabanal's group, we were exploring the potential of cyclodextrin as a solvent, rather than the current DMSO, to enhance the solubility

of peptidomimetics, thereby improving their bioavailability. Cyclodextrins (Figure 52) represents a diverse array of cyclic oligosaccharides, collectively serving as a promising avenue for optimizing drug delivery and efficacy (Jambhekar & Breen, 2016).

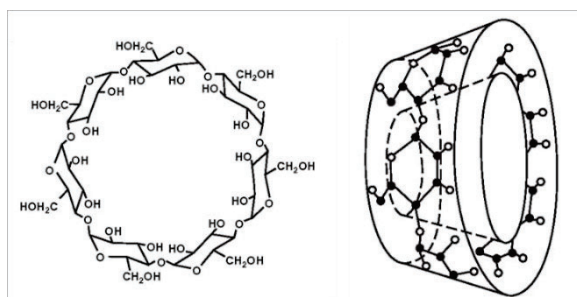


Figure 52: Structure of cyclodextrin and toroidal shape it adopts. *Extracted from (Jambhekar & Breen, 2016).*

The first compelling results have been recently obtained in the laboratory: first, the protocol of solubilisation of P1.3 has been successfully set up; and secondly, P1.70 solubilized with cyclodextrin displays a higher cell mortality effect than with DMSO in PDAC cells, but not in normal cells.

A model explaining the biological effect of P1.3 on KRAS signalling pathways is shown in Figure 53.

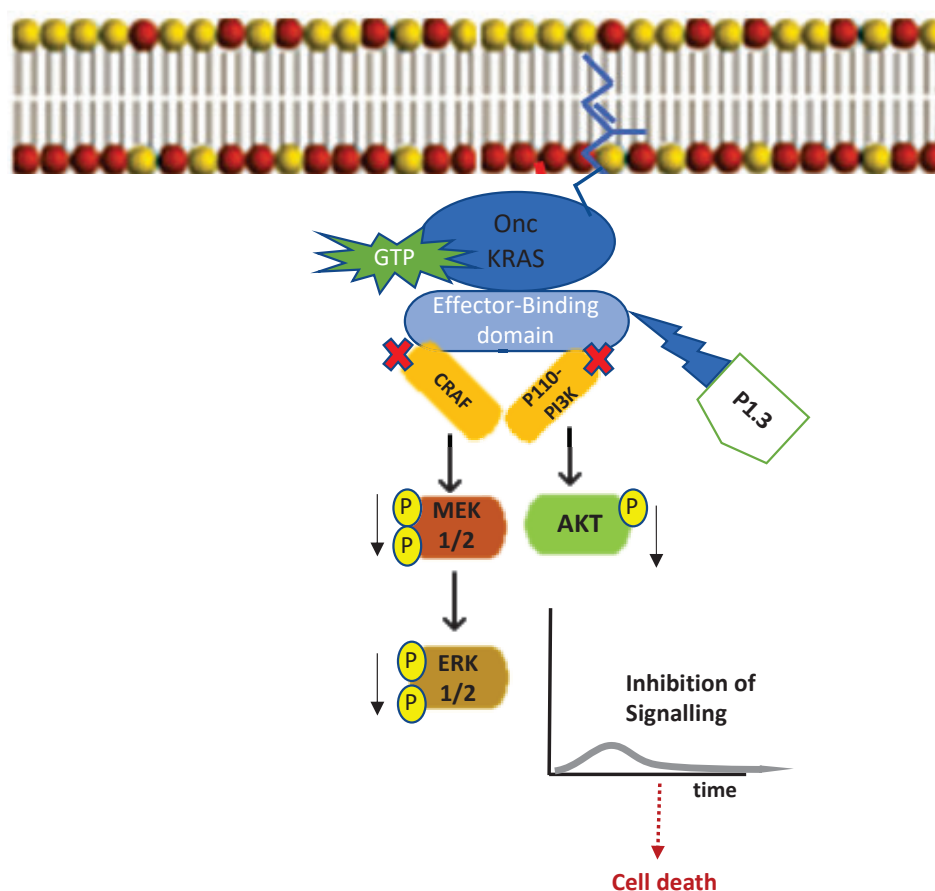


Figure 53: Model representation summarising the biological effect of peptidomimetic P1.3 targeting KRAS effector-binding domain.

5.2. Small molecule binds directly to $\alpha 4$ - $\alpha 5$ helices on surface of KRAS increases its signalling while inducing colorectal cancer (CRC) cell death

In this study, we unveil a **promising druggable pocket nestled within the $\alpha 4$ - $\alpha 5$ helices regions of KRAS**, employing advanced molecular modelling techniques. This site, previously recognized for its significance in the interaction with calmodulin (CaM) (Garrido et al., 2018a; Lopez-Alcalá et al., 2008b), emerges as a focal point for therapeutic intervention. Taking advantage of docking and molecular dynamics simulations, we pinpointed a compound, which we named **P14**, capable of accommodating into this pocket. After reformulating this compound, several derivatives were generated and between them, **P14B** was chosen as the most promising candidate to continue the research. Experimental validation, by surface plasmon resonance, not only affirmed **its binding affinity with KRAS** but also, by a competition assay, demonstrated its **ability to impede CaM binding**, thereby orchestrating a modulation of RAS signalling pathways. Extensive investigations have elucidated the intricate organization of RAS proteins into nanoclusters, typically encompassing 6-7 molecules within a radius of ~ 9 nm, thus serving as highly dynamic hubs for RAS-mediated signalling events (Zhou & Hancock, 2014). Notably, disrupting RAS function can be achieved through the inhibition of RAS dimerization/nanoclustering (Spencer-Smith et al., 2017). Building upon this foundation, Spencer-Smith and collaborators unveiled the development of a synthetic binding protein, NS1 monobody, adept at robustly inhibiting oncogenic RAS-driven signalling and transformation, that significantly reduced co-localisation of KRAS-G12V with CRAF at the plasma membrane (Spencer-Smith et al., 2017). This inhibition is accomplished through precise targeting of the $\alpha 4$ and $\alpha 5$ helices within the G-domain, as detailed in their seminal work (Spencer-Smith et al., 2019). Furthermore, it is noteworthy that the K13 and K19 DARPins (Anti-RAS designed ankyrin repeat proteins macromolecules) exert inhibitory effects on KRAS binding within the $\alpha 3$ - $\alpha 4$ allosteric lobe, thereby perturbing the integrity of RAS dimerization and nanocluster formation (Bery et al., 2019).

In contrast to these findings, the compounds that we have identified as putative drugs accommodating in a pocket within $\alpha 4$ - $\alpha 5$ helices of KRAS, **P14 and P14B**, unexpectedly **activated RAS signalling in treated CRC cells expressing oncogenic KRAS**. A possible explanation for this discrepancy, could be that although P14 and P14B might be interacting with the same KRAS surface as the previously reported molecules, the specific amino acids of

KRAS interacting with the compounds may differ and, hence, the differences observed in KRAS signalling.

Since our aim was to analyse if P14 and P14B treatment of cancer cells might have an impact on signalling pathways activated by oncogenic KRAS, we used DLD-1 cells, which are CRC cancer cells harbouring one oncogenic KRAS allele. Although DLD-1 cells harbour a different oncogenic mutation in KRAS (G13D) that the model structure used in the KRAS modelling and in docking analysis (G12V) (Garrido et al., 2018b), we know from our previous work that CaM binds to KRAS independently of being or not mutated in this region of the protein. The unique restriction is that CaM binds to KRAS only if the latter is GTP-loaded and non-phosphorylated at S181 (Garrido et al., 2018a; Lopez-Alcalá et al., 2008a).

Our primary objective was to scrutinize the impact of P14B on signalling pathways activated by oncogenic KRAS. Prior research has underscored the elevated levels of ERK1/2 and AKT phosphorylation in DLD-1 cells, indicative of heightened signalling activity (Tsubaki et al., 2019). Although these cells have a KRAS oncogenic allele, the addition of foetal bovine serum (FBS) to serum-starved cells triggered a notable surge in phosphorylated MEK, ERK, and AKT, underscoring the capacity of growth factors to induce robust activation of signal transduction pathways. Strikingly, administration of P14B in isolation to serum starved DLD-1 cells was sufficient to provoke a similar level of activation of these KRAS downstream kinases. Furthermore, the phosphorylation of ERK exhibited a more sustained profile in P14B-treated cells compared to FBS-treated cells.

The sustained ERK activation observed in the context of RAS mutations or expression alterations in the pathway has been primarily attributed to the absence of negative feedback regulation from ERK (Fritsche-Guenther et al., 2011), suggesting that certain negative feedback pathways responsible for ERK deactivation might not be activated due to the P14B treatment. It is important to note that ERK phosphorylation was maintained over time, but not CRAF phosphorylation (Ser338). One possibility is that CRAF activity was maintained even in the absence of Ser338 phosphorylation (frequently considered a readout of CRAF activity) (Oehrl et al., 2003) Figure 54. In this sense, an additional study proposed that tyrosine phosphorylation of CRAF may augment ERK activation independently to its role in facilitating Ser338 CRAF phosphorylation. This hypothesis was supported by experiments utilising phosphomimetic mutations (tyrosine (Y) to aspartate (D)) of both tyrosines (SSDD instead of

SSYY). These mutant cells exhibited a significant increase in ERK activation compared to wild type cells expressing (SSYY), despite no further elevation in the level of Ser338 phosphorylation was detected (Takahashi et al., 2017).

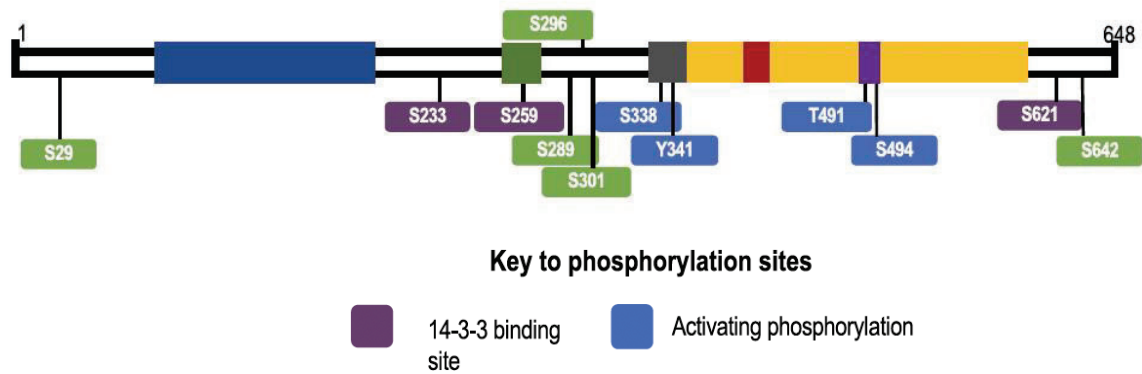


Figure 54: Representative image showing CRAF structure and its phosphorylation sites necessary for full CRAF activation. *Adapted from* (Cook et al., 2021).

Additionally, the increase in ERK activity observed when cells are treated with P14B could be due to variation in the stoichiometry of CRAF/BRAF heterodimers, which play a pivotal role in dimerization induced ERK activation, as highlighted by multiple studies (Freeman et al., 2013; Garnett et al., 2006; Rushworth et al., 2006).

Consistent with the induction of MEK and ERK phosphorylation in **P14B-treated DLD-1 cells**, **alterations in RAF binding to KRAS** were also observed by co-IP in DLD-1 cells exogenously stably expressing HA-KRAS-G12V. As anticipated, oncogenic KRAS exhibited binding to CRAF even under serum-starved conditions, a phenomenon previously reported, albeit without concomitant RAS pathway activation (Lerner et al., 1995). However, growth factor stimulation was indispensable for phosphorylation and subsequent activation of KRAS-bound CRAF (J. Zhao & Luo, 2022). Interestingly, P14B addition bypasses this requirement, since we could see active CRAF (P-CRAF (Ser338)) bound to KRAS upon P14B addition to serum starved cells. Conversely, no binding of BRAF to oncogenic KRAS was detected in serum-starved HA-KRAS-G12V cells. It has been proposed that in RAS mutant cells, BRAF adopts an inactive conformation through its intrinsic kinase activity, either via auto-phosphorylation or by phosphorylating a partner protein that maintains it in an inactive state (Heidorn et al., 2010).

Intriguingly, our findings revealed that P14B treatment completely mirrors the effect of growth factors in terms of the association of BRAF with oncogenic KRAS.

As intended, in this study we determined how P14B interacts with the globular region of oncogenic KRAS and showed that it inhibits the interaction of CaM with this domain. Our previous studies indicated that CaM interacts with KRAS *in vivo* and that inhibition of CaM enhances both wild-type and oncogenic KRAS signalling. It seems that interruption of KRAS-CaM binding could be a reason of the sustained activation of ERK pathway as indicated in Figure 38. Interestingly, highly sustained activation of the ERK pathway induces overexpression of P21^{cip1}, cyclin-dependent kinase inhibitor 1, which in turn leads to growth arrest of the cells, while transient activation followed by a sustained but lower level of ERK activity induces cell proliferation in many systems (Kahan et al., 1992; Pumiglia & Decker, 1997; Qiu & Green, 1992; Roovers & Assoian, 2000). In agreement with that, other studies have shown that sustained ERK activation induces a program cell-withdrawal in intestinal epithelial cells through the activation of protein kinase c α (PKC α). This process, alongside its role in cell proliferation, is considered to be important for maintaining intestinal homeostasis (Clark et al., 2004; Frey et al., 1997, 2000).

In accordance with the fact that CaM prevents a too-sustained ERK1/2 activation and cell proliferation upon growth factors stimulation (Bosch et al., 1998; Villalonga et al., 2001), our cell viability assay clearly showed a reduction in cell proliferation of DLD-1 cells harbouring an oncogenic KRAS allele upon P14B treatment, corroborated with the increased level of apoptosis. Congruent with that evidence, DLD-1 cells harbouring knockout oncogenic allele of KRAS and non-transformed hTERT-RPE cells do not show such a high increase in ERK phosphorylation upon P14B treatment and did not undergo cell death upon P14B treatment. This is apparently contradictory but the promotion of apoptosis by RAS, and specifically by the RAS/RAF/ERK pathway, has been described previously (Kauffmann-Zeh et al., 1997; Pylayeva-Gupta et al., 2011). It is also possible that other KRAS effectors are engaged by P14B and not by FBS treatment and are responsible for the observed cell death.

Additionally, P14B could exhibit multifaceted actions beyond its interaction with CaM. It would be interesting to know whether P14B is capable of directly modulating the interaction of various proteins with the critical $\alpha 4$ - $\alpha 5$ helices region of KRAS, thus influencing downstream signalling pathways independently of its role in preventing CaM interaction.

Notably, in the context of ovarian, lung and pancreatic cancers, the tumour suppressor DIRAS3 has been found to bind to the α 5-helix region of KRAS within the same binding pocket as P14B (Sutton et al., 2019). By doing so, DIRAS3 effectively impedes KRAS clustering and attenuates its signalling cascade. Given these findings, it presents an intriguing avenue of investigation to ascertain whether DIRAS3 exerts a similar inhibitory effect in CRC cells and whether P14B disrupts this interaction.

Moreover, emerging evidence suggests a complex assembly of RAS proteins into higher-order helical complexes termed RAS-RAF signalosomes. Within these assemblies, not all RAS members make direct contact with the plasma membrane. Notably, the β 4- α 3, β 5- α 4, and β 6- α 5 loops of KRAS play pivotal roles in mediating the formation of asymmetric KRAS dimers within these structures (Mysore et al., 2021). Consequently, it raises the question of whether P14B may modulate the generation of such superstructures, potentially influencing downstream signalling pathways. Further investigations are warranted to elucidate the precise mechanisms by which P14B impacts the assembly and function of RAS-RAF signalosomes.

Furthermore, our study has elucidated the impact of P14B on colony formation using DLD-1 cells within a 3D environment. Notably, our findings reveal that **P14B effectively reduces the capacity for colony formation**, accompanied by a noticeable decrease in the size of established colonies. Extending our investigations to patient-derived colorectal cancer organoids (PDCOs), we observed a **significant inhibitory effect of P14B treatment on the proliferation rate of these PDCOs**, distinguishing them markedly from patient-derived normal organoids. Importantly, this inhibitory effect was consistently studied across various constitutive passages of PDCOs. However, it is noteworthy that our results (data not shown) were not completely reproducibly and yielded a contradictory outcome upon P14B treatment, wherein a significant impediment to organoid growth in PDCOs was not observed. This discrepancy underscores the importance of considering factors such as P14B solubility to optimize its efficacy in organoids or when transitioning to *in vivo* models. Moreover, exploring structural modifications to generate derivatives aimed at enhancing the efficacy of P14B *in vivo* represents a promising avenue for future research efforts. These endeavours hold the potential to significantly improve therapeutic outcomes in the treatment of CRC, offering novel strategies for combating this challenging disease. Further exploration in animal models

and clinical trials will be crucial to validate and translate these findings into effective therapeutic interventions for CRC patients.

A model explaining the biological effect of P14B on oncogenic KRAS signalling pathways is shown in Figure 55.

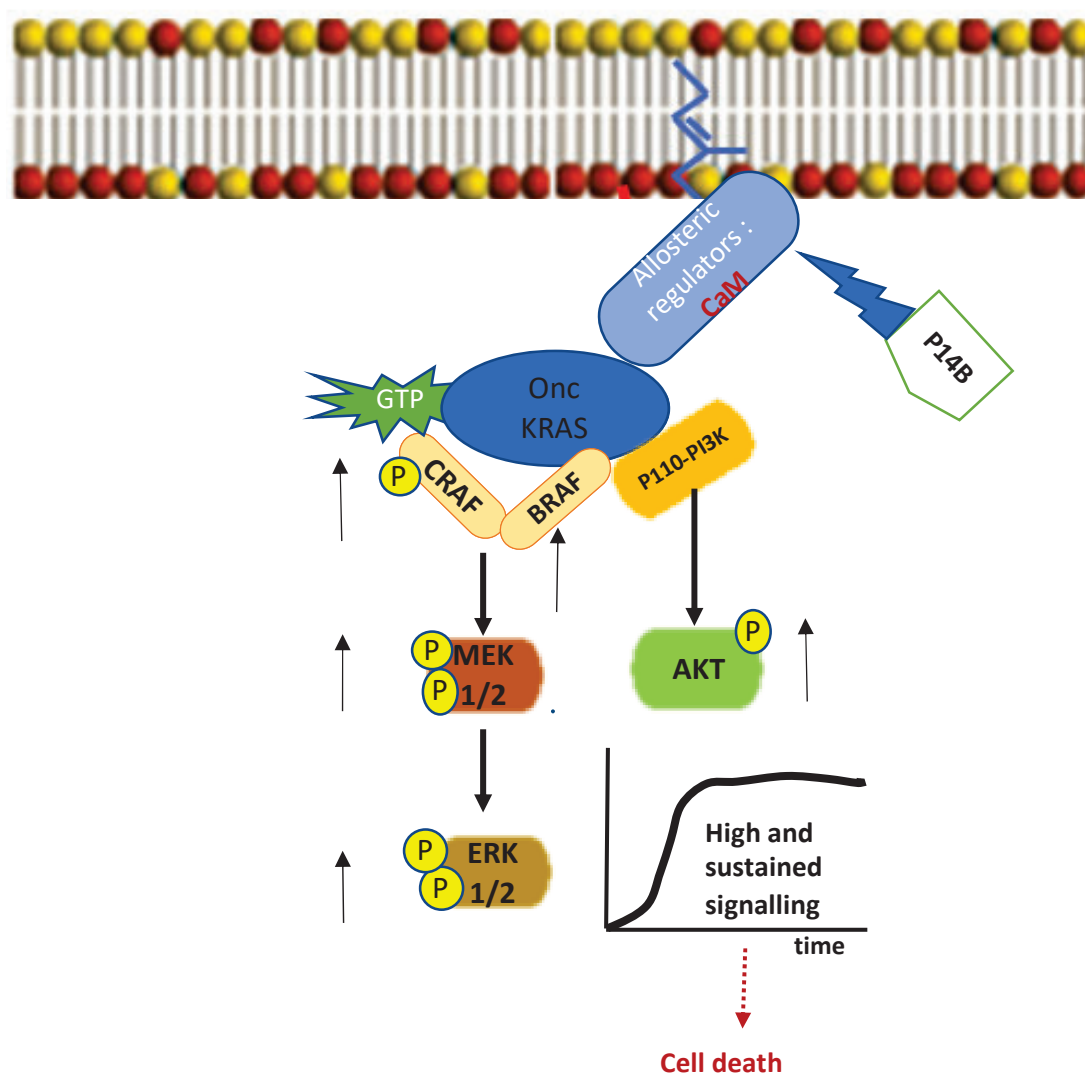


Figure 55: Model representation summarising the biological effects of small molecule P14B directly targeting the allosteric domain of KRAS.

One of our objectives was to gain a comprehensive understanding of the **KRAS interaction landscape upon P14B treatment**. To achieve this, we employed UltraID, the smallest enzyme for proximity-dependent biotinylation (PDB) studies, measuring 44% smaller than BioID. This affords us a distinct advantage, as larger tag sizes are often associated with increased likelihood of interference with protein function trafficking, and interactions (Vandemoortele et al., 2019). Given that our focus was on investigating the effect of P14B treatment on

oncogenic KRAS interactome within a short timeframe of one hour, the use of UltraID addresses the limitations posed by BioID. Unlike BioID, which requires prolonged incubation periods with biotin due to its slower kinetics labelling, UltraID enables rapid labeling of the interacting proteins. Consequently, this mitigates the risk of high background labelling prior to P14B treatment and to the supplementation of additional biotin in the medium (May et al., 2020).

After confirming the functionality of the UltraID-KRAS-G12V expression vector, our liquid chromatography coupled to mass spectrometry (LC/MS) protein analysis of the PDB experiment (performed in P14B-treated and not-treated DLD-1 colorectal cancer (CRC) cells), revealed a total of 116 high-confidence KRAS-proximal interactors. Among these, 16 proteins were previously conclusively identified with high confidence as physical interactors with KRAS, showcasing notable candidates such as MAPK1, EGFR, BRAF, and ARAF. It's worth noting that certain biotinylated proteins that were expected to be identified as KRAS interactors, including PI3K-p110 and CRAF, couldn't be verified by LC/MS, suggesting that the sensitivity of LC/MS analysis may fall below the threshold for specific proteins. This could suggest a higher stability in the interaction of these proteins with KRAS, leading to a reduced turnover of bound molecules and consequently lower levels of biotinylated proteins. Thus, additional fractionation methods to enrich for some proteins could be considered for future UltraID-LC/MS work. Nonetheless, our results analysed using Proteome Discoverer and SAINT softwares highlighted changes in the interaction of KRAS with some partners upon P14B treatment.

Another aspect to consider from our data exploration is that, while we successfully identified calmodulin (CaM) and BRAF as KRAS interactors, the anticipated changes following P14B treatment were not observed: specifically, an expected increase in BRAF and a decrease in CaM. This discrepancy might be attributed to the possibility that within one-hour of P14B treatment, any initial differences had already diminished.

Among the proteins showing an increased interaction with KRAS following P14B treatment, we found, **junctophilin 1**, **importin subunit alpha-1**, and **aspartate—tRNA ligase**, which interact directly with KRAS or through different protein complexes according to the BioGrid database as depicted in Figure 56 and in Figure 49 of the Results section of this thesis. For instance, aspartate—tRNA ligase was previously found to interact with KRAS in a high throughput analysis (affinity capture-MS) (Rosenbluh et al., 2016), but also with growth factor

receptor-bound protein 2 (GRB2) (Brehme et al., 2009) that directly interacts with KRAS (Bigenzahn et al., 2018b) or indirectly through SOS1 (Huttlin et al., 2021), as indicated in Figure 56B. This same high-throughput analysis (Rosenbluh et al., 2016), along with additional studies utilising affinity capture-MS and proximity label-MS (Go et al., 2021a), identified interactions between several members of the importin complexes with KRAS. Interestingly, some of these members also interact with CaM and CaM-like proteins, which are known strong interactors of KRAS (Figure 56C). Furthermore, three independent high-throughput studies have pinpointed an interaction between KRAS and junctophilin 1 (Adhikari & Counter, 2018; Go et al., 2021a; Kovalski et al., 2019). Remarkably, this protein also interacts with CaM-like proteins (Figure 56A).

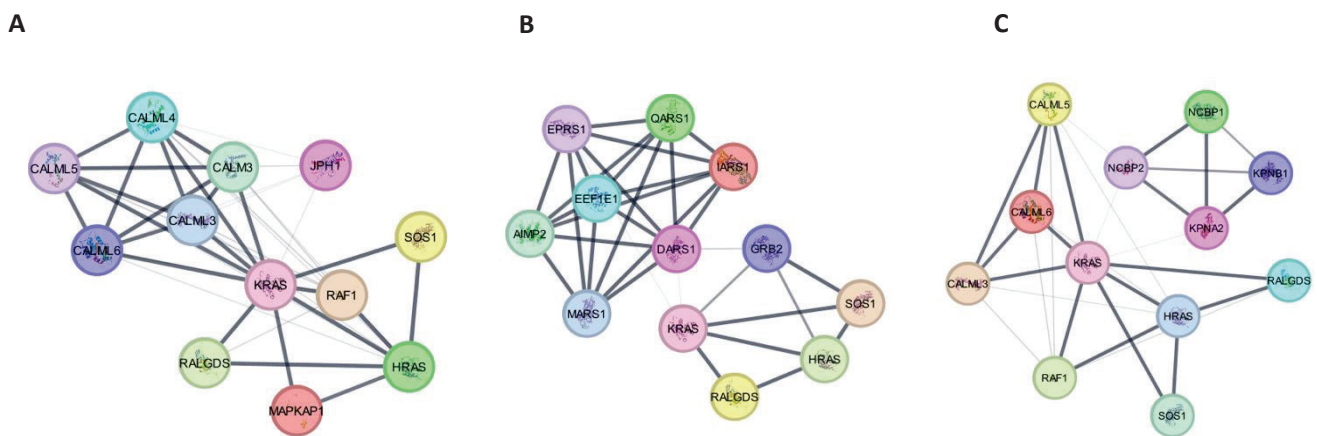


Figure 56: Direct KRAS physical interactions revealed by UltraID proximity-dependent biotinylation assay in DLD-1 cells, analysed using Cytoscape. 10 strong KRAS binding proteins were incorporated into the analysis. A cut score of 0,1 was employed for the detection of the physical interactions. (A) Illustrates potential interacting partners of Junctophilin 1 (JPH1), highlighting its network of association. (B) Displays a representative image of the interacting partners of aspartate—tRNA ligase (DARS1). (C) Exploration of the potential interacting proteins associated with importin subunit alpha-1 (KPNA2).

While these interactions identified by LC/MS await validation through co-immunoprecipitation performed in lysates from KRAS-G12V expressing cells, and/or through streptavidin pull-down followed by western blot (WB) in lysates of cells expressing Ultra-ID-KRAS G12V and incubated with biotin; we can speculate on the potential involvement of these

proteins in the decrease in cell viability following P14B treatment observed in DLD-1 but not in normal cells.

Junctophilins (JPHs) belong to members of the family of junctional membrane complex (JMC) proteins, which play a crucial role in stabilizing the junctional membrane complex between the endoplasmic reticulum (ER) and plasma membrane (PM). Among these proteins, JPH3 has emerged as a tumour suppressor downregulated and methylated in colorectal and gastric cancers (X. Hu et al., 2017). Studies have confirmed that restoring of JPH3 increases ER stress-induced apoptosis and upregulates several unfolded protein response (UPR) pathways, which may initiate apoptotic cascades to eliminate stressed cells (Woehlbier & Hetz, 2011) in colorectal and gastric cancer cells due to the sustained or extensive stress (X. Hu et al., 2017). Furthermore, JPH3 expression triggers calpain activation leading to mitochondrial membrane depolarization, followed by the release of cytochrome C and Smac from the mitochondria, consequently activating caspase -9 and -3 (Figure 57) (X. Hu et al., 2017). These findings are consistent with our results observing apoptotic cell death and increased direct interaction of JPH1 with KRAS following P14B treatment of CRC cells.

Interestingly, regarding **aspartate—tRNA ligase** and **importin subunit alpha-1**, previously described binding proteins of these two direct KRAS interactors identified in our study, are found in our differentially biotinylated proteins (DBPs) list, and also, they display a highly interconnect network with other proteins of the list (refer to Figure 49 in results). Among them, **condensin complex subunit 2**, **E3 ubiquitin-protein ligase (HUWE1)**, **glutamine--fructose-6-phosphate aminotransferase**, **methionine--tRNA ligase** and **CRK-I**. These proteins showed increased level of interaction with KRAS upon P14B treatment except CRK-1, which indicates a negative modulation with KRAS interaction upon P14B treatment.

We will highlight here the role of some of those proteins and discuss their relationship with KRAS.

To begin with, the protein **HUWE1** could interact with KRAS through Shoc2 protein (Figure 58A). HUWE1 interacts with Shoc2 (Jang et al., 2014) and it has been illustrated that GTP-bound H/N/KRAS forms productive holoenzyme complexes with Shoc2 (Liau et al., 2022), although we did not identify Shoc2 in our analysis.

the binding capacity of P-CRAF (S338) and BRAF with oncogenic KRAS upon P14B treatment, leading to sustained activation of ERK1/2. Shoc2 also recruits numerous proteins of the ubiquitin machinery to fine-tune signals transmitted via the module. An earlier study confirmed the E3 ubiquitin ligase HUWE1 as a new partner in the Shoc2-RAS-CRAF scaffold complex (Jang et al., 2014). Additionally, it was demonstrated that activation of the ERK1/2 pathway triggers Shoc2 and CRAF ubiquitylation by the E3 ligase HUWE1 as part of a negative feedback loop, inhibiting Shoc2's ability to accelerate ERK1/2 activation (Jang et al., 2014). The ERK activity observed over the treatment course with P14B in DLD-1 cells, suggests that this negative feedback loop is inhibited upon P14B treatment (Figure 59). Furthermore, a study demonstrated that USP7 de-ubiquitylating enzyme interacts with Shoc2 and HUWE1 in response to EGF-induced activation of ERK1/2 and regulates the HUWE1-mediated negative feedback loop that modulates the amplitude of Shoc2-ERK1/2 signals (Wilson et al., 2021). We did not observe a degradation of CRAF upon P14B, suggesting that the ubiquitination by HUWE1 was also inhibited **Figure 59**.

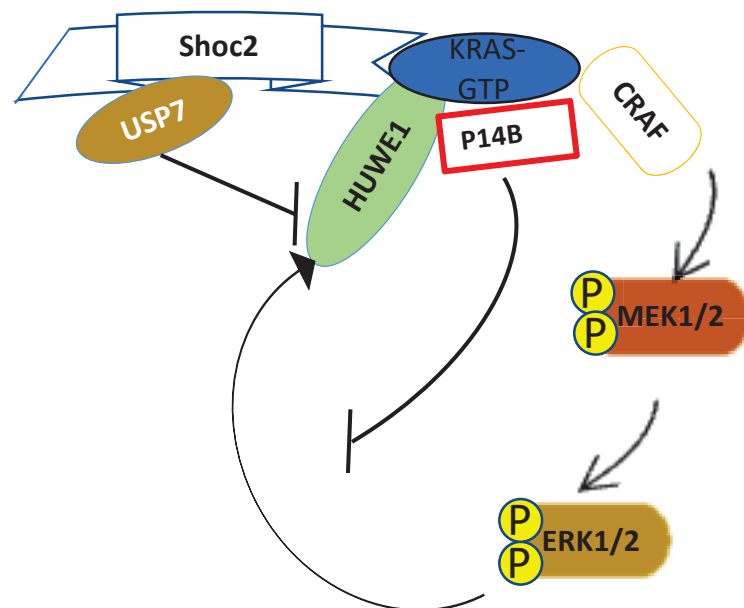


Figure 59: Model depicting the sustained activation of the ERK1/2 pathway following exposure to P14B: P14B potentially inhibiting the negative feedback mechanism mediated by the E3 ubiquitin ligase HUWE1.

As mentioned above, the analysis of DBPs obtained in our experiment, revealed a notable decrease in the level of interaction of **CRK** with KRAS upon P14B treatment. CRK emerges as a pivotal pro-apoptotic cue essential for executing cell death triggered by ER-stress (Austgen

et al., 2012). Notably, CRK-I exhibit elevated expression in various human cancers (Miller et al., 2003; Sriram & Birge, 2010). Both CRK isoforms, CRK-I and CRK-II, harbour a BH3-death domain, empowering mitochondria to respond to BID stimulation by releasing cytochrome C, thereby amplifying apoptotic signals within the cells (Austgen et al., 2012). Interestingly, during ER-stress, an unidentified cysteine protease cleaves CRK-I and CRK-II, yielding N-terminal fragments endowed with robust apoptotic potential (Austgen et al., 2012). Given that cancer cells inherently harbour basal ER stress, coupled with the fact that the heightened ERK signalling triggered by P14B treatment can exacerbates this stress, it is tempting to speculate that interaction of oncogenic KRAS with CRK-I obstructs its cleavage by the cysteine protease. Upon administration of P14B treatment, this obstruction may be alleviated, leading to the liberation and subsequent cleavage of CRK-I, thereby enabling its proapoptotic role (Figure 60).

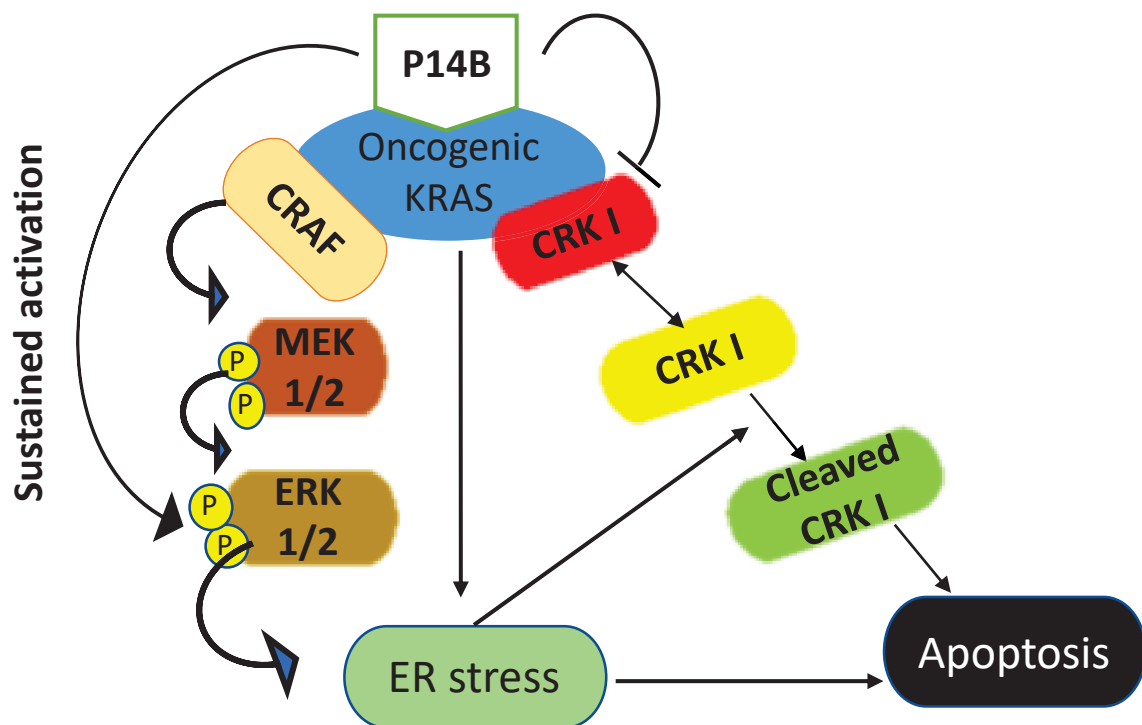


Figure 60: Model depicting how the sustained activation of ERK1/2 in P14B treated cells may potentiate ER stress, and synergistically how P14B may affect the interaction of oncogenic KRAS with CRK-I, yielding in CRK-I release and cleavage, and culminating in apoptotic cell death.

Furthermore, our findings following P14B treatment of the cells, revealed a noteworthy observation within DBPs. Specifically, a significant increased representation of proteins

involved in metabolic and biosynthesis pathways is observed. They could potentially exert positive or negative influences. It is widely acknowledged that the relentless growth of tumours necessitates a continuous influx of micronutrients to sustain both bioenergetic and macromolecule biosynthesis (Cluntun et al., 2017). However, this process inevitably confines nutrient availability within the tumour microenvironment (Ahmadiankia et al., 2019; Cluntun et al., 2017). Notably, oncogenic KRAS plays a pivotal role in upregulating key glycolytic enzymes to meet the energy demands of cancer cells (Ying et al., 2012). The heightened metabolic requirements stemming from uncontrolled tumour proliferation contribute significantly to metabolic stress, a pathway known to trigger apoptosis (White, 2006). Thus, it would be interesting to investigate the extent to which P14B treatment influences metabolism, potentially inducing cellular stress pathways and ultimately leading to apoptosis.

6. CONCLUSIONS

1. The peptidomimetic P1.3, *in silico* designed to bind to the RAS protein within its effector domain, exerts a downregulatory effect on RAS main signalling pathways RAF/MAPK and PI3K/AKT in non-transformed cells, without affecting the levels of GTP-KRAS.
2. P1.3 exhibits direct binding affinity with oncogenic KRAS *in vitro* by surface plasmon resonance (affinity constant of 15.7 μ M).
3. The maximum tolerated dose of P1.3 administration in nude mice is 20mg/kg, demonstrating no discernible organ toxicity in the spleen, pancreas, or liver; however, the intraperitoneal injection may induce coagulative necrosis in liver.
4. The small molecule P14, selected for being able to accommodate into an allosteric pocket near α 5 helix of KRAS, induces an activation of KRAS signalling pathways RAF/MAPK and PI3K/AKT in colorectal cancer (CRC) and in pancreatic ductal adenocarcinoma (PDAC) cell lines expressing oncogenic KRAS.
5. P14B, an improved derivative of P14, induces an increased activation of KRAS signalling pathways RAF/MAPK and PI3K/AKT in CRC cells, with a sustained ERK activation. In contrast, P14B treatment, induces a mild increase in signalling in CRC cells expressing wild type KRAS and in normal cells.
6. P14B treatment of CRC cells expressing oncogenic KRAS favours *in vivo* KRAS interaction with its effectors P-CRAF (Ser338) and BRAF.
7. P14B exhibits direct binding affinity with the globular domain of oncogenic KRAS *in vitro* by surface plasmon resonance (affinity constant of 32.8 μ M).
8. P14B competes with calmodulin for binding to the globular domain of oncogenic KRAS *in vitro*.
9. P14B treatment decreases the viability of CRC cells expressing oncogenic KRAS (with an IC₅₀ of 80 μ M), and increases apoptosis, but not that of CRC cells expressing wild type KRAS or normal cells.
10. P14B treatment reduces the colony-forming capacity of CRC cells growing in 3D conditions (Matrigel).
11. The UltraID-KRAS-G12V proximity dependent biotinylation -LC/MS method (UltraID-LC/MS) has successfully been set up, being appropriate for the identification of oncogenic KRAS-binding proteins *in vivo*. More than 100 KRAS-proximal interactors have been identified by UltraID-LC/MS in DLD-1 CRC cells.
12. P14B treatment of CRC cells alters the protein interaction profile of oncogenic KRAS, revealing differential abundances of proteins that bind directly or indirectly to KRAS:
13. A total number of 33 proteins exhibit differential biotinylation (DBPs) upon P14B treatment with 32 of them showing increased interaction with KRAS, while only 1 demonstrated decreased interaction. Among the DBPs, Junctophilin-1, importin subunit α -1 and aspartate-tRNA ligase were previously described as direct KRAS interactors.

7. References

- Abankwa, D., Gorfe, A. A., & Hancock, J. F. (2007). Ras nanoclusters: Molecular structure and assembly. *Seminars in Cell & Developmental Biology*, 18(5), 599–607. <https://doi.org/https://doi.org/10.1016/j.semcdb.2007.08.003>
- Abuasaker, B., Garrido, E., Vilaplana, M., Gómez-Zepeda, J. D., Brun, S., Garcia-Cajide, M., Mauvezin, C., Jaumot, M., Pujol, M. D., Rubio-Martínez, J., & Agell, N. (2023). $\alpha 4$ - $\alpha 5$ Helices on Surface of KRAS Can Accommodate Small Compounds That Increase KRAS Signaling While Inducing CRC Cell Death. *International Journal of Molecular Sciences*, 24(1). <https://doi.org/10.3390/ijms24010748>
- Adhikari, H., & Counter, C. M. (2018). Interrogating the protein interactomes of RAS isoforms identifies PIP5K1A as a KRAS-specific vulnerability. *Nature Communications*, 9(1), 3646. <https://doi.org/10.1038/s41467-018-05692-6>
- Aguirre, A. J., & Hahn, W. C. (2018). Synthetic Lethal Vulnerabilities in KRAS-Mutant Cancers. *Cold Spring Harbor Perspectives in Medicine*, 8(8). <https://doi.org/10.1101/cshperspect.a031518>
- Ahmadiankia, N., Bagheri, M., & Fazli, M. (2019). Nutrient deprivation modulates the metastatic potential of breast cancer cells. *Reports of Biochemistry & Molecular Biology*, 8(2), 139.
- Alvarez-Moya, B., Barceló, C., Tebar, F., Jaumot, M., & Agell, N. (2011). Cam interaction and ser181 phosphorylation as new k-ras signaling modulators. *Small GTPases*, 2(2), 99–103. <https://doi.org/10.4161/sgtp.2.2.15555>
- Alvarez-Moya, B., López-Alcalá, C., Drosten, M., Bachs, O., & Agell, N. (2010). K-Ras4B phosphorylation at Ser181 is inhibited by calmodulin and modulates K-Ras activity and function. *Oncogene*, 29(44), 5911–5922. <https://doi.org/10.1038/onc.2010.298>
- Aoyama, Y., Avruch, J., & Zhang, X. (2004). Nore1 inhibits tumor cell growth independent of Ras or the MST1/2 kinases. *Oncogene*, 23(19), 3426–3433. <https://doi.org/10.1038/sj.onc.1207486>
- Apolloni, A., Prior, I. A., Lindsay, M., Parton, R. G., & Hancock, J. F. (2000). H-ras but Not K-ras Traffics to the Plasma Membrane through the Exocytic Pathway. *Molecular and Cellular Biology*, 20(7), 2475–2487. <https://doi.org/10.1128/MCB.20.7.2475-2487.2000>
- Austgen, K., Johnson, E. T., Park, T. J., Curran, T., & Oakes, S. A. (2012). The adaptor protein CRK is a pro-apoptotic transducer of endoplasmic reticulum stress. *Nature Cell Biology*, 14(1), 87–92. <https://doi.org/10.1038/ncb2395>
- Avruch, J., Xavier, R., Bardeesy, N., Zhang, X., Praskova, M., Zhou, D., & Xia, F. (2009). Rassf Family of Tumor Suppressor Polypeptides*. *Journal of Biological Chemistry*, 284(17), 11001–11005. <https://doi.org/https://doi.org/10.1074/jbc.R800073200>
- Baker, R., Wilkerson, E. M., Sumita, K., Isom, D. G., Sasaki, A. T., Dohlman, H. G., & Campbell, S. L. (2013). Differences in the regulation of K-Ras and H-Ras isoforms by monoubiquitination. *The Journal of Biological Chemistry*, 288(52), 36856–36862. <https://doi.org/10.1074/jbc.c113.525691>
- Ballester, R., Furth, M. E., & Rosen, O. M. (1987). Phorbol ester- and protein kinase C-mediated phosphorylation of the cellular Kirsten ras gene product. *Journal of Biological Chemistry*, 262(6), 2688–2695. [https://doi.org/https://doi.org/10.1016/S0021-9258\(18\)61562-5](https://doi.org/https://doi.org/10.1016/S0021-9258(18)61562-5)
- Bange, E., Marmarelis, M. E., Hwang, W.-T., Yang, Y.-X., Thompson, J. C., Rosenbaum, J., Bauml, J. M., Ciunci, C., Alley, E. W., Cohen, R. B., Langer, C. J., Carpenter, E., & Aggarwal, C. (2019). Impact of KRAS and TP53 Co-Mutations on Outcomes After First-

- Line Systemic Therapy Among Patients With STK11-Mutated Advanced Non–Small-Cell Lung Cancer. *JCO Precision Oncology*, 3, 1–11. <https://doi.org/10.1200/PO.18.00326>
- Barbacid, M. (n.d.). *ras GENES*. www.annualreviews.org
- Barceló, C., Etschin, J., Mansour, M. R., Sanda, T., Ginesta, M. M., Sanchez-Arévalo Lobo, V. J., Real, F. X., Capellà, G., Estanyol, J. M., Jaumot, M., Look, A. T., & Agell, N. (2014). Ribonucleoprotein HNRNPA2B1 Interacts With and Regulates Oncogenic KRAS in Pancreatic Ductal Adenocarcinoma Cells. *Gastroenterology*, 147(4), 882–892.e8. <https://doi.org/https://doi.org/10.1053/j.gastro.2014.06.041>
- Barceló, C., Paco, N., Morell, M., Alvarez-Moya, B., Bota-Rabassedas, N., Jaumot, M., Vilardell, F., Capella, G., & Agell, N. (2014a). Phosphorylation at Ser-181 of Oncogenic KRAS Is Required for Tumor Growth. *Cancer Research*, 74(4), 1190–1199. <https://doi.org/10.1158/0008-5472.CAN-13-1750>
- Barceló, C., Paco, N., Morell, M., Alvarez-Moya, B., Bota-Rabassedas, N., Jaumot, M., Vilardell, F., Capella, G., & Agell, N. (2014b). Phosphorylation at Ser-181 of Oncogenic KRAS Is Required for Tumor Growth. *Cancer Research*, 74(4), 1190–1199. <https://doi.org/10.1158/0008-5472.CAN-13-1750>
- Basso, A. D., Kirschmeier, P., & Bishop, W. R. (2006). Thematic review series: Lipid Posttranslational Modifications. Farnesyl transferase inhibitors. *Journal of Lipid Research*, 47(1), 15–31. <https://doi.org/https://doi.org/10.1194/jlr.R500012-JLR200>
- Becher, I., Savitski, M. M., Savitski, M. F., Hopf, C., Bantscheff, M., & Drewes, G. (2013). Affinity Profiling of the Cellular Kinome for the Nucleotide Cofactors ATP, ADP, and GTP. *ACS Chemical Biology*, 8(3), 599–607. <https://doi.org/10.1021/cb3005879>
- Beck, T. W., Huleihel, M., Gunnell, M. A., Bonner, T. I., & Rapp, U. R. (1987). The complete coding sequence of the human A-raf-1 oncogene and transforming activity of a human A-raf carrying retrovirus. *Nucleic Acids Research*, 15 2, 595–609. <https://api.semanticscholar.org/CorpusID:42763478>
- Bellio, H., Fumet, J. D., & Ghiringhelli, F. (2021). Targeting BRAF and RAS in Colorectal Cancer. *Cancers*, 13(9). <https://doi.org/10.3390/cancers13092201>
- Berg, T. J., Gastonguay, A. J., Lorimer, E. L., Kuhnmuench, J. R., Li, R., Fields, A. P., & Williams, C. L. (2010). Splice variants of SmgGDS control small GTPase prenylation and membrane localization. *The Journal of Biological Chemistry*, 285(46), 35255–35266. <https://doi.org/10.1074/jbc.m110.129916>
- Bergo, M. O., Wahlstrom, A. M., Fong, L. G., & Young, S. G. (2008). Genetic analyses of the role of RCE1 in RAS membrane association and transformation. *Methods in Enzymology*, 438, 367–389. <https://api.semanticscholar.org/CorpusID:28368996>
- Bery, N., Legg, S., Debreczeni, J., Breed, J., Embrey, K., Stubbs, C., Kolasinska-Zwierz, P., Barrett, N., Marwood, R., Watson, J., Tart, J., Overman, R., Miller, A., Phillips, C., Minter, R., & Rabbitts, T. H. (2019). KRAS-specific inhibition using a DARPIn binding to a site in the allosteric lobe. *Nature Communications*, 10(1). <https://doi.org/10.1038/s41467-019-10419-2>
- Betzig, E., Patterson, G. H., Sougrat, R., Lindwasser, O. W., Olenych, S., Bonifacino, J. S., Davidson, M. W., Lippincott-Schwartz, J., & Hess, H. F. (2006). Imaging Intracellular Fluorescent Proteins at Nanometer Resolution. *Science*, 313(5793), 1642–1645. <https://doi.org/10.1126/science.1127344>
- Bigenzahn, J. W., Collu, G. M., Kartnig, F., Pieraks, M., Vladimer, G. I., Heinz, L. X., Sedlyarov, V., Schischlik, F., Fauster, A., Rebsamen, M., Parapatics, K., Blomen, V. A., Müller, A. C., Winter, G. E., Kralovics, R., Brummelkamp, T. R., Mlodzik, M., & Superti-Furga, G.

- (2018a). LZTR1 is a regulator of RAS ubiquitination and signaling. *Science (New York, N.Y.)*, 362(6419), 1171–1177. <https://doi.org/10.1126/science.aap8210>
- Bigenzahn, J. W., Collu, G. M., Kartnig, F., Pieraks, M., Vladimer, G. I., Heinz, L. X., Sedlyarov, V., Schischlik, F., Fauster, A., Rebsamen, M., Parapatics, K., Blomen, V. A., Müller, A. C., Winter, G. E., Kralovics, R., Brummelkamp, T. R., Mlodzik, M., & Superti-Furga, G. (2018b). LZTR1 is a regulator of RAS ubiquitination and signaling. *Science*, 362(6419), 1171–1177. <https://doi.org/10.1126/science.aap8210>
- Bivona, T. G., Pérez de Castro, I., Ahearn, I. M., Grana, T. M., Chiu, V. K., Lockyer, P. J., Cullen, P. J., Pellicer, A., Cox, A. D., & Philips, M. R. (2003). Phospholipase C γ activates Ras on the Golgi apparatus by means of RasGRP1. *Nature*, 424(6949), 694–698. <https://doi.org/10.1038/nature01806>
- Bivona, T. G., Quatela, S. E., Bodemann, B. O., Ahearn, I. M., Soskis, M. J., Mor, A., Miura, J., Wiener, H. H., Wright, L. P., Saba, S., Yim, D. G., Fein, A., de Castro, I. P., Li, C., Thompson, C. B., Cox, A. D., & Philips, M. R. (2006). PKC regulates a farnesyl-electrostatic switch on K-Ras that promotes its association with Bcl-XL on mitochondria and induces apoptosis. *Molecular Cell*, 21 4, 481–493. <https://api.semanticscholar.org/CorpusID:21139511>
- Blair, H. A. (2021). Sotorasib: First Approval. *Drugs*, 81(13), 1573–1579. <https://doi.org/10.1007/s40265-021-01574-2>
- Bonner, T. I., Oppermann, H., Seeburg, P., Kerby, S. B., Gunnell, M. A., Young, A. C., & Rapp, U. R. (1986). The complete coding sequence of the human raf oncogene and the corresponding structure of the c-raf-1 gene. *Nucleic Acids Research*, 14(2), 1009–1015. <https://doi.org/10.1093/nar/14.2.1009>
- Bos, J. L., Rehmann, H., & Wittinghofer, A. (2007). GEFs and GAPs: Critical Elements in the Control of Small G Proteins. In *Cell* (Vol. 129, Issue 5, pp. 865–877). Elsevier B.V. <https://doi.org/10.1016/j.cell.2007.05.018>
- Bosch, M., Gil, J., Bachs, O., & Agell, N. (1998). Calmodulin Inhibitor W13 Induces Sustained Activation of ERK2 and Expression of p21cip1. *The Journal of Biological Chemistry*, 273, 22145–22150. <https://doi.org/10.1074/jbc.273.34.22145>
- Boulton, T. G., Nye, S. H., Robbins, D. J., Ip, N. Y., Radziejewska, E., Morgenbesser, S. D., DePinho, R. A., Panayotatos, N., Cobb, M. H., & Yancopoulos, G. D. (1991). ERKs: A family of protein-serine/threonine kinases that are activated and tyrosine phosphorylated in response to insulin and NGF. *Cell*, 65(4), 663–675. [https://doi.org/https://doi.org/10.1016/0092-8674\(91\)90098-J](https://doi.org/https://doi.org/10.1016/0092-8674(91)90098-J)
- Bourne, H. R., Sanders, D. A., & McCormick, F. (1991). The GTPase superfamily: conserved structure and molecular mechanism. *Nature*, 349(6305), 117–127. <https://doi.org/10.1038/349117a0>
- Brehme, M., Hantschel, O., Colinge, J., Kaupe, I., Planyavsky, M., Köcher, T., Mechtler, K., Bennett, K. L., & Superti-Furga, G. (2009). Charting the molecular network of the drug target Bcr-Abl. *Proceedings of the National Academy of Sciences*, 106(18), 7414–7419. <https://doi.org/10.1073/pnas.0900653106>
- Bunda, S., Burrell, K., Heir, P., Zeng, L., Alamsahebpour, A., Kano, Y., Raught, B., Zhang, Z.-Y., Zadeh, G., & Ohh, M. (2015). Inhibition of SHP2-mediated dephosphorylation of Ras suppresses oncogenesis. *Nature Communications*, 6, 8859. <https://doi.org/10.1038/ncomms9859>
- Cabot, D., Brun, S., Paco, N., Ginesta, M. M., Gendreau-Sanclemente, N., Abuasaker, B., Ruiz-Fariña, T., Barceló, C., Cuatrecasas, M., Bosch, M., Rentero, C., Pons, G., Estanyol, J. M.,

- Capellà, G., Jaumot, M., & Agell, N. (2021). KRAS phosphorylation regulates cell polarization and tumorigenic properties in colorectal cancer. *Oncogene*, 40(38), 5730–5740. <https://doi.org/10.1038/s41388-021-01967-3>
- Caetano, M. S., Zhang, H., Cumpian, A. M., Gong, L., Unver, N., Ostrin, E. J., Daliri, S., Chang, S. H., Ochoa, C. E., Hanash, S., Behrens, C., Wistuba, I. I., Sternberg, C., Kadara, H., Ferreira, C. G., Watowich, S. S., & Moghaddam, S. J. (2016). IL6 Blockade Reprograms the Lung Tumor Microenvironment to Limit the Development and Progression of K-ras–Mutant Lung Cancer. *Cancer Research*, 76(11), 3189–3199. <https://doi.org/10.1158/0008-5472.CAN-15-2840>
- Cai, L., Wang, Y., Wang, J.-F., & Chou, K.-C. (2011). Identification of Proteins Interacting with Human SP110 During the Process of Viral Infections. *Medicinal Chemistry (Shāriqah (United Arab Emirates))*, 7, 121–126. <https://doi.org/10.2174/157340611794859343>
- Calvisi, D. F., Donninger, H., Vos, M. D., Birrer, M. J., Gordon, L., Leaner, V., & Clark, G. J. (2009). NORE1A tumor suppressor candidate modulates p21CIP1 via p53. *Cancer Research*, 69(11), 4629–4637. <https://doi.org/10.1158/0008-5472.can-08-3672>
- Calvisi, D. F., Pinna, F., Pellegrino, R., Sanna, V., Sini, M., Daino, L., Simile, M. M., De Miglio, M. R., Frau, M., Tomasi, M. L., Seddaiu, M. A., Muronì, M. R., Feo, F., & Pascale, R. M. (2008). Ras-driven proliferation and apoptosis signaling during rat liver carcinogenesis is under genetic control. *International Journal of Cancer*, 123(9), 2057–2064. <https://doi.org/https://doi.org/10.1002/ijc.23720>
- Canon, J., Rex, K., Saiki, A. Y., Mohr, C., Cooke, K., Bagal, D., Gaida, K., Holt, T., Knutson, C. G., Koppada, N., Lanman, B. A., Werner, J., Rapaport, A. S., San Miguel, T., Ortiz, R., Osgood, T., Sun, J.-R., Zhu, X., McCarter, J. D., ... Lipford, J. R. (2019). The clinical KRAS(G12C) inhibitor AMG 510 drives anti-tumour immunity. *Nature*, 575(7781), 217–223. <https://doi.org/10.1038/s41586-019-1694-1>
- Castel, P., Dharmaiah, S., Sale, M., Messing, S., Rizzuto, G., Cuevas-Navarro, A., Cheng, A., Trnka, M., Urisman, A., Esposito, D., & Simanshu, D. (2021). RAS interaction with Sin1 is dispensable for mTORC2 assembly and activity. *Proceedings of the National Academy of Sciences of the United States of America*, 118. <https://doi.org/10.1073/pnas.2103261118>
- Ceddia, S., Landi, L., & Cappuzzo, F. (2022). KRAS-Mutant Non-Small-Cell Lung Cancer: From Past Efforts to Future Challenges. *International Journal of Molecular Sciences*, 23. <https://api.semanticscholar.org/CorpusID:251754251>
- Chandra, A., Grecco, H. E., Pisupati, V., Perera, D., Cassidy, L., Skoulidis, F., Ismail, S. A., Hedberg, C., Hanzal-Bayer, M., Venkitaraman, A. R., Wittinghofer, A., & Bastiaens, P. I. H. (2011). The GDI-like solubilizing factor PDEδ sustains the spatial organization and signalling of Ras family proteins. *Nature Cell Biology*, 14(2), 148–158. <https://doi.org/10.1038/ncb2394>
- Chang, E. H., Gondat, M. A., Ellist, R. W., Scolnick, E. M., & Lowy, D. R. (1982). Human genome contains four genes homologous to transforming genes of Harvey and Kirsten murine sarcoma viruses (molecular cloning/restriction endonuclease mapping/heteroduplex analysis/intervening sequences/gene family). In *Proc. Natl Acad. Sci. USA* (Vol. 79).
- Changeux, J.-P. (2013). The concept of allosteric modulation: an overview. *Drug Discovery Today: Technologies*, 10(2), e223–e228. <https://doi.org/https://doi.org/10.1016/j.ddtec.2012.07.007>

- Chen, J., Lui, W.-O., Vos, M. D., Clark, G. J., Takahashi, M., Schoumans, J., Khoo, S. K., Petillo, D., Lavery, T., Sugimura, J., Astuti, D., Zhang, C., Kagawa, S., Maher, E. R., Larsson, C., Alberts, A. S., Kanayama, H., & Teh, B. T. (2003). The t(1;3) breakpoint-spanning genes LSAMP and NORE1 are involved in clear cell renal cell carcinomas. *Cancer Cell*, 4(5), 405–413. [https://doi.org/https://doi.org/10.1016/S1535-6108\(03\)00269-1](https://doi.org/https://doi.org/10.1016/S1535-6108(03)00269-1)
- Cheng, A., Coleman, R., Smyth, K., Cao, Q., Soulard, P., Caffrey, D., Salzberg, A., & Huang, E. (2007). Structure-based maximal affinity model predicts small-molecule druggability. *Nature Biotechnology*, 25, 71–75. <https://doi.org/10.1038/nbt1273>
- Cheng, H., Fan, K., Luo, G., Fan, Z., Yang, C., Huang, Q., Jin, K., Xu, J., Yu, X., & Liu, C. (2019). KrasG12D mutation contributes to regulatory T cell conversion through activation of the MEK/ERK pathway in pancreatic cancer. *Cancer Letters*, 446, 103–111. <https://doi.org/https://doi.org/10.1016/j.canlet.2019.01.013>
- Cheung, W. L., Ajiro, K., Samejima, K., Kloc, M., Cheung, P., Mizzen, C. A., Beeser, A., Etkin, L. D., Chernoff, J., Earnshaw, W. C., & Allis, C. D. (2003). Apoptotic Phosphorylation of Histone H2B Is Mediated by Mammalian Sterile Twenty Kinase. *Cell*, 113(4), 507–517. [https://doi.org/https://doi.org/10.1016/S0092-8674\(03\)00355-6](https://doi.org/https://doi.org/10.1016/S0092-8674(03)00355-6)
- Chiu, V. K., Bivona, T., Hach, A., Sajous, J. B., Silletti, J., Wiener, H., Johnson, R. L., Cox, A. D., & Philips, M. R. (2002). Ras signalling on the endoplasmic reticulum and the Golgi. *Nature Cell Biology*, 4(5), 343–350. <https://doi.org/10.1038/ncb783>
- Cho, K., Casteel, D. E., Prakash, P., Tan, L., van der Hoeven, D., Salim, A. A., Kim, C., Capon, R. J., Lacey, E., Cunha, S. R., Gorfe, A. A., & Hancock, J. F. (2016). AMPK and Endothelial Nitric Oxide Synthase Signaling Regulates K-Ras Plasma Membrane Interactions via Cyclic GMP-Dependent Protein Kinase 2. *Molecular and Cellular Biology*, 36(24), 3086–3099. <https://doi.org/10.1128/MCB.00365-16>
- Clark, J. A., Black, A. R., Leontieva, O. V., Frey, M. R., Pysz, M. A., Kunneva, L., Woloszynska-Read, A., Roy, D., & Black, J. D. (2004). Involvement of the ERK Signaling Cascade in Protein Kinase C-mediated Cell Cycle Arrest in Intestinal Epithelial Cells*. *Journal of Biological Chemistry*, 279(10), 9233–9247. <https://doi.org/https://doi.org/10.1074/jbc.M312268200>
- Cluntun, A. A., Lukey, M. J., Cerione, R. A., & Locasale, J. W. (2017). Glutamine metabolism in cancer: understanding the heterogeneity. *Trends in Cancer*, 3(3), 169–180.
- Cook, F. A., & Cook, S. J. (2021). Inhibition of RAF dimers: It takes two to tango. In *Biochemical Society Transactions* (Vol. 49, Issue 1, pp. 237–251). Portland Press Ltd. <https://doi.org/10.1042/BST20200485>
- Cuesta, C., Arévalo-Alameda, C., & Castellano, E. (2021). The Importance of Being PI3K in the RAS Signaling Network. *Genes*, 12(7). <https://doi.org/10.3390/genes12071094>
- Cullis, J., Das, S., & Bar-Sagi, D. (2018). Kras and Tumor Immunity: Friend or Foe? *Cold Spring Harbor Perspectives in Medicine*, 8(9). <https://doi.org/10.1101/cshperspect.a031849>
- Dharmaiah, S., Bindu, L., Tran, T. H., Gillette, W. K., Frank, P. H., Ghirlando, R., Nissley, D. V., Esposito, D., McCormick, F., Stephen, A. G., & Simanshu, D. K. (2016). Structural basis of recognition of farnesylated and methylated KRAS4b by PDEδ. *Proceedings of the National Academy of Sciences of the United States of America*, 113(44), E6766–E6775. <https://doi.org/10.1073/pnas.1615316113>
- Dharmaiah, S., Tran, T. H., Messing, S., Agamasu, C., Gillette, W. K., Yan, W., Waybright, T., Alexander, P., Esposito, D., Nissley, D. V., McCormick, F., Stephen, A. G., & Simanshu, D. K. (2019). Structures of N-terminally processed KRAS provide insight into the role of N-

- acetylation. *Scientific Reports*, 9(1), 10512. <https://doi.org/10.1038/s41598-019-46846-w>
- Dhillon, A. S., Yip, Y. Y., Grindlay, G. J., Pakay, J. L., Dangers, M., Hillmann, M., Clark, W., Pitt, A., Mischak, H., & Kolch, W. (2009). The C-terminus of Raf-1 acts as a 14-3-3-dependent activation switch. *Cellular Signalling*, 21(11), 1645–1651. <https://doi.org/https://doi.org/10.1016/j.cellsig.2009.07.001>
- Dhillon, S. (2023). Adagrasib: First Approval. *Drugs*, 83(3), 275–285. <https://doi.org/10.1007/s40265-023-01839-y>
- Dias Carvalho, P., Machado, A. L., Martins, F., Seruca, R., & Velho, S. (2019a). Targeting the Tumor Microenvironment: An Unexplored Strategy for Mutant KRAS Tumors. *Cancers*, 11(12). <https://doi.org/10.3390/cancers11122010>
- Dias Carvalho, P., Machado, A. L., Martins, F., Seruca, R., & Velho, S. (2019b). Targeting the Tumor Microenvironment: An Unexplored Strategy for Mutant KRAS Tumors. *Cancers*, 11(12). <https://doi.org/10.3390/cancers11122010>
- Díaz-Eufracio, B. I., Naveja, J. J., & Medina-Franco, J. L. (2018). Protein-Protein Interaction Modulators for Epigenetic Therapies. *Advances in Protein Chemistry and Structural Biology*, 110, 65–84. <https://doi.org/10.1016/bs.apcsb.2017.06.002>
- Donninger, H., Schmidt, M. L., Mezzanotte, J., Barnoud, T., & Clark, G. J. (2016). Ras signaling through RASSF proteins. In *Seminars in Cell and Developmental Biology* (Vol. 58, pp. 86–95). Academic Press. <https://doi.org/10.1016/j.semcd.2016.06.007>
- Donninger, H., Vos, M. D., & Clark, G. J. (2007a). The RASSF1A tumor suppressor. *Journal of Cell Science*, 120(18), 3163–3172. <https://doi.org/10.1242/jcs.010389>
- Donninger, H., Vos, M. D., & Clark, G. J. (2007b). The RASSF1A tumor suppressor. *Journal of Cell Science*, 120(18), 3163–3172. <https://doi.org/10.1242/jcs.010389>
- Durisic, N., Cuervo, L. L., & Lakadamyali, M. (2014). Quantitative super-resolution microscopy: pitfalls and strategies for image analysis. *Current Opinion in Chemical Biology*, 20, 22–28. <https://doi.org/https://doi.org/10.1016/j.cbpa.2014.04.005>
- Elmetwali, T., Salman, A., & Palmer, D. H. (2016). NORE1A induction by membrane-bound CD40L (mCD40L) contributes to CD40L-induced cell death and G1 growth arrest in p21-mediated mechanism. *Cell Death & Disease*, 7(3), e2146–e2146. <https://doi.org/10.1038/cddis.2016.52>
- Evans, B. J., King, A. T., Katsifis, A., Matesic, L., & Jamie, J. F. (2020). Methods to Enhance the Metabolic Stability of Peptide-Based PET Radiopharmaceuticals. *Molecules*, 25(10). <https://doi.org/10.3390/molecules25102314>
- Fang, Z., Marshall, C. B., Nishikawa, T., Gossert, A. D., Jansen, J. M., Jahnke, W., & Ikura, M. (2018). Inhibition of K-RAS4B by a Unique Mechanism of Action: Stabilizing Membrane-Dependent Occlusion of the Effector-Binding Site. *Cell Chemical Biology*, 25(11), 1327–1336.e4. <https://doi.org/10.1016/j.chembiol.2018.07.009>
- Fell, J. B., Fischer, J. P., Baer, B. R., Blake, J. F., Bouhana, K., Briere, D. M., Brown, K. D., Burgess, L. E., Burns, A. C., Burkard, M. R., Chiang, H., Chicarelli, M. J., Cook, A. W., Gaudino, J. J., Hallin, J., Hanson, L., Hartley, D. P., Hicken, E. J., Hingorani, G. P., ... Marx, M. A. (2020). Identification of the Clinical Development Candidate MRTX849, a Covalent KRASG12C Inhibitor for the Treatment of Cancer. *Journal of Medicinal Chemistry*, 63(13), 6679–6693. <https://doi.org/10.1021/acs.jmedchem.9b02052>
- Fischer, A., Hekman, M., Kuhlmann, J., Rubio, I., Wiese, S., & Rapp, U. R. (2007). B- and C-RAF display essential differences in their binding to Ras: the isotype-specific N terminus

- of B-Raf facilitates Ras binding. *The Journal of Biological Chemistry*, 282(36), 26503–26516. <https://doi.org/10.1074/jbc.m607458200>
- Freeman, A. K., Ritt, D. A., & Morrison, D. K. (2013). Effects of Raf Dimerization and Its Inhibition on Normal and Disease-Associated Raf Signaling. *Molecular Cell*, 49(4), 751–758. <https://doi.org/https://doi.org/10.1016/j.molcel.2012.12.018>
- Frey, M. R., Clark, J. A., Leontieva, O., Uronis, J. M., Black, A. R., & Black, J. D. (2000). Protein Kinase C Signaling Mediates a Program of Cell Cycle Withdrawal in the Intestinal Epithelium. *Journal of Cell Biology*, 151(4), 763–778. <https://doi.org/10.1083/jcb.151.4.763>
- Frey, M. R., Saxon, M. L., Zhao, X., Rollins, A., Evans, S. S., & Black, J. D. (1997). Protein Kinase C Isozyme-mediated Cell Cycle Arrest Involves Induction of p21waf1/cip1 and p27kip1 and Hypophosphorylation of the Retinoblastoma Protein in Intestinal Epithelial Cells*. *Journal of Biological Chemistry*, 272(14), 9424–9435. <https://doi.org/https://doi.org/10.1074/jbc.272.14.9424>
- Fritsche-Guenther, R., Witzel, F., Sieber, A., Herr, R., Schmidt, N., Braun, S., Brummer, T., Sers, C., & Blüthgen, N. (2011). Strong negative feedback from Erk to Raf confers robustness to MAPK signalling. *Molecular Systems Biology*, 7. <https://doi.org/10.1038/msb.2011.27>
- Fruman, D. A., Chiu, H., Hopkins, B. D., Bagrodia, S., Cantley, L. C., & Abraham, R. T. (2017). The PI3K Pathway in Human Disease. *Cell*, 170(4), 605–635. <https://doi.org/https://doi.org/10.1016/j.cell.2017.07.029>
- Fu, X., Wang, X., Duanmu, J., Li, T., & Jiang, Q. (2020). KRAS mutations are negatively correlated with immunity in colon cancer. *Aging*, 13(1), 750–768. <https://doi.org/10.18632/aging.202182>
- Gao, G., Liao, W., Ma, Q., Zhang, B., Chen, Y., & Wang, Y. (2020). KRAS G12D mutation predicts lower TMB and drives immune suppression in lung adenocarcinoma. *Lung Cancer (Amsterdam, Netherlands)*, 149, 41–45. <https://doi.org/10.1016/j.lungcan.2020.09.004>
- Garnett, M., Rana, S., Paterson, H., Barford, D., & Marais, R. (2006). Wild-Type and Mutant B-Raf Activate C-Raf through Distinct Mechanisms Involving Heterodimerization. *Molecular Cell*, 20, 963–969. <https://doi.org/10.1016/j.molcel.2005.10.022>
- Garrido, E., Lázaro, J., Jaumot, M., Agell, N., & Rubio-Martinez, J. (2018a). Modeling and subtleties of K-Ras and Calmodulin interaction. *PLOS Computational Biology*, 14(10), e1006552-. <https://doi.org/10.1371/journal.pcbi.1006552>
- Garrido, E., Lázaro, J., Jaumot, M., Agell, N., & Rubio-Martinez, J. (2018b). Modeling and subtleties of K-Ras and Calmodulin interaction. *PLOS Computational Biology*, 14(10), e1006552-. <https://doi.org/10.1371/journal.pcbi.1006552>
- Gestwicki, J. E., & Smith, M. C. (2012). Features of protein–protein interactions that translate into potent inhibitors: topology, surface area and affinity. *Expert Reviews in Molecular Medicine*, 14, e16. <https://doi.org/DOI: 10.1017/erm.2012.10>
- Gilmartin, A. G., Bleam, M. R., Groy, A., Moss, K. G., Minthorn, E. A., Kulkarni, S. G., Rominger, C. M., Erskine, S., Fisher, K. E., Yang, J., Zappacosta, F., Annan, R., Sutton, D., & Laquerre, S. G. (2011). GSK1120212 (JTP-74057) Is an Inhibitor of MEK Activity and Activation with Favorable Pharmacokinetic Properties for Sustained In Vivo Pathway Inhibition. *Clinical Cancer Research*, 17(5), 989–1000. <https://doi.org/10.1158/1078-0432.CCR-10-2200>

- Go, C. D., Knight, J. D. R., Rajasekharan, A., Rathod, B., Hesketh, G. G., Abe, K. T., Youn, J.-Y., Samavarchi-Tehrani, P., Zhang, H., Zhu, L. Y., Popiel, E., Lambert, J.-P., Coyaud, É., Cheung, S. W. T., Rajendran, D., Wong, C. J., Antonicka, H., Pelletier, L., Palazzo, A. F., ... Gingras, A.-C. (2021a). A proximity-dependent biotinylation map of a human cell. *Nature*, 595(7865), 120–124. <https://doi.org/10.1038/s41586-021-03592-2>
- Go, C. D., Knight, J. D. R., Rajasekharan, A., Rathod, B., Hesketh, G. G., Abe, K. T., Youn, J.-Y., Samavarchi-Tehrani, P., Zhang, H., Zhu, L. Y., Popiel, E., Lambert, J.-P., Coyaud, É., Cheung, S. W. T., Rajendran, D., Wong, C. J., Antonicka, H., Pelletier, L., Palazzo, A. F., ... Gingras, A.-C. (2021b). A proximity-dependent biotinylation map of a human cell. *Nature*, 595(7865), 120–124. <https://doi.org/10.1038/s41586-021-03592-2>
- Goebel, L., Müller, M. P., Goody, R. S., & Rauh, D. (2020). KRasG12C inhibitors in clinical trials: a short historical perspective. *RSC Med. Chem.*, 11(7), 760–770. <https://doi.org/10.1039/D0MD00096E>
- Goodwin, J. S., Drake, K. R., Rogers, C., Wright, L. P., Lippincott-Schwartz, J., Philips, M. R., Kenworthy, A. K., & Kenworthy, A. K. (2005). Depalmitoylated Ras traffics to and from the Golgi complex via a nonvesicular pathway. *The Journal of Cell Biology*, 170, 261–272. <https://api.semanticscholar.org/CorpusID:7283631>
- Grant, B. J., Lukman, S., Hocker, H. J., Sayyah, J., Brown, J. H., McCammon, J. A., & Gorfe, A. A. (2011). Novel Allosteric Sites on Ras for Lead Generation. *PLOS ONE*, 6(10), e25711-. <https://doi.org/10.1371/journal.pone.0025711>
- Guillard, S., Kolasinska-Zwierz, P., Debreczeni, J., Breed, J., Zhang, J., Bery, N., Marwood, R., Tart, J., Overman, R., Stocki, P., Mistry, B., Phillips, C., Rabbitts, T., Jackson, R., & Minter, R. (2017). Structural and functional characterization of a DARPin which inhibits Ras nucleotide exchange. *Nature Communications*, 8, 16111. <https://doi.org/10.1038/ncomms16111>
- Guo, C., Zhang, X., & Pfeifer, G. (2011). The tumor suppressor RASSF1A prevents dephosphorylation of the mammalian STE20-like kinases MST1 and MST2. *The Journal of Biological Chemistry*, 286, 6253–6261. <https://doi.org/10.1074/jbc.M110.178210>
- Guo, Y., Pan, W., Liu, S., Shen, Z., Xu, Y., & Hu, L. (2020). ERK/MAPK signalling pathway and tumorigenesis (Review). *Experimental and Therapeutic Medicine*. <https://doi.org/10.3892/etm.2020.8454>
- Hallin, J., Bowcut, V., Calinisan, A., Briere, D. M., Hargis, L., Engstrom, L. D., Laguer, J., Medwid, J., Vanderpool, D., Lifset, E., Trinh, D., Hoffman, N., Wang, X., David Lawson, J., Gunn, R. J., Smith, C. R., Thomas, N. C., Martinson, M., Bergstrom, A., ... Christensen, J. G. (2022). Anti-tumor efficacy of a potent and selective non-covalent KRASG12D inhibitor. *Nature Medicine*, 28(10), 2171–2182. <https://doi.org/10.1038/s41591-022-02007-7>
- Hallin, J., Engstrom, L. D., Hargis, L., Calinisan, A., Aranda, R., Briere, D. M., Sudhakar, N., Bowcut, V., Baer, B. R., Ballard, J. A., Burkard, M. R., Fell, J. B., Fischer, J. P., Vigers, G. P., Xue, Y., Gatto, S., Fernandez-Banet, J., Pavlicek, A., Velastagui, K., ... Christensen, J. G. (2020). The KRASG12C Inhibitor MRTX849 Provides Insight toward Therapeutic Susceptibility of KRAS-Mutant Cancers in Mouse Models and Patients. *Cancer Discovery*, 10(1), 54–71. <https://doi.org/10.1158/2159-8290.CD-19-1167>
- Hamarsheh, S., Groß, O., Brummer, T., & Zeiser, R. (2020). Immune modulatory effects of oncogenic KRAS in cancer. *Nature Communications*, 11(1), 5439. <https://doi.org/10.1038/s41467-020-19288-6>

- Hancock, J. F., Magee, A. I., Childs, J. E., & Marshall, C. J. (1989). All ras proteins are polyisoprenylated but only some are palmitoylated. *Cell*, 57(7), 1167–1177. [https://doi.org/https://doi.org/10.1016/0092-8674\(89\)90054-8](https://doi.org/https://doi.org/10.1016/0092-8674(89)90054-8)
- Harwood, S. J., Smith, C. R., Lawson, J. D., & Ketcham, J. M. (2023). Selected Approaches to Disrupting Protein–Protein Interactions within the MAPK/RAS Pathway. In *International Journal of Molecular Sciences* (Vol. 24, Issue 8). Multidisciplinary Digital Publishing Institute (MDPI). <https://doi.org/10.3390/ijms24087373>
- Hatzivassiliou, G., Liu, B., O'Brien, C., Spoerke, J., Hoeflich, K., Haverty, P., Soriano, R., Forrest, W., Heldens, S., Chen, H., Toy, K., Ha, C., Zhou, W., Song, K., Friedman, L., Amler, L., Hampton, G., Moffat, J., Belvin, M., & Lackner, M. (2012). ERK Inhibition Overcomes Acquired Resistance to MEK Inhibitors. *Molecular Cancer Therapeutics*, 11, 1143–1154. <https://doi.org/10.1158/1535-7163.MCT-11-1010>
- Haza, K., Martin, H., Rao, A., Turner, A., Saunders, S., Petersen, B., Tiede, C., Tipping, K., Tang, A., Ajayi, M., Taylor, T., Harvey, M., Fishwick, K., Adams, L., Gaule, T., Trinh, C., Johnson, M., Breeze, A., Edwards, T., & Tomlinson, D. (2021). RAS-inhibiting biologics identify and probe druggable pockets including an SII- α 3 allosteric site. *Nature Communications*, 12, 4045. <https://doi.org/10.1038/s41467-021-24316-0>
- Heidorn, S. J., Milagre, C., Whittaker, S., Nourry, A., Niculescu-Duvas, I., Dhomen, N., Hussain, J., Reis-Filho, J. S., Springer, C. J., Pritchard, C., & Marais, R. (2010). Kinase-Dead BRAF and Oncogenic RAS Cooperate to Drive Tumor Progression through CRAF. *Cell*, 140(2), 209–221. <https://doi.org/10.1016/j.cell.2009.12.040>
- Hesson, L., Dallol, A., Minna, J. D., Maher, E. R., & Latif, F. (2003). NORE1A, a homologue of RASSF1A tumour suppressor gene is inactivated in human cancers. *Oncogene*, 22(6), 947–954. <https://doi.org/10.1038/sj.onc.1206191>
- Hill, T. A., Shepherd, N. E., Diness, F., & Fairlie, D. P. (2014). Constraining Cyclic Peptides To Mimic Protein Structure Motifs. *Angewandte Chemie International Edition*, 53(48), 13020–13041. <https://doi.org/https://doi.org/10.1002/anie.201401058>
- Hillig, R. C., Sautier, B., Schroeder, J., Moosmayer, D., Hilpmann, A., Stegmann, C. M., Werbeck, N. D., Briem, H., Boemer, U., Weiske, J., Badock, V., Mastouri, J., Petersen, K., Siemeister, G., Kahmann, J. D., Wegener, D., Böhnke, N., Eis, K., Graham, K., ... Bader, B. (2019). Discovery of potent SOS1 inhibitors that block RAS activation via disruption of the RAS–SOS1 interaction. *Proceedings of the National Academy of Sciences*, 116(7), 2551–2560. <https://doi.org/10.1073/pnas.1812963116>
- Hoeflich, K. P., O'Brien, C., Boyd, Z., Cavet, G., Guerrero, S., Jung, K., Januario, T., Savage, H., Punnoose, E., Truong, T., Zhou, W., Berry, L., Murray, L., Amler, L., Belvin, M., Friedman, L. S., & Lackner, M. R. (2009). In vivo Antitumor Activity of MEK and Phosphatidylinositol 3-Kinase Inhibitors in Basal-Like Breast Cancer Models. *Clinical Cancer Research*, 15(14), 4649–4664. <https://doi.org/10.1158/1078-0432.CCR-09-0317>
- Hoxhaj, G., & Manning, B. D. (2020). The PI3K–AKT network at the interface of oncogenic signalling and cancer metabolism. *Nature Reviews Cancer*, 20(2), 74–88. <https://doi.org/10.1038/s41568-019-0216-7>
- Hu, J., Stites, E. C., Yu, H., Yu, H., Germino, E. A., Meharena, H. S., Stork, P. J. S., Kornev, A. P., Taylor, S. S., & Shaw, A. S. (2013). Allosteric activation of functionally asymmetric RAF kinase dimers. *Cell*, 154(5), 1036–1046. <https://doi.org/10.1016/j.cell.2013.07.046>
- Hu, X., Kuang, Y., Li, L., Tang, H., Shi, Q., Shu, X., Zhang, Y., Chan, F. K. L., Tao, Q., & He, C. (2017). Epigenomic and functional characterization of Junctophilin 3 (JPH3) as a novel

tumor suppressor being frequently inactivated by promoter CpG methylation in digestive cancers. *Theranostics*, 7(7), 2150–2163. <https://doi.org/10.7150/THNO.18185>

Huang, B., & Schroeder, M. (2006). LIGSITEcsc: predicting ligand binding sites using the Connolly surface and degree of conservation. *BMC Structural Biology*, 6(1), 19. <https://doi.org/10.1186/1472-6807-6-19>

Huang, L., Guo, Z., Wang, F., & Fu, L. (2021). KRAS mutation: from undruggable to druggable in cancer. In *Signal Transduction and Targeted Therapy* (Vol. 6, Issue 1). Springer Nature. <https://doi.org/10.1038/s41392-021-00780-4>

Huleihel, M., Goldsborough, M., Cleveland, J., Gunnell, M., Bonner, T., & Rapp, U. R. (1986). Characterization of murine A-raf, a new oncogene related to the v-raf oncogene. *Molecular and Cellular Biology*, 6(7), 2655–2662. <https://doi.org/10.1128/mcb.6.7.2655-2662.1986>

Hunter, J. C., Manandhar, A., Carrasco, M. A., Gurbani, D., Gondi, S., & Westover, K. D. (2015). Biochemical and Structural Analysis of Common Cancer-Associated KRAS Mutations. *Molecular Cancer Research*, 13(9), 1325–1335. <https://doi.org/10.1158/1541-7786.MCR-15-0203>

Huttlin, E. L., Bruckner, R. J., Navarrete-Perea, J., Cannon, J. R., Baltier, K., Gebreab, F., Gygi, M. P., Thornock, A., Zarraga, G., Tam, S., Szpyt, J., Gassaway, B. M., Panov, A., Parzen, H., Fu, S., Golbazi, A., Maenpaa, E., Stricker, K., Guha Thakurta, S., ... Gygi, S. P. (2021). Dual proteome-scale networks reveal cell-specific remodeling of the human interactome. *Cell*, 184(11), 3022-3040.e28. <https://doi.org/https://doi.org/10.1016/j.cell.2021.04.011>

Inder, K. L., Hill, M. M., & Hancock, J. F. (2010). Nucleophosmin and nucleolin regulate K-Ras signaling. *Communicative & Integrative Biology*, 3(2), 188–190. <https://doi.org/10.4161/cib.3.2.10923>

Ivanov, A. A., Khuri, F. R., & Fu, H. (2013). Targeting protein-protein interactions as an anticancer strategy. *Trends in Pharmacological Sciences*, 34 7, 393–400. <https://api.semanticscholar.org/CorpusID:30001148>

Iverson, C., Larson, G., Lai, C., Yeh, L.-T., Dadson, C., Weingarten, P., Appleby, T., Vo, T., Maderna, A., Vernier, J.-M., Hamatake, R., Miner, J. N., & Quart, B. (2009). RDEA119/BAY 869766: A Potent, Selective, Allosteric Inhibitor of MEK1/2 for the Treatment of Cancer. *Cancer Research*, 69(17), 6839–6847. <https://doi.org/10.1158/0008-5472.CAN-09-0679>

Jambhekar, S. S., & Breen, P. (2016). Cyclodextrins in pharmaceutical formulations I: structure and physicochemical properties, formation of complexes, and types of complex. *Drug Discovery Today*, 21(2), 356–362. <https://doi.org/https://doi.org/10.1016/j.drudis.2015.11.017>

Jang, E. R., Shi, P., Bryant, J., Chen, J., Dukhande, V., Gentry, M. S., Jang, H., Jeoung, M., & Galperin, E. (2014). HUWE1 Is a Molecular Link Controlling RAF-1 Activity Supported by the Shoc2 Scaffold. *Molecular and Cellular Biology*, 34(19), 3579–3593. <https://doi.org/10.1128/MCB.00811-14>

Jänne, P. A., Riely, G. J., Gadgeel, S. M., Heist, R. S., Ou, S.-H. I., Pacheco, J. M., Johnson, M. L., Sabari, J. K., Leventakos, K., Yau, E., Bazhenova, L., Negrao, M. V., Pennell, N. A., Zhang, J., Anderes, K., Der-Torossian, H., Kheoh, T., Velastegui, K., Yan, X., ... Spira, A. I. (2022). Adagrasib in Non–Small-Cell Lung Cancer Harboring a KRASG12C Mutation. *New England Journal of Medicine*, 387(2), 120–131. <https://doi.org/10.1056/NEJMoa2204619>

- Jiang, Q., Wang, L., & Hei, X. (2015). Parameter identification of chaotic systems using artificial raindrop algorithm. *Journal of Computational Science*, 8, 20–31. <https://doi.org/https://doi.org/10.1016/j.jocs.2015.02.004>
- Jiao, X.-D., Qin, B.-D., Xu, Y., Gong, F., & Zang, Y.-S. (2020). 1987P Discordant genomic correlates of PD-L1 expression in lung adenocarcinoma among multiple cohorts using dissimilar PD-L1 testing techniques. *Annals of Oncology*, 31. <https://api.semanticscholar.org/CorpusID:225196001>
- Johnson, C. W., Lin, Y.-J., Reid, D., Parker, J. A., Pavlopoulos, S., Dischinger, P. S., Graveel, C., Aguirre, A. J., Steensma, M. R., Haigis, K. M., & Mattos, C. (2019). Isoform-Specific Destabilization of the Active Site Reveals a Molecular Mechanism of Intrinsic Activation of KRas G13D. *Cell Reports*, 28, 1538-1550.e7. <https://api.semanticscholar.org/CorpusID:199508231>
- Kahan, C., Seuwen, K., Meloche, S., & Pouyssegur, J. (1992). Coordinate, biphasic activation of p44 mitogen-activated protein kinase and S6 kinase by growth factors in hamster fibroblasts. Evidence for thrombin-induced signals different from phosphoinositide turnover and adenylylcyclase inhibition. *Journal of Biological Chemistry*, 267(19), 13369–13375. [https://doi.org/https://doi.org/10.1016/S0021-9258\(18\)42220-X](https://doi.org/https://doi.org/10.1016/S0021-9258(18)42220-X)
- Kalidas, Y., & Chandra, N. (2008). PocketDepth: A new depth based algorithm for identification of ligand binding sites in proteins. *Journal of Structural Biology*, 161(1), 31–42. <https://doi.org/https://doi.org/10.1016/j.jsb.2007.09.005>
- Kano, Y., Gebregiorgis, T., Marshall, C. B., Radulovich, N., Poon, B. P. K., St-Germain, J. R., Cook, J. D., Valencia-Sama, I., Grant, B. M. M., Herrera, S. G., Miao, J., Raught, B., Irwin, M. S., Lee, J. E., Yeh, J. J., Zhang, Z.-Y., Tsao, M.-S., Ikura, M., & Ohh, M. (2019). Tyrosyl phosphorylation of KRAS stalls GTPase cycle via alteration of switch I and II conformation. *Nature Communications*, 10. <https://api.semanticscholar.org/CorpusID:58010448>
- Karandikar, M., Xu, S., & Cobb, M. H. (2000). MEKK1 Binds Raf-1 and the ERK2 Cascade Components*. *Journal of Biological Chemistry*, 275(51), 40120–40127. <https://doi.org/https://doi.org/10.1074/jbc.M005926200>
- Karnoub, A. E., & Weinberg, R. A. (2008). Ras oncogenes: Split personalities. In *Nature Reviews Molecular Cell Biology* (Vol. 9, Issue 7, pp. 517–531). <https://doi.org/10.1038/nrm2438>
- Kato, K., Cox, A. D., Hisaka, M. M., Graham, S. M., Buss, J. E., & Der, C. J. (1992). Isoprenoid addition to Ras protein is the critical modification for its membrane association and transforming activity. *Proceedings of the National Academy of Sciences*, 89(14), 6403–6407. <https://doi.org/10.1073/pnas.89.14.6403>
- Kattan, W. E., & Hancock, J. F. (2020). RAS Function in cancer cells: Translating membrane biology and biochemistry into new therapeutics. In *Biochemical Journal* (Vol. 477, Issue 15, pp. 2893–2919). Portland Press Ltd. <https://doi.org/10.1042/BCJ20190839>
- Kauffmann-Zeh, A., Rodriguez-Viciana, P., Ulrich, E., Gilbert, C., Coffey, P., Downward, J., & Evan, G. (1997). Suppression of c-Myc-induced apoptosis by Ras signalling through PI(3)K and PKB. *Nature*, 385(6616), 544–548. <https://doi.org/10.1038/385544a0>
- Kessler, D., Gmachl, M., Mantoulidis, A., Martin, L. J., Zoephel, A., Mayer, M., Gollner, A., Covini, D., Fischer, S., Gerstberger, T., Gmaschitz, T., Goodwin, C., Greb, P., Häring, D., Hela, W., Hoffmann, J., Karolyi-Oezguer, J., Knesl, P., Kornigg, S., ... McConnell, D. B. (2019). Drugging an undruggable pocket on KRAS. *Proceedings of the National Academy of Sciences*, 116(32), 15823–15829. <https://doi.org/10.1073/pnas.1904529116>

- Khokhlatchev, A., Rabizadeh, S., Xavier, R., Nedwidek, M., Chen, T., Zhang, X., Seed, B., & Avruch, J. (2002a). Identification of a Novel Ras-Regulated Proapoptotic Pathway. *Current Biology*, 12(4), 253–265. [https://doi.org/https://doi.org/10.1016/S0960-9822\(02\)00683-8](https://doi.org/https://doi.org/10.1016/S0960-9822(02)00683-8)
- Khokhlatchev, A. V., Rabizadeh, S., Xavier, R. J., Nedwidek, M., Chen, T., Zhang, X., Seed, B., & Avruch, J. (2002b). Identification of a Novel Ras-Regulated Proapoptotic Pathway. *Current Biology*, 12, 253–265. <https://api.semanticscholar.org/CorpusID:14053233>
- Kilic, U., Caglayan, A. B., Beker, M. C., Gunal, M. Y., Caglayan, B., Yalcin, E., Kelestemur, T., Gundogdu, R. Z., Yulug, B., Yilmaz, B., Kerman, B. E., & Kilic, E. (2017). Particular phosphorylation of PI3K/Akt on Thr308 via PDK-1 and PTEN mediates melatonin's neuroprotective activity after focal cerebral ischemia in mice. *Redox Biology*, 12, 657–665. <https://doi.org/https://doi.org/10.1016/j.redox.2017.04.006>
- Köhler, M., & Brummer, T. (2016). B-Raf activation loop phosphorylation revisited. *Cell Cycle*, 15(9), 1171–1173. <https://doi.org/10.1080/15384101.2016.1159111>
- Kolch, W., Heidecker, G., Lloyd, P., & Rapp, U. R. (1991). Raf-1 protein kinase is required for growth of induced NIH/3T3 cells. *Nature*, 349(6308), 426–428. <https://doi.org/10.1038/349426a0>
- Kondo, Y., Ognjenović, J., Banerjee, S., Karandur, D., Merk, A., Kulhanek, K., Wong, K., Roose, J. P., Subramaniam, S., & Kuriyan, J. (2019a). Cryo-EM structure of a dimeric B-Raf:14-3-3 complex reveals asymmetry in the active sites of B-Raf kinases. *Science*, 366(6461), 109–115. <https://doi.org/10.1126/science.aay0543>
- Kondo, Y., Ognjenović, J., Banerjee, S., Karandur, D., Merk, A., Kulhanek, K., Wong, K., Roose, J. P., Subramaniam, S., & Kuriyan, J. (2019b). Cryo-EM structure of a dimeric B-Raf:14-3-3 complex reveals asymmetry in the active sites of B-Raf kinases. *Science (New York, N.Y.)*, 366(6461), 109–115. <https://doi.org/10.1126/science.aay0543>
- Kovalski, J. R., Bhaduri, A., Zehnder, A. M., Neela, P. H., Che, Y., Wozniak, G. G., & Khavari, P. A. (2019). The functional proximal proteome of oncogenic Ras includes mTORC2. *Molecular Cell*, 73(4), 830–844.
- Kozak, C. A., Gunnell, M. A., & Rapp, A. U. R. (1984). A new oncogene, c-raf, is located on mouse chromosome 6. *Journal of Virology*, 49, 297–299. <https://api.semanticscholar.org/CorpusID:34688021>
- Kubitz, L., Bitsch, S., Zhao, X., Schmitt, K., Deweid, L., Roehrig, A., Barazzone, E. C., Valerius, O., Kolmar, H., & Béthune, J. (2022). Engineering of ultraID, a compact and hyperactive enzyme for proximity-dependent biotinylation in living cells. *Communications Biology*, 5(1). <https://doi.org/10.1038/s42003-022-03604-5>
- Kuppusamy, R., Willcox, M., Black, & Kumar, N. (2019). Short Cationic Peptidomimetic Antimicrobials. *Antibiotics*, 8, 44. <https://doi.org/10.3390/antibiotics8020044>
- Laude, A. J., & Prior, I. A. (2008). Palmitoylation and localisation of RAS isoforms are modulated by the hypervariable linker domain. *Journal of Cell Science*, 121(4), 421–427. <https://doi.org/10.1242/jcs.020107>
- Lee, C.-S., Lee, L. C., Yuan, T. L., Chakka, S., Fellmann, C., Lowe, S. W., Caplen, N. J., McCormick, F., & Luo, J. (2019). MAP kinase and autophagy pathways cooperate to maintain RAS mutant cancer cell survival. *Proceedings of the National Academy of Sciences*, 116(10), 4508–4517. <https://doi.org/10.1073/pnas.1817494116>
- Lee, G., Kenny, P., Lee, E., & Bissell, M. (2007). Lee GY, Kenny PA, Lee EH, Bissell MJ.. Three-dimensional culture models of normal and malignant breast epithelial cells. *Nat*

- Methods 4: 359–365. *Nature Methods*, 4, 359–365.
<https://doi.org/10.1038/nmeth1015>
- Lee, J. K., Sivakumar, S., Schrock, A. B., Madison, R., Fabrizio, D., Gjoerup, O., Ross, J. S., Frampton, G. M., Napalkov, P., Montesion, M., Schutzman, J. L., Ye, X., Hegde, P. S., Nagasaka, M., Oxnard, G. R., Sokol, E. S., Ou, S. H. I., & Shi, Z. (2022). Comprehensive pan-cancer genomic landscape of KRAS altered cancers and real-world outcomes in solid tumors. *Npj Precision Oncology*, 6(1). <https://doi.org/10.1038/s41698-022-00334-z>
- Lee, S., Jeong, W., Cho, Y., Cha, P., Yoon, J., Ro, E. J., Choi, S., Oh, J., Heo, Y., Kim, H., Min, D. S., Han, G., Lee, W., & Choi, K. (2018). Catenin-RAS interaction serves as a molecular switch for RAS degradation via GSK3; *EMBO Reports*, 19(12), e46060. <https://doi.org/https://doi.org/10.15252/embr.201846060>
- Leonard, Presta, G., Chen, H., O'Connor, S. J., Vanessa, Chisholm, Meng, Y. G., Krummen, L. A., Marjorie, Winkler, Napoléone, & Ferrara. (1997). Humanization of an anti-vascular endothelial growth factor monoclonal antibody for the therapy of solid tumors and other disorders. *Cancer Research*, 57 20, 4593–4599.
<https://api.semanticscholar.org/CorpusID:7328553>
- Lerner, E. C., Qian, Y., Blaskovich, M. A., Fossum, R. D., Vogt, A., Sun, J., Cox, A. D., Der, C. J., Hamilton, A. D., & Sefti, S. M. (1995). Ras CAAX Peptidomimetic FTI-277 Selectively Blocks Oncogenic Ras Signaling by Inducing Cytoplasmic Accumulation of Inactive Ras-Raf Complexes (*). *Journal of Biological Chemistry*, 270(45), 26802–26806.
<https://doi.org/https://doi.org/10.1074/jbc.270.45.26802>
- Li, C., Vides, A., Kim, D., Xue, J. Y., Zhao, Y., & Lito, P. (2021). The G protein signaling regulator RGS3 enhances the GTPase activity of KRAS. *Science*, 374, 197–201.
<https://api.semanticscholar.org/CorpusID:238476861>
- Liao, Q., Gao, Q.-Z., Wei, J., & Chou, K.-C. (2011). Docking and Molecular Dynamics Study on the Inhibitory Activity of Novel Inhibitors on Epidermal Growth Factor Receptor (EGFR). *Medicinal Chemistry (Shāriqah (United Arab Emirates))*, 7, 24–31.
<https://doi.org/10.2174/157340611794072698>
- Liau, N. P. D., Johnson, M. C., Izadi, S., Gerosa, L., Hammel, M., Bruning, J. M., Wendorff, T. J., Phung, W., Hymowitz, S. G., & Sudhamsu, J. (2022). Structural basis for SHOC2 modulation of RAS signalling. *Nature*, 609(7926), 400–407.
<https://doi.org/10.1038/s41586-022-04838-3>
- Liu, C., Zheng, S., Jin, R., Wang, X., Wang, F., Zang, R., Xu, H., Lu, Z., Huang, J., Lei, Y., Mao, S., Wang, Y., Feng, X., Sun, N., Wang, Y., & He, J. (2020). The superior efficacy of anti-PD-1/PD-L1 immunotherapy in KRAS-mutant non-small cell lung cancer that correlates with an inflammatory phenotype and increased immunogenicity. *Cancer Letters*, 470, 95–105. <https://doi.org/https://doi.org/10.1016/j.canlet.2019.10.027>
- Liu, G., Qin, Q., Chan, K. W. Y., Li, Y., Bulte, J. W. M., McMahon, M. T., van Zijl, P. C. M., & Gilad, A. A. (2014). Non-invasive temperature mapping using temperature-responsive water saturation shift referencing (T-WASSR) MRI. *NMR in Biomedicine*, 27(3), 320–331. <https://doi.org/https://doi.org/10.1002/nbm.3066>
- Liu, J., & Nussinov, R. (2016). Allosteric: An Overview of Its History, Concepts, Methods, and Applications. *PLOS Computational Biology*, 12(6), e1004966-.
<https://doi.org/10.1371/journal.pcbi.1004966>

- Liu, P., Wang, Y., & Li, X. (2019). Targeting the untargetable KRAS in cancer therapy. In *Acta Pharmaceutica Sinica B* (Vol. 9, Issue 5, pp. 871–879). Chinese Academy of Medical Sciences. <https://doi.org/10.1016/j.apsb.2019.03.002>
- Liu, S., Gönen, M., Stadler, Z., Weiser, M., Hechtman, J., Vakiani, E., Wang, T., Vyas, M., Joneja, U., Al-Bayati, M., Segal, N., Smith, J., King, S., Guercio, S., Ntiamuah, P., Markowitz, A., Zhang, L., Cercek, A., Garcia-Aguilar, J., & Shia, J. (2018). Cellular localization of PD-L1 expression in mismatch-repair-deficient and proficient colorectal carcinomas. *Modern Pathology*, 32, 1. <https://doi.org/10.1038/s41379-018-0114-7>
- Lopez-Alcalá, C., Alvarez-Moya, B., Villalonga, P., Calvo, M., Bachs, O., & Agell, N. (2008a). Identification of essential interacting elements in K-Ras/calmodulin binding and its role in K-Ras localization. *The Journal of Biological Chemistry*, 283(16), 10621–10631. <https://doi.org/10.1074/jbc.M706238200>
- Lopez-Alcalá, C., Alvarez-Moya, B., Villalonga, P., Calvo, M., Bachs, O., & Agell, N. (2008b). Identification of Essential Interacting Elements in K-Ras/Calmodulin Binding and Its Role in K-Ras Localization * . *Journal of Biological Chemistry*, 283(16), 10621–10631. <https://doi.org/10.1074/jbc.M706238200>
- Luo, J., Solimini, N. L., & Elledge, S. J. (2009). Principles of Cancer Therapy: Oncogene and Non-oncogene Addiction. *Cell*, 136(5), 823–837. <https://doi.org/https://doi.org/10.1016/j.cell.2009.02.024>
- Macerelli, M., Caramella, C., Faivre, L., Besse, B., Planchard, D., Polo, V., Ngo Camus, M., Celebic, A., Koubi-Pick, V., Lacroix, L., Pignon, J. P., & Soria, J. C. (2014). Does KRAS mutational status predict chemoresistance in advanced non-small cell lung cancer (NSCLC)? *Lung Cancer*, 83(3), 383–388. <https://doi.org/https://doi.org/10.1016/j.lungcan.2013.12.013>
- Mahmoudi Gomari, M., Saraygord-Afshari, N., Farsimadan, M., Rostami, N., Aghamiri, S., & Farajollahi, M. M. (2020). Opportunities and challenges of the tag-assisted protein purification techniques: Applications in the pharmaceutical industry. *Biotechnology Advances*, 45, 107653. <https://doi.org/10.1016/j.biotechadv.2020.107653>
- Manolaridis, I., Kulkarni, K., Dodd, R. B., Ogasawara, S., Zhang, Z., Bineva, G., O'Reilly, N., Hanrahan, S. J., Thompson, A. J., Cronin, N., Iwata, S., & Barford, D. (2013). Mechanism of farnesylated CAAX protein processing by the intramembrane protease Rce1. *Nature*, 504(7479), 301–305. <https://doi.org/10.1038/nature12754>
- Mansour, M. A. (2018). Ubiquitination: Friend and foe in cancer. *The International Journal of Biochemistry & Cell Biology*, 101, 80–93. <https://doi.org/https://doi.org/10.1016/j.biocel.2018.06.001>
- Matallanas, D., Romano, D., Al-Mulla, F., O'Neill, E., Al-Ali, W., Crespo, P., Doyle, B., Nixon, C., Sansom, O., Drosten, M., Barbacid, M., & Kolch, W. (2011). Mutant K-Ras Activation of the Proapoptotic MST2 Pathway Is Antagonized by Wild-Type K-Ras. *Molecular Cell*, 44(6), 893–906. <https://doi.org/https://doi.org/10.1016/j.molcel.2011.10.016>
- Maurer, T., Garrenton, L. S., Oh, A., Pitts, K., Anderson, D. J., Skelton, N. J., Fauber, B. P., Pan, B., Malek, S., Stokoe, D., Ludlam, M. J. C., Bowman, K. K., Wu, J., Giannetti, A. M., Starovasnik, M. A., Mellman, I., Jackson, P. K., Rudolph, J., Wang, W., & Fang, G. (2012). Small-molecule ligands bind to a distinct pocket in Ras and inhibit SOS-mediated nucleotide exchange activity. *Proceedings of the National Academy of Sciences*, 109(14), 5299–5304. <https://doi.org/10.1073/pnas.1116510109>

- May, D. G., Scott, K. L., Campos, A. R., & Roux, K. J. (2020). Comparative Application of BioID and TurboID for Protein-Proximity Biotinylation. *Cells*, 9(5). <https://doi.org/10.3390/cells9051070>
- Mazhab-Jafari, M. T., Marshall, C. B., Smith, M. J., Gasmi-Seabrook, G. M. C., Stathopoulos, P. B., Inagaki, F., Kay, L. E., Neel, B. G., & Ikura, M. (2015). Oncogenic and RASopathy-associated K-RAS mutations relieve membrane-dependent occlusion of the effector-binding site. *Proceedings of the National Academy of Sciences of the United States of America*, 112(21), 6625–6630. <https://doi.org/10.1073/pnas.1419895112>
- Mcbride, O. W., Swan+, D. C., Tronick+, S. R., Gol+, R., Klimanis+, D., Moore, D. E., & Aaronson, S. A. (n.d.). *Nucleic Acids Research Regional chromosomal localization of N-ras, K-ras-1, K-ras-2 and myb oncogenes in human cells* (Vol. 1).
- Michaelson, D., Silletti, J., Murphy, G., D'Eustachio, P., Rush, M., & Philips, M. R. (2001). Differential Localization of Rho Gtpases in Live Cells: Regulation by Hypervariable Regions and Rhogdi Binding. *Journal of Cell Biology*, 152(1), 111–126. <https://doi.org/10.1083/jcb.152.1.111>
- Miller, C., Chen, G., Gharib, T., Thomas, D., Misek, D., Giordano, T., Yee, J., Orringer, M., Hanash, S., & Beer, D. (2003). Increased C-CRK proto-oncogene expression is associated with an aggressive phenotype in lung adenocarcinomas. *Oncogene*, 22, 7950–7957. <https://doi.org/10.1038/sj.onc.1206529>
- Mirzoeva, O. K., Das, D., Heiser, L. M., Bhattacharya, S., Siwak, D., Gendelman, R., Bayani, N., Wang, N. J., Neve, R. M., Guan, Y., Hu, Z., Knight, Z., Feiler, H. S., Gascard, P., Parvin, B., Spellman, P. T., Shokat, K. M., Wyrobek, A. J., Bissell, M. J., ... Korn, W. M. (2009). Basal Subtype and MAPK/ERK Kinase (MEK)-Phosphoinositide 3-Kinase Feedback Signaling Determine Susceptibility of Breast Cancer Cells to MEK Inhibition. *Cancer Research*, 69(2), 565–572. <https://doi.org/10.1158/0008-5472.CAN-08-3389>
- Moelling, K., Heimann, B., Beiming, P., Rapp, U. R., & Sander, T. (1984). Serine- and threonine-specific protein kinase activities of purified gag-mil and gag-raf proteins. *Nature*, 312(5994), 558–561. <https://doi.org/10.1038/312558a0>
- Molina, J. R., & Adjei, A. A. (2006). The Ras/Raf/MAPK Pathway. *Journal of Thoracic Oncology*, 1(1), 7–9. [https://doi.org/10.1016/s1556-0864\(15\)31506-9](https://doi.org/10.1016/s1556-0864(15)31506-9)
- Mysore, V. P., Zhou, Z. W., Ambrogio, C., Li, L., Kapp, J. N., Lu, C., Wang, Q., Tucker, M. R., Okoro, J. J., Nagy-Davidescu, G., Bai, X., Plückthun, A., Jänne, P. A., Westover, K. D., Shan, Y., & Shaw, D. E. (2021). A structural model of a Ras–Raf signalosome. *Nature Structural and Molecular Biology*, 28(10), 847–857. <https://doi.org/10.1038/s41594-021-00667-6>
- Nakayama, A., Nagashima, T., Nishizono, Y., Kuramoto, K., Mori, K., Homboh, K., Yuri, M., & Shimazaki, M. (2022). Characterisation of a novel KRAS G12C inhibitor ASP2453 that shows potent anti-tumour activity in KRAS G12C-mutated preclinical models. *British Journal of Cancer*, 126(5), 744–753. <https://doi.org/10.1038/s41416-021-01629-x>
- Nan, X., Tamgüney, T. M., Collisson, E. A., Lin, L. J., Pitt, C., Galeas, J., Lewis, S., Gray, J. W., McCormick, F., & Chu, S. (2015). Ras-GTP dimers activate the Mitogen-Activated Protein Kinase (MAPK) pathway. *Proceedings of the National Academy of Sciences of the United States of America*, 112(26), 7996–8001. <https://doi.org/10.1073/pnas.1509123112>
- Nevola, L., & Giral, E. (2015). Modulating protein–protein interactions: the potential of peptides. *Chemical Communications*, 51(16), 3302–3315. <https://doi.org/10.1039/C4CC08565E>

- Niv, H., Gutman, O., Kloog, Y., & Henis, Y. I. (2002). Activated K-Ras and H-Ras display different interactions with saturable nonraft sites at the surface of live cells. *Journal of Cell Biology*, 157(5), 865–872. <https://doi.org/10.1083/jcb.200202009>
- O'Bryan, J. P. (2019). Pharmacological targeting of RAS: Recent success with direct inhibitors. *Pharmacological Research*, 139, 503–511. <https://doi.org/10.1016/j.phrs.2018.10.021>
- Oehrl, W., Rubio, I., & Wetzker, R. (2003). Serine 338 Phosphorylation Is Dispensable for Activation of c-Raf1*. *Journal of Biological Chemistry*, 278(20), 17819–17826. <https://doi.org/10.1074/jbc.M209951200>
- Orsburn, B. (2021). Proteome Discoverer—A Community Enhanced Data Processing Suite for Protein Informatics. *Proteomes*, 9, 15. <https://doi.org/10.3390/proteomes9010015>
- Ortiz-Vega, S., Khokhlatchev, A., Nedwidek, M., Zhang, X., Dammann, R., Pfeifer, G. P., & Avruch, J. (2002). The putative tumor suppressor RASSF1A homodimerizes and heterodimerizes with the Ras-GTP binding protein Nore1. *Oncogene*, 21(9), 1381–1390. <https://doi.org/10.1038/sj.onc.1205192>
- Osta, B. El, Behera, M., Kim, S., Berry, L. D., Sica, G. L., Pillai, R. N., Owonikoko, T. K., Kris, M. G., Johnson, B. E., Kwiatkowski, D. J., Sholl, L. M., Aisner, D. L., Bunn, P. A., Khuri, F. R., & Ramalingam, S. S. (2019). Characteristics and Outcomes of Patients With Metastatic KRAS-Mutant Lung Adenocarcinomas: The Lung Cancer Mutation Consortium Experience. *Journal of Thoracic Oncology*, 14, 876–889. <https://api.semanticscholar.org/CorpusID:73426557>
- Ostrem, J. M. L., & Shokat, K. M. (2016). Direct small-molecule inhibitors of KRAS: from structural insights to mechanism-based design. *Nature Reviews Drug Discovery*, 15(11), 771–785. <https://doi.org/10.1038/nrd.2016.139>
- Ostrem, J. M., Peters, U., Sos, M. L., Wells, J. A., & Shokat, K. M. (2013). K-Ras(G12C) inhibitors allosterically control GTP affinity and effector interactions. *Nature*, 503(7477), 548–551. <https://doi.org/10.1038/nature12796>
- Ottiano, A., Nasti, G., Santorsola, M., Altieri, V., Fruscio, G., Circelli, L., Luce, A., Cossu, A., Scognamiglio, G., Perri, F., Correr, M., Belli, A., Delrio, P., Botti, G., & Caraglia, M. (2021). KRAS Mutational Regression Is Associated With Oligo-Metastatic Status and Good Prognosis in Metastatic Colorectal Cancer. *Frontiers in Oncology*, 11. <https://doi.org/10.3389/fonc.2021.632962>
- Otto, J. C., Kim, E., Young, S. G., & Casey, P. J. (1999). Cloning and Characterization of a Mammalian Prenyl Protein-specific Protease*. *Journal of Biological Chemistry*, 274(13), 8379–8382. <https://doi.org/10.1074/jbc.274.13.8379>
- Pacold, M., Suire, S., Perisic, O., Lara-Gonzalez, S., Davis, C., Walker, E., Hawkins, P., Stephens, L., Eccleston, J., & Williams, R. (2000). Crystal Structure and Functional Analysis of Ras Binding to Its Effector Phosphoinositide 3Kinase ?? *Cell*, 103, 931–944. [https://doi.org/10.1016/S0092-8674\(00\)00196-3](https://doi.org/10.1016/S0092-8674(00)00196-3)
- Pallara, C., Cabot, D., Rivas, J., Brun, S., Seco, J., Abuasaker, B., Tarragó, T., Jaumot, M., Prades, R., & Agell, N. (2022). Peptidomimetics designed to bind to RAS effector domain are promising cancer therapeutic compounds. *Scientific Reports*, 12(1). <https://doi.org/10.1038/s41598-022-19703-6>
- Palma, G., Khurshid, F., Lu, K., Woodward, B., & Husain, H. (2021). Selective KRAS G12C inhibitors in non-small cell lung cancer: chemistry, concurrent pathway alterations, and clinical outcomes. *Npj Precision Oncology*, 5(1), 98. <https://doi.org/10.1038/s41698-021-00237-5>

- Pan, D. (2010). The Hippo Signaling Pathway in Development and Cancer. *Developmental Cell*, 19(4), 491–505. <https://doi.org/https://doi.org/10.1016/j.devcel.2010.09.011>
- Panka, D. J., Atkins, M. B., & Mier, J. W. (2006). Targeting the Mitogen-Activated Protein Kinase Pathway in the Treatment of Malignant Melanoma. *Clinical Cancer Research*, 12(7), 2371s–2375s. <https://doi.org/10.1158/1078-0432.CCR-05-2539>
- Pantsar, T. (2020). The current understanding of KRAS protein structure and dynamics. In *Computational and Structural Biotechnology Journal* (Vol. 18, pp. 189–198). Elsevier B.V. <https://doi.org/10.1016/j.csbj.2019.12.004>
- Papke, B., Azam, S. H., Feng, A. Y., Swearingen, A. E. D. Van, Gutierrez-Ford, C., Pallan, P. S., Egli, M., Cox, A. D., Der, C. J., & Pecot, C. V. (2020). Silencing of oncogenic KRAS by mutant-selective small interfering RNA. *BioRxiv*, 2020.10.08.331835. <https://doi.org/10.1101/2020.10.08.331835>
- Park, E., Rawson, S., Li, K., Kim, B.-W., Ficarro, S. B., Pino, G. G.-D., Sharif, H., Marto, J. A., Jeon, H., & Eck, M. J. (2019). Architecture of autoinhibited and active BRAF–MEK1–14-3-3 complexes. *Nature*, 575(7783), 545–550. <https://doi.org/10.1038/s41586-019-1660-y>
- Park, J., Kang, S. I., Lee, S.-Y., Zhang, X. F., Kim, M. S., Beers, L. F., Lim, D.-S., Avruch, J., Kim, H.-S., & Lee, S. B. (2010a). Tumor Suppressor Ras Association Domain Family 5 (RASSF5/NORE1) Mediates Death Receptor Ligand-induced Apoptosis*. *Journal of Biological Chemistry*, 285(45), 35029–35038. <https://doi.org/https://doi.org/10.1074/jbc.M110.165506>
- Park, J., Kang, S. I., Lee, S.-Y., Zhang, X. F., Kim, M. S., Beers, L. F., Lim, D.-S., Avruch, J., Kim, H.-S., & Lee, S. B. (2010b). Tumor Suppressor Ras Association Domain Family 5 (RASSF5/NORE1) Mediates Death Receptor Ligand-induced Apoptosis*. *Journal of Biological Chemistry*, 285(45), 35029–35038. <https://doi.org/https://doi.org/10.1074/jbc.M110.165506>
- Parker, M. I., Meyer, J. E., Golemis, E. A., & Dunbrack Roland L. Jr. (2022). Delineating the RAS Conformational Landscape. *Cancer Research*, 82(13), 2485–2498. <https://doi.org/10.1158/0008-5472.CAN-22-0804>
- Patricelli, M. P., Janes, M. R., Li, L.-S., Hansen, R., Peters, U., Kessler, L. V, Chen, Y., Kucharski, J. M., Feng, J., Ely, T., Chen, J. H., Firdaus, S. J., Babbar, A., Ren, P., & Liu, Y. (2016). Selective Inhibition of Oncogenic KRAS Output with Small Molecules Targeting the Inactive State. *Cancer Discovery*, 6(3), 316–329. <https://doi.org/10.1158/2159-8290.CD-15-1105>
- Pereira, F., Ferreira, A., Reis, C. A., Sousa, M. J., Oliveira, M. J., & Preto, A. (2022). KRAS as a Modulator of the Inflammatory Tumor Microenvironment: Therapeutic Implications. *Cells*, 11(3). <https://doi.org/10.3390/cells11030398>
- Plowman, S. J., Muncke, C., Parton, R. G., Hancock, J. F., & Simons, K. (2005). H-ras, K-ras, and inner plasma membrane raft proteins operate in nanoclusters with differential dependence on the actin cytoskeleton. In *PNAS October* (Vol. 25, Issue 43). www.pnas.org/cgi/doi/10.1073/pnas.0504114102
- Poon, E., Mullins, S., Watkins, A., Williams, G. S., Koopmann, J.-O., Genova, G. Di, Cumberbatch, M., Veldman-Jones, M., Grosskurth, S. E., Sah, V., Schuller, A., Reimer, C., Dovedi, S. J., Smith, P. D., Stewart, R., & Wilkinson, R. W. (2017). The MEK inhibitor selumetinib complements CTLA-4 blockade by reprogramming the tumor immune microenvironment. *Journal for ImmunoTherapy of Cancer*, 5(1), 63. <https://doi.org/10.1186/s40425-017-0268-8>

- Poulikakos, P., Zhang, C., Bollag, G., Shokat, K., & Rosen, N. (2010). RAF inhibitors transactivate RAF dimers and ERK signaling in cells with wild-type BRAF. *Nature*, 464, 427–430. <https://doi.org/10.1038/nature08902>
- Praskova, M., Khoklatchev, A., Ortiz-Vega, S., & Avruch, J. (2004). Regulation of the MST1 kinase by autophosphorylation, by the growth inhibitory proteins, RASSF1 and NORE1, and by Ras. *Biochemical Journal*, 381(2), 453–462. <https://doi.org/10.1042/BJ20040025>
- Prior, I. A., Lewis, P. D., & Mattos, C. (2012). A Comprehensive Survey of Ras Mutations in Cancer. *Cancer Research*, 72(10), 2457–2467. <https://doi.org/10.1158/0008-5472.CAN-11-2612>
- Pumiglia, K. M., & Decker, S. J. (1997). Cell cycle arrest mediated by the MEK/mitogen-activated protein kinase pathway. *Proceedings of the National Academy of Sciences*, 94(2), 448–452. <https://doi.org/10.1073/pnas.94.2.448>
- Pylayeva-Gupta, Y., Grabocka, E., & Bar-Sagi, D. (2011). RAS oncogenes: Weaving a tumorigenic web. *Nature Reviews. Cancer*, 11, 761–774. <https://doi.org/10.1038/nrc3106>
- Qiu, M.-S., & Green, S. H. (1992). PC12 cell neuronal differentiation is associated with prolonged p21ras activity and consequent prolonged ERK activity. *Neuron*, 9(4), 705–717. [https://doi.org/10.1016/0896-6273\(92\)90033-A](https://doi.org/10.1016/0896-6273(92)90033-A)
- Quintal, N., & Campos, M. (2020). Bioactive Peptides as Therapeutic Adjuvants for Cancer. *Nutrition and Cancer*, 73, 1–13. <https://doi.org/10.1080/01635581.2020.1813316>
- Rabara, D., Tran, T. H., Dharmaiah, S., Stephens, R. M., McCormick, F., Simanshu, D. K., & Holderfield, M. (2019). KRAS G13D sensitivity to neurofibromin-mediated GTP hydrolysis. *Proceedings of the National Academy of Science*, 116(44), 22122–22131. <https://doi.org/10.1073/pnas.1908353116>
- Rajakulendran, T., Sahmi, M., Lefrançois, M., Sicheri, F., & Therrien, M. (2009). A dimerization-dependent mechanism drives RAF catalytic activation. *Nature*, 461(7263), 542–545. <https://doi.org/10.1038/nature08314>
- Rapp, U. R., & Todaro, G. J. (1978). Generation of New Mouse Sarcoma Viruses in Cell Culture. *Science*, 201(4358), 821–824. <https://doi.org/10.1126/science.210501>
- Riaud, M., Maxwell, J., Soria-Bretones, I., Dankner, M., Li, M., & Rose, A. A. N. (2024). The role of CRAF in cancer progression: from molecular mechanisms to precision therapies. *Nature Reviews Cancer*, 24(2), 105–122. <https://doi.org/10.1038/s41568-023-00650-x>
- Riss, T. L., Moravec, R. A., & Niles, A. L. (2013). Cell Viability Assays. In *Cell Viability Assays*.
- Rodriguez-Viciano, P., Oses-Prieto, J., Burlingame, A., Fried, M., & McCormick, F. (2006). A Phosphatase Holoenzyme Comprised of Shoc2/Sur8 and the Catalytic Subunit of PP1 Functions as an M-Ras Effector to Modulate Raf Activity. *Molecular Cell*, 22(2), 217–230. <https://doi.org/10.1016/j.molcel.2006.03.027>
- Roovers, K., & Assoian, R. (2000). Integrating the MAP kinase signal into the G1 phase cell cycle machinery. *BioEssays*, 22, 818–826. [https://doi.org/10.1002/1521-1878\(200009\)22:9<818::AID-BIES7>3.3.CO;2-Y](https://doi.org/10.1002/1521-1878(200009)22:9<818::AID-BIES7>3.3.CO;2-Y)
- Rosenbluh, J., Mercer, J., Shrestha, Y., Oliver, R., Tamayo, P., Doench, J. G., Tirosh, I., Piccioni, F., Hartenian, E., & Horn, H. (2016). Genetic and proteomic interrogation of lower confidence candidate genes reveals signaling networks in β -catenin-active cancers. *Cell Systems*, 3(3), 302–316.
- Roux, K. J., Kim, D. I., Raida, M., & Burke, B. (2012). A promiscuous biotin ligase fusion protein identifies proximal and interacting proteins in mammalian cells. *Journal of Cell Biology*, 196(6), 801–810. <https://doi.org/10.1083/jcb.201112098>

- Rushworth, L. K., Hindley, A. D., O'Neill, E., & Kolch, W. (2006). Regulation and Role of Raf-1/B-Raf Heterodimerization. *Molecular and Cellular Biology*, 26(6), 2262–2272. <https://doi.org/10.1128/MCB.26.6.2262-2272.2006>
- Ryan, M. B., de la Cruz, F. F., Phat, S., Myers, D. T., Wong, E., Shahzade, H. A., Hong, C. B., & Corcoran, R. B. (2019). Vertical Pathway Inhibition Overcomes Adaptive Feedback Resistance to KRASG12C Inhibition. *Clinical Cancer Research*, 26, 1633–1643. <https://api.semanticscholar.org/CorpusID:208336026>
- Sabari, J. K., Velcheti, V., Shimizu, K., Strickland, M. R., Heist, R. S., Singh, M., Nayyar, N., Giobbie-Hurder, A., Digumarthy, S. R., Gainor, J. F., Rajan, A. P., Nieblas-Bedolla, E., Burns, A. C., Hallin, J., Olson, P., Christensen, J. G., Kurz, S. C., Brastianos, P. K., & Wakimoto, H. (2022). Activity of Adagrasib (MRTX849) in Brain Metastases: Preclinical Models and Clinical Data from Patients with KRASG12C-Mutant Non–Small Cell Lung Cancer. *Clinical Cancer Research*, 28(15), 3318–3328. <https://doi.org/10.1158/1078-0432.CCR-22-0383>
- Santos, R., Ursu, O., Gaulton, A., Bento, A., Donadi, R., Bologa, C., Karlsson, A., Al-Lazikani, B., Hersey, A., Oprea, T., & Overington, J. (2016). A comprehensive map of molecular drug targets. *Nature Reviews Drug Discovery*, 16. <https://doi.org/10.1038/nrd.2016.230>
- Santra, T., Herrero, A., Rodriguez, J., von Kriegsheim, A., Iglesias-Martinez, L. F., Schwarzl, T., Higgins, D., Aye, T.-T., Heck, A. J. R., Calvo, F., Agudo-Ibáñez, L., Crespo, P., Matallanas, D., & Kolch, W. (2019). An Integrated Global Analysis of Compartmentalized HRAS Signaling. *Cell Reports*, 26(11), 3100–3115.e7. <https://doi.org/10.1016/j.celrep.2019.02.038>
- Sasaki, A. T., Carracedo, A., Locasale, J. W., Anastasiou, D., Takeuchi, K., Kahoud, E. R., Haviv, S., Asara, J. M., Pandolfi, P. P., & Cantley, L. C. (2011). Ubiquitination of K-Ras enhances activation and facilitates binding to select downstream effectors. *Science Signaling*, 4(163), ra13. <https://doi.org/10.1126/scisignal.2001518>
- Schlesinger, T. K., Fanger, G. R., Yujiri, T., & Johnson, G. L. (1998). The TAO of MEKK. *Frontiers in Bioscience : A Journal and Virtual Library*, 3, D1181–6. <https://doi.org/10.2741/a354>
- Schmick, M., Kraemer, A., & Bastiaens, P. I. H. (2015). Ras moves to stay in place. *Trends in Cell Biology*, 25(4), 190–197. <https://doi.org/10.1016/j.tcb.2015.02.004>
- Schmick, M., Vartak, N., Papke, B., Kovacevic, M., Truxius, D. C., Rossmannek, L., & Bastiaens, P. I. H. (2014). KRas Localizes to the Plasma Membrane by Spatial Cycles of Solubilization, Trapping and Vesicular Transport. *Cell*, 157(2), 459–471. <https://doi.org/https://doi.org/10.1016/j.cell.2014.02.051>
- Schmid, S., Gautschi, O., Rothschild, S., Mark, M., Froesch, P., Klingbiel, D., Reichegger, H., Jochum, W., Diebold, J., & Früh, M. (2017). Clinical Outcome of ALK-Positive Non–Small Cell Lung Cancer (NSCLC) Patients with De Novo EGFR or KRAS Co-Mutations Receiving Tyrosine Kinase Inhibitors (TKIs). *Journal of Thoracic Oncology*, 12(4), 681–688. <https://doi.org/https://doi.org/10.1016/j.jtho.2016.12.003>
- Seabra, M. C., Reiss, Y., Casey, P. J., Brown, M. S., & Goldstein, J. L. (1991). Protein farnesyltransferase and geranylgeranyltransferase share a common α subunit. *Cell*, 65(3), 429–434. [https://doi.org/https://doi.org/10.1016/0092-8674\(91\)90460-G](https://doi.org/https://doi.org/10.1016/0092-8674(91)90460-G)
- Seguin, L., Camargo, M., Wettersten, H., Kato, S., Desgrosellier, J., Schalscha, T., Elliott, K., Cosset, É., Lesperance, J., Weis, S., & Cheresch, D. (2017). Galectin-3, a Druggable Vulnerability for KRAS-Addicted Cancers. *Cancer Discovery*, 7, CD-17. <https://doi.org/10.1158/2159-8290.CD-17-0539>

- Shalom-Feuerstein, R., Plowman, S. J., Rotblat, B., Ariotti, N., Tian, T., Hancock, J. F., & Kloog, Y. (2008). K-Ras Nanoclustering Is Subverted by Overexpression of the Scaffold Protein Galectin-3. *Cancer Research*, 68(16), 6608–6616. <https://doi.org/10.1158/0008-5472.CAN-08-1117>
- Shannon, P., Markiel, A., Ozier, O., Baliga, N., Wang, J., Ramage, D., Amin, N., Schwikowski, B., & Ideker, T. (2003). Cytoscape: A Software Environment for Integrated Models of Biomolecular Interaction Networks. *Genome Research*, 13, 2498–2504. <https://doi.org/10.1101/gr.1239303>
- She, Q.-B., Solit, D. B., Ye, Q., O'Reilly, K. E., Lobo, J., & Rosen, N. (2005). The BAD protein integrates survival signaling by EGFR/MAPK and PI3K/Akt kinase pathways in PTEN-deficient tumor cells. *Cancer Cell*, 8(4), 287–297. <https://doi.org/https://doi.org/10.1016/j.ccr.2005.09.006>
- Sieburth, D. S., Sun, Q., & Han, M. (1998). SUR-8, a Conserved Ras-Binding Protein with Leucine-Rich Repeats, Positively Regulates Ras-Mediated Signaling in *C. elegans*. *Cell*, 94(1), 119–130. [https://doi.org/10.1016/S0092-8674\(00\)81227-1](https://doi.org/10.1016/S0092-8674(00)81227-1)
- Silvius, J. R., Bhagatji, P., Leventis, R., & Terrone, D. (2005). K-ras4B and Prenylated Proteins Lacking “Second Signals” Associate Dynamically with Cellular Membranes. *Molecular Biology of the Cell*, 17(1), 192–202. <https://doi.org/10.1091/mbc.e05-05-0408>
- Simons, K., & Toomre, D. (2000). Lipid rafts and signal transduction. *Nature Reviews Molecular Cell Biology*, 1(1), 31–39. <https://doi.org/10.1038/35036052>
- Siprashvili, Z., Webster, D. E., Johnston, D., Shenoy, R. M., Ungewickell, A. J., Bhaduri, A., Flockhart, R., Zarnegar, B. J., Che, Y., Meschi, F., Puglisi, J. D., & Khavari, P. A. (2016). The noncoding RNAs SNORD50A and SNORD50B bind K-Ras and are recurrently deleted in human cancer. *Nature Genetics*, 48(1), 53–58. <https://doi.org/10.1038/ng.3452>
- Skoulidis, F., Byers, L. A., Diao, L., Papadimitrakopoulou, V. A., Tong, P., Izzo, J., Behrens, C., Kadara, H., Parra, E. R., Canales, J. R., Zhang, J., Giri, U., Gudikote, J., Cortez, M. A., Yang, C., Fan, Y., Peyton, M., Girard, L., Coombes, K. R., ... Heymach, J. V. (2015). Co-occurring Genomic Alterations Define Major Subsets of KRAS-Mutant Lung Adenocarcinoma with Distinct Biology, Immune Profiles, and Therapeutic Vulnerabilities. *Cancer Discovery*, 5(8), 860–877. <https://doi.org/10.1158/2159-8290.CD-14-1236>
- Skoulidis, F., Goldberg, M. E., Greenawalt, D. M., Hellmann, M. D., Awad, M. M., Gainor, J. F., Schrock, A. B., Hartmaier, R. J., Trabucco, S. E., Gay, L., Ali, S. M., Elvin, J. A., Singal, G., Ross, J. S., Fabrizio, D., Szabo, P. M., Chang, H., Sasson, A., Srinivasan, S., ... Heymach, J. V. (2018). STK11/LKB1 Mutations and PD-1 Inhibitor Resistance in KRAS-Mutant Lung Adenocarcinoma. *Cancer Discovery*, 8(7), 822–835. <https://doi.org/10.1158/2159-8290.CD-18-0099>
- Skoulidis, F., & Heymach, J. V. (2019). Co-occurring genomic alterations in non-small-cell lung cancer biology and therapy. *Nature Reviews Cancer*, 19(9), 495–509. <https://doi.org/10.1038/s41568-019-0179-8>
- Smakman, N., Veenendaal, L. M., van Diest, P., Bos, R., Offringa, R., Borel Rinkes, I. H. M., & Kranenburg, O. (2005). Dual effect of KrasD12 knockdown on tumorigenesis: increased immune-mediated tumor clearance and abrogation of tumor malignancy. *Oncogene*, 24(56), 8338–8342. <https://doi.org/10.1038/sj.onc.1208995>
- Song, H. Y., Biancucci, M., Kang, H.-J., O'Callaghan, C., Park, S.-H., Principe, D., Jiang, H., Yan, Y., Satchell, K., Raparia, K., Gius, D., & Vassilopoulos, A. (2016). SIRT2 deletion enhances

- KRAS-induced tumorigenesis in vivo by regulating K147 acetylation status. *Oncotarget*, 7. <https://doi.org/10.18632/oncotarget.12015>
- Sos, M., Fischer, S., Ullrich, R., Peifer, M., Heuckmann, J., Koker, M., Heynck, S., Stückerath, I., Weiss, J., Malchers, F., Michel, K., Goel, A., Regales, L., Politi, K., Perera, S., Getlik, M., Heukamp, L., Ansén, S., Zander, T., & Thomas, R. (2009). Identifying genotype-dependent efficacy of single and combined PI3K-and MAPK-pathway inhibition in cancer. *Proceedings of the National Academy of Sciences of the United States of America*, 106, 18351–18356. <https://doi.org/10.1073/pnas.0907325106>
- Spencer-Smith, R., Koide, A., Zhou, Y., Eguchi, R. R., Sha, F., Gajwani, P., Santana, D., Gupta, A., Jacobs, M., Herrero-Garcia, E., Cobbert, J., Lavoie, H., Smith, M., Rajakulendran, T., Dowdell, E., Okur, M. N., Dementieva, I., Sicheri, F., Therrien, M., ... O'Bryan, J. P. (2017). Inhibition of RAS function through targeting an allosteric regulatory site. *Nature Chemical Biology*, 13(1), 62–68. <https://doi.org/10.1038/nchembio.2231>
- Spencer-Smith, R., Li, L., Prasad, S., Koide, A., Koide, S., & O'Bryan, J. P. (2019). Targeting the $\alpha 4$ - $\alpha 5$ interface of RAS results in multiple levels of inhibition. *Small GTPases*, 10(5), 378–387. <https://doi.org/10.1080/21541248.2017.1333188>
- Sriram, G., & Birge, R. B. (2010). Emerging Roles for Crk in Human Cancer. *Genes & Cancer*, 1(11), 1132–1139. <https://doi.org/10.1177/1947601910397188>
- Stalneck, C. A., & Der, C. J. (2020). RAS, wanted dead or alive: Advances in targeting RAS mutant cancers. *Science Signaling*, 13(624), eaay6013. <https://doi.org/10.1126/scisignal.aay6013>
- Storz, P. (2015). The crosstalk between acinar cells with Kras mutations and M1-polarized macrophages leads to initiation of pancreatic precancerous lesions. *Oncotarget*, 4(6), e1008794. <https://doi.org/10.1080/2162402X.2015.1008794>
- Sun, Q., Burke, J. P., Phan, J., Burns, M. C., Olejniczak, E. T., Waterson, A. G., Lee, T., Rossanese, O. W., & Fesik, S. W. (2012). Discovery of Small Molecules that Bind to K-Ras and Inhibit Sos-Mediated Activation. *Angewandte Chemie International Edition*, 51(25), 6140–6143. <https://doi.org/10.1002/anie.201201358>
- Sutton, M. N., Lu, Z., Li, Y. C., Zhou, Y., Huang, T., Reger, A. S., Hurwitz, A. M., Palzkill, T., Logsdon, C., Liang, X., Gray, J. W., Nan, X., Hancock, J., Wahl, G. M., & Bast, R. C. (2019). DIRAS3 (ARHI) Blocks RAS/MAPK Signaling by Binding Directly to RAS and Disrupting RAS Clusters. *Cell Reports*, 29(11), 3448–3459.e6. <https://doi.org/10.1016/j.celrep.2019.11.045>
- Takahashi, M., Li, Y., Dillon, T. J., Kariya, Y., & Stork, P. J. S. (2017). *Phosphorylation of the C-Raf N Region Promotes Raf Dimerization*. <https://doi.org/10.1128/MCB>
- Teo, G., Liu, G., Zhang, J., Nesvizhskii, A. I., Gingras, A.-C., & Choi, H. (2014). SAINTexpress: improvements and additional features in Significance Analysis of INTERactome software. *Journal of Proteomics*, 100, 37–43. <https://doi.org/10.1016/j.jprot.2013.10.023>
- Terrell, E. M., & Morrison, D. K. (2019). Ras-mediated activation of the Raf family kinases. *Cold Spring Harbor Perspectives in Medicine*, 9(1). <https://doi.org/10.1101/cshperspect.a033746>
- Tian, T., Harding, A., Inder, K., Plowman, S., Parton, R. G., & Hancock, J. F. (2007). Plasma membrane nanoswitches generate high-fidelity Ras signal transduction. *Nature Cell Biology*, 9(8), 905–914. <https://doi.org/10.1038/ncb1615>
- Tsai, F. D., Lopes, M. S., Zhou, M., Court, H., Ponce, O., Fiordalisi, J. J., Gierut, J. J., Cox, A. D., Haigis, K. M., & Philips, M. R. (2015). K-Ras4A splice variant is widely expressed in

- cancer and uses a hybrid membrane-targeting motif. *Proceedings of the National Academy of Science*, 112(3), 779–784. <https://doi.org/10.1073/pnas.1412811112>
- Tsai, M.-J., Chang, W.-A., Huang, M.-S., & Kuo, P.-L. (2014). Tumor Microenvironment: A New Treatment Target for Cancer. *ISRN Biochemistry*, 2014, 351959. <https://doi.org/10.1155/2014/351959>
- Tsubaki, M., Takeda, T., Noguchi, M., Jinushi, M., Seki, S., Morii, Y., Shimomura, K., Imano, M., Satou, T., & Nishida, S. (2019). Overactivation of akt contributes to MEK inhibitor primary and acquired resistance in colorectal cancer cells. *Cancers*, 11(12). <https://doi.org/10.3390/cancers11121866>
- Tsuchida, N., Ryder, T., & Ohtsubo, E. (1982). Nucleotide Sequence of the Oncogene Encoding the p21 Transforming Protein of Kirsten Murine Sarcoma Virus. *Science*, 217(4563), 937–939. <https://doi.org/10.1126/science.6287573>
- Upadhyaya, P., Qian, Z., Habir, N. A. A., & Pei, D. (2014). Direct Ras inhibitors identified from a structurally rigidified bicyclic peptide library. *Tetrahedron*, 70(42), 7714–7720. <https://doi.org/https://doi.org/10.1016/j.tet.2014.05.113>
- Uras, I. Z., Moll, H. P., & Casanova, E. (2020). Targeting KRAS Mutant Non-Small-Cell Lung Cancer: Past, Present and Future. *International Journal of Molecular Sciences*, 21(12). <https://doi.org/10.3390/ijms21124325>
- Vandemoortele, G., Eyckerman, S., & Gevaert, K. (2019). Pick a Tag and Explore the Functions of Your Pet Protein. *Trends in Biotechnology*, 37(10), 1078–1090. <https://doi.org/https://doi.org/10.1016/j.tibtech.2019.03.016>
- Vavvas, D., Li, X., Avruch, J., & Zhang, X.-F. (1998). Identification of Nore1 as a Potential Ras Effector*. *Journal of Biological Chemistry*, 273(10), 5439–5442. <https://doi.org/https://doi.org/10.1074/jbc.273.10.5439>
- Vetter, I. R., & Wittinghofer, A. (2001). The Guanine Nucleotide-Binding Switch in Three Dimensions. *Science*, 294(5545), 1299–1304. <https://doi.org/10.1126/science.1062023>
- Villalonga, P., López-Alcalá, C., Bosch, M., Chiloeches, A., Rocamora, N., Gil, J., Marais, R., Marshall, C. J., Bachs, O., & Agell, N. (2001). Calmodulin Binds to K-Ras, but Not to H- or N-Ras, and Modulates Its Downstream Signaling. *Molecular and Cellular Biology*, 21(21), 7345–7354. <https://doi.org/10.1128/MCB.21.21.7345-7354.2001>
- Villalonga, P., López-Alcalá, C., Chiloeches, A., Gil, J., Marais, R., Bachs, O., & Agell, N. (2002). Calmodulin Prevents Activation of Ras by PKC in 3T3 Fibroblasts*. *Journal of Biological Chemistry*, 277(40), 37929–37935. <https://doi.org/https://doi.org/10.1074/jbc.M202245200>
- Vivanco, I., & Sawyers, C. L. (2002). The phosphatidylinositol 3-Kinase–AKT pathway in human cancer. *Nature Reviews Cancer*, 2(7), 489–501. <https://doi.org/10.1038/nrc839>
- Vos, M. D., Ellis, C. A., Bell, A., Birrer, M. J., & Clark, G. J. (2000). Ras Uses the Novel Tumor Suppressor RASSF1 as an Effector to Mediate Apoptosis*. *Journal of Biological Chemistry*, 275(46), 35669–35672. <https://doi.org/https://doi.org/10.1074/jbc.C000463200>
- Vos, M. D., Martinez, A., Ellis, C. A., Vallecorsa, T., & Clark, G. J. (2003). The Pro-apoptotic Ras Effector Nore1 May Serve as a Ras-regulated Tumor Suppressor in the Lung*. *Journal of Biological Chemistry*, 278(24), 21938–21943. <https://doi.org/https://doi.org/10.1074/jbc.M211019200>
- Walker, J. E., Saraste, M., Runswick, M. J., & Gay, N. J. (1982). Distantly related sequences in the alpha- and beta-subunits of ATP synthase, myosin, kinases and other ATP-requiring

- enzymes and a common nucleotide binding fold. *The EMBO Journal*, 1.
<https://api.semanticscholar.org/CorpusID:10530046>
- Wang, M.-T., Holderfield, M., Galeas, J., Delrosario, R., To, M. D., Balmain, A., & McCormick, F. (2015). K-Ras Promotes Tumorigenicity through Suppression of Non-canonical Wnt Signaling. *Cell*, 163(5), 1237–1251. <https://doi.org/10.1016/j.cell.2015.10.041>
- Wang, W. hua, Yuan, T., Qian, M. jia, Yan, F. jie, Yang, L., He, Q. jun, Yang, B., Lu, J. jian, & Zhu, H. (2021). Post-translational modification of KRAS: potential targets for cancer therapy. In *Acta Pharmacologica Sinica* (Vol. 42, Issue 8, pp. 1201–1211). Springer Nature. <https://doi.org/10.1038/s41401-020-00542-y>
- Wang, Z., Zheng, X., Wang, X., Chen, Y., Li, Z., Yu, J., Yang, W., Mao, B., Zhang, H., Li, J., & Shen, L. (2021). Genetic differences between lung metastases and liver metastases from left-sided microsatellite stable colorectal cancer: next generation sequencing and clinical implications. *Annals of Translational Medicine*, 9(12), 967.
<https://doi.org/10.21037/atm-21-2221>
- Weiss, J., Yaeger, R. D., Johnson, M. L., Spira, A., Klempner, S., Barve, M. A., Christensen, J. G., Chi, A., Der-Torossian, H., Velastegui, K., Kheoh, T., & Ou, S.-H. I. (2021). LBA6 KRYSTAL-1: Adagrasib (MRTX849) as monotherapy or combined with cetuximab (Cetux) in patients (Pts) with colorectal cancer (CRC) harboring a KRASG12C mutation. *Annals of Oncology*, 32, S1294. <https://doi.org/10.1016/j.annonc.2021.08.2093>
- Weng, C., Faure, A. J., Escobedo, A., & Lehner, B. (2023). The energetic and allosteric landscape for KRAS inhibition. *Nature*. <https://doi.org/10.1038/s41586-023-06954-0>
- White, E. (2006). Mechanisms of apoptosis regulation by viral oncogenes in infection and tumorigenesis. *Cell Death & Differentiation*, 13(8), 1371–1377.
<https://doi.org/10.1038/sj.cdd.4401941>
- Whyte, D. B., Kirschmeier, P., Hockenberry, T. N., Nunez-Oliva, I., James, L., Catino, J. J., Bishop, W. R., & Pai, J. K. (1997). K- and N-Ras are geranylgeranylated in cells treated with farnesyl protein transferase inhibitors. *The Journal of Biological Chemistry*, 272(22), 14459–14464. <https://doi.org/10.1074/jbc.272.22.14459>
- Wilson, P., Abdelmoti, L., Norcross, R., Jang, E. R., Palayam, M., & Galperin, E. (2021). The role of USP7 in the Shoc2-ERK1/2 signaling axis and Noonan-like syndrome with loose anagen hair. *Journal of Cell Science*, 134(21). <https://doi.org/10.1242/jcs.258922>
- Winter-Vann, A., & Casey, P. (2005). Winter-Vann AM, Casey PJ.. Post-prenylation-processing enzymes as new targets in oncogenesis. *Nat Rev Cancer* 5: 405-412. *Nature Reviews. Cancer*, 5, 405–412. <https://doi.org/10.1038/nrc1612>
- Wittinghofer, A., & Vetter, I. R. (2011). Structure-Function Relationships of the G Domain, a Canonical Switch Motif. *Annual Review of Biochemistry*, 80(1), 943–971.
<https://doi.org/10.1146/annurev-biochem-062708-134043>
- Woehlbier, U., & Hetz, C. (2011). Modulating stress responses by the UPRosome: a matter of life and death. *Trends in Biochemical Sciences*, 36(6), 329–337.
<https://doi.org/10.1016/j.tibs.2011.03.001>
- Wood, K., Hensing, T. A., Malik, R., & Salgia, R. (2016). Prognostic and Predictive Value in KRAS in Non-Small-Cell Lung Cancer: A Review. *JAMA Oncology*, 2 6, 805–812.
<https://api.semanticscholar.org/CorpusID:23908243>
- Wright, L. P., & Philips, M. R. (2006). Thematic review series: Lipid Posttranslational Modifications CAAX modification and membrane targeting of Ras. *Journal of Lipid Research*, 47(5), 883–891. <https://doi.org/https://doi.org/10.1194/jlr.R600004-JLR200>

- Wu, X., Upadhyaya, P., Villalona-Calero, M. A., Briesewitz, R., & Pei, D. (2013). Inhibition of Ras–effector interactions by cyclic peptides. *MedChemComm*, 4(2), 378–382. <https://doi.org/10.1039/C2MD20329D>
- Xue, J. Y., Zhao, Y., Aronowitz, J., Mai, T. T., Vides, A., Qeriqi, B., Kim, D., Li, C., de Stanchina, E., Mazutis, L., Risso, D., & Lito, P. (2020). Rapid non-uniform adaptation to conformation-specific KRAS(G12C) inhibition. *Nature*, 577(7790), 421–425. <https://doi.org/10.1038/s41586-019-1884-x>
- Yagoda, N., von Rechenberg, M., Zaganjor, E., Bauer, A. J., Yang, W. S., Fridman, D. J., Wolpaw, A. J., Smukste, I., Peltier, J. M., Boniface, J. J., Smith, R., Lessnick, S. L., Sahasrabudhe, S., & Stockwell, B. R. (2007). RAS–RAF–MEK-dependent oxidative cell death involving voltage-dependent anion channels. *Nature*, 447(7146), 865–869. <https://doi.org/10.1038/nature05859>
- Yang, M. H., Laurent, G., Bause, A. S., Spang, R., German, N., Haigis, M. C., & Haigis, K. M. (2013). HDAC6 and SIRT2 regulate the acetylation state and oncogenic activity of mutant K-RAS. *Molecular Cancer Research : MCR*, 11(9), 1072–1077. <https://doi.org/10.1158/1541-7786.mcr-13-0040-t>
- Yang, M. H., Nickerson, S., Kim, E. T., Liot, C., Laurent, G., Spang, R., Philips, M. R., Shan, Y., Shaw, D. E., Bar-Sagi, D., Haigis, M. C., & Haigis, K. M. (2012a). Regulation of RAS oncogenicity by acetylation. *Proceedings of the National Academy of Sciences of the United States of America*, 109(27), 10843–10848. <https://doi.org/10.1073/pnas.1201487109>
- Yang, M. H., Nickerson, S., Kim, E. T., Liot, C., Laurent, G., Spang, R., Philips, M. R., Shan, Y., Shaw, D. E., Bar-Sagi, D., Haigis, M. C., & Haigis, K. M. (2012b). Regulation of RAS oncogenicity by acetylation. *Proceedings of the National Academy of Sciences of the United States of America*, 109(27), 10843–10848. <https://doi.org/10.1073/pnas.1201487109>
- Yang, M. H., Tran, T. H., Hunt, B., Agnor, R., Johnson, C. W., Waybright, T. J., Nowak, J. A., Stephen, A. G., Simanshu, D. K., & Haigis, K. M. (n.d.). *Allosteric regulation of switch-II controls K-Ras oncogenicity Running title: Regulating oncogenic K-Ras by second site mutations*. <https://doi.org/10.1101/2022.09.20.508702>
- Yang, Y., Zhang, H., Huang, S., & Chu, Q. (2023a). KRAS Mutations in Solid Tumors: Characteristics, Current Therapeutic Strategy, and Potential Treatment Exploration. In *Journal of Clinical Medicine* (Vol. 12, Issue 2). MDPI. <https://doi.org/10.3390/jcm12020709>
- Yang, Y., Zhang, H., Huang, S., & Chu, Q. (2023b). KRAS Mutations in Solid Tumors: Characteristics, Current Therapeutic Strategy, and Potential Treatment Exploration. In *Journal of Clinical Medicine* (Vol. 12, Issue 2). MDPI. <https://doi.org/10.3390/jcm12020709>
- Yap, J., Yuan, J., Tee, Z. H., Huang, X., Ng, W. H., & Hu, J. (2019). Characterize Disease-related Mutants of RAF Family Kinases by Using a Set of Practical and Feasible Methods. *Journal of Visualized Experiments : JoVE*, 149. <https://doi.org/10.3791/59795>
- Yee, K., Grochola, L., Hamilton, G., Grawenda, A., Bond, E., Taubert, H., Würl, P., Bond, G., & O'Neill, E. (2012). A RASSF1A Polymorphism Restricts p53/p73 Activation and Associates with Poor Survival and Accelerated Age of Onset of Soft Tissue Sarcoma. *Cancer Research*, 72, 2206–2217. <https://doi.org/10.1158/0008-5472.CAN-11-2906>
- Yeh, T. C., Marsh, V., Bernat, B. A., Ballard, J., Colwell, H., Evans, R. J., Parry, J., Smith, D., Brandhuber, B. J., Gross, S., Marlow, A., Hurley, B., Lyssikatos, J., Lee, P. A., Winkler, J.

- D., Koch, K., & Wallace, E. (2007). Biological Characterization of ARRY-142886 (AZD6244), a Potent, Highly Selective Mitogen-Activated Protein Kinase Kinase 1/2 Inhibitor. *Clinical Cancer Research*, 13(5), 1576–1583. <https://doi.org/10.1158/1078-0432.CCR-06-1150>
- Yin, G., Kistler, S., George, S. D., Kuhlmann, N., Garvey, L., Huynh, M., Bagni, R. K., Lammers, M., Der, C. J., & Campbell, S. L. (2017). A KRAS GTPase K104Q Mutant Retains Downstream Signaling by Offsetting Defects in Regulation*. *Journal of Biological Chemistry*, 292(11), 4446–4456. <https://doi.org/https://doi.org/10.1074/jbc.M116.762435>
- Ying, H., Kimmelman, A. C., Lyssiotis, C. A., Hua, S., Chu, G. C., Fletcher-Sananikone, E., Locasale, J. W., Son, J., Zhang, H., Coloff, J. L., Yan, H., Wang, W., Chen, S., Viale, A., Zheng, H., Paik, J., Lim, C., Guimaraes, A. R., Martin, E. S., ... DePinho, R. A. (2012). Oncogenic Kras Maintains Pancreatic Tumors through Regulation of Anabolic Glucose Metabolism. *Cell*, 149(3), 656–670. <https://doi.org/10.1016/j.cell.2012.01.058>
- Young, L. C., Hartig, N., Muñoz-Alegre, M., Oses-Prieto, J. A., Durdu, S., Bender, S., Vijayakumar, V., Vietri Rudan, M., Gewinner, C., Henderson, S., Jathoul, A. P., Ghatrora, R., Lythgoe, M. F., Burlingame, A. L., & Rodriguez-Vician, P. (2013). An MRAS, SHOC2, and SCRIB Complex Coordinates ERK Pathway Activation with Polarity and Tumorigenic Growth. *Molecular Cell*, 52(5), 679–692. <https://doi.org/10.1016/j.molcel.2013.10.004>
- Yuan, J., Ng, W. H., Lam, P. Y. P., Wang, Y., Xia, H., Yap, J., Guan, S. P., Lee, A. S. G., Wang, M., Baccarini, M., & Hu, J. (2018). The dimer-dependent catalytic activity of RAF family kinases is revealed through characterizing their oncogenic mutants. *Oncogene*, 37(43), 5719–5734. <https://doi.org/10.1038/s41388-018-0365-2>
- Yuan, T. L., Amzallag, A., Bagni, R., Yi, M., Afghani, S., Burgan, W., Fer, N., Strathern, L. A., Powell, K., Smith, B., Waters, A. M., Drubin, D., Thomson, T., Liao, R., Greninger, P., Stein, G. T., Murchie, E., Cortez, E., Egan, R. K., ... McCormick, F. (2018). Differential Effector Engagement by Oncogenic KRAS. *Cell Reports*, 22(7), 1889–1902. <https://doi.org/https://doi.org/10.1016/j.celrep.2018.01.051>
- Zacharias, D. A., Violin, J. D., Newton, A. C., & Tsien, R. Y. (2002). Partitioning of lipid-modified monomeric GFPs into membrane microdomains of live cells. *Science (New York, N.Y.)*, 296(5569), 913–916. <https://doi.org/10.1126/science.1068539>
- Zeitouni, D., Pylayeva-Gupta, Y., Der, C. J., & Bryant, K. L. (2016). KRAS Mutant Pancreatic Cancer: No Lone Path to an Effective Treatment. *Cancers*, 8(4). <https://doi.org/10.3390/cancers8040045>
- Zhang, J., Zhang, J., Liu, Q., Fan, X.-X., Leung, E. L.-H., Yao, X.-J., & Liu, L. (2022). Resistance looms for KRAS G12C inhibitors and rational tackling strategies. *Pharmacology & Therapeutics*, 229, 108050. <https://doi.org/https://doi.org/10.1016/j.pharmthera.2021.108050>
- Zhao, B., Li, L., Tumaneng, K., Wang, C.-Y., & Guan, K.-L. (2010). A coordinated phosphorylation by Lats and CK1 regulates YAP stability through SCF β -TRCP. *Genes & Development*, 24(1), 72–85. <https://doi.org/10.1101/gad.1843810>
- Zhao, B., Wei, X., Li, W., Udan, R. S., Yang, Q., Kim, J., Xie, J., Ikenoue, T., Yu, J., Li, L., Zheng, P., Ye, K., Chinnaiyan, A., Halder, G., Lai, Z.-C., & Guan, K.-L. (2007). Inactivation of YAP oncoprotein by the Hippo pathway is involved in cell contact inhibition and tissue growth control. *Genes & Development*, 21(21), 2747–2761. <https://doi.org/10.1101/gad.1602907>

- Zhao, J., & Luo, Z. (2022). Discovery of Raf Family Is a Milestone in Deciphering the Ras-Mediated Intracellular Signaling Pathway. *International Journal of Molecular Sciences*, 23(9). <https://doi.org/10.3390/ijms23095158>
- Zheng, Y., Ding, L., Meng, X., Potter, M., Kearney, A. L., Zhang, J., Sun, J., James, D. E., Yang, G., & Zhou, C. (2022). Structural insights into Ras regulation by SIN1. *Proceedings of the National Academy of Sciences*, 119(19), e2119990119. <https://doi.org/10.1073/pnas.2119990119>
- Zhou, Y., & Hancock, J. (2014). Ras nanoclusters: Versatile lipid-based signaling platforms. *Biochimica et Biophysica Acta*, 1853. <https://doi.org/10.1016/j.bbamcr.2014.09.008>
- Zhou, Y., & Hancock, J. F. (2015). Ras nanoclusters: Versatile lipid-based signaling platforms. In *Biochimica et Biophysica Acta - Molecular Cell Research* (Vol. 1853, Issue 4, pp. 841–849). Elsevier B.V. <https://doi.org/10.1016/j.bbamcr.2014.09.008>
- Zhou, Y., & Hancock, J. F. (2023). RAS nanoclusters are cell surface transducers that convert extracellular stimuli to intracellular signalling. In *FEBS Letters* (Vol. 597, Issue 6, pp. 892–908). John Wiley and Sons Inc. <https://doi.org/10.1002/1873-3468.14569>
- Zhou, Y., Prakash, P., Gorfe, A. A., & Hancock, J. F. (2018a). Ras and the Plasma Membrane: A Complicated Relationship. In *Cold Spring Harbor perspectives in medicine* (Vol. 8, Issue 10). NLM (Medline). <https://doi.org/10.1101/cshperspect.a031831>
- Zhou, Y., Prakash, P., Gorfe, A. A., & Hancock, J. F. (2018b). Ras and the Plasma Membrane: A Complicated Relationship. *Cold Spring Harbor Perspectives in Medicine*, 8(10). <https://doi.org/10.1101/CSHPERSPECT.A031831>
- Zimmermann, G., Papke, B., Ismail, S., Vartak, N., Chandra, A., Hoffmann, M., Hahn, S. A., Triola, G., Wittinghofer, A., Bastiaens, P. I. H., & Waldmann, H. (2013). Small molecule inhibition of the KRAS–PDE δ interaction impairs oncogenic KRAS signalling. *Nature*, 497(7451), 638–642. <https://doi.org/10.1038/nature12205>